

POLITECNICO DI MILANO

School of Civil, Environmental and Land Management Engineering
Master of Science in Civil Engineering for Risk Mitigation



POLITECNICO
MILANO 1863

**Flood hazard assessment by 2D hydrodynamic
modelling for rivers North of Milan**

Supervisor: Dr. Alessio Radice
Co-Supervisor: Ing. Rocco Bonora

Master thesis of:
Thomas Cannella – Matr. 946321
Alessandro Caretto – Matr. 944267

Academic year 2020-2021

Sometimes it's in the small rivers which are big troubles....

Acknowledgments

We would like to express our gratitude to our thesis advisor Dr. Alessio Radice of the school of Civil, Environmental and Land Management Engineering at Politecnico di Milano. His availability and support are not common, so we are proud of having experienced this journey together.

Special thanks to Rocco for sharing with us his experience and for bearing us even in the hardest times. No model can run without his touch!

Grazie!

Thomas and Alessandro

Lecco, December 2021

Abstract

Riverine floods endanger lives and cause heavy economic losses. In addition to economic and social damage, floods can have severe environmental consequences, for example when installations holding large quantities of toxic chemicals are inundated or wetland areas are destroyed. Flood impacts may be reduced by appropriate measures, whose design needs to be supported by appropriate assessment of the spatial distribution of hazard and risk.

The legislation of the European Union includes the Directive 2007/60/EC on the assessment and management of flood risks, entered into force on 26 November 2007. In Italy the Directive 2007/60/EC has been adopted with D.Lgs. 49/2010 and with the operative tool PGRA - Piano di Gestione del Rischio Alluvioni, whose use is required by the Italian law to characterize and plan the necessary actions aimed at reducing the negative consequences of flood events on human health, territory, goods, environment, cultural heritage and the economic and social activities.

The present work is framed in the area prone to flood risk called “Milano Nord”, and its aim consists in defining a methodology for a full 2-dimensional unsteady modelling at the river scale, for two of the streams in the area: the Seveso and the Bozzente. The numerical model adopted in this case is embodied in the code PARFLOOD of the “Università degli Studi di Parma” (UNIPR). The input data for the hydrodynamic simulations have been produced merging different pieces of information (hydrological/hydraulic data from past reports, topographic data from digital terrain models and ground surveys of river sections, soil use databases). The proposed approach has been used to produce flood hazard maps (showing maximum values of water depth and velocity within a design event) for the return periods of 10, 100, and 500 years.

The final maps have been compared with the results from the previous flood hazard assessments (last update of the flood maps was performed in 2019 with 0D models), in order to highlight the major differences between the results obtained with the two approaches. A critical analysis of the procedure and of the results produced in this thesis has been carried out, highlighting several limitations of the performed work (probable overestimation of the flood hazard, possible geometric misrepresentations due to the large scale of the models, lack of building block inclusion); some further developments are thus proposed to overcome such limitations and produce more reliable inundation maps.

Abstract (Italian version)

Le inondazioni fluviali mettono in pericolo vite umane e causano pesanti perdite economiche. Oltre ai danni economici e sociali, le inondazioni possono avere gravi conseguenze ambientali, per esempio quando vengono inondate stabilimenti che contengono grandi quantità di sostanze chimiche tossiche o quando vengono distrutti ecosistemi paludosi. Gli impatti delle inondazioni possono essere ridotti con misure appropriate, la cui progettazione deve essere supportata da un'adeguata valutazione della distribuzione spaziale del pericolo e del rischio.

La legislazione dell'Unione Europea include la Direttiva 2007/60/CE sulla valutazione e gestione dei rischi da alluvione, entrata in vigore il 26 novembre 2007. In Italia la Direttiva 2007/60/CE è stata adottata con il D.Lgs. 49/2010 e con lo strumento operativo PGRA - Piano di Gestione del Rischio Alluvioni, il cui utilizzo è previsto dalla normativa italiana per caratterizzare e pianificare le azioni necessarie volte a ridurre le conseguenze negative degli eventi alluvionali sulla salute umana, sul territorio, sui beni, sull'ambiente, sul patrimonio culturale e sulle attività economiche e sociali.

Il presente lavoro è inquadrato nell'area a rischio di alluvione denominata "Milano Nord", e il suo scopo consiste nel definire una metodologia per una modellazione a moto vario bidimensionale a scala fluviale, per due dei torrenti della zona: il Seveso e il Bozzente. Il modello numerico adottato in questo caso è incorporato nel codice PARFLOOD dell'Università degli Studi di Parma (UNIPR). I dati di input per le simulazioni idrodinamiche sono stati prodotti utilizzando diverse informazioni (dati idrologici/idraulici da relazioni precedenti, dati topografici da modelli digitali del terreno e rilievi in sito delle sezioni del fiume, database sull'uso del suolo). L'approccio proposto è stato usato per produrre mappe di pericolo di inondazione (che mostrano i valori massimi di altezza e velocità dell'acqua in un evento di progetto) per i periodi di ritorno di 10, 100 e 500 anni.

Le mappe finali sono state confrontate con i risultati delle precedenti valutazioni della pericolosità da inondazione (l'ultimo aggiornamento delle mappe di inondazione è stato eseguito nel 2019 con modelli 0D), al fine di evidenziare le principali differenze tra i risultati ottenuti con i due approcci. È stata effettuata un'analisi critica della procedura e dei risultati prodotti in questa tesi, evidenziando diversi limiti del lavoro svolto (probabile sovrastima della pericolosità alluvionale, possibili travisamenti geometrici dovuti alla grande scala dei modelli, mancata inclusione degli edifici); vengono quindi proposti alcuni ulteriori sviluppi per superare tali limiti e produrre mappe di inondazione più affidabili.

Contents

1. Introduction and objectives	1
1.1 The European Floods Directive and the PGRA in the Po district of Italy	1
1.2 Area of interest	3
1.3 Starting situation for the present work.....	5
1.3.1 Previous studies and models.....	5
1.3.2 Updating of the maps from 2019	7
1.4 Aim and structure of the work	8
2. Hazard Mapping with 2D hydraulic simulations	12
2.1 Two-dimensional flow modelling	12
2.1.1 Boundary Conditions.....	14
2.2 Numerical model	14
2.2.1 Internal Boundary Condition	16
2.3 Flood modelling in urban context.....	19
3. Method for hydraulic simulations using available data.....	22
3.1 Terrain geometry representation	22
3.2 Roughness modelling	25
3.3 Division of a river into modelling reaches	28
3.4 Downstream boundary conditions	30
3.5 Input files for PARFLOOD code.....	32
3.6 Output files from PARFLOOD code	32
3.7 Result check and representation.....	33
3.7.1 Control sections for the flow rate distribution.....	34
3.7.2 Cumulated Frequency Distribution (CFD) of water depth and velocity.....	35
3.7.3 Comparison with Vs without bridges	37
3.7.4 Comparison with previous results (2019 perimeter)	41
4. Setup of the models and results.....	43
4.1 Seveso	43
4.1.1 Longitudinal peak flow rate distribution and its discretization	43
4.1.2 Boundary conditions.....	46
4.1.3 Control sections for the flow rate distribution.....	51
4.1.4 Maps of the results.....	54
4.2 Bozzente	73
4.2.1 Longitudinal peak flow rate distribution and its discretization	73
4.2.2 Boundary conditions.....	75

4.2.3 Control sections for the flow rate distribution.....	79
4.2.4 Maps of the results.....	83
4.3 General comments.....	102
5. Critical discussion of the results and further developments	103
5.1 Observations.....	103
5.1.1 Downstream BC.....	103
5.1.2 PARFLOOD vs Perimeters 2019.....	104
5.2 Limitations of the model	105
5.2.1 Boundary conditions for consecutive reaches	105
5.2.2 Punctual inflows.....	106
5.2.3 Junction of maps for consecutive reaches.....	109
5.2.4 Bathymetry: construction and sections geometry.....	111
5.2.5 Bridge input.....	114
5.2.6 Culvert representation.....	114
5.3 Future developments.....	115
5.4 Attempt to implement some improvements.....	117
5.4.1 Reconstruction of the bathymetry	117
5.4.2 2D model with PARFLOOD with the new bathymetry.....	120
5.4.3 1D modelling for comparison.....	126
5.4.4 Observations	129
6. Conclusions	131

List of Figures

Figure 1.1: Sub basins included in the Po River District	2
Figure 1.2: Territories included in the Po river District	3
Figure 1.3: APSFR Milano Nord, with the main watercourses (in blue), the irrigation channels (in yellow), the artificial channels for the flood management in (orange)	4
Figure 1.4: Flooded area upstream the culvert at the entrance of Milan, for different return periods (2003 version)	6
Figure 1.5: Water depth maps for Bozzente (left) and Seveso (right), 2019 version	8
Figure 1.6: Modelled reaches of Bozzente and Seveso streams	9
Figure 2.1: Example of Bridge scheme	17
Figure 2.2: Example of Bridge geometry and different flow conditions	17
Figure 2.3: Representation of the Manning's roughness embedded in a larger computational domain	20
Figure 2.4: Example of void method [Alcrudo, 2004]	20
Figure 2.5: Examples of bottom elevation techniques on a coarse mesh (on the left) and on a finer mesh (on the right) [Alcrudo, 2004]	21
Figure 2.6: Examples of Porosity method.....	21
Figure 3.1: DTM correction procedure.....	24
Figure 3.2: Flood extension in correspondence of the underpass in Barlassina, before (left) and after (right) the correction of the DTM	25
Figure 3.3: Urbanized area representation from OSM (left) and Dusaf 6.0 (right)	26
Figure 3.4: Polygons for Manning coefficient distribution	28
Figure 3.5: Longitudinal distribution of the peak flow rate along the river	29
Figure 3.6: Discretization of the distribution	29
Figure 3.7.a and 3.7.b: Rating curves defined by potential and linear function respectively	31
Figure 3.8: Control sections distribution.....	34
Figure 3.9: Input Hydrograph and Hydrographs at different control sections	35
Figure 3.10: Water depth map with few anomalous values	36
Figure 3.11: CFD of Water Depth	36
Figure 3.12: Difference between depth Bridges-No Bridges	37
Figure 3.13: Difference between velocity Bridges-No Bridges.....	38
Figure 3.14: CFD Depth Bridges-No Bridges	39
Figure 3.15: CFD Velocity Bridges-No Bridges	39
Figure 3.16: Overlap of the flooded areas	40

Figure 3.17: Detail of the flooded area without (left) and with (right) the presence of the bridge (in red)	41
Figure 3.18: Comparison between PARFLOOD results and 2019 perimeter in one of the reaches of the Seveso	42
Figure 4.1: Peak flow rate distribution for the Seveso	44
Figure 4.2: Subdivision of the Seveso	45
Figure 4.3 a-c: Hydrographs set as upstream BCs for the Seveso for T=10, 100, 500 years respectively	47
Figure 4.4: Control sections for the reach 2	51
Figure 4.5: Control sections for the reach 6	52
Figure 4.6: Hydrographs extracted from the control sections for the reach 2	52
Figure 4.7: Hydrographs extracted from the control sections for the reach 6	53
Figure 4.8: Peak flow rate distribution for the Bozzente	73
Figure 4.9: Subdivision of the Bozzente	74
Figure 4.10 a-c: Hydrographs set as upstream BCs for the Bozzente for T=10, 100, 500 years respectively	76
Figure 4.11: Control sections for the reach 1	80
Figure 4.12: Control sections for the reach 3	81
Figure 4.13: Hydrographs extracted from the control sections for the reach 1	82
Figure 4.14: Hydrographs extracted from the control sections for the reach 3	82
Figure 5.1: Comparison between results imposing condition 5 (left) and condition 4 (right)	104
Figure 5.2: Representation of control section of reach 2 and upstream section of reach 3, Bozzente river	105
Figure 5.3: Flow rate distributions at downstream control section reach 2 and input hydrograph reach 3	106
Figure 5.4: Sketch of computational domain needed to insert punctual inflows	107
Figure 5.5: Sketch of computational domain needed to insert affluent, if affluent sections are available	108
Figure 5.6: Sketch of shrinkage of the domain in the upstream area of the reach	109
Figure 5.7: Example of junction between partition 4 (left) and partition 5 (right) of Bozzente river	110
Figure 5.8: Result of junction between partitions 4 and 5 of Bozzente river	111
Figure 5.9: Comparison between surveyed section BZ 2.1 and its representation in GIS	112
Figure 5.10: Comparison between surveyed section BZ 20 and its representation in GIS	113
Figure 5.11: Representation of removed bridges in red, and the inserted one in green - reach 6 of Seveso stream	114

Figure 5.12: Representation of culvert section in Bozzente River.....	115
Figure 5.13: Sections representation in the bathymetry of the Bozzente (a-b) and of the Seveso (c-d)	119
Figure 5.14: Flood maps for the Bozzente - Reach 5 (T=10 y).....	121
Figure 5.15: Flood maps for the Seveso - Reach 4 (T=10 y)	122
Figure 5.16: Overflow of the Bozzente between section BZ 9 bis and BZ 8	123
Figure 5.17: Local correction of the riverbed elevation.....	124
Figure 5.18: Water depth distribution after the local correction of the bathymetry.....	125
Figure 5.19: Detail of the water level in correspondence of the curve.....	125
Figure 5.20: HEC-RAS profile for the Bozzente – Reach 5.....	126
Figure 5.21: HEC-RAS profile for the Seveso – Reach 4	126
Figure 5.22: Superposition of the profiles for the Bozzente.....	127
Figure 5.23: Superposition of the profiles for the Seveso	128

1. Introduction and objectives

1.1 The European Floods Directive and the PGRA in the Po district of Italy

Riverine floods endanger lives and cause heavy economic losses. In addition to economic and social damage, floods can have severe environmental consequences, for example when installations holding large quantities of toxic chemicals are inundated or wetland areas are destroyed. Between 1998 and 2009, Europe suffered over 213 major damaging floods, which have caused some 1126 deaths, the displacement of about half a million people and at least €52 billion in insured economic losses. Overall losses as a consequence of floods have increased over the last few decades in Europe. Evidence suggests that increases in population and wealth in the affected areas are the main factors contributing to the increase in losses. Additionally, improvements in data collection in recent decades could bias trends over time [European Environmental Agency (EEA), 2010]. Although the share of losses attributable to climate change is currently impossible to determine accurately, it is likely to increase in the future, since the frequency and intensity of extreme weather events are projected to grow. On the other hand, flood impacts may be reduced by appropriate measures, whose design needs to be supported by appropriate assessment of the spatial distribution of hazard and risk.

The legislation of the European Union (EU henceforth) includes the Directive 2007/60/EC on the assessment and management of flood risks, entered into force on 26 November 2007. This Directive requires the Member States to assess the flood risk for all their water courses and coast lines, to map the expected flood extent, to identify and list assets and humans at risk in these areas, and to take adequate and coordinated measures to reduce the flood risk. This Directive also aims at reinforcing the rights of the public to access information, and to adopt a participatory approach in the planning process. The Floods Directive indicates spatial planning as a suitable mean to achieve its objectives; the related work is carried out in coordination with that for the Water Framework Directive (issued in 2002), because flood risk management plans and river basin management plans need to be integrated.

In Italy the Directive 2007/60/EC has been adopted with D.Lgs. 49/2010 and it represents an opportunity to re-examine, upgrade and improve the actions for the flood risk management, already defined in any PAI (Piano di Assetto Idrogeologico) in force, taking in account the need to adapt to climate change and to increase the level of resilience towards disasters. A plan for the flood risk management (PGRA - Piano di Gestione del Rischio Alluvioni), is the

1.2 Area of interest

The AdBPo has identified 21 areas with potential significant flood risk (APSFR) within the Po district. These APSFRs may correspond to a river (for example, this is the case of the Po with its delta) or to a town (for example, the town of Brescia with some rivers flowing in its surroundings). Given the large size of the river districts that includes territories with different morphologies and levels of urbanization, the characteristics of the APSFRs may be quite different from one another.

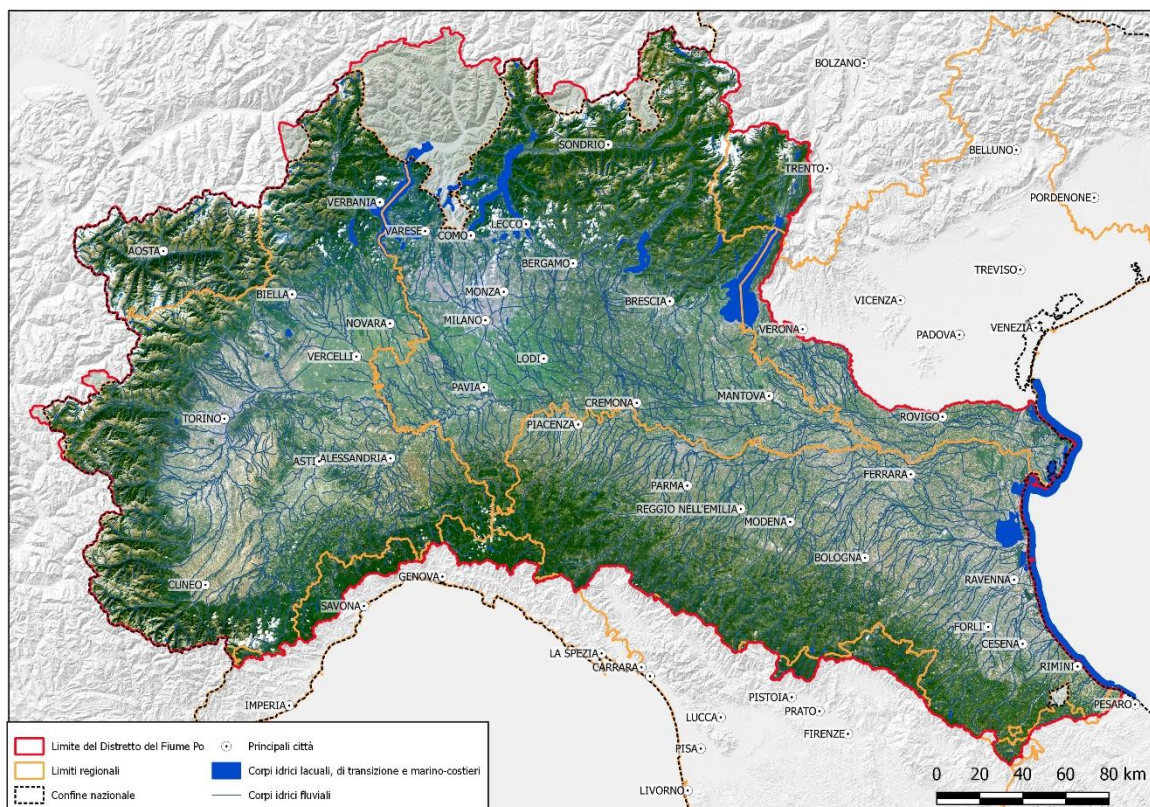


Figure 1.2: Territories included in the Po river District

The present work is framed in the “APSFR Milano Nord” (Figure 1.3). It includes all the municipalities of the Management Unit named “Lambro-Olona” and it comprehends the flood-prone areas related to the watercourses flowing around Milan (particularly at the North of the city). In particular, the area covers 111 municipalities in Lombardia Region, belonging to the Metropolitan City of Milan and to the Provinces of Monza-Brianza, Como, Lecco and Varese. The extent of the flood prone areas related to the main network of the APSFR is around 110 km². The overall network includes around 420 km of river stretches. The APSFR mainly follows two main axes, orthogonal to each other, because the rivers mostly have a

South-ward direction while irrigation and flood diversion channels have East-ward or West-ward direction. The involved natural watercourses (from East to West) are the Lambro (until the confluence with the Cavo Redefossi), Seveso, torrenti delle Groane (Garbogera, Pudiga-Cisnara, Nirone and Guisa), Lura, Bozzente, Olona.

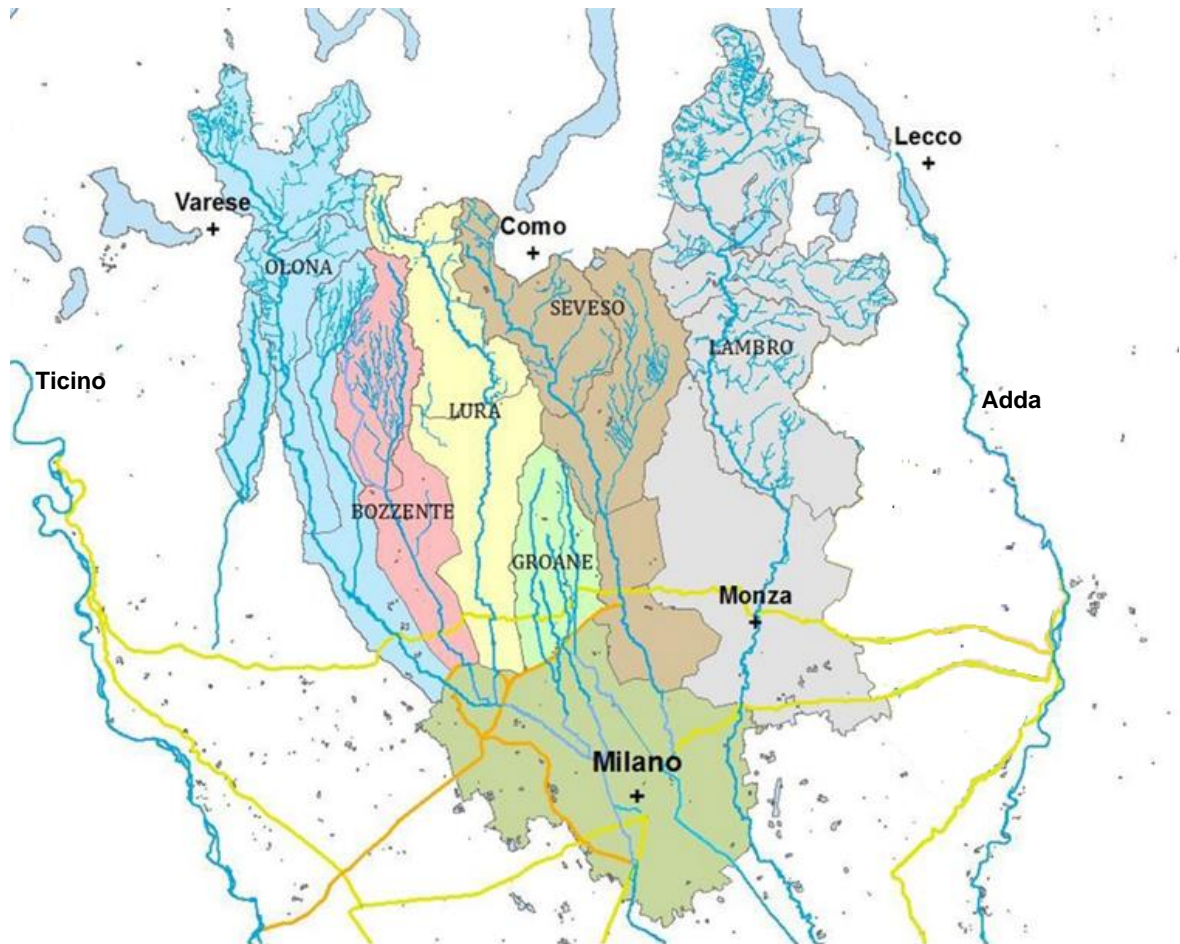


Figure 1.3: APSFR Milano Nord, with the main watercourses (in blue), the irrigation channels (in yellow), the artificial channels for the flood management in (orange)

All the mentioned reaches are strongly interconnected from the functional point of view. The numerous natural waterways in the area converge into the urban area of the city and its hinterland. In the city area, all the streams except the Lambro flow in culverts and completely channelised riverbeds which, for several kilometres, cross the city centre underground. The underground culverts represent a sort of calibrated mouth, which strongly limits the flow rate that can be conveyed. In fact, all the waterways of the network, with the exception of the Lambro, have a consolidated conformation with progressively decreasing flow capacity from

upstream to downstream. The whole network, from a functional point of view, can essentially be considered as a single river system that flows into the Lambro river downstream of Milan. This system has a specifically arranged set-up that makes it a unique case in the Po basin. It is the result, in fact, of a centuries-old human activity intended to supply water to a city that, from Roman times until the period of the first industrialization, has become more and more water demanding, due to its progressive development. Civil and industrial settlements have led to the creation of new sewer networks and, together with the transformed conditions of land use, an increase in the volume of water discharged into rivers and streams. Moreover, a reduction in the time of concentration is another direct consequence of urbanization that gives rise to significant increases in flood volumes and peak discharges. This situation is further worsened by the development over time of interfering works, which decrease the discharge capacity, triggering large and frequent floods of the main waterways and consequent flooding of highly urbanized areas. This leads to great amount of damage and severe inconveniences to the resident population, together with long interruptions in traffic and public transport services.

1.3 Starting situation for the present work

1.3.1 Previous studies and models

The hydrologic analysis and the hydraulic modelling of the network “Nord Milano” have been performed in previous studies, by hydraulic consultancy companies or by municipalities which issued specific interventions on the streams; the latter is the case of the several flood retention basins realised in the APFSR. Furthermore, on the website of the Municipalities crossed by the watercourses of the network, a local hydraulic analysis could be found in the context of the PGT (Piano di Governo del Territorio), an urban planning tool at the municipal level with the purpose of defining the set up of the entire municipal area. Among all, the most extensive, referred to the entire APFSR, are represented by “*Studio di fattibilità della sistemazione idraulica dei corsi d’acqua naturali e artificiali all’interno dell’ambito idrografico di pianura Lambro – Olona.*”. These have been performed in 2003 by the company Lotti & Associati and commissioned by the Po basin District Authority. The aim of these studies is the assessment of the water network design, which guarantees the achievement of safety conditions in such a densely inhabited territory around the metropolitan city of Milan. This has been pursued through a mono dimensional modelling of unsteady flow, for assigned return period, for all the watercourses

in *Table 1.1*. It is worth noticing that not the entire length of the rivers has been surveyed and so characterized by measured cross sections, so the modelled length for each river is reported as well in *Table 1.1*.

River	Olona	Bozzente	Lura	Guisa	Nirone	Pudiga	Garbogera	Seveso	Lambro
Length of the stream [km]	70	39	47	22	8	23	24	48	140
Length of the model [km]	56	19	21	16	6	12	14	35	60

Table 1.1: Length of the natural watercourses in the APSFR Milano Nord

Figure 1.4 provides an example of the results coming from the mono dimensional modelling in a sub-section of the Seveso stream:

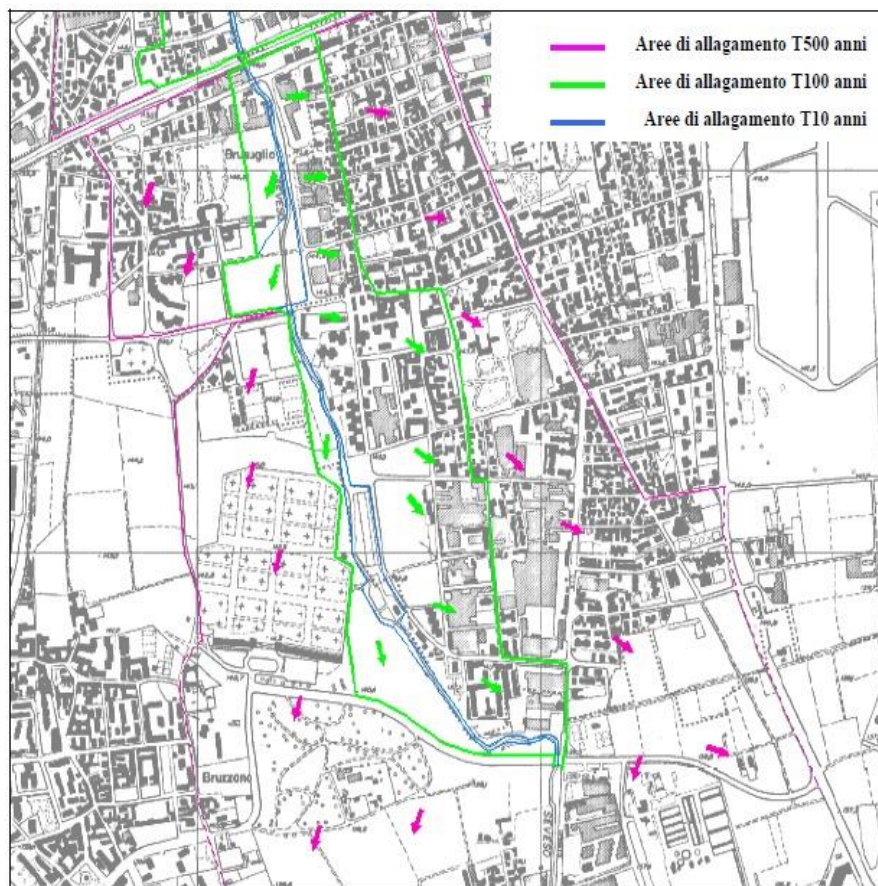


Figure 1.4: Flooded area upstream the culvert at the entrance of Milan, for different return periods (2003 version)

1.3.2 Updating of the maps from 2019

On December 2019 the activities in support of the update of the hazard maps have led to new developments: to produce maps for the flood scenarios with high (H), medium (M) and low (L) probability of occurrence, simplified methods have been followed, assessing the distribution of water surface elevation starting from the results of a 1D model, where possible, and from the perimeter of the flooded area, where no results were available.

Reconstruction of the water surface from the 1D model results

The first method is called TIRANTI and it is implemented considering as input the results of a one-dimensional hydrodynamic modelling: in particular here the results come from the above mentioned “Studio di fattibilità”.

TIRANTI is a GIS-based tool which defines the water surface through three subsequent operations, here briefly described:

- First, the value of water surface elevation coming from the 1D model is assigned to all the points of the respective cross section;
- Second, two-dimensional interpolation of the water surface elevation is performed through Natural Neighbor method;
- Finally, the results of the interpolation are clipped with the boundaries of the flooded area.

The need of results from a hydraulic mono-dimensional modelling has limited the extension of the modelled area to the same reaches characterized by the previously mentioned “Studio di fattibilità (2003)”.

Reconstruction of the water surface from the perimeter of the flooded area

The second method is called RAPIDE (RAPid GIS tool for Inundation Depth Estimation). It can be applied where there is no availability of results from a previous 1D hydrodynamic modelling, so the only starting piece of information is represented by the perimeter of the flooded area. The latter is defined as the locus of points where the water surface elevation coincides with the terrain elevation. Also RAPIDE requires three operations to be performed:

- First, the auxiliary lines, perpendicular to the watercourse, are defined between the two points belonging to the aforementioned perimeter of the flooded area;
- Second, through the Natural Neighbor interpolation, the water surface is generated;

- Finally, the results of the interpolation are clipped with the boundaries of the flooded area.

The method RAPIDE is less accurate than the previously described TIRANTI. Nevertheless, it allows to get results even in reaches where no results are available from a previous mono-dimensional modelling.

Here below, some examples of maps coming from the just described simplified methods are illustrated:



Figure 1.5: Water depth maps for Bozzente (left) and Seveso (right), 2019 version

1.4 Aim and structure of the work

With the PGRA 2021 the AdBPo intends to redefine the boundaries of the flood-prone areas in the context of the APSFR North of Milan, shifting from the maps produced with the simplified methods in 2019 to an extensive two-dimensional modelling of all the main waterways included in the network of the Metropolitan City of Milan. The present thesis work is thus motivated by a general need for defining a methodology suitable for a full 2-dimensional flood modelling on a large scale, that represents a major update to the previous PGRA 2015 and the additional maps produced in 2019.

The numerical model adopted in this case is embodied in the code PARFLOOD of the “Università degli Studi di Parma” (UNIPR). PARFLOOD is a GPU-enhanced finite volume SWE solver for fast flood simulations, firstly developed by Vacondio et al. [2014]. The use of a numerical solver executable on specific hardware is beneficial (compared to using a solver that runs on normal PCs) when one has to model rivers along large distances maintaining a fine spatial resolution.

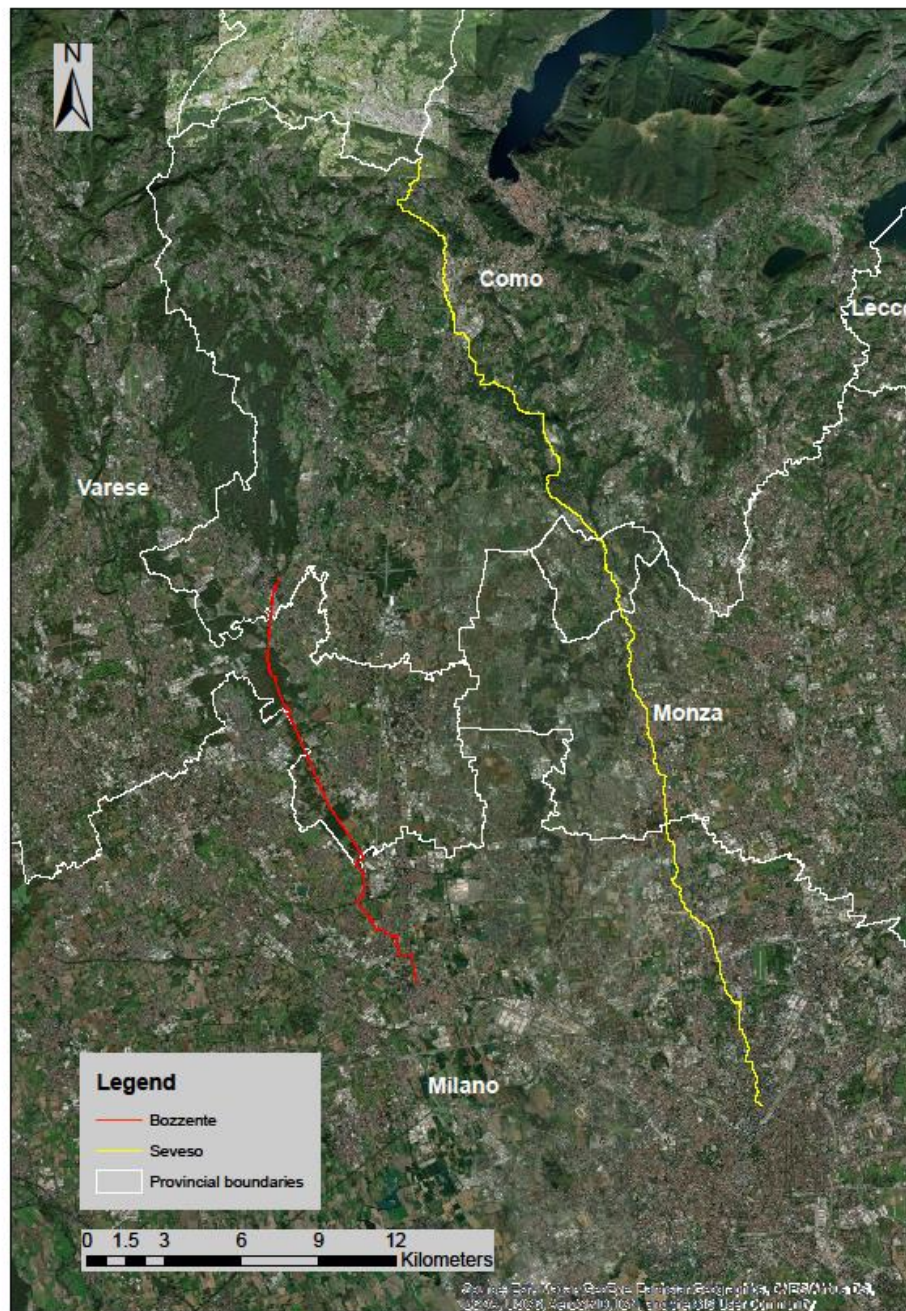


Figure 1.6: Modelled reaches of Bozzente and Seveso streams

The present thesis is focused on two of the main waterways in the APSFR, the Bozzente and the Seveso, whose modelled reaches are represented in *Figure 1.6*. These two streams have been chosen because their different characteristics pose multiple challenges to a numerical solver and its operator.

The Bozzente originates inside the Pineta park near Olgiate Comasco, a municipality of the Como province, and flows into the Olona river in Rho, after about 39 Km. The watercourse is fed by two main discharge sources: a natural one, resulting from the runoff of rainwater, and an artificial one, resulting from the discharges of urban drainage and purification systems. The average width of the riverbed is around 5 m, but, in many cases, it results drastically reduced up to 2-3 meters by the presence of interfering works; indeed, moving from upstream to the downstream more urbanized area, the number of transversal structures increases, in addition to the presence of some culverts in the neighbourhood and inside the town of Rho. In 1960 the stream was diverted into the Olona river, canalising its waters from Origgio to Rho. Moreover, the woods surrounding the Bozzente not only represent a precious ecological resource for the territory, but also a strategic area for the mitigation of alluvial events, as they allow the natural attenuation of the flood wave. The hydraulic risk, however, is not the only problem of this stream: in fact, the quality of the water results quite poor, due both to the high polluting inflows converging into the basin, and to the poor diluting capability, as a consequence of the small flow rate in low water conditions.

The Seveso originates in the province of Como near the border with the Canton Ticino, at about 490 meters a.s.l. It crosses various towns in the Brianza area and enters Milan until it flows into the Naviglio della Martesana, in the center of Milan. The average width of the stream ranges from 10-12 m, in the upstream region where the riverbed is flanked by floodplains, to 5-6 m, mainly downstream, in correspondence of the urbanized areas. As all the other rivers in the APSFR, the Seveso is affected by heavy flow limitations, coming from a consolidated conformation of the riverbed, developed over time: the arrangement includes a set of constraints posed by the reduced size of the riverbed, the uninterrupted succession of bridges and the discontinuity of the defensive system in crossing the urbanized areas. In flood situations, the Seveso is partially drained by the artificial channel "Canale Scolmatore di Nord Ovest" (CSNO). The CSNO has a length of about 34 Km and derives the flood waters from the Seveso stream in the Municipality of Paderno Dugnano to deliver them to the Olona deviator and, in exceptional cases, to the Ticino river. The Seveso reaches Milan and then flows in culverts, whose "bottlenecks" are one of the contributing causes of the periodic inundations of the city (2.6 per year in average).

In addition to the already mentioned PGRA 20215 and “Studio di fattibilità della sistemazione idraulica”, the reports related to previous studies have been taken as reference for the two rivers purposes of the present work. In particular, for the Bozzente, among the available in literature, the following reports have been considered:

- Agenzia Interregionale per il Po (AIPO) – Approfondimenti idrologici relativi alla realizzazione della vasca di laminazione lungo il Torrente Bozzente in comune di Nerviano (MI) [March 2011]
- Comune di Uboldo – Aggiornamento a seguito dei pareri della Provincia di Varese e dell’ARPA – Dipartimento di Varese [April 2014].

For the Seveso, the reports at issue are:

- AIPO – Studio idraulico del Torrente Seveso [June 2011]
- ADBPo – Relazione Tecnica T. Seveso [June 2016]
- Autorità di Bacino Distrettuale del Fiume Po – Relazione sull’aggiornamento delle analisi idrologiche e idrauliche del Torrente Seveso [November 2017]
- Comune di Milano – Area di laminazione del Torrente Seveso [April 2019].

This thesis is structured as follows: *Chapter 2* contains an overview of the theoretical basis supporting the 2-dimensional flood modelling performed through the PARFLOOD code; in *Chapter 3*, a description of the methodology defined and followed during the thesis work is presented; *Chapter 4* illustrates the results in terms of maps for the streams under study, Seveso and Bozzente; finally, *Chapter 5* offers a critical discussion about the several issues that revolve around the flood modelling work, followed by the conclusions in *Chapter 6*.

2. Hazard Mapping with 2D hydraulic simulations

Flood propagation modelling can be defined as “the art of quantitatively describing the characteristics and evolution of the flow that is set up when a large amount of water moves along the Earth surface in an uncontrolled way” [Alcrudo, 2004]. This chapter describes the mathematical approach followed in this thesis to describe the flood propagation in the areas of study.

2.1 Two-dimensional flow modelling

Mathematically, the flow propagation over the Earth surface is a three-dimensional time dependent, incompressible, fluid dynamics problem [Alcrudo, 2004]. The equations that describe the dynamics of the flood propagation are the Navier-Stokes (NS) equations. However, unfortunately, in the case of a turbulent flow with large (in both space and time) computational domain, the attempts to solve the same equations can be compromised. To overcome the problem of the turbulent flow, the NS equations can be averaged in time [Spurk, 1997], obtaining the Reynold Averaged Navier-Stokes (RANS) equations that describe the time-mean flow.

The RANS are widely used in industrial fluid mechanics and aerodynamics fields, but they are still too complex to describe flood propagations for large areas. In order to simplify the mathematical problem, the NS equations are averaged over the depth, obtaining the Shallow Water equations (SWE) [Benquè et al., 1982]. The depth-averaging procedure simplifies the free surface location problem which is now placed as a unique value of water depth above the terrain surface. This set of equations can also be derived from the momentum conservation and the continuity equation in the plane of motion [Cunge, 2003] and they are widely used for flood modelling, inundation, and dam breaks, among others. The depth-averaged representation of the equations reduces the 3D problem to a 2D one, where the depth of the water layer plays the role of the pressure [Landau and Lifshitz, 1959]. These equations can be written in vectorial representation as shown in *Equation (2.1)*, where \mathbf{U} is the vector of the unknowns, \mathbf{F} and \mathbf{G} are the convective flux vectors in the x-direction and the y-direction respectively (in the plane of movement), and \mathbf{F}_d and \mathbf{G}_d are the diffusive flux vectors in the x-direction and the y-direction respectively. At the same time, \mathbf{H} is the friction and \mathbf{I} the slope source term vector. The full vectors are shown in *Equations (2.2), (2.3) and (2.4)*.

$$\frac{\delta U}{\delta t} + \frac{\delta}{\delta x}(F + F_d) + \frac{\delta}{\delta y}(G + G_d) = H + I \quad (2.1)$$

$$U = \begin{pmatrix} h \\ hu \\ hv \end{pmatrix} \quad F = \begin{pmatrix} hu \\ hu^2 + \frac{gh^2}{2} \\ huv \end{pmatrix} \quad G_d = \begin{pmatrix} 0 \\ huv \\ hv^2 + \frac{gh^2}{2} \end{pmatrix} \quad (2.2)$$

$$F_d = \begin{pmatrix} 0 \\ -\varepsilon h \frac{\delta u}{\delta x} \\ -\varepsilon h \frac{\delta v}{\delta x} \end{pmatrix} \quad G_d = \begin{pmatrix} 0 \\ -\varepsilon h \frac{\delta u}{\delta y} \\ -\varepsilon h \frac{\delta v}{\delta y} \end{pmatrix} \quad (2.3)$$

$$H = \begin{pmatrix} 0 \\ gh(S_{0x} + S_{fx}) \\ gh(S_{0y} + S_{fy}) \end{pmatrix} \quad (2.4)$$

Here, h is the water depth, u and v are the depth-averaged velocities in turbulent flow [Alcrudo, 2004], respectively in the x-direction and y-direction; g is the acceleration of gravity. The diffusive fluxes are indicated by ε as the kinematic viscosity coefficient, that comprises the fluid kinematic viscosity, the turbulent eddy viscosity and the apparent viscosity due to velocity variations in the vertical direction. S_{0x} and S_{0y} are the bed slopes along the two cartesian directions, with z the bottom surface. S_{fx} and S_{fy} are the friction slopes, represented through the empirical formula with the Manning's coefficients (n).

$$S_{0x} = -\frac{\delta z}{\delta x}; S_{0y} = -\frac{\delta z}{\delta y} \quad (2.5)$$

$$S_{fx} = -\frac{n^2 u \sqrt{u^2 + v^2}}{h^{4/3}}; S_{fy} = -\frac{n^2 v \sqrt{u^2 + v^2}}{h^{4/3}} \quad (2.6)$$

It is important to acknowledge that the SWE approach is based on the following approximations:

1. vertical velocities are neglected;
2. hydrostatic pressure is assumed;
3. the slope of the river is small enough so that the sine of the slope can be approximated with the value of the angle;
4. the friction approach is taken from the uniform flow conditions.

2.1.1 Boundary Conditions

Obviously, to solve 3 partial differential equations one needs of 3 initial boundary conditions (BCs) for the three unknowns: depth and velocities. In function of the type of the flow, it must be necessary to define 3 upstream conditions to describe super-critical flow or 2 upstream and 1 downstream BC for defining sub-critical flow. In particular, in addition to an initial water depth value, the upstream BC can be defined as the flow rate that can be constant over time and will therefore be referred to as permanent flow, or as a hydrograph if modelled under conditions of varied flow. The downstream condition instead can be a rating curve or a constant water level over time. It is important to specify that in a 2D model it should be required a different BC for each cell that intersects the computational domain at upstream or downstream, but, to simplify the problem, the BCs can be assumed valid for all cells at issue, introducing the following assumptions:

- at the downstream section there is no cross slope of the free surface and therefore the flow can be considered one-dimensional;
- orthogonality between upstream section and vectors of velocity.

2.2 Numerical model

The numerical solution of differential equations, like the SWE, is defined by the space and time discretization strategy, the used mesh configuration and the numerical scheme employed. The spatial discretization can be performed with the Finite Differences, the Finite Volume, or the Finite Element Method. The Finite Volume formulation has a flexible geometrical treatment and it is, conceptually, a simple method: this makes it the most widespread flood modelling strategy [Alcrudo, 2004]. Moreover, this procedure ensures the conservation of mass and momentum. The studied domain is divided into non overlapping finite volumes over which the integral form of the SWE is applied.

The numerical model adopted in this thesis is implemented in the already mentioned PARFLOOD code, provided by Università degli Studi di Parma (UNIPR). Further details about the PARFLOOD code user guide can be found in *Appendix A*. This model is capable to solve, in a finite volume framework, the integral form of the SWE presented in *Equation (2.7)* coming from the work of Toro [2001] and modified according to the study of Liang and Borthwick [2009]. The main advantage of the modified version of the SWEs reported in *Equation (2.7)* is that it guarantees the capability of preserving still water at rest [Vázquez-Cendón, 1999], regardless of the adopted discretization form of the slope source term. This modification is the adaptation for wet-dry interfaces of the derived algebraic modification performed by Rogers et al. [2003] that were able to balance the hyperbolic system of equations regardless of the adopted numerical scheme. From the original formulation described in the previous paragraphs, the modified entities are the vectors \mathbf{U} into \mathbf{U}' , \mathbf{F} into \mathbf{F}' , \mathbf{G} into \mathbf{G}' and the bed slope representation shown in *Equation (2.10)*. Here \mathbf{T} is the tensor of fluxes described in (2.9), $\eta = h + z$ is the free surface elevation above datum, A is the area of the integration element, C is the element boundary, \mathbf{n} is the outward unit vector normal to C .

$$\frac{d}{dt} \int_A \mathbf{U}' dA + \int_C \mathbf{T} \cdot \mathbf{n} dC = \int_A S_0 + S_f dA \quad (2.7)$$

$$\mathbf{U}' = \begin{pmatrix} \eta \\ hu \\ hv \end{pmatrix} \quad (2.8)$$

$$\mathbf{T} = \begin{pmatrix} uh & vh \\ u^2h + 0.5g(\eta^2 - 2\eta z) & uvh \\ uvh & v^2h + 0.5g(\eta^2 - 2\eta z) \end{pmatrix} = (\mathbf{F}', \mathbf{G}') \quad (2.9)$$

$$S_0 + S_f = \begin{pmatrix} 0 \\ -g\eta \frac{\delta z}{\delta x} + ghS_{fx} \\ -g\eta \frac{\delta z}{\delta y} + ghS_{fy} \end{pmatrix} \quad (2.10)$$

The partial differential *Equation (2.7)* is solved on a Cartesian grid. Both a first order and a second order accurate (in space and time) Finite Volume (FV) numerical approximation of the SWEs

have been implemented [Vacondio et al., 2014]. For the first order approximation, the vector of the conserved physical quantities $\mathbf{U}_{i,j}$ is updated in time as follows in *Equation (2.11)*.

$$U_{i,j}^{n+1} = U_{i,j}^n - \frac{\Delta t^n}{\Delta x} (F'_{i+\frac{1}{2},j} - F'_{i-\frac{1}{2},j}) - \frac{\Delta t^n}{\Delta y} (G'_{i,j+\frac{1}{2}} - G'_{i,j-\frac{1}{2}}) + \Delta t^n (S_0 + S_f) \quad (2.11)$$

The superscript n represents the time level, the subscripts i, j and $\Delta x, \Delta y$ are the cell position and the grid size in x and y directions respectively. On the other domain, Δt^n is the time step calculated accordingly to the Courant-Friedrichs-Lewy stability condition as described in *Equation (2.12)* for each time level [Dazzi et al., 2018], where the Cr is the Courant number (≤ 1).

$$\Delta t_{i,j} = \frac{1}{2} Cr \min\left(\frac{\Delta x}{u_{i,j} + \sqrt{gh_{i,j}}}, \frac{\Delta y}{v_{i,j} + \sqrt{gh_{i,j}}}\right), \Delta t = \min(\Delta t_{i,j}) \quad (2.12)$$

The second order of accuracy in time is obtained by a second order Runge-Kutta method as exhibited in *Equation (2.13)*, where it is present the operator $\mathbf{D}_i(\mathbf{U}_{i,j})$ that is defined according to *Equation (2.14)*, while $\mathbf{U}^{n+1/2}$ can be obtained from *Equation (2.15)*.

$$U_{i,j}^{n+1} = U_{i,j}^n + 0.5\Delta t^n (D_i(U_{i,j}^n) + D_i(U_{i,j}^{n+1/2})) \quad (2.13)$$

$$D_i(U_{i,j}) = -\frac{F'_{i+\frac{1}{2},j} - F'_{i-\frac{1}{2},j}}{\Delta x} - \frac{G'_{i,j+\frac{1}{2}} - G'_{i,j-\frac{1}{2}}}{\Delta y} + S_0 + S_f \quad (2.14)$$

$$U_{i,j}^{n+1/2} = U_{i,j}^n + \Delta t^n D_i(U_{i,j}^n) \quad (2.15)$$

To avoid the arising of high velocities and instabilities, if the water depth $h_{i,j}$ is lower than a small threshold h_ε the cell is dried ($h = 0$). The PARFLOOD code has been used in several cases of study testing its capacities in different scenarios such as in Vacondio et al. [2016], Dazzi et al. [2018] and Dazzi et al. [2019].

2.2.1 Internal Boundary Condition

Internal Boundary Conditions (IBC) are needed to solve the structures along the reach. In the present section, the algorithm adopted to introduce the internal boundary conditions in the

PARFLOOD solver are described briefly. As explained by Dazzi et al. [2020] the planimetric position of a hydraulic structure is identified by means of a line or polyline, which is discretized through a number of cell edges at the pre-processing stage (*Figure 2.1*). Cells facing at least one of these internal edges are then identified and marked as “upstream” or “downstream” IBC cells. The input data must include the bridge geometry (*Figure 2.2*), in particular the low chord elevations: a “ceiling” elevation for pressurization is assigned to each IBC cell, so that complex geometries like single or multiple arched bridges can be described adequately. An overtopping elevation is also provided. Abutments and piers can be either handled as holes in the mesh or included in the bridge geometry as *Figure 2.1*: sketch of IBC elements for a bridge (orthoimage in background). In the same picture, the bridge is identified by the dashed blue line, which the model discretizes as IBC cell edges (red). Upstream and downstream IBC cells are colored in yellow and cyan, respectively. The “zero opening” cells (piers and abutments) are marked with a cross (see for example the ones circled in green).

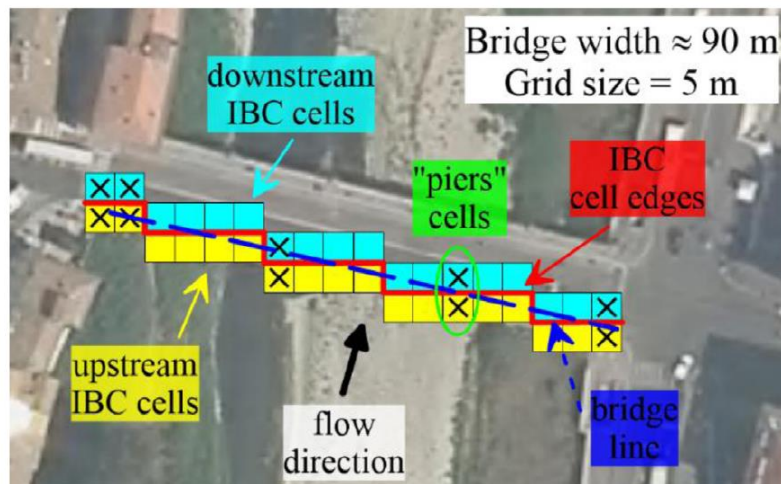


Figure 2.1: Example of Bridge scheme

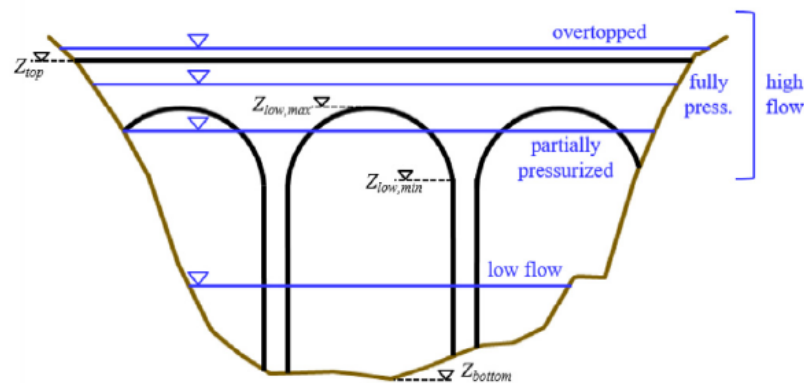


Figure 2.2: Example of Bridge geometry and different flow conditions

The basic idea is to compute the average water level upstream and downstream the bridge/structure, and to compare it with the minimum and maximum ceiling elevations, to distinguish different flow conditions: low flow, partially pressurized, fully pressurized, overtopped (*Figure 2.2*). These values are then used for estimating the flow rate through the bridge by adopting a discharge formula. The involved parameters are: $Z_{low,min}$ and $Z_{low,max}$, respectively the minimum and maximum elevations of the bridge low chord; Z_{top} , the elevation of the top chord; Z_{bottom} , the minimum bottom elevation along the bridge section; the mean levels upstream (η_U) and downstream (η_D) of the bridge and total heads (H_U and H_D). So, according to the flow condition the discharge will be differently evaluated:

1. For low flow conditions (no interaction with the deck), IBCs are not activated, and all cells behave as ordinary inner cells.
2. For a partially pressurized only a subset of IBC cells interacts with the bridge deck. This partial obstruction is considered by reducing the normal specific discharge q_{\perp} in the upstream cells whose water surface elevation exceeds the local ceiling as follows:

$$\overline{(q_{\perp})_k} = (q_{\perp})_k \frac{Z_{low,k} - z_k}{\eta_k - z_k} \text{ if } \eta_k > Z_{low,k} \quad (2.16)$$

here q_{\perp} coincides with uh or vh depending on the IBC edge inclination (both components are modified if the cell shares two IBC edges). Then, the same specific discharge (overlined) is assigned to the corresponding downstream IBC cell. Note that the specific discharge in all IBC cells with $\eta < Z_{low}$ remains unchanged, while the specific discharge in “zero opening” cells (e.g. with $Z_{low,k} \leq z_k$) is zeroed.

3. If the bridge is fully pressurized, two possible flow conditions, namely free-flow and submerged flow, can occur. In the former case, the discharge Q passing through the bridge is evaluated as follows:

$$Q = C_d A \sqrt{2g(H_u - 0.5(Z_{low,max} - Z_{bottom}))} \quad (2.17)$$

For submerged flow, on the other hand, the pressure flow equation is used:

$$Q = C_d A \sqrt{2g(H_u - \eta_D)} \quad (2.18)$$

In Eqs. (2.17) and (2.18), A represents the total area of the bridge opening, while C_d and C_Q are discharge coefficients for the two flow conditions. Typical values used in the practice are 0.5 and 0.8 [Bradley, 1978].

4. If the bridge is overtopped, compared to the previous case, the discharge is increased according to the weir equation:

$$Q = C_w L \sqrt{2g} (H_u - Z_{top})^{3/2} \quad (2.19)$$

where L is the bridge length normal to flow, and C_w is a weir coefficient.

Conversely, for high flow conditions the (specific) discharge is imposed in upstream IBC cells. It is worth pointing out that the water level is not modified in any cell, so that mass is neither added nor subtracted to the domain. The same specific discharge assigned to each upstream IBC cell is replicated in its companion downstream IBC cell. The model assumes that the flow is normal to the IBC edge, hence the specific discharge in the tangential direction is set equal to zero. This hypothesis may induce directionality to flow, which can be particularly noticeable in the case of skewed bridges, but in the meantime, it guarantees that mass is conserved through the IBC edge. Moreover, this effect is expected to affect the flow field only locally, while the overall prediction of flood propagation and backwater should not be much influenced.

2.3 Flood modelling in urban context

In an urban context, one of the key points for representative modelling is the choice of how to fit the buildings into the model. It is well known that the highly urbanized fabric has a significant influence on the flood water flow. Depending on the scale of the modelled reach, the available information and the modelling purpose, the buildings can be considered with 4 different methods.

The first method consists in a local friction-based representation of buildings in a 2D approach, in which the space containing the urban fabric is considered as area with increased friction coefficient, to capture the energy losses due to the impact against buildings (*Figure 2.3*). This method can be implemented when the scale of the case study is large enough that local effects

and a detailed local description of the physical effect of buildings could be neglected. Local friction is treated as another field variable, thus one of the difficulties of this method is the determination of the correct roughness coefficient to be assigned. Several tables provide Manning's values according to different land uses but every case must be treated singularly because friction coefficients may depend on building density, scale of the flooded area and ratio of flow depth to buildings height.



Figure 2.3: Representation of the Manning's roughness embedded in a larger computational domain

Another method consists in excluding buildings from the computational space by creating voids (*Figure 2.4*). This choice is the most accurate for describing an urban fabric but is

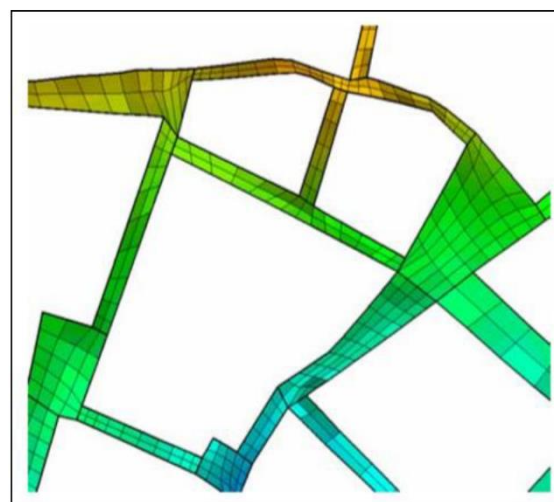


Figure 2.4: Example of void method [Alcrudo, 2004]

recommended if the scale of the case study is not very large, unless a complete dataset of all buildings represented by polygons is already available in GIS environment.

A similar concept for building representation is to use the bottom elevation technique, increasing the elevation of grid points that fall within the footprint area of a building. The main problem of this method is the representation of the slope between the higher point and the ground point, which can be of order 1 if the discretization is coarse (mesh size similar to building elevation) or reach several orders of magnitude if the discretization is fine (mesh size much smaller than building elevation). This fact violates the mild slope assumption of the SWE. However, the model does not fail because buildings act as internal boundaries causing water stagnation and water around buildings is still considered shallow. As in the previous case this method is most used in small to medium-scale models.

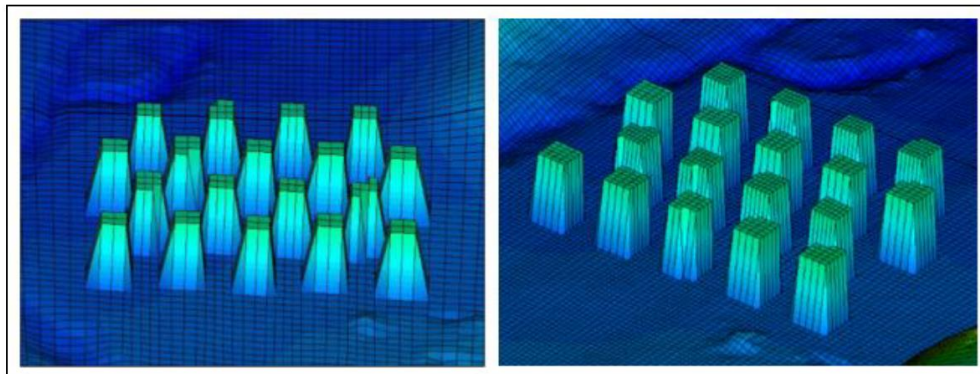


Figure 2.5: Examples of bottom elevation techniques on a coarse mesh (on the left) and on a finer mesh (on the right) [Alcrudo, 2004]

Lastly, an additional method for representing buildings in two-dimensional models could consist in assigning a “porosity” to the urban fabric. This method is used to take into account the volume of water that can be stored in the buildings and that, therefore, no longer participates in the surface flood.

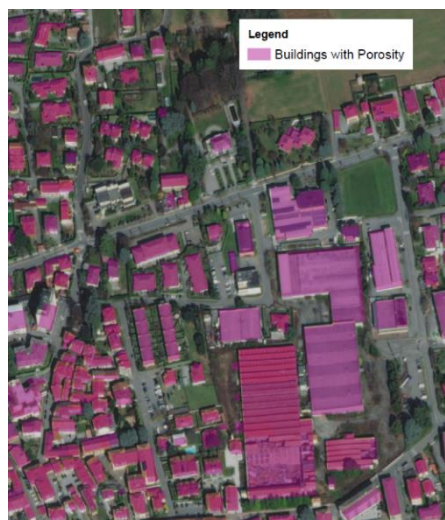


Figure 2.6: Examples of Porosity method

3. Method for hydraulic simulations using available data

Quantitative flood hazard assessment is a challenging task given the complexity of the natural and territorial systems at stake. During the modelling process, assumptions and simplifications are unavoidable. In this chapter, a description of the methodology defined and followed during the thesis work is presented. The devised modelling procedure combines and exploits the data that were available in terms of river geometry (river cross sections, floodplain elevations from digital terrain models), flow rates (peak values and design hydrographs), soil cover. First, the procedure to create the input files for the PARFLOOD code is illustrated, regarding both the digital terrain model and the roughness modelling. Then, a need to divide a river model into a number of reach models is stated, in relation with the availability and structure of input data for flow rate distribution. Furthermore, the approach to define the required downstream boundary conditions is described. Finally, an overview of the steps followed to assess the quality and the physical consistency of the results is presented.

3.1 Terrain geometry representation

To perform a 2D flood simulation a Digital Terrain Model (DTM) is necessary as input. In the case of the present work, different DTMs have been combined to obtain a river and floodplain geometry as a suitable input for the modelling. In particular, the 3 following datasets were necessary to have the final, complete and corrected terrain model:

1. “DTM 5x5 - Modello digitale del terreno (ed. 2015)”: free dataset from *Geoportale della Lombardia*, which covers the area of the whole Lombardia with a resolution of 5 meters;
2. DTM 1x1 from “MATTM, Ministero dell'ambiente e della tutela del territorio e del mare (ed. 2008)”: it has a resolution of 1 m and covers the area of the APSFR (determined in the previous studies for the highest return period) plus a 100-m buffer.
3. Cross sections of the rivers and interfering structures as surveyed for the “Studio di fattibilità della sistemazione idraulica” (2003), characterized by an average spacing of around 400 m between each other along the direction of the watercourses.

The cross sections of the river are enough for a one-dimensional modelling but are evidently not enough to create a 2D bathymetry of the main channel. Therefore, the cross sections are converted into a raster of the riverbed limited to the main channel. A DTM 1x1 is obtained

through a MATLAB code, developed ad hoc for the present work. The code takes as input the point cloud with the coordinates of the surveyed cross sections and returns the bed bathymetry in the form of a third raster (after the Regione Lombardia and MATTM ones). Further details about the code and the procedure for the creation of the excavated DTM for the riverbed are available in *Appendix B*. For convenience, in the following, the three raster datasets will be referred to as *number 1*, *number 2* and *number 3*, respectively.

The main reasons why a combination of those three DTMs is necessary are:

- The fact that the original datasets, *number 1* and *number 2*, contain the information about the highest elevation value in correspondence of that cell: this implies that, first, the value of the raster along the river is referred to water surface elevation and not to the dry riverbed, second, that in the case of intersection between the watercourse and a raised structure (e.g. bridges), the elevation of the DTM is referred to the latter, thus the stream results interrupted as a wall is present inside the riverbed.
- The need of increasing the resolution in correspondence of the riverbed and the immediate vicinity; indeed, raster *number 1* covers the entire area interested by the model, but the resolution of 5 meters is not representative of the dimension of the rivers under analyses, which width ranges from approximately 3 to 10 meters. Thus, the DTM 1x1 which covers a stripe of terrain around the waterway has been superposed to the former to increase the level of detail in the riverbed.

In the next page an illustrative example is reported to clarify the concept:

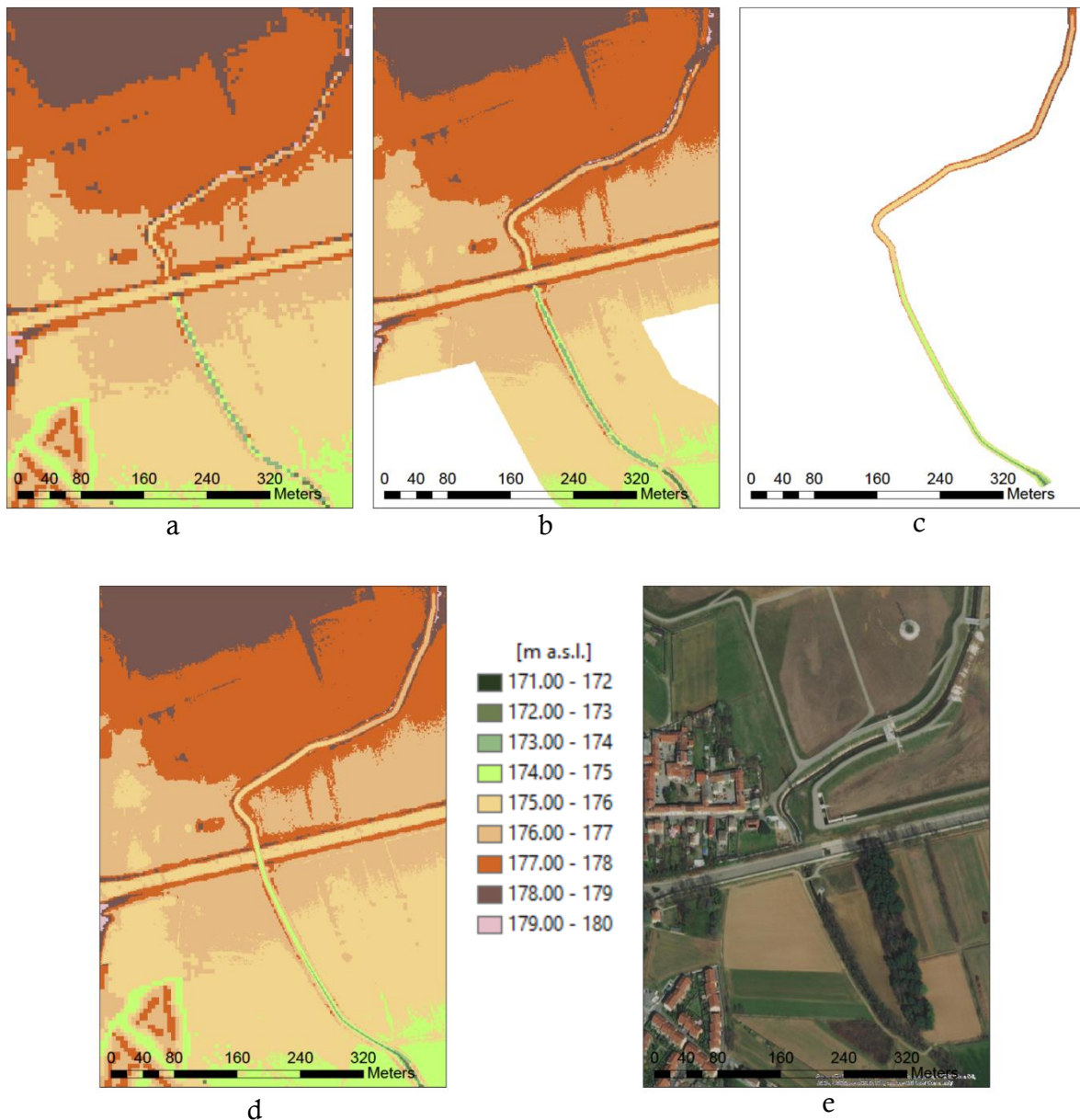


Figure 3.1: DTM correction procedure

In *Figure 3.1 a-c* the three raster datasets are displayed in the same area at the intersection between the river Bozzente (North-South) and an artificial channel (East-West). The elevation of the latter is above that of the river. The DTMs *number 1* (*Figure 3.1.a*) and *number 2* (*Figure 3.1.b*) describe this fact in agreement with the satellite imagery (*Figure 3.1.e*). This creates a step in elevation, thus a fictitious obstacle in the water course. To correct this inconsistency, the “DTM 1x1 for the riverbed” (*Figure 3.1.c*) has been superposed to recreate the actual geometry of the bed.

The final DTM representing the input for the model is shown in *Figure 3.1.d*: it has been obtained superposing the three raster datasets in order from 1 to 3, with raster number 3 on top.

It is worth noticing that not only in correspondence of the riverbed it has been necessary to correct the DTM and to restore the actual terrain elevation; indeed, in the case of the Seveso in the Municipality of Barlassina, the absence of the underpass in the original DTM, obstructed by the elevation of the above roads, heavily influences the actual physical behaviour of the water in the surrounding floodplains. From *Figure 3.2* it is possible to understand that here the effect of the road (East-West axis) is macroscopic.

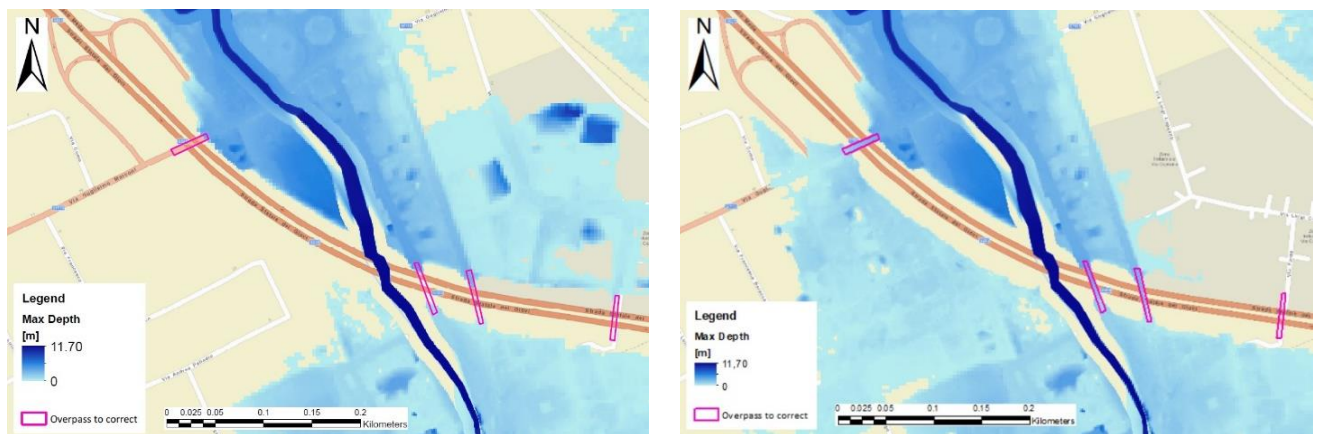


Figure 3.2: Flood extension in correspondence of the underpass in Barlassina, before (left) and after (right) the correction of the DTM

Such operations have not been performed for minor cases, where the effect of those interfering structures could be considered negligible with respect to the flooding phenomenon development.

3.2 Roughness modelling

In the case of the present study, two datasets have been compared in order to choose the one which better represents the urbanized areas and, so, it could be suitable to define the roughness distribution:

- the open dataset *Usa e copertura del suolo 2018 (DUSAF 6.0)*, that is provided by Lombardia Region and it can be free downloaded from *Geoportale della Lombardia*. It

contains information about land use and cover with a resolution of 20 m, integrated with hedges and rows with a minimum length of 40 m at the ground level. Each polygon of the dataset represents a specific area on the ground surface and its identity is expressed through a code and a brief description in terms of use and land cover.

- The open-source Open Street Map (OSM): it provides free data that can be downloaded through a query in order to select the specific subset the user needs (here buildings footprint).

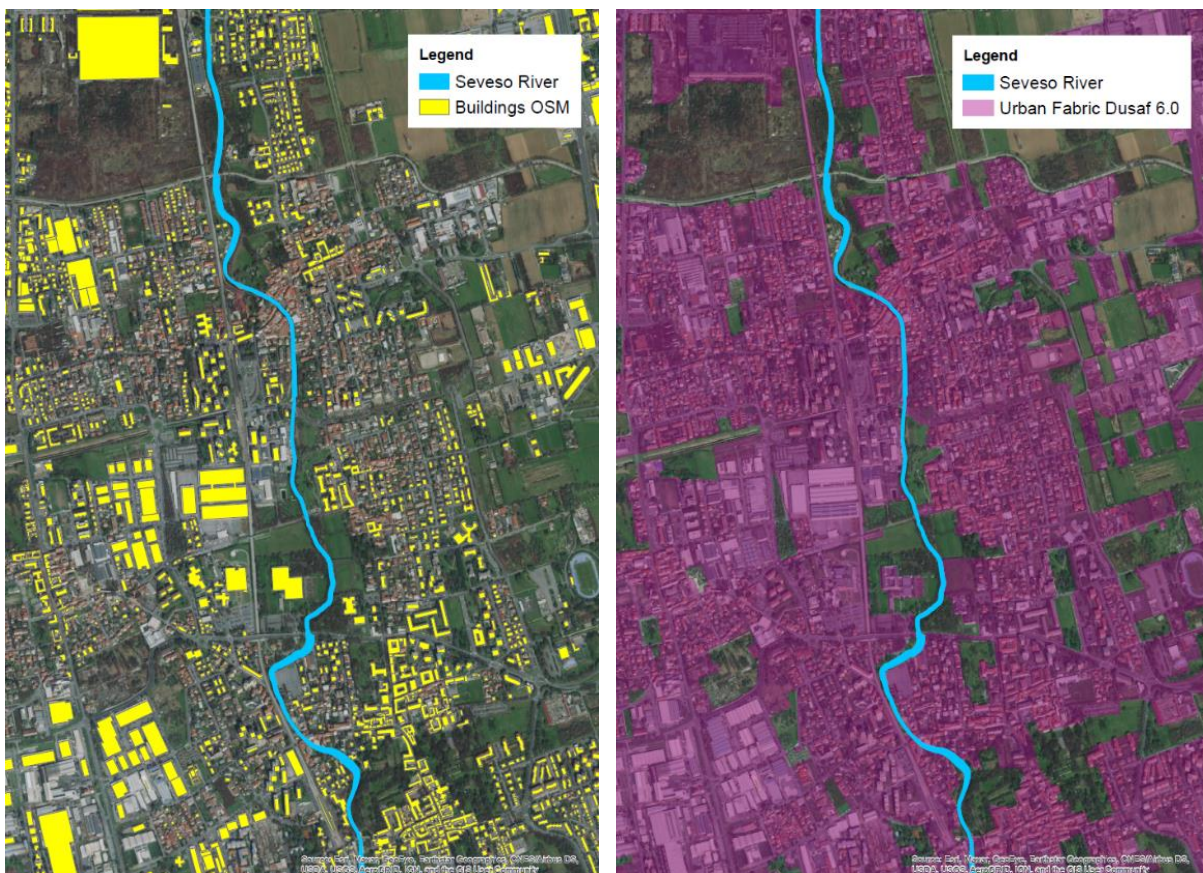


Figure 3.3: Urbanized area representation from OSM (left) and Dusaf 6.0 (right)

For the aim of this work the Dusaf 6.0 has been chosen because it provides a complete and extensive data coverage, so it results suitable for the aim of mapping a vast area such as the APFSR is. Indeed, as one can see from *Figure 3.3*, where the Seveso in the municipality of Paderno Dugnano is represented, the footprint, at a scale of the single building, from OSM database is not available for all the buildings in the interested area.

Moreover, the values of the roughness, expressed in terms of Manning value n , have been set to:

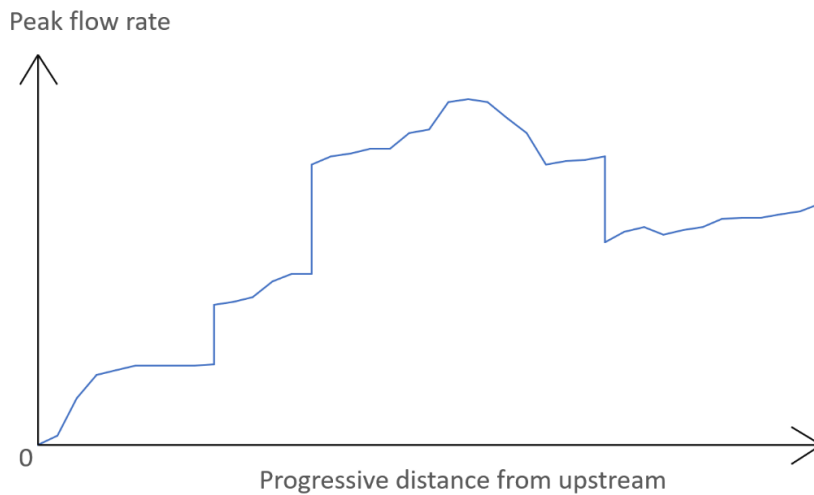
- $n = 0.035$ for the riverbed,
- $n = 0.4$ for the urbanized areas,
- $n = 0.08$ for the remaining areas.

To define the regions to be considered as urbanized, the dataset Dusaf 6.0 has been filtered out according to the ID code related to each item of the collection. In particular, in *Table 3.1* the areas considered as belonging to the “urbanized” class with $n=0.4$ are reported.

ID code	Description
1111	Dense residential area
1112	Discontinuous residential area
1121	Continuous and averagely dense residential area
1122	Sparse residential area
1123	Scattered residential buildings
11231	Farmsteads
12111	Commercial, artisanal, industrial settlements
12112	Agricultural productive settlements
12121	Hospitals
12122	Private and public services plants
12123	Technological plants
12125	Military areas
12124	Graveyards

Table 3.1: ID codes of the areas classified as urbanized

The application of this classification can be seen in *Figure 3.4*, in which the river reach polygon of the Bozzente is highlighted with respect to the urbanized area and the background, in order to assign the aforementioned values of n accordingly.



⏪ ⏩ ✎ *Figure 3.5: Longitudinal distribution of the peak flow rate along the river*

Figure 3.6 describes the division procedure with reference to ideal discharge data in terms of a continuous variability of the flow rate and of local values as those one can find in a table of any hydraulic study (Cfr. Sections 4.1.1 and 4.2.1). These data can be taken as a reference to move from a continuous distribution to a finite set of values of flow rate. To “build” the upstream BC of the river sub-sections, the distribution of Q can be discretized as shown. In other words, one considers that, in each sub-section of the stream, the actual distribution of the discharge (Figure 3.5) is quite uniform and, as a consequence, it can be represented by a constant value of the peak flow rate.

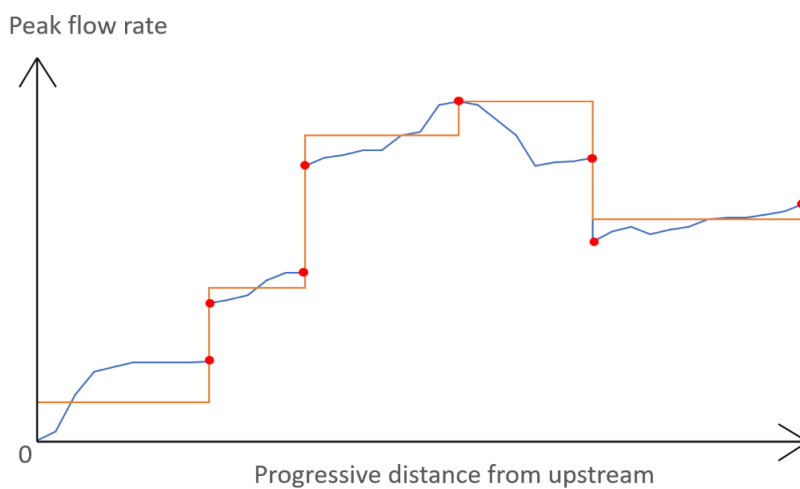


Figure 3.6: Discretization of the distribution

The presence of physical discontinuities (e.g. tributaries, water intake works) represents hydraulic disconnections, in the sense that they require a change in BC to follow the behaviour of the flow rate distribution. Such a discretization obviously discards progressive variabilities but it has been considered suitable for the modelling purposes of the present thesis.

It is important to point out that a hydrograph to be considered as upstream BC for the defined sub-reaches is not available for all of them (the discharge data used in this thesis come from the “Studio di fattibilità della sistemazione idraulica” that provides peak flow rates and associated hydrographs at some cross sections, from the PGRA that provides peak values of the discharge at some sections, generally in agreement with the “Studio di fattibilità” and from any other hydrological/hydraulic report available). Therefore, at the entry section of the modelled subdivisions, the actual reference hydrograph coming from previous hydrological studies can be applied where available. For the remaining sections, the hydrograph corresponding to the immediately upstream sub-reach should be adapted by scaling the values with respect to the reference peak discharge corresponding to the steps already shown in *Figure 3.6*.

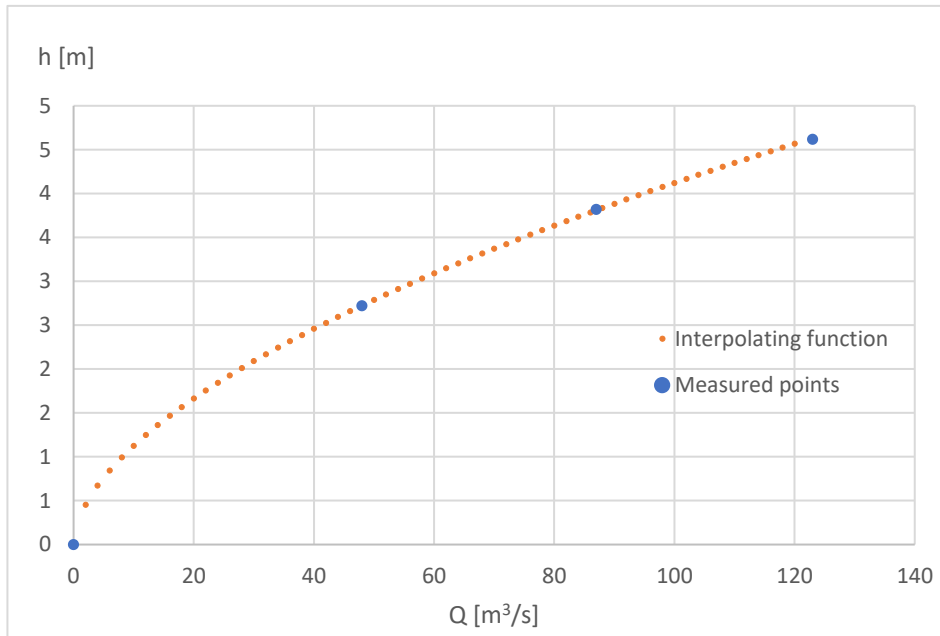
A final remark is needed about the fact that, all the process above described, has to be repeated for each discharge distribution corresponding to the three different return periods T , here considered, which are $T=10$ years (frequent events), $T=100$ years (events with intermediate frequency) and $T=500$ years (rare events).

3.4 Downstream boundary conditions

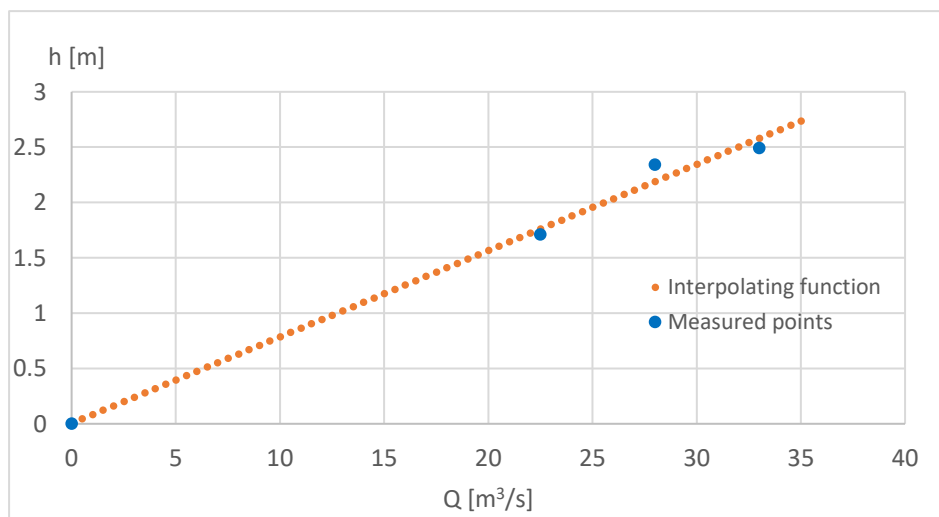
Downstream the previously described partitions of the main watercourse, a boundary condition (BC) is required as well. A situation analogous to that of the upstream BC occurs, in the sense that not for all the sub-reaches a specific dataset that describes the particular BC is available.

In the case of the present work, rating curves have been applied to the closure section of the aforementioned reaches, where the data was already available. In all the other cases, to describe the variation of water surface elevation as a function of the flow rate, a rating curve has been built, interpolating the known values coming from PGRA 2015. More specifically, the values of maximum water surface elevation have been combined with the peak flow rates for every return period T , through the interpolation function that best fits the data (and imposing a zero depth for zero flow rate). In the cases where the distribution of the three

measured points can be described by a power law, the results is analogous as the one displayed in *Figure 3.7.a*. In the other cases, a linear trend has been considered suitable to interpolate the data (*Figure 3.7.b*)



a



b

Figure 3.7.a and 3.7.b: Rating curves defined by potential and linear function respectively

3.5 Input files for PARFLOOD code

To solve the SWE, PARFLOOD requires the definition of the terrain model and the roughness of the modelled area, as well as initial and boundary conditions. So, to run a hydraulic simulation on this code, some ad hoc input files need to be prepared. Moreover, they should be named coherently with the name of the modelled reach, then specialized to their function by adding the following file extensions:

1. .BTM: GRID file describing the terrain model;
2. .MAN: GRID file describing the roughness of the terrain expressed through Manning coefficient;
3. .BLN: definition of the computational domain and related external boundary conditions;
4. .BCC: external boundary conditions (specialization of the file .BLN); in detail, the typology of BC, set for each segment of the polygon delimiting the computational domain, is indicated by means of a specific number:
 - 21 → hydrograph: for the upstream BC
 - 1 → wall: to indicate that the segment of the domain acts as a wall so it cannot be crossed by water
 - 4 → far field: the water can cross the segment as if there was a flat, indefinite and free of obstacles terrain
 - 3 → level: a specific value of water level is imposed along the segment
 - 5 → rating curve: for the downstream BC
5. .INH: GRID file defining the initial conditions, to ensure the presence of wetted cells at the inflow section of the computational domain;
6. .ILN: definition of the coordinates of the extremities of the internal boundary conditions;
7. .IBC: internal boundary conditions (specialization of the file .ILN);
8. .PTS: list of the points for the multi-resolution computational grid.

3.6 Output files from PARFLOOD code

Once the simulation has successfully completed the required modelling time, some operations of decoding of the results are necessary to obtain the files representing the output. In particular,

through a script specially-made for the solver running with PARFLOOD code, the so called “Decode Simulation”, it is possible to manually select the output files and physical quantities to extract from the solver itself. There are three basic types of data that can be obtained by decoding the output files:

1. Maps of physical quantities (water surface elevation, water depth, velocities, etc...) as distribution in a specific instant of the simulation or as maximum values;
2. Flow rate in correspondence of control sections;
3. Water depth in control points.

To visualize the results map, it has to be converted from binary to Surfer's .grd. The available output formats are Surfer 6 Text Grid and Surfer 6 Binary Grid. Moreover, the user can choose whether to extract the whole map containing outputs related to the entire duration of the flood event (i.e. the duration of the input hydrograph), or to select a specific range both in space and time.

To assess the quality and the physical coherence of the so obtained output, some checks are required, as explained in the following.

3.7 Result check and representation

To evaluate the success of the simulation and to have a quantitative description of the outputs, in support to understanding the results, the following operations are carried out:

1. Control section for the flow rate distribution
2. Cumulated frequency distribution of water depth and velocity
3. Comparison with/without bridges
4. Comparison with previous results (TIRANTI/RAPIDE)

It is important to point out that these operations are carried out with different perspectives, in the sense that they target specific aspects of the results evaluation. More specifically, points 1. and 2. refer to quality checks, in the sense that they provide a guide to point out possible anomalies which could be due to numerical issues, thus they are not in agreement with the physics of the phenomenon. Point 3. represents a procedure which aim is to give an idea about the influence, on the final map, of the presence of interfering structures along the reach. Finally, the comparison mentioned in point 4. is necessary to understand how far the updated maps are from the previous version from 2019.

3.7.1 Control sections for the flow rate distribution

The first verification to be performed is that the flow input is consistent with the upstream boundary condition defined in the .BCC and .BLN files. To do this, a control section is inserted nearby the upstream segment of the computational domain, as shown in *Figure 3.8* with “control section 1”. To verify the consistency of the simulation, additional control sections can be inserted along the modelled reach, as shown in the figure below, where a reach from the Seveso is taken as example.

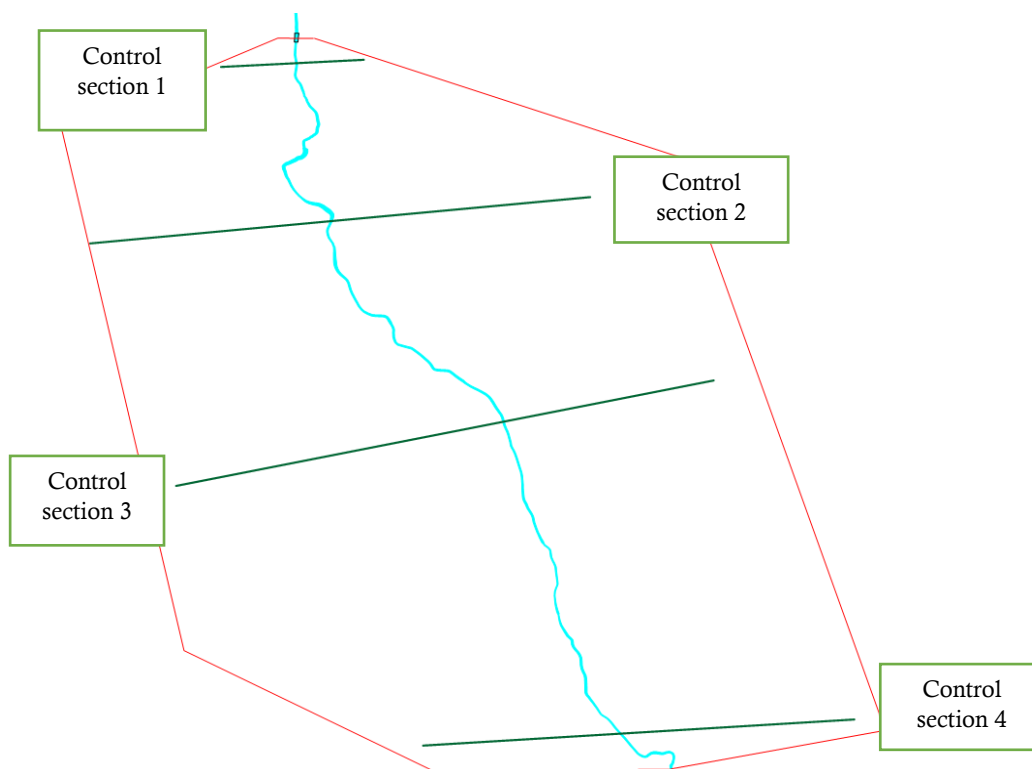


Figure 3.8: Control sections distribution

Thanks to the control sections it is possible to record the trend of the related flow rate, passing through them over time, as shown in *Figure 3.9*. In fact, comparing the hydrographs extrapolated from these sections, one of the phenomena that can be observed is a delay of the wave, expected to occur in the downstream ones. The control sections inserted to check the flood wave propagation must be crossed not only by the water present in the riverbed but also by the overflowed water, for this reason they have to be sufficiently wide.

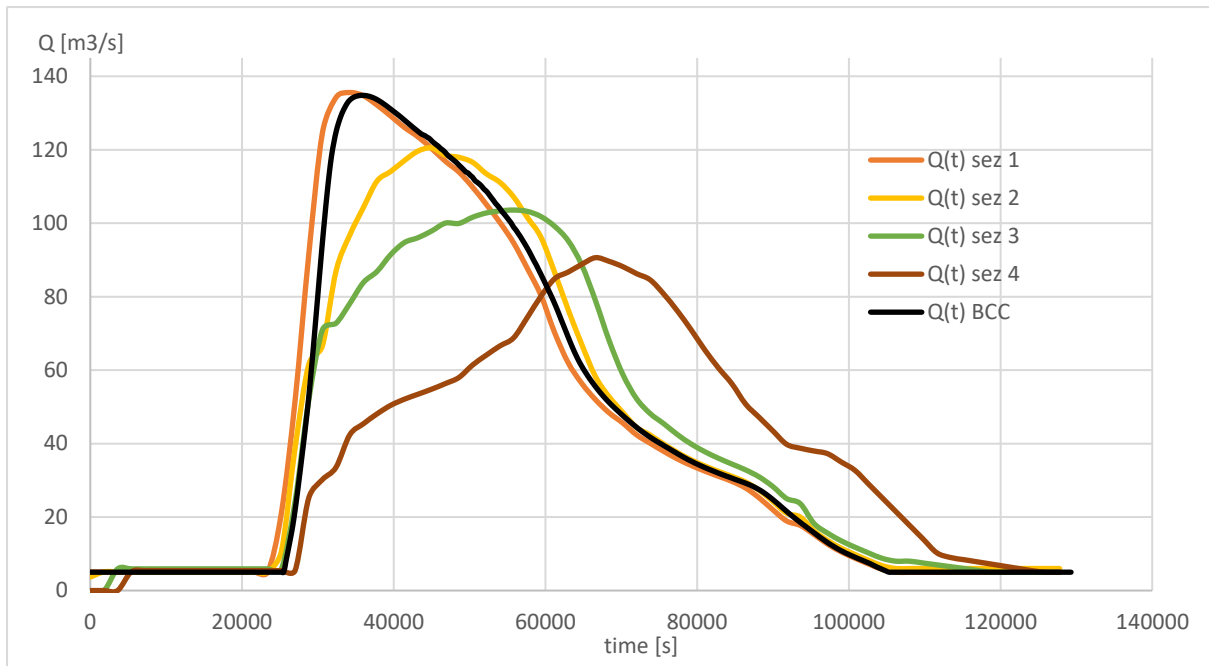


Figure 3.9: Input Hydrograph and Hydrographs at different control sections

3.7.2 Cumulated Frequency Distribution (CFD) of water depth and velocity

The second check is useful for verifying the distribution of results in terms of both water and velocity. Indeed, due to numerical instability, it can happen that abnormal results arise in correspondence of the boundary conditions, so that the simulation could stop running before completing the required time. In case the simulation completes the set duration of the event, still it is likely that numerical instabilities have led to anomalous values of water depth or velocity. The cumulative frequency distribution makes it possible to understand how much weight the different values have in the distribution. An example is shown in *Figure 3.10* where it is possible to observe that the maximum value of water depth is greater than 14 metres, but from the cumulative distributed frequencies (*Figure 3.11*) values greater than 3 metres do not affect the realism of the model given the very low frequency of high values.

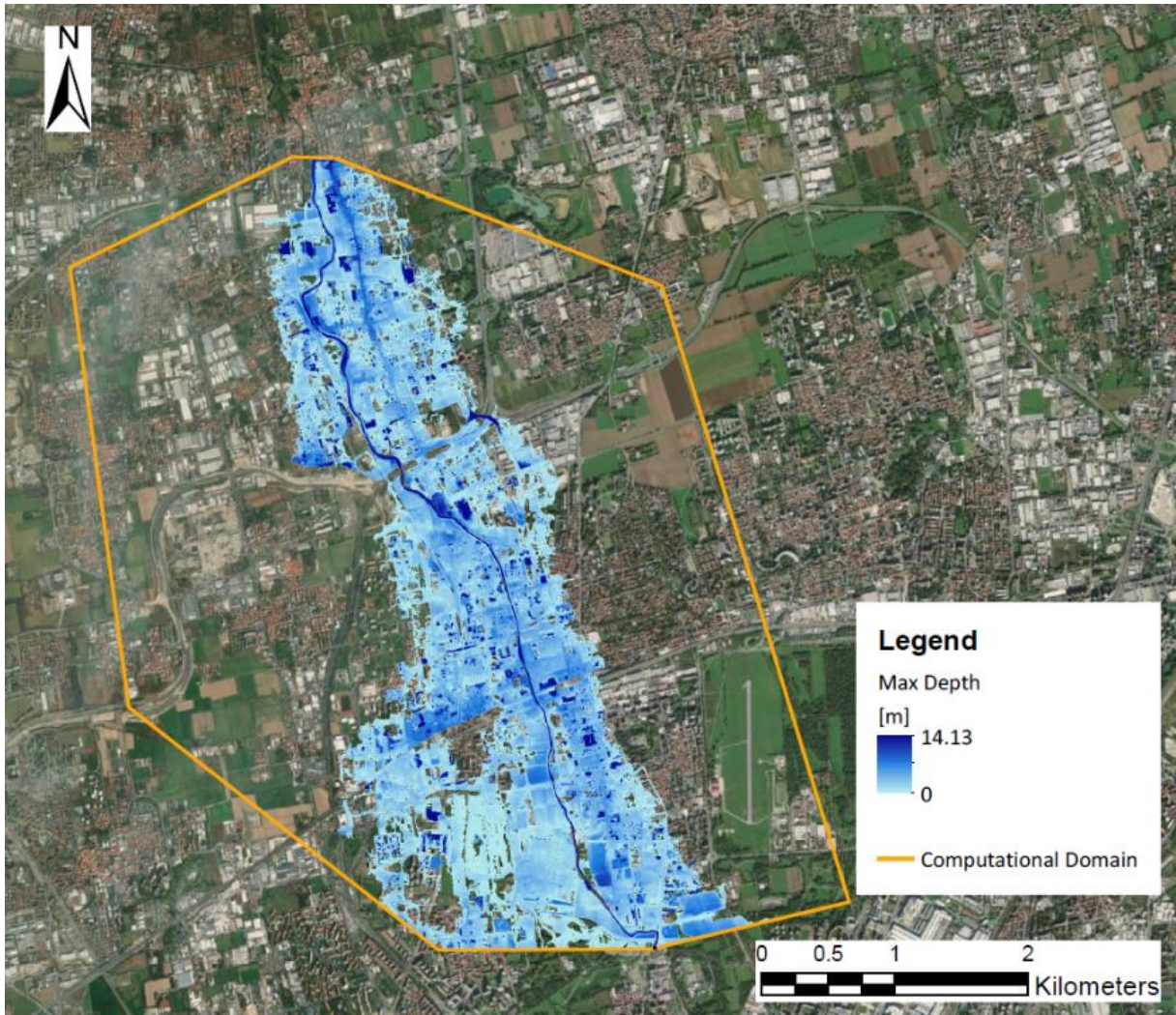


Figure 3.10: Water depth map with few anomalous values

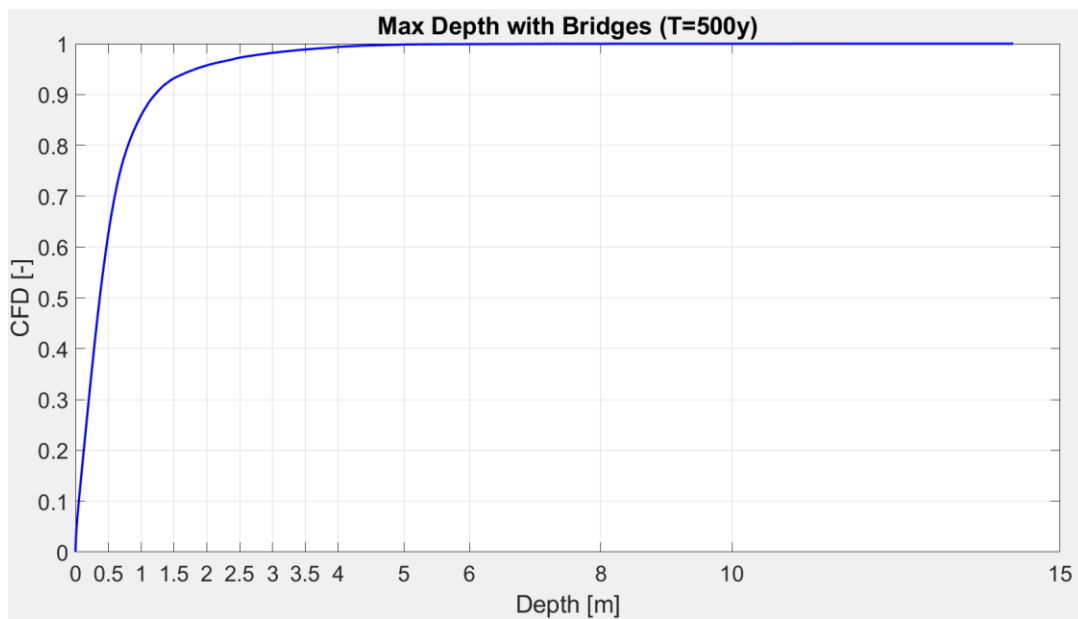


Figure 3.11: CFD of Water Depth

3.7.3 Comparison with Vs without bridges

To observe the influence of the bridges in the modelled stretches, it is useful to compare:

- Water depth and velocity distribution
- Extension of the flooded area

Water depth and velocity distribution

To obtain results from a flood modelling which does not take into account the presence of bridges, it is enough to run the simulation without the input files which are strictly related to internal boundary conditions (i.e.. INL and .IBC). Once the maps of the differences (*Figure 3.12* and *3.13*) have been produced, it is useful to evaluate the cumulative frequency distribution (*Figure 3.14* and *3.15*) to assess the weight of the peak values in the range of data.

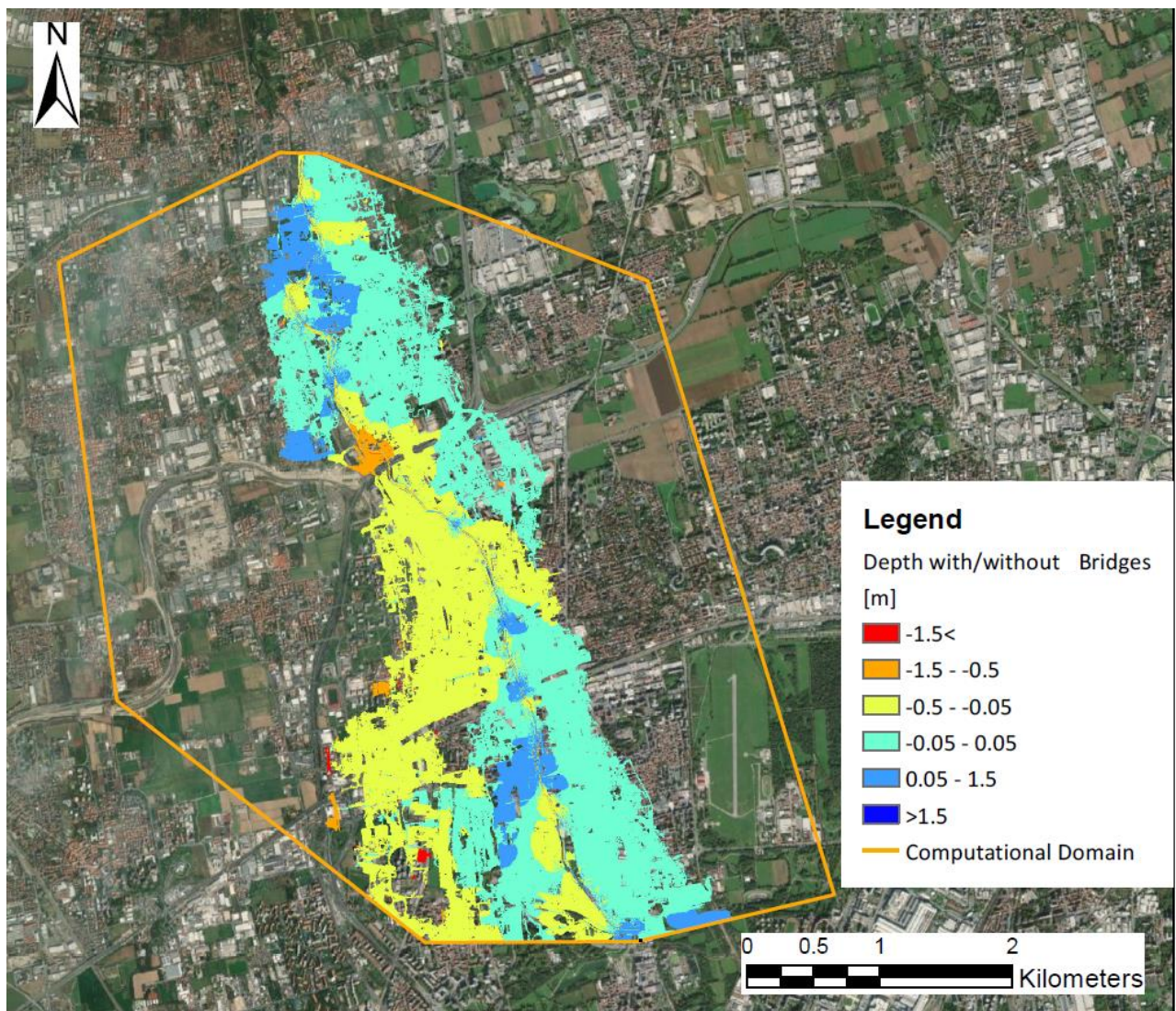


Figure 3.12: Difference between depth Bridges-No Bridges

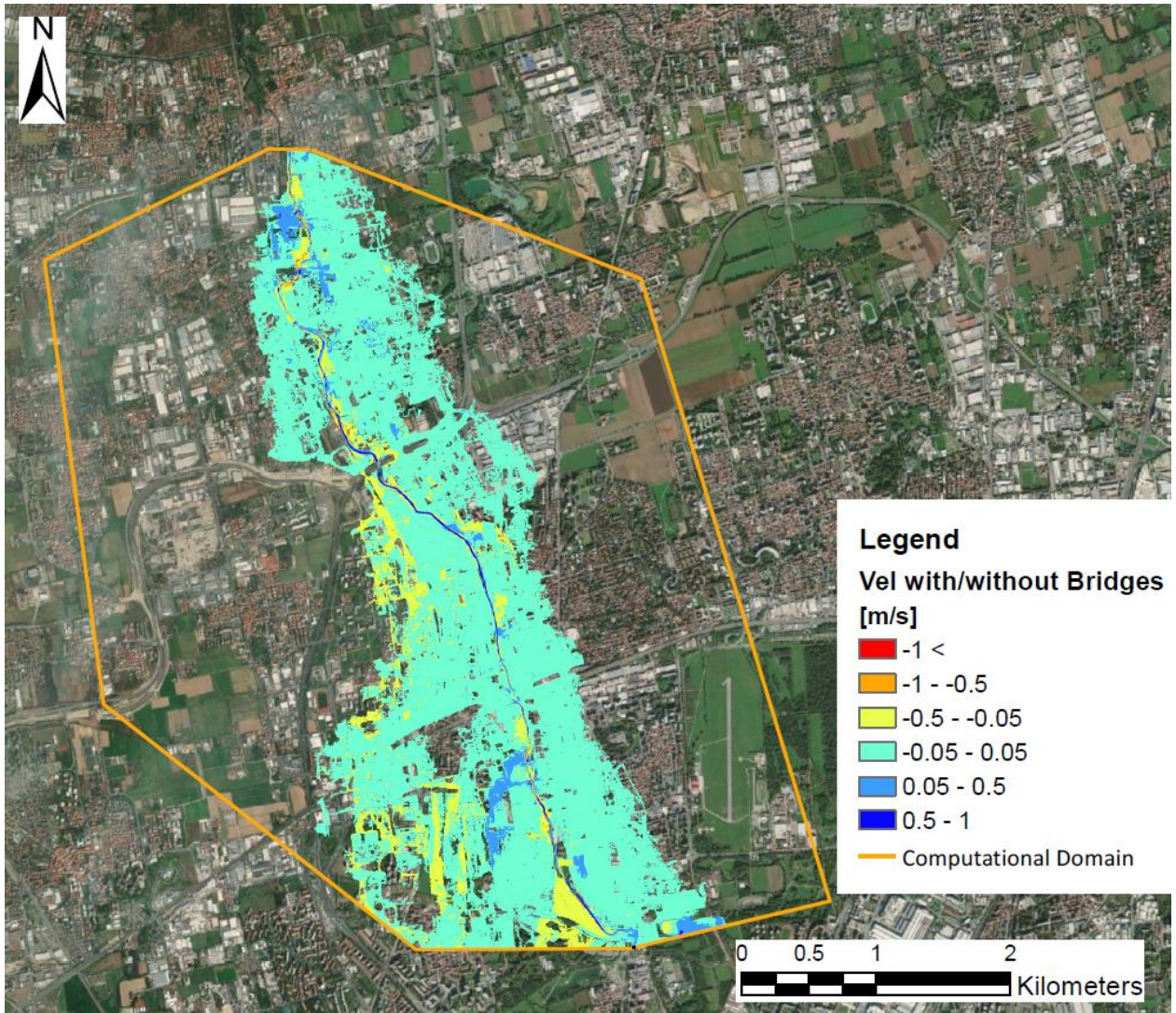


Figure 3.13: Difference between velocity Bridges-No Bridges

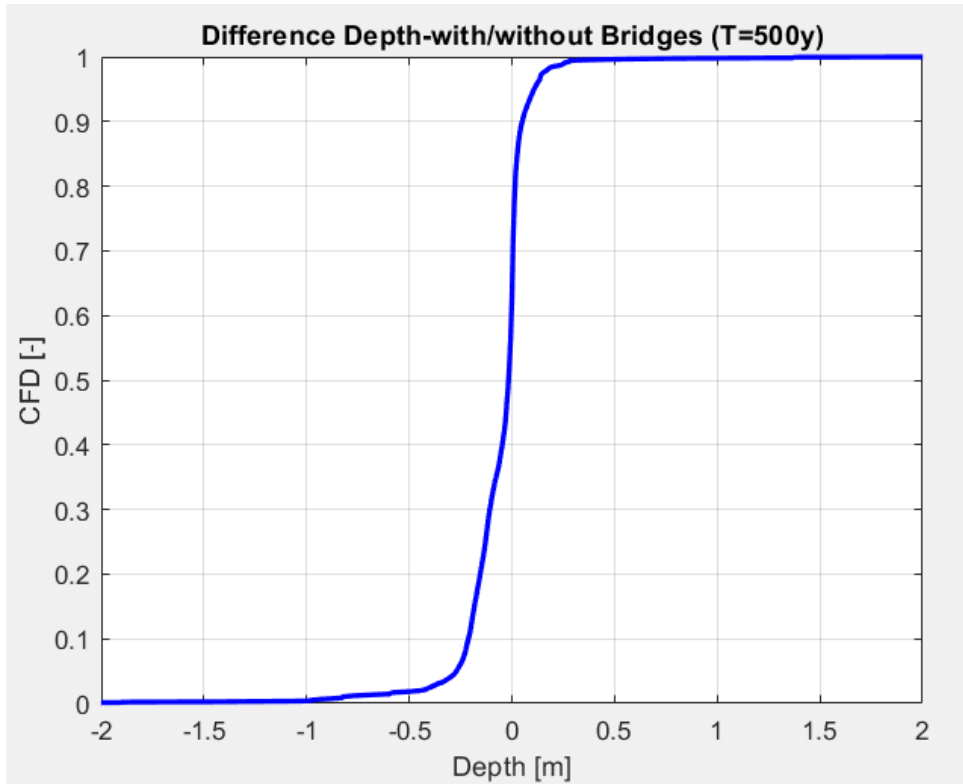


Figure 3.14: CFD Depth Bridges-No Bridges

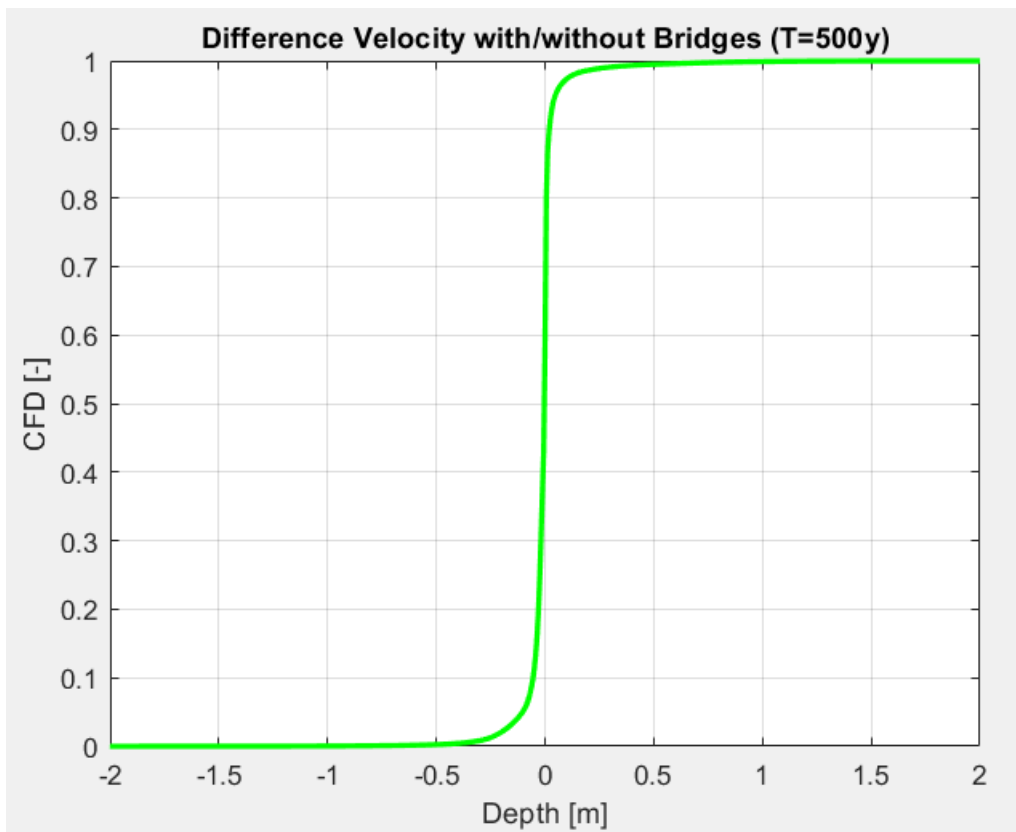


Figure 3.15: CFD Velocity Bridges-No Bridges

CFD helps to interpret to which extent the bridges affect the results, in the sense that, the distributions which move away the most from the verticality of the curve in correspondence of the y-axis, are characterized by a more evident influence of the bridges on the final flood map.

Extension of the flooded area

After the calculation of the flooded area for both simulations, it is convenient to compare them to understand if a series of bridges affects the result or not in terms of extension of interested area. It is useful to observe the overlap of the layers as shown in *Figure 3.16*.

In this case, for example, it is possible to observe an increment of the flooded area due to the presence of bridges, hence bridges interacting with the flow in the riverbed generate the backwater phenomenon (*Figure 3.17*) that causes the water level to rise and thus the flooded area to increase.

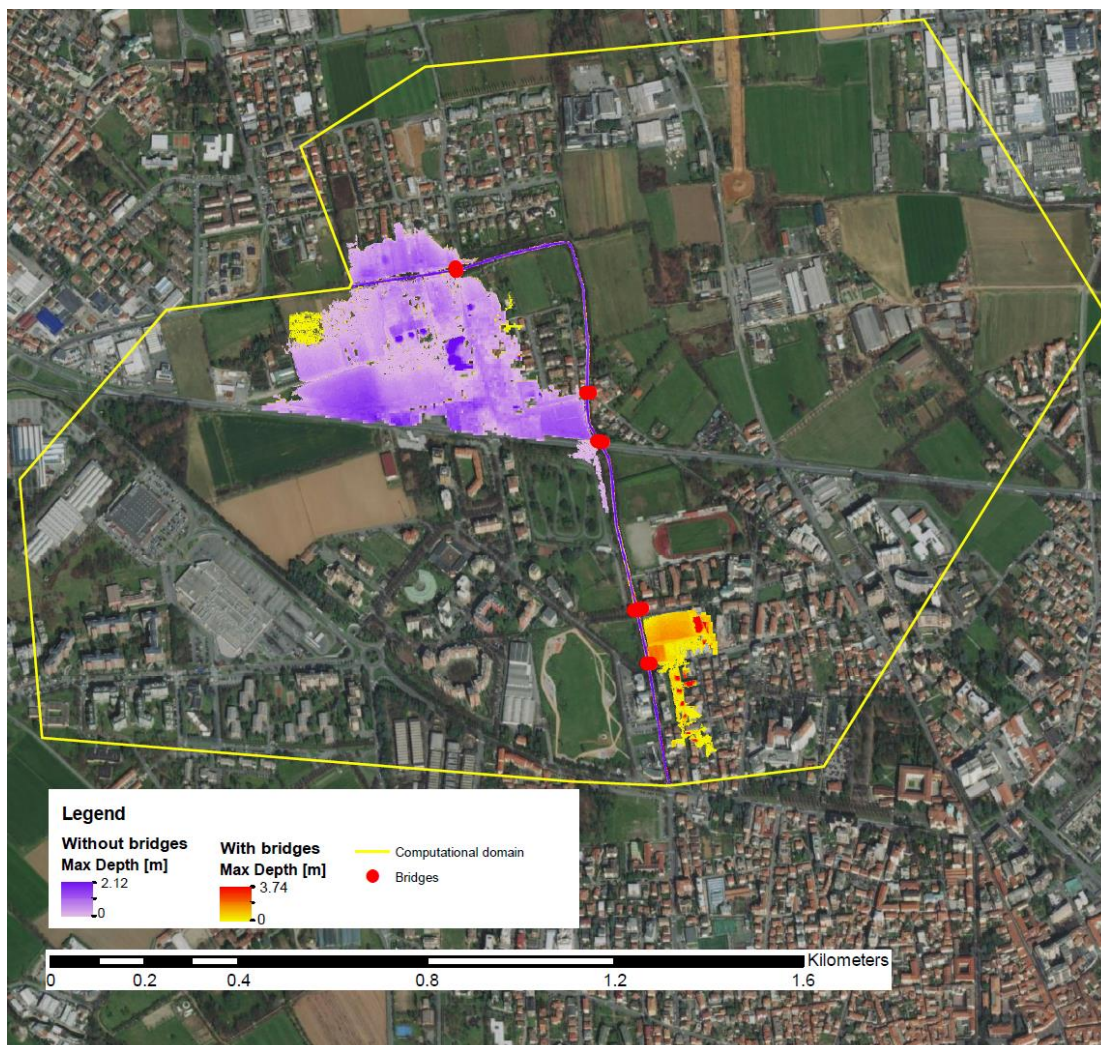


Figure 3.16: Overlap of the flooded areas

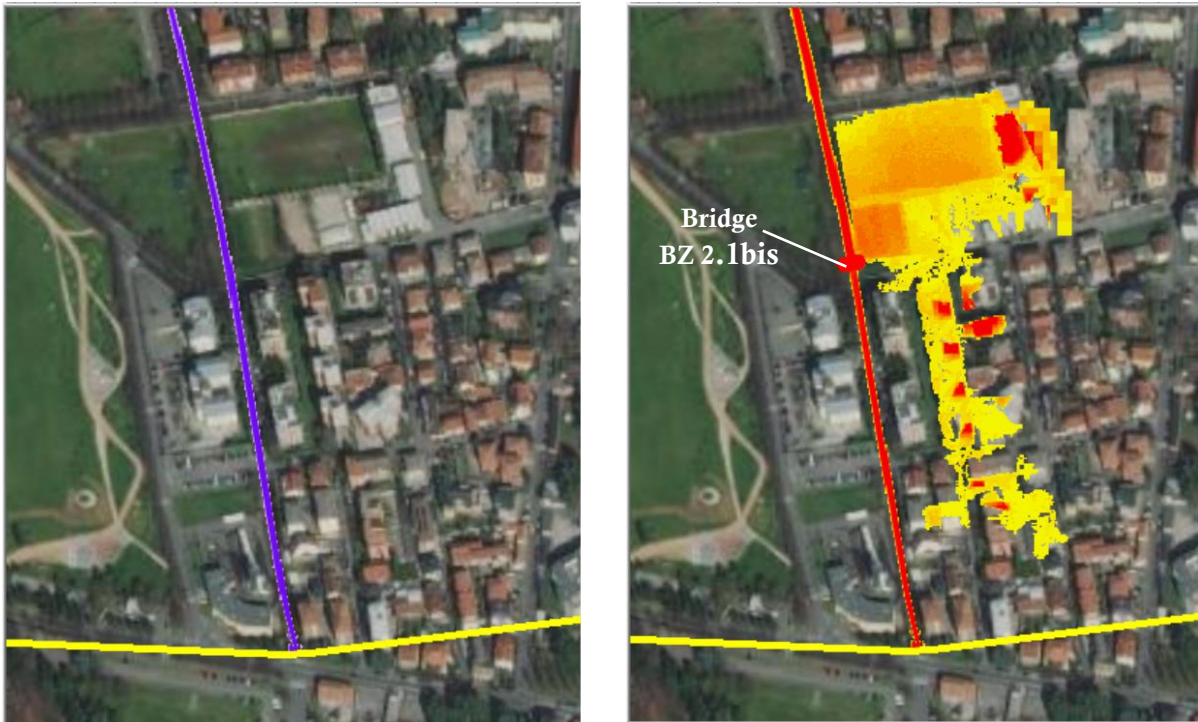


Figure 3.17: Detail of the flooded area without (left) and with (right) the presence of the bridge (in red)

3.7.4 Comparison with previous results (2019 perimeter)

A comparison in terms of flooding areas has been carried out, between the perimeters defined by the previous PGRA and those of the updated modelling illustrated in the present work. It is useful to highlight those areas where the differences are more pronounced and therefore where more intensive updating may be required. In *Figure 3.18* there is an example.

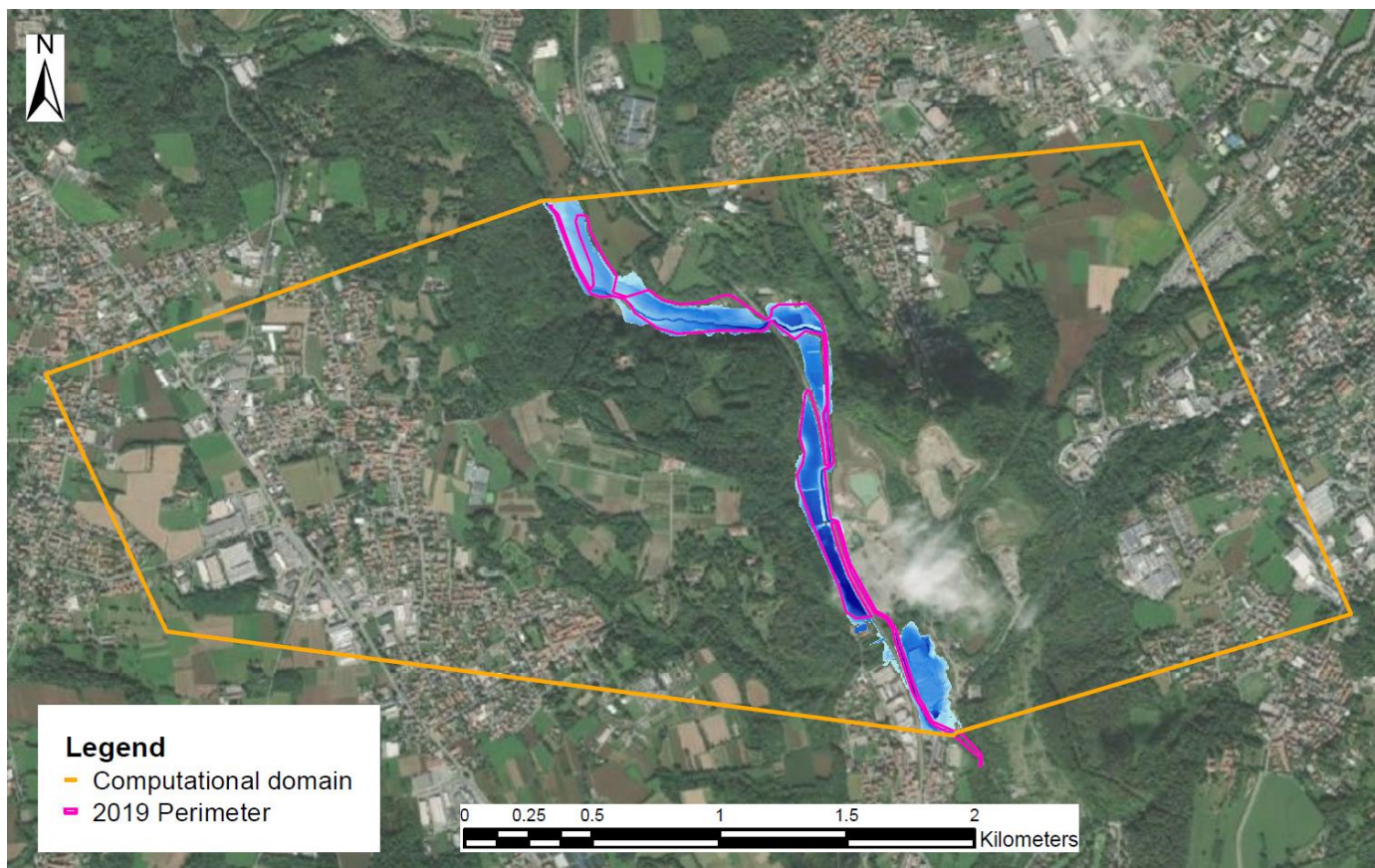


Figure 3.18: Comparison between PARFLOOD results and 2019 perimeter in one of the reaches of the Seveso

One can observe that, in some areas, the contours defined in 2019 are very similar to those in the updated maps, such as in the upper part of the reach shown in *Figure 3.18*, while in others it is not possible to find a matching between them, like in the downstream part of the same figure.

4. Setup of the models and results

In this chapter an overview of the setup of the models, in terms of partition of the whole river in sub-reaches and relative boundary conditions, and the results obtained from the 2D flood simulations of the Seveso and Bozzente are presented. First, the partition of the rivers in sub-reaches is shown as a consequence of the longitudinal peak flow rate distribution. Second, a focus on the boundary conditions applied to the single sub-reach is illustrated by means of maps, hydrographs and rating curves. Then, the procedure intended to monitor the evolution of the flow rate through the control sections is described. Eventually, the maps with the results in terms of water depth and velocity are plotted.

First, the results for the modelling of the stream Seveso will be illustrated, followed by those related to the Bozzente. The results obtained during the present thesis cannot be considered the final ones, due to several shortcomings that are critically considered in *Chapter 5*.

4.1 Seveso

4.1.1 Longitudinal peak flow rate distribution and its discretization

As described in *Section 3.1*, the longitudinal distribution of the peak flow rate along the watercourse, for a given return period, has been discretized with a finite number of steps, representing the reference value of Q set for the corresponding reach. In *Figure 4.1* the three distributions for the Seveso corresponding to $T = 10, 100$ and 500 years are graphed.

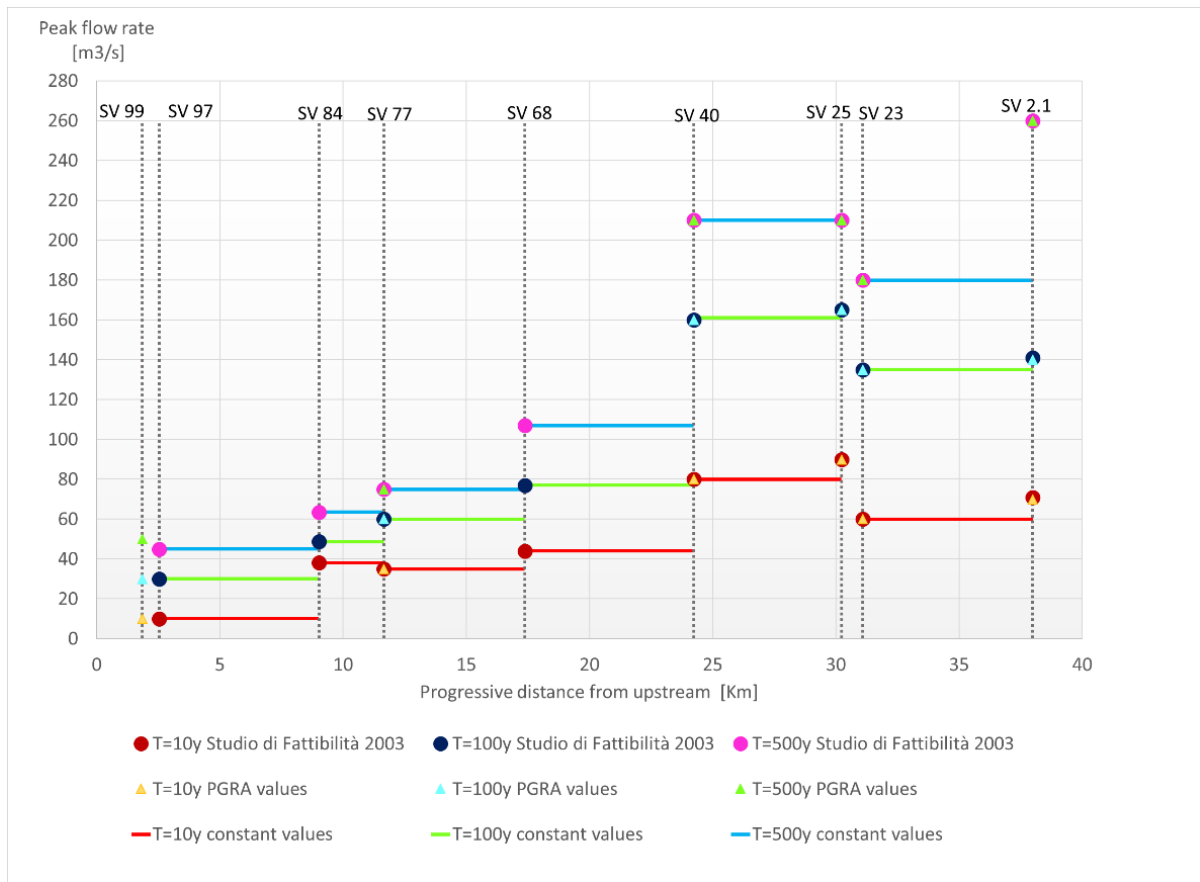


Figure 4.1: Peak flow rate distribution for the Seveso

The graph above displays data coming from two sources, namely the PGRA 2015 and the “Studio di Fattibilità (2003)”. This has been possible thanks to the fact that, where the data from both sources are present, the values are the same, so no ambiguity has resulted from their interpretation. In particular the “Studio di Fattibilità” has been fundamental in defining the increases in flow rate given by the intake of the Rio Acquanegra at section SV84 and that of the Serenza at section SV68. The peak flow rate distribution determined the subdivision of the Seveso in 6 separate sub-reaches:

- 1) From section SV97 to section SV84 due to the presence of the Rio Acquanegra.
- 2) From section SV84 to section SV77 due to the input of the Val Sant'Antonio stream.
- 3) From section SV77 to section SV68 due to the confluence with Serenza river.
- 4) From section SV68 to section SV40 due to confluence with Certesa river.
- 5) From section SV40 to section SV24 because of the intake work for the “Canale Scolmatore di Nord-Ovest (CSNO)”.
- 6) From section SV24 to section SV2.1 at the culvert at the entrance of the city of Milan.

The reach between SV99 and SV97 has been excluded from the model because of the lack of information necessary to model the entry section of the culvert at SV99. However, the fluvial

channel has been split according to the change in upstream boundary condition. Thus, the 6 reaches of the Seveso, represented in *Figure 4.2*, have been modelled independently from each other. The following pages present the complete description of the boundary conditions applied at the single sub-reaches of the Seveso.

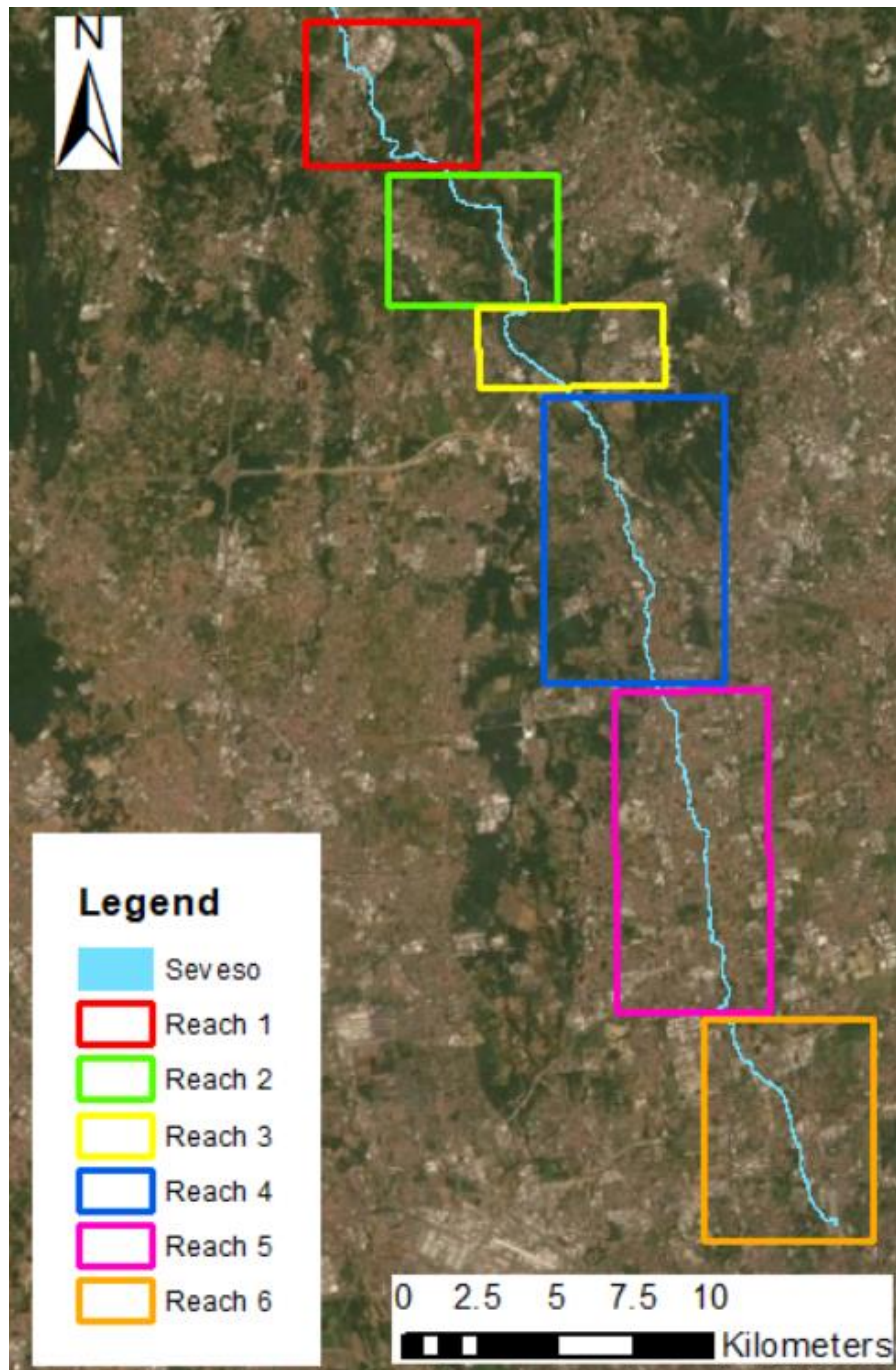
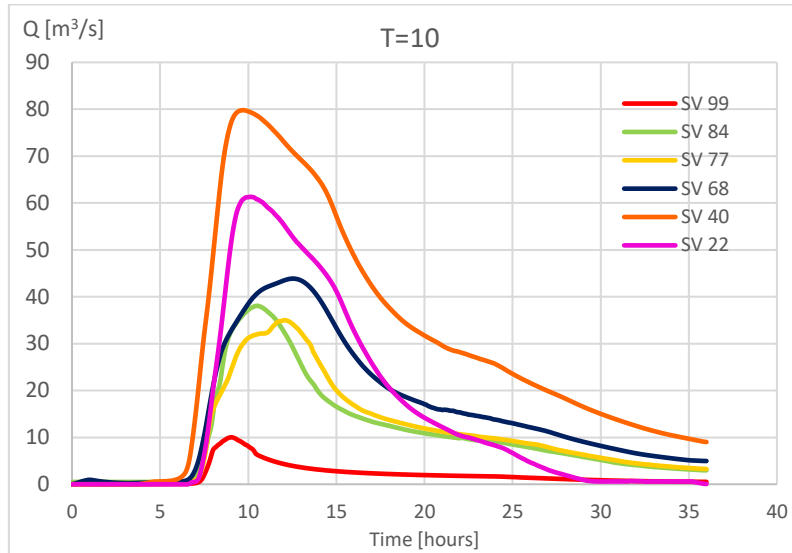


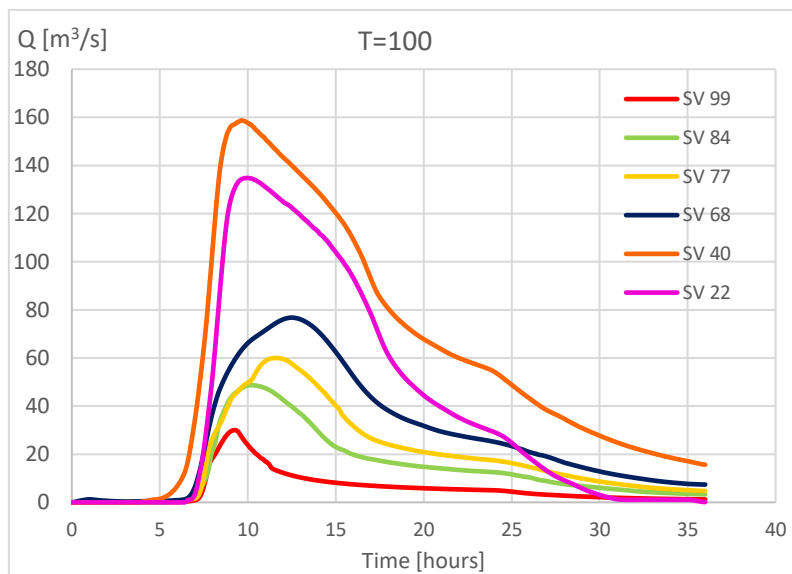
Figure 4.2: Subdivision of the Seveso

4.1.2 Boundary conditions

Figure 4.3 shows all the hydrographs applied at the upstream section of the sub-reaches, for each return period (10, 100 and 500 y). As one can notice, they describe an event which lasts 36 hours.



a



b

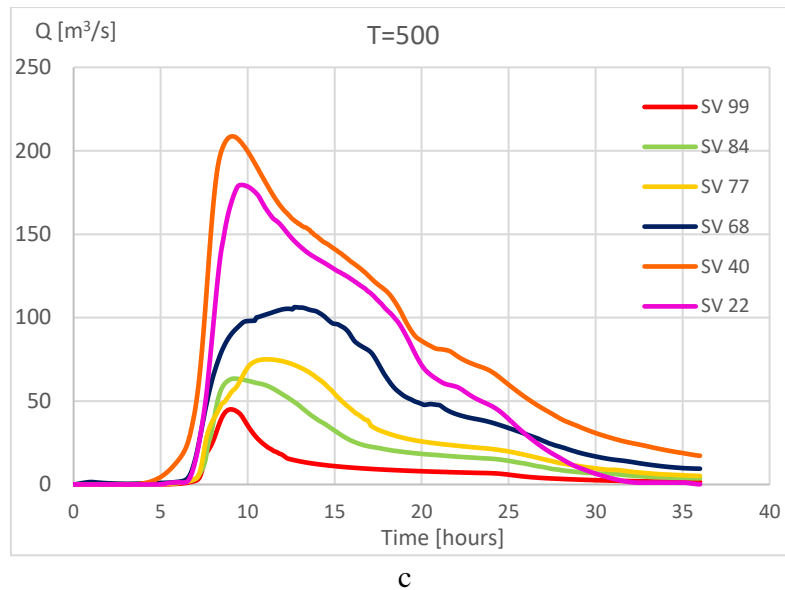
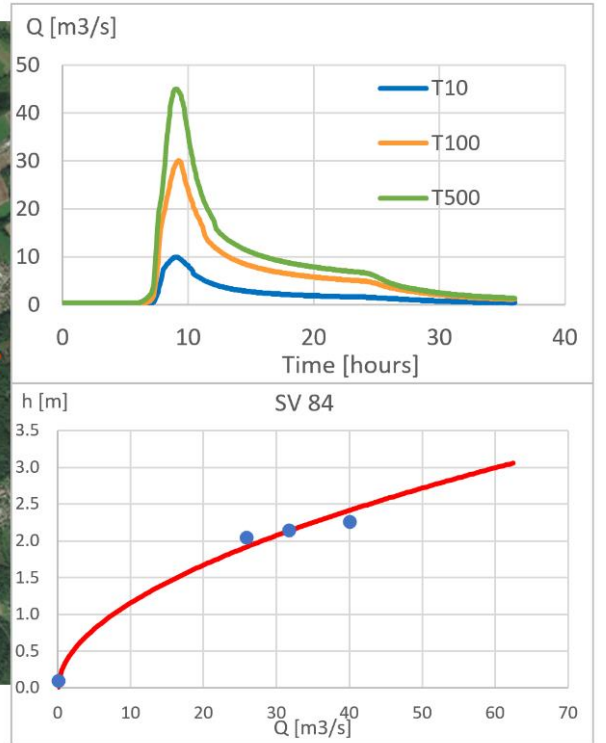
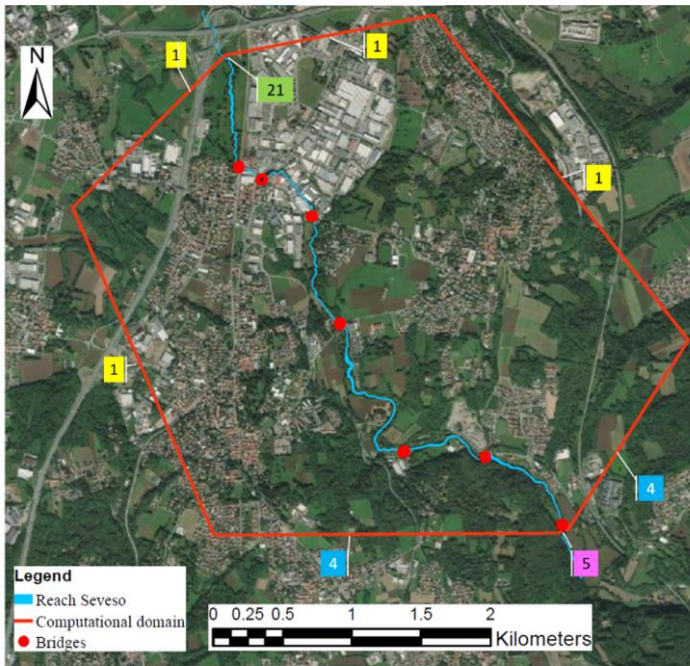


Figure 4.3 a-c: Hydrographs set as upstream BCs for the Seveso for $T=10$, 100, 500 years respectively

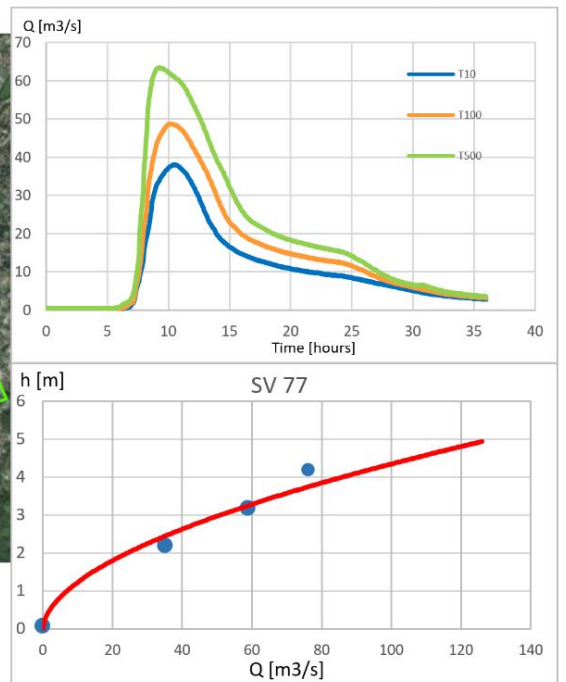
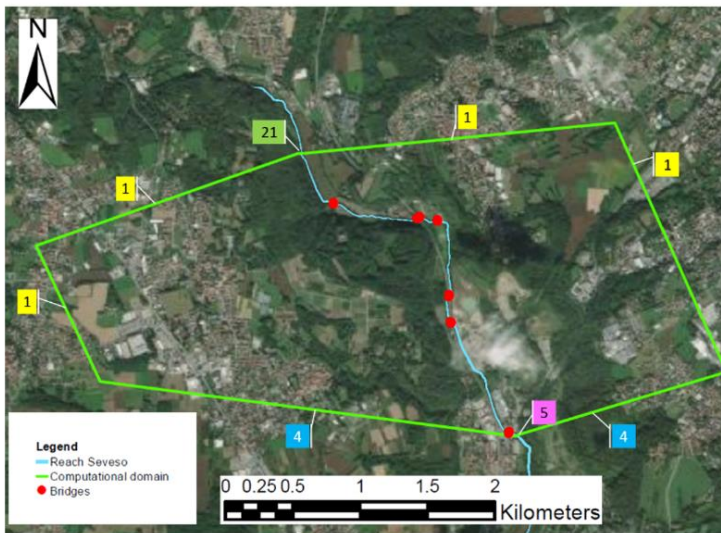
In the following, an overview of the boundary conditions per each sub-reach of the Seveso is illustrated. Beside the map of the reach, the upstream BCs (i.e. hydrographs) for the three return periods are plotted, together with the respective downstream BC which (apart from reach 6) is represented by a rating curve. In particular, the rating curves for the Seveso have been obtained by a power law, having as known values the water elevations coming from the PGRA 2015 (Cfr. *Section 3.4*).

The numbers 1, 3, 4, 5, 21 on the following maps refer to the typology of BC imposed on the segment, respectively “wall”, “level”, “far field”, “rating curve” and “hydrograph” (Cfr. *Section 3.5*).

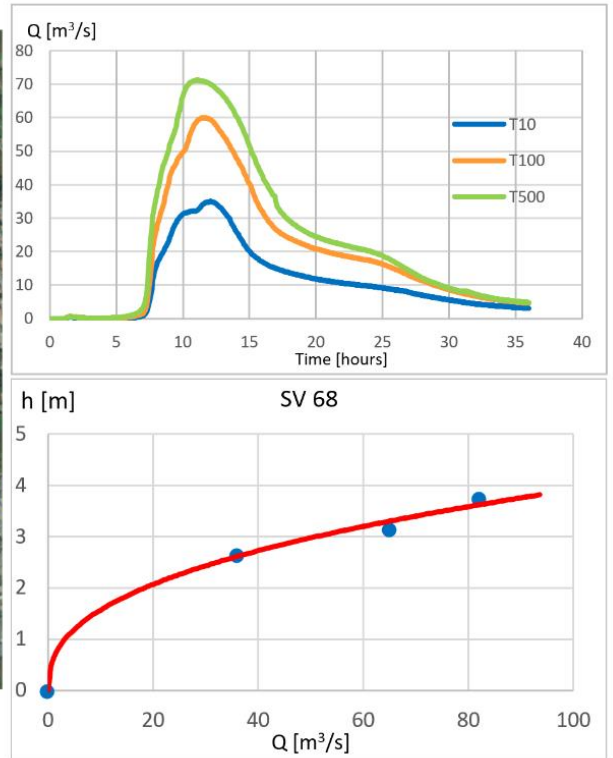
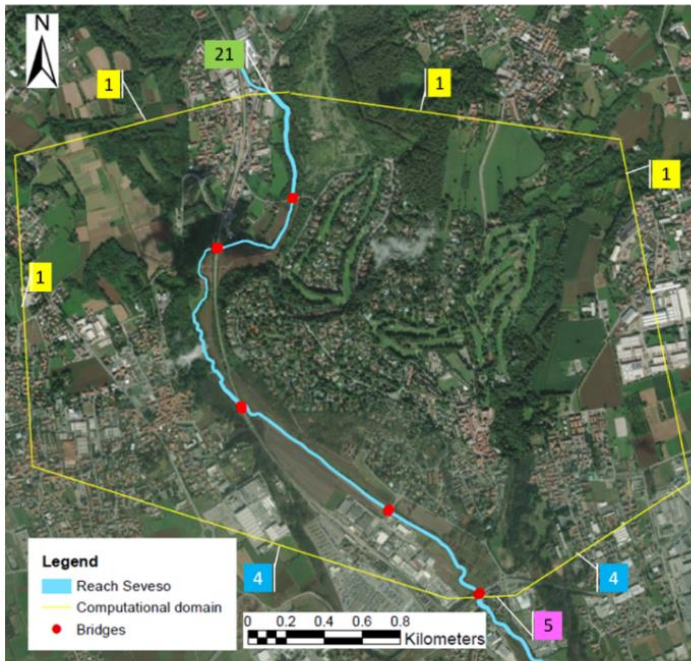
Reach	Length [km]	Upstream section	Downstream section	Transversal structures	Q (T=10) [m ³ /s]	Q (T=100) [m ³ /s]	Q (T=500) [m ³ /s]
1	7.20	SV 97	SV 84	7	10	30	45



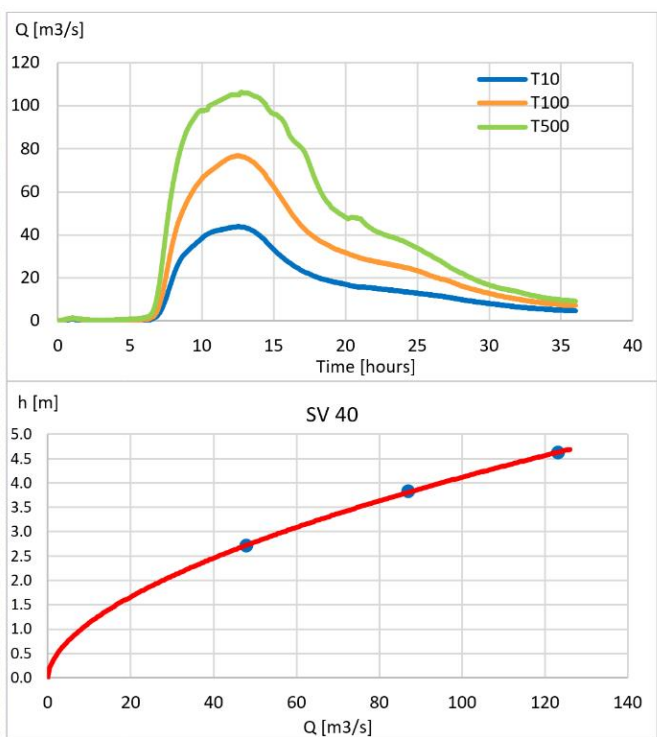
Reach	Length [km]	Upstream section	Downstream section	Transversal structures	Q (T=10) [m ³ /s]	Q (T=100) [m ³ /s]	Q (T=500) [m ³ /s]
2	2.65	SV 84	SV 77	7	38	49	63



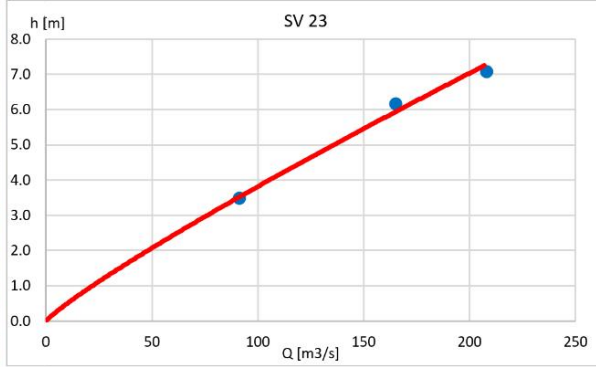
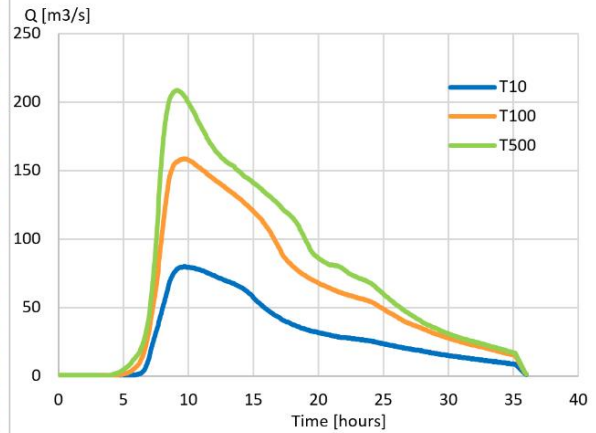
Reach	Length [km]	Upstream section	Downstream section	Transversal structures	Q (T=10) [m ³ /s]	Q (T=100) [m ³ /s]	Q (T=500) [m ³ /s]
3	5.70	SV 77	SV 68	6	35	60	75



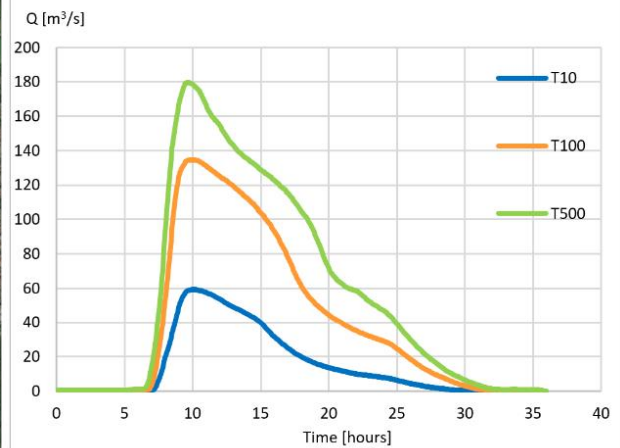
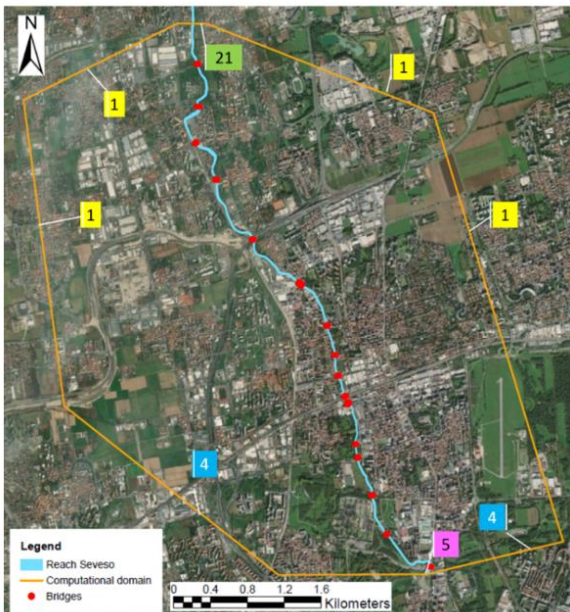
Reach	Length [km]	Upstream section	Downstream section	Transversal structures	Q (T=10) [m ³ /s]	Q (T=100) [m ³ /s]	Q (T=500) [m ³ /s]
4	5.85	SV 68	SV 40	20	45	77	107



Reach	Length [km]	Upstream section	Downstream section	Transversal structures	Q (T=10) [m ³ /s]	Q (T=100) [m ³ /s]	Q (T=500) [m ³ /s]
5	7.75	SV 40	SV 23	19	80	160	210



Reach	Length [km]	Upstream section	Downstream section	Transversal structures	Q (T=10) [m ³ /s]	Q (T=100) [m ³ /s]	Q (T=500) [m ³ /s]
6	6.90	SV 23	SV 2.1	18	60	135	180



As downstream BC, a constant level equal to the elevation of the upper edge of the entry section of the culvert has been set (139 m a.s.l.).

4.1.3 Control sections for the flow rate distribution

To monitor the evolution of the flow rate over time along the river reach, control sections have been inserted to extract the necessary data in correspondence of them (Cfr. *Section 3.7.1*). *Figures 4.4* and *4.5* show respectively reaches 2 and 6 with the relative control sections. It is worth noticing that their span is large enough to consider the entire width of the flood perimeter, here referred, in both the reaches, to a return period of 100 years. The results consist of hydrographs like those plotted in *Figures 4.6* and *4.7*. In both cases one can notice that the control sections number 1, immediately after the upstream section of the sub-reaches, follows faithfully the shape of the initial flow rate distribution represented by the upstream BC. Further confirmations about the correspondence between the flood simulation development and the information coming from the hydrographs could be found in the trend of the latter: indeed, moving downstream, their peak values decrease and result delayed, as a result of the propagation of the flood wave.

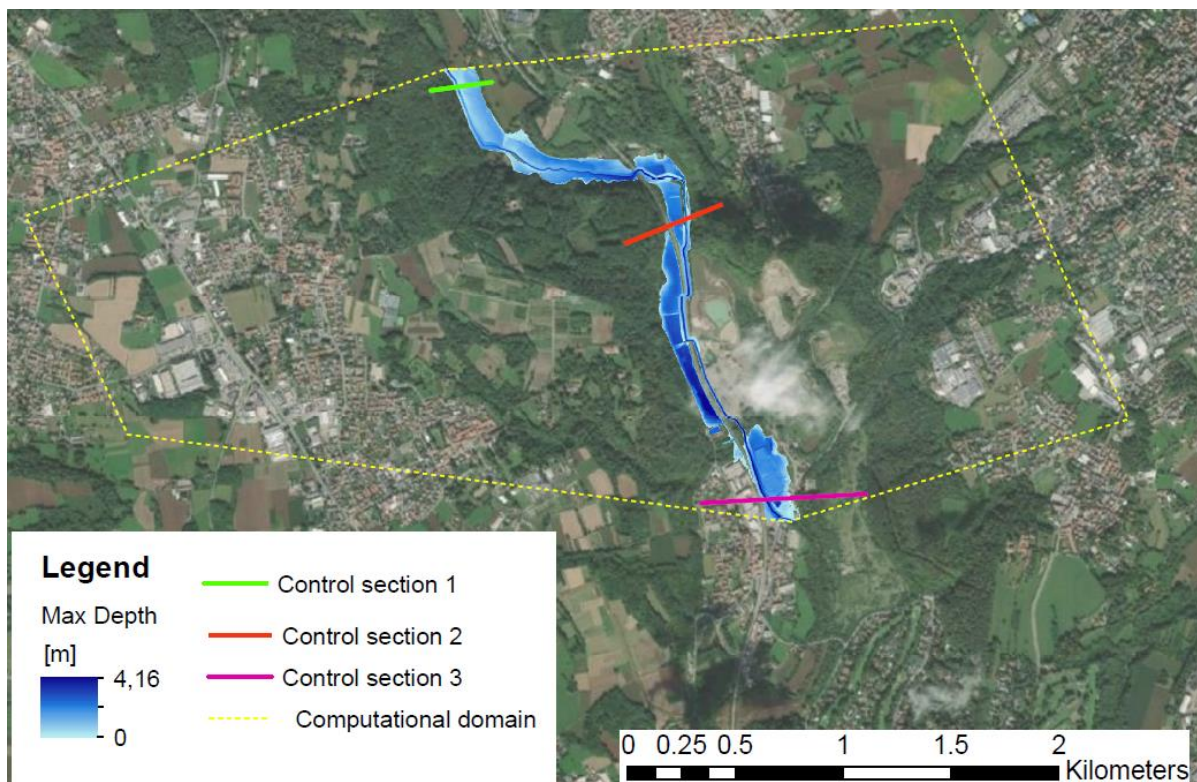


Figure 4.4: Control sections for the reach 2

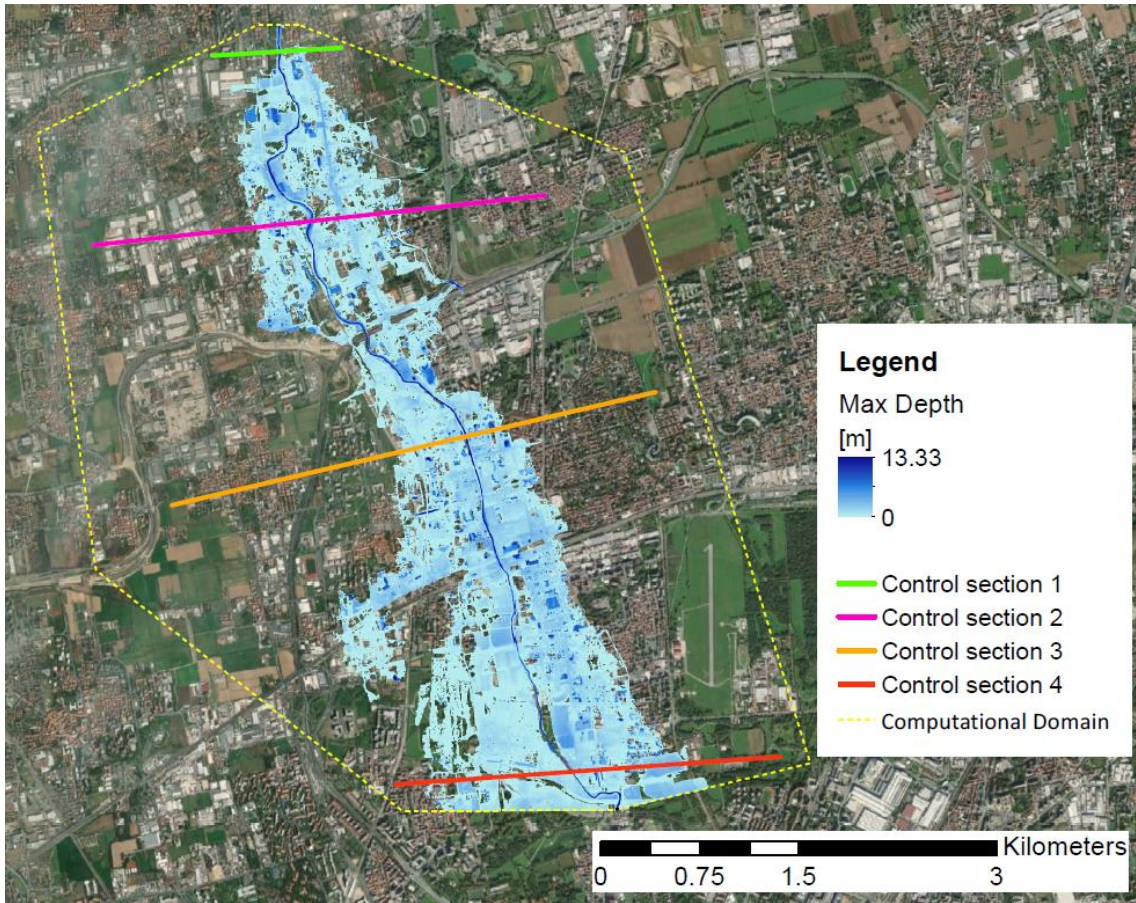


Figure 4.5: Control sections for the reach 6

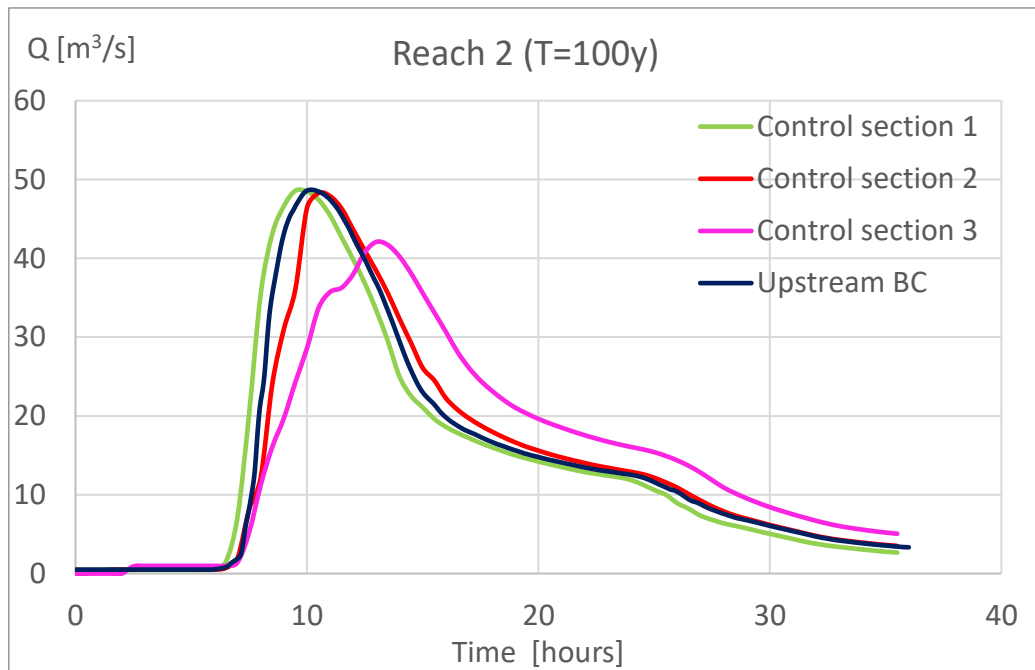


Figure 4.6: Hydrographs extracted from the control sections for the reach 2

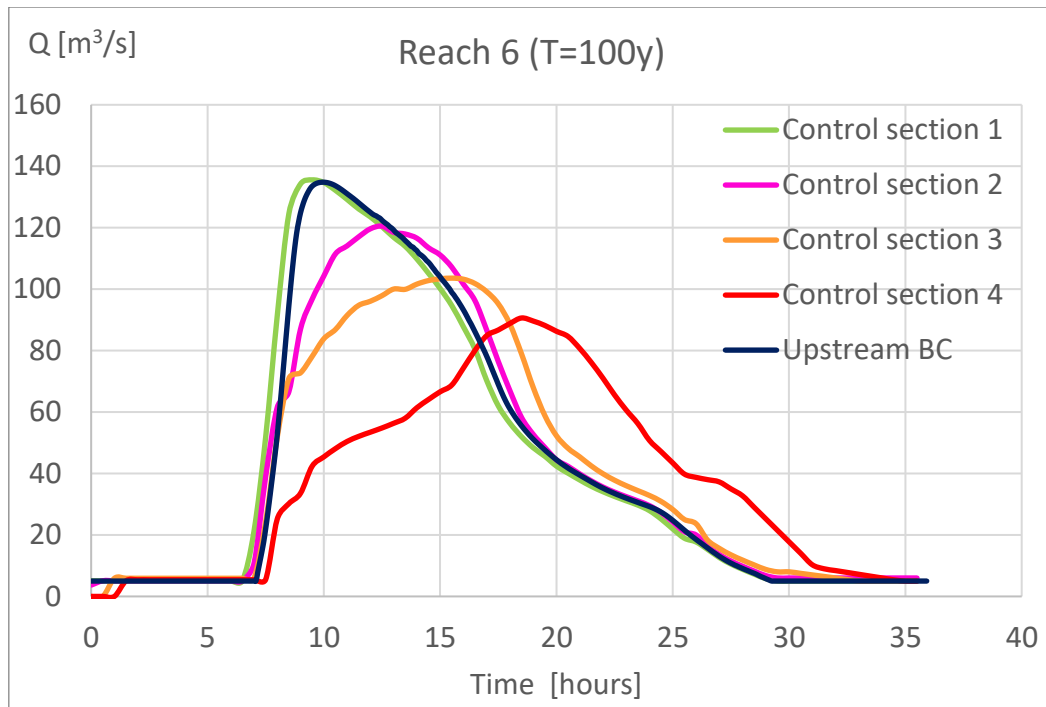


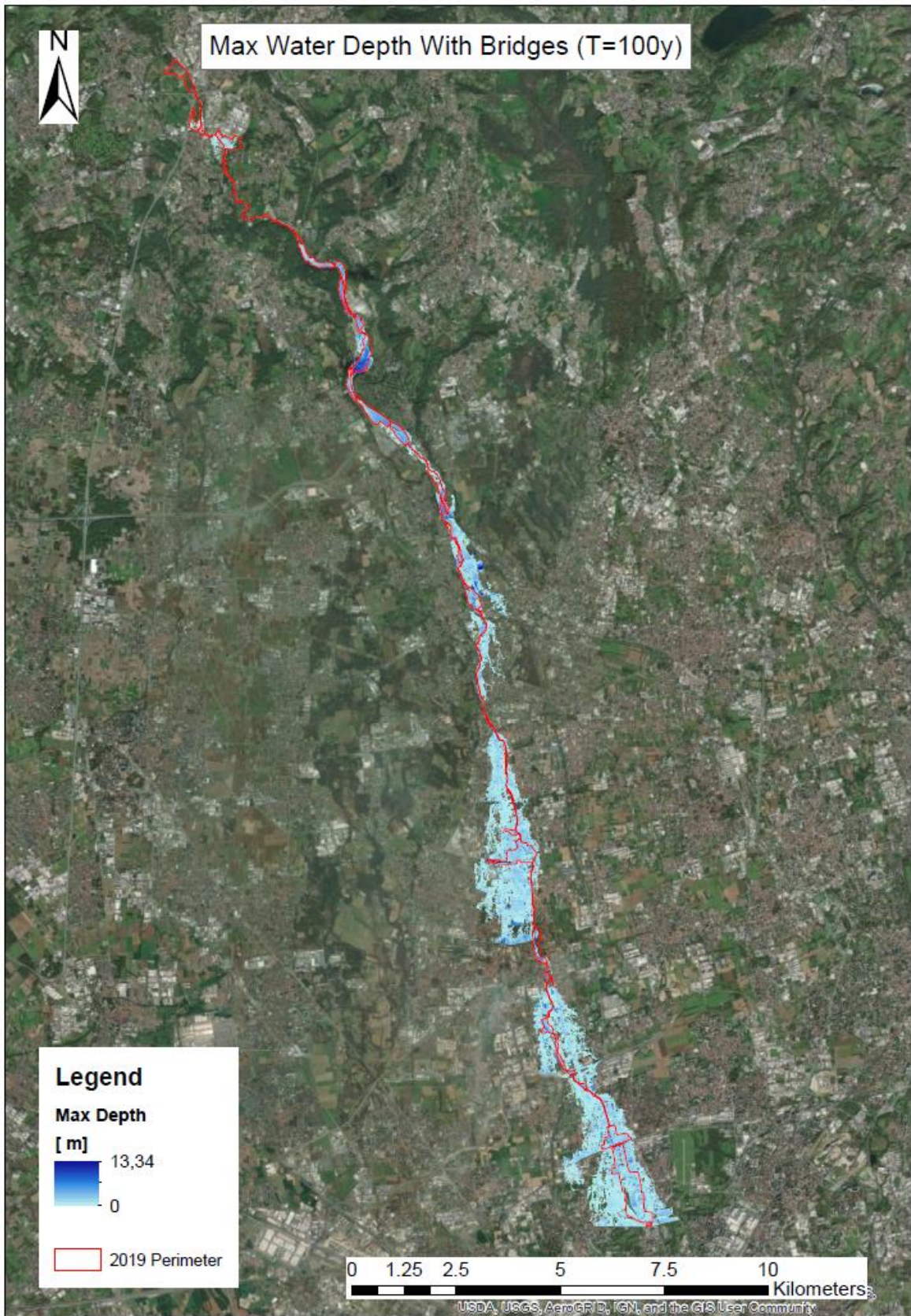
Figure 4.7: Hydrographs extracted from the control sections for the reach 6

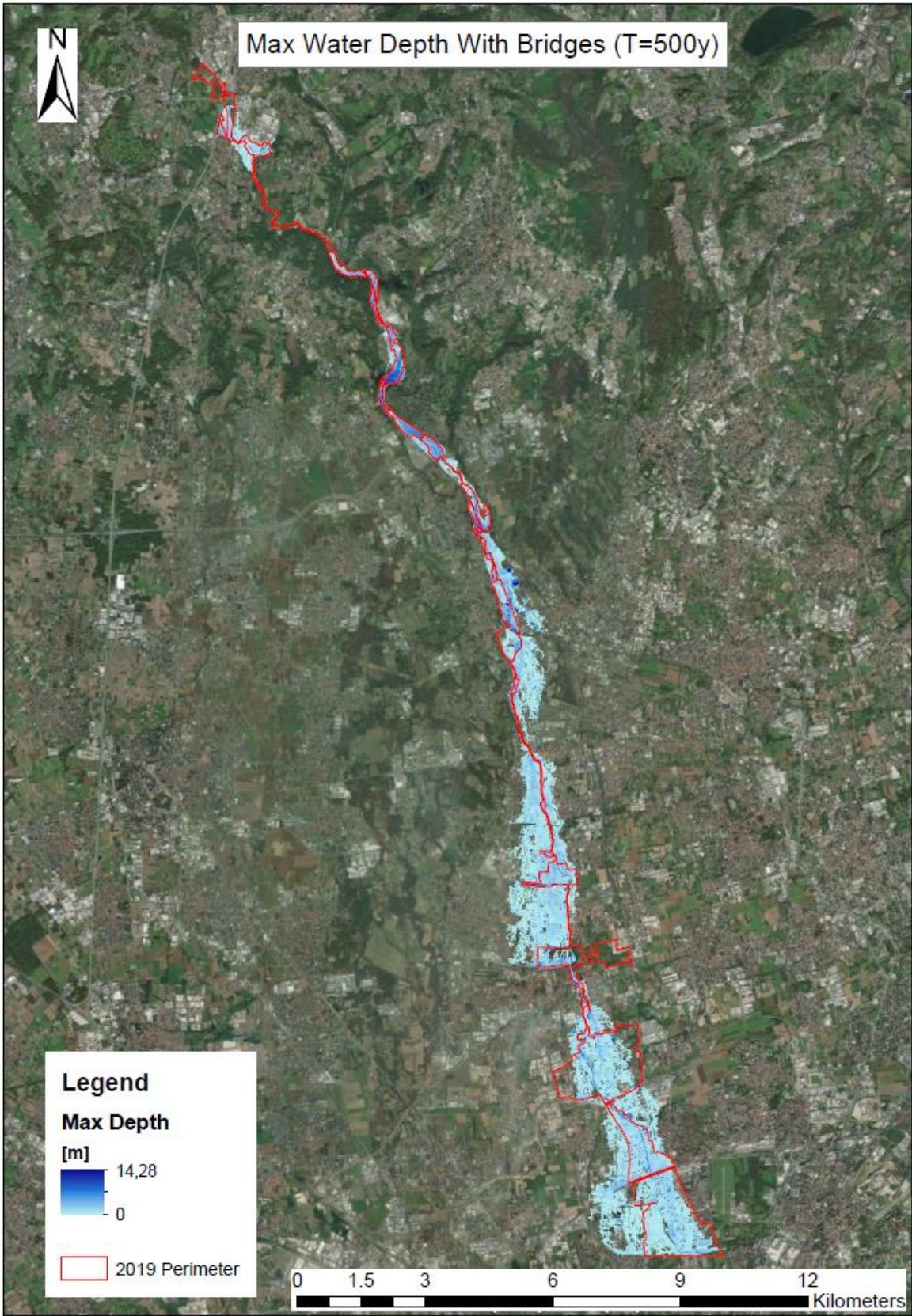
4.1.4 Maps of the results

In this section, the maps of the final results coming from the 2-dimensional simulations, performed through PARFLOOD code, are plotted.

Max Water Depth	
Spatial distribution with bridges compared with the perimeter of the flood maps from 2019	Pp. 55-57
Spatial distribution without bridges	Pp. 58-60
Differences between max water depth distribution with and without bridges	Pp. 61-63
Max Velocity	
Spatial distribution with bridges compared with the perimeter of the flood maps from 2019	Pp. 64-66
Spatial distribution without bridges	Pp. 67-69
Differences between max velocity distribution with and without bridges	Pp. 70-72



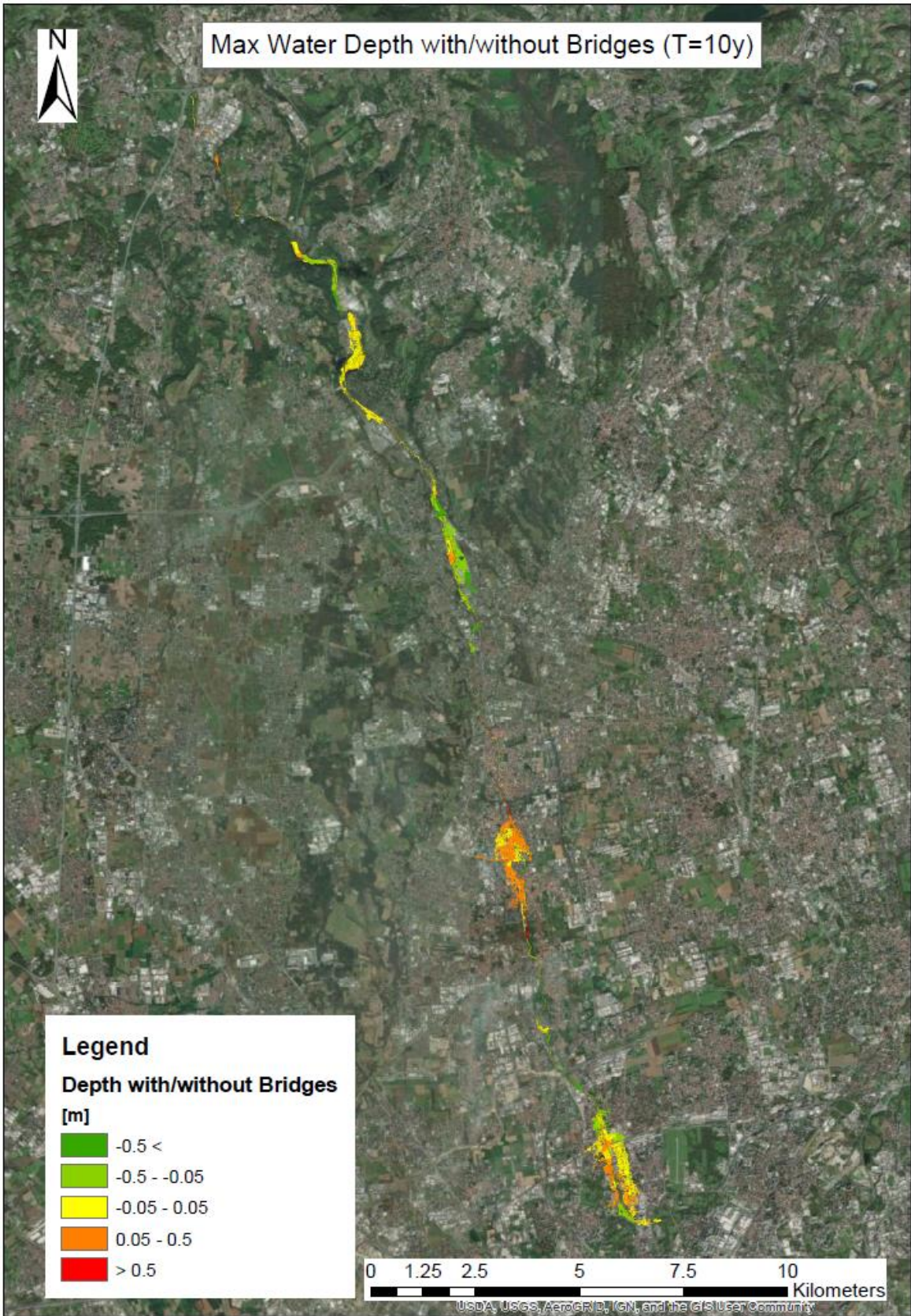


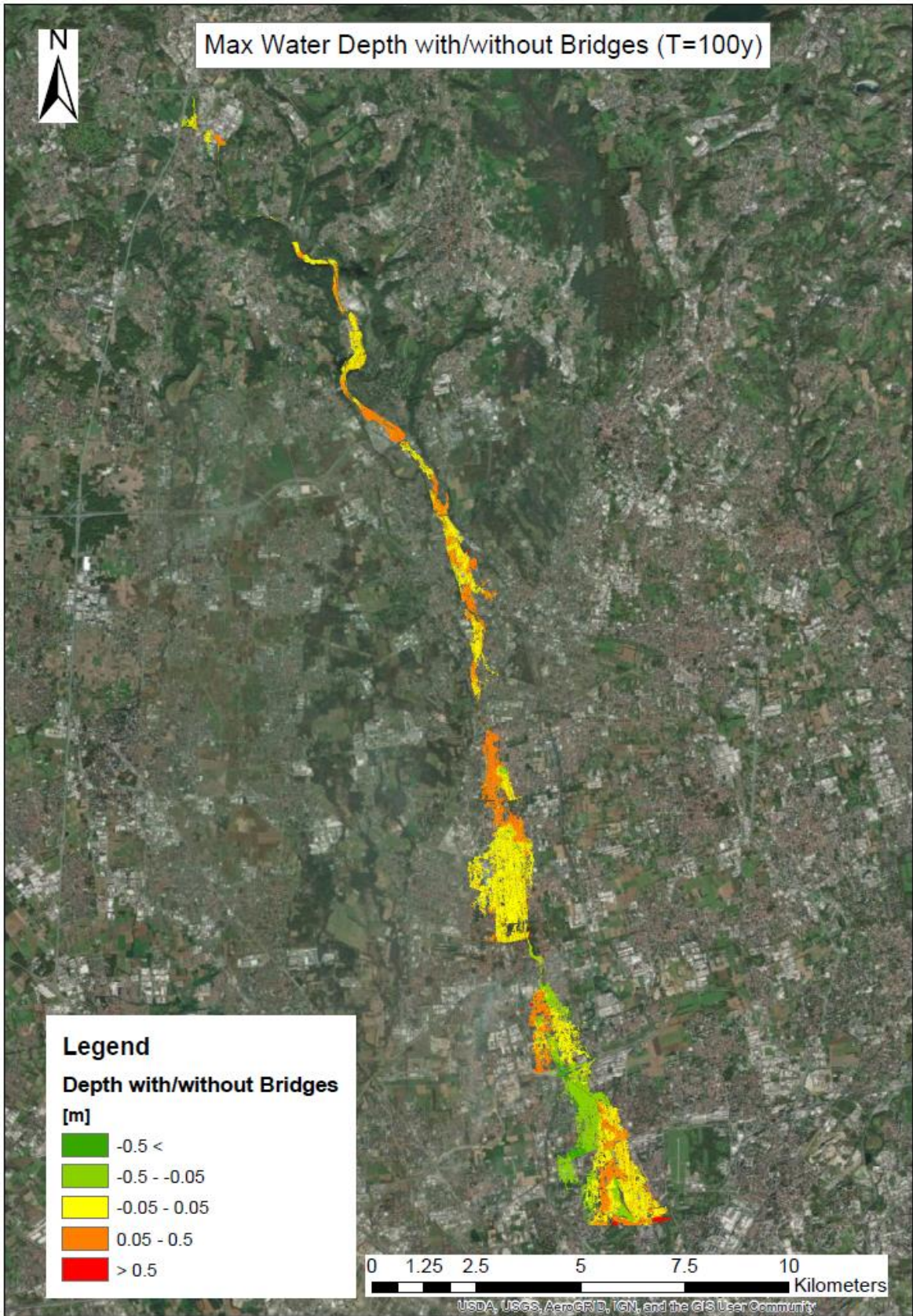


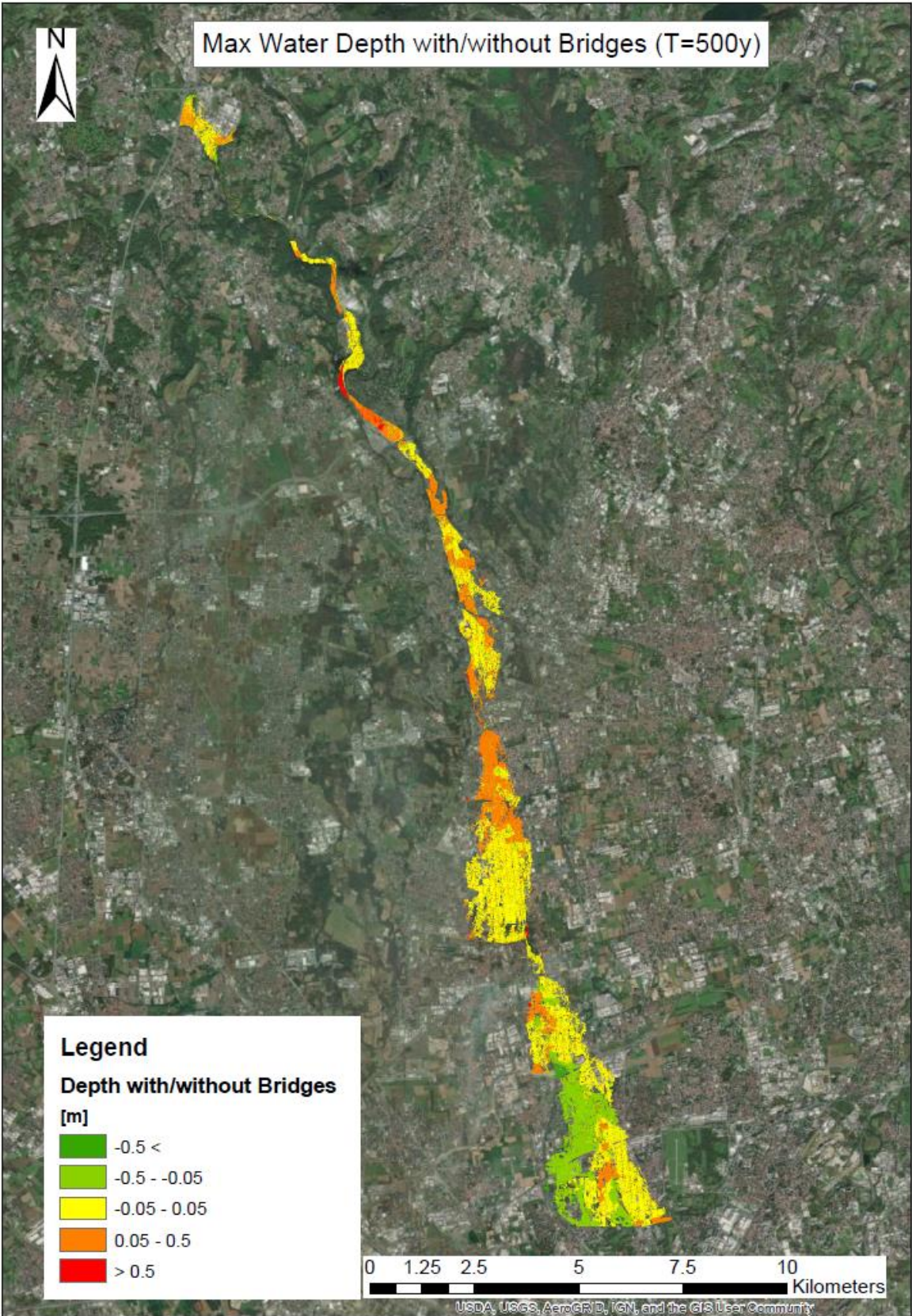


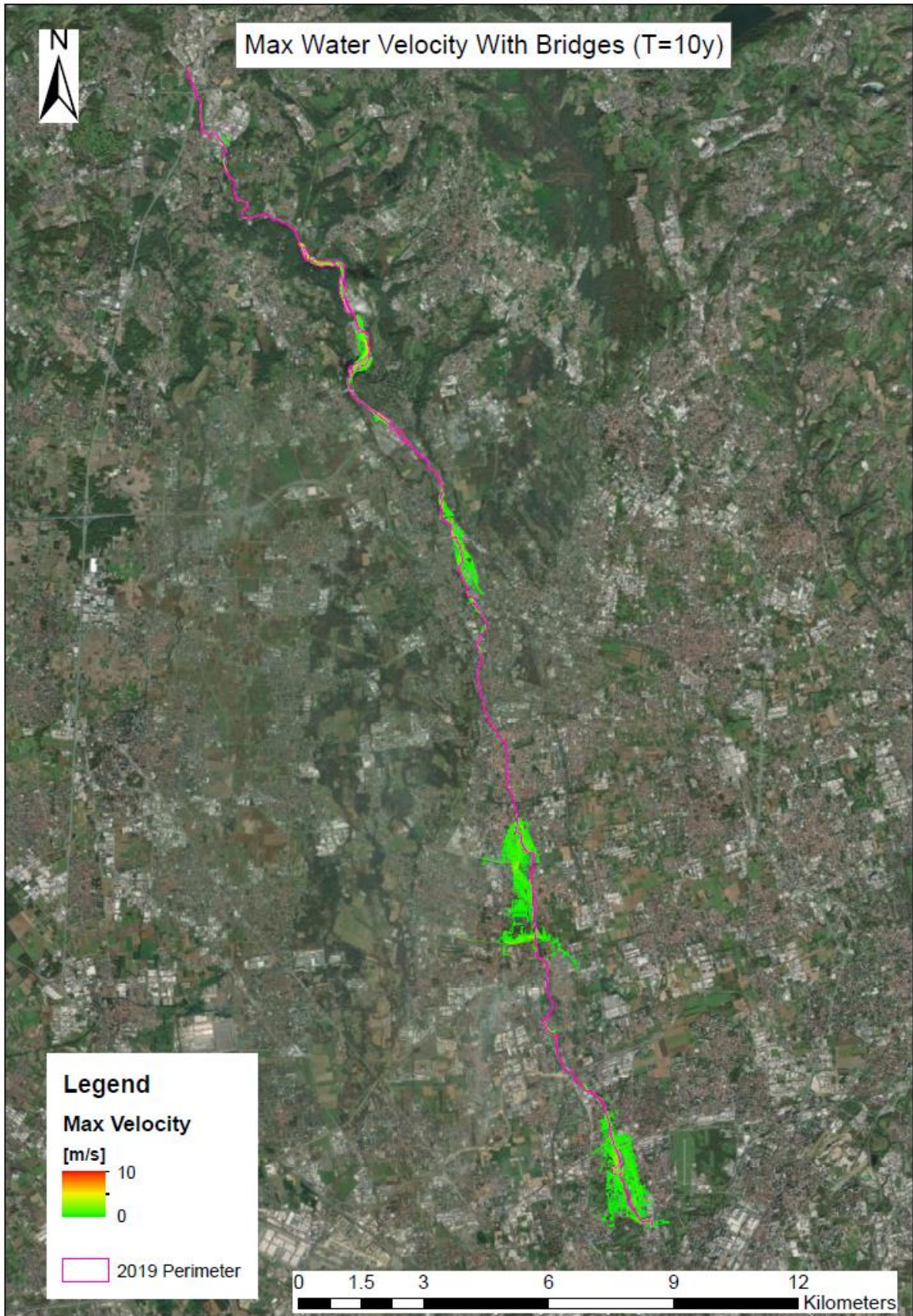


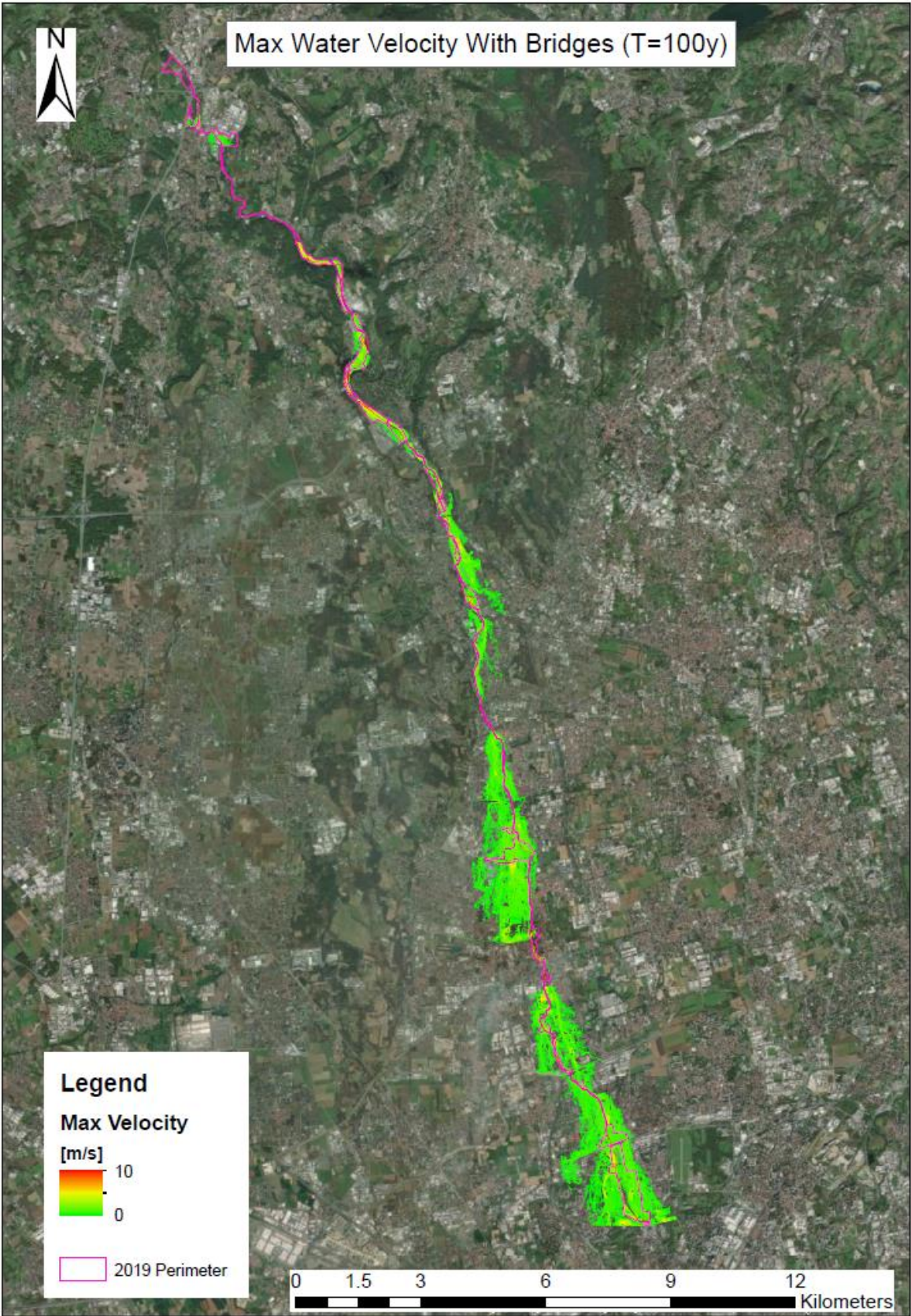


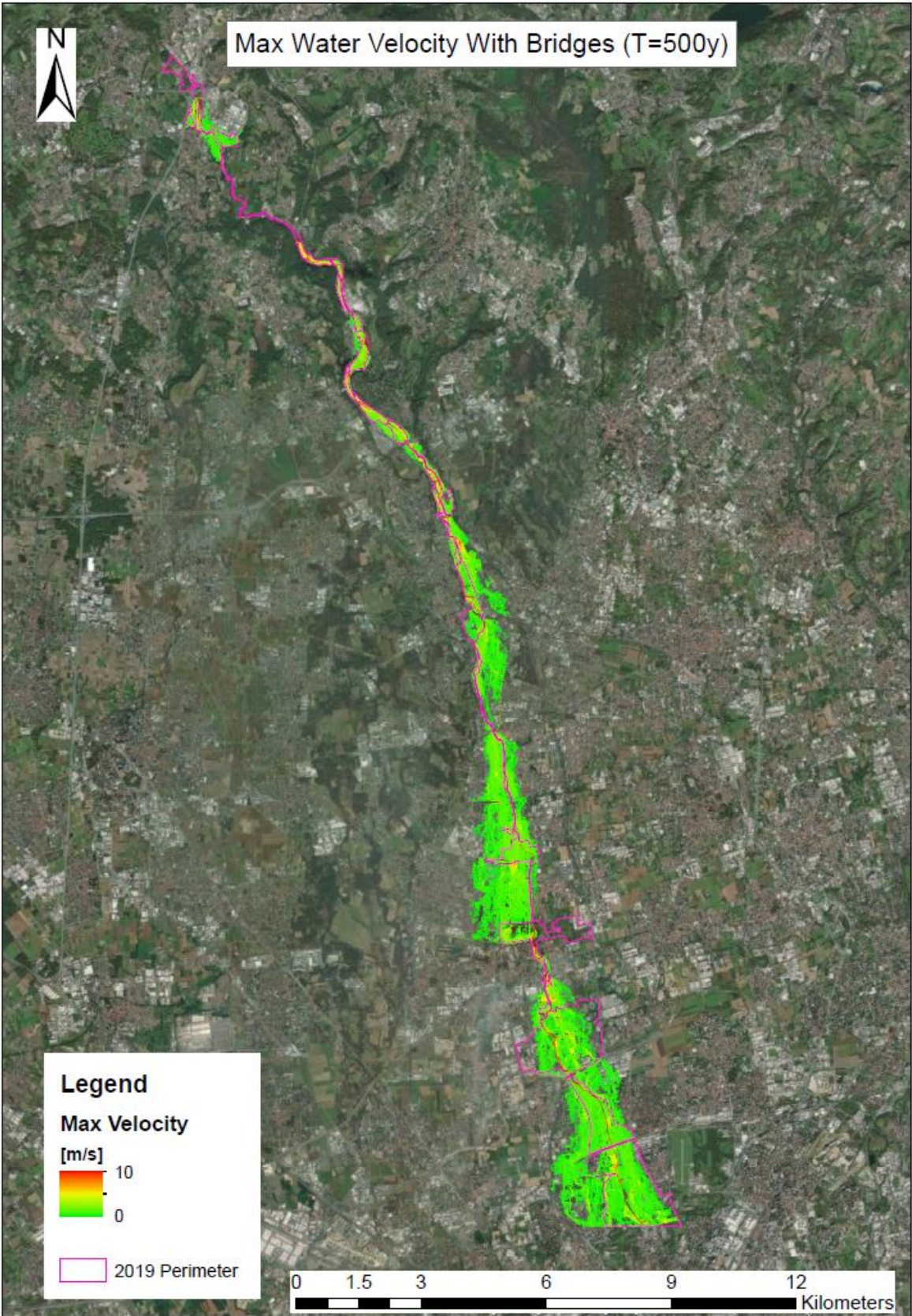


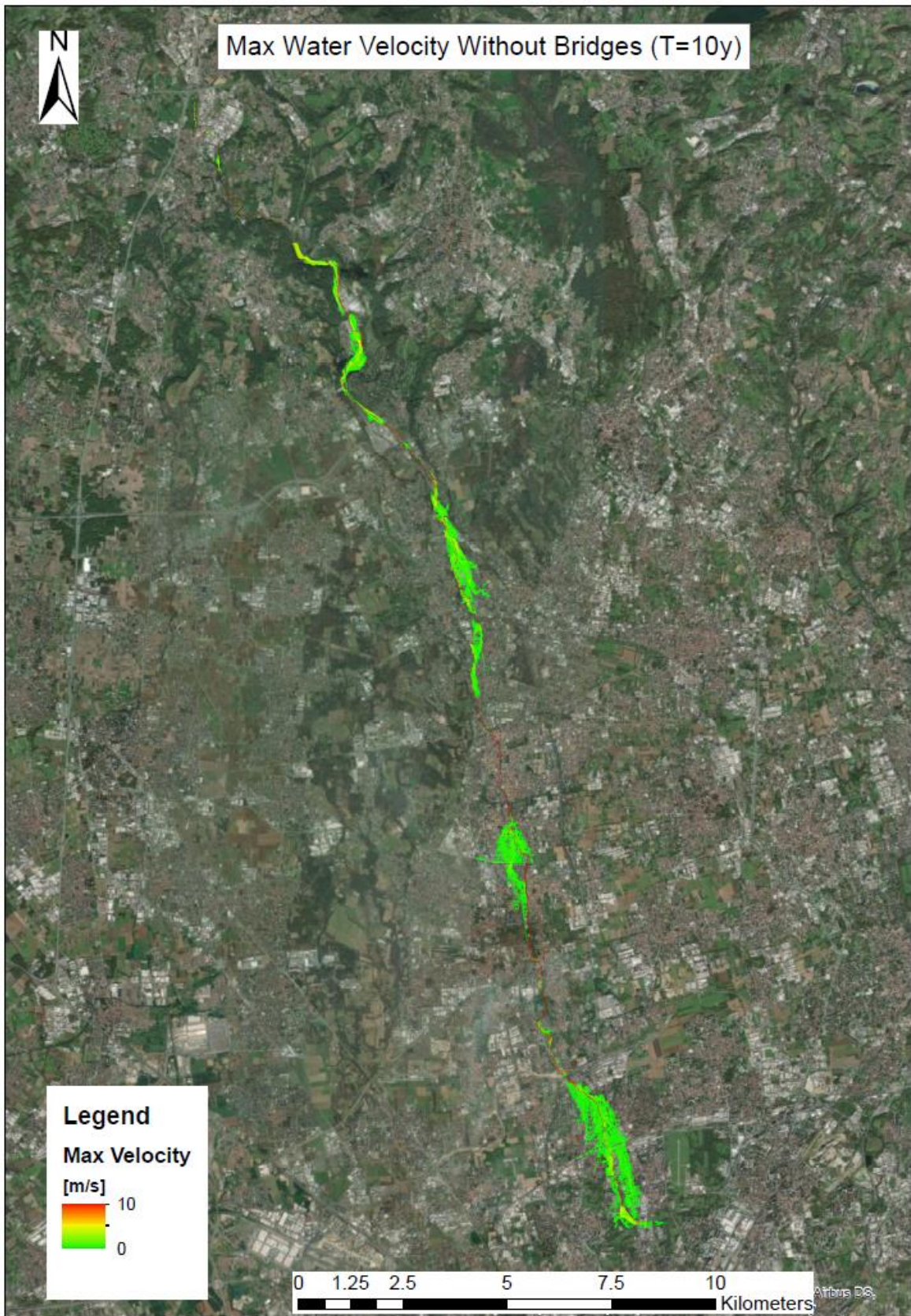


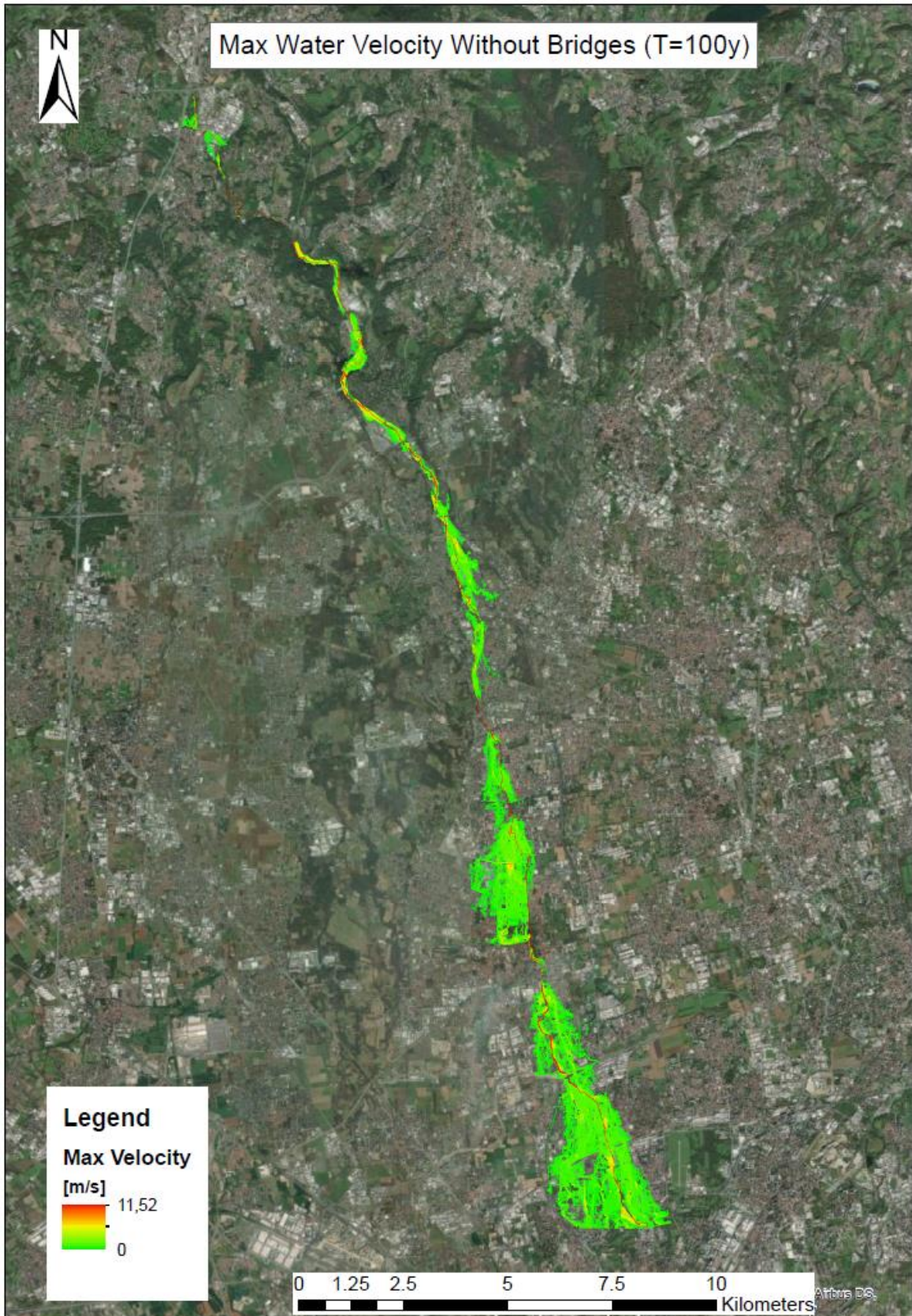


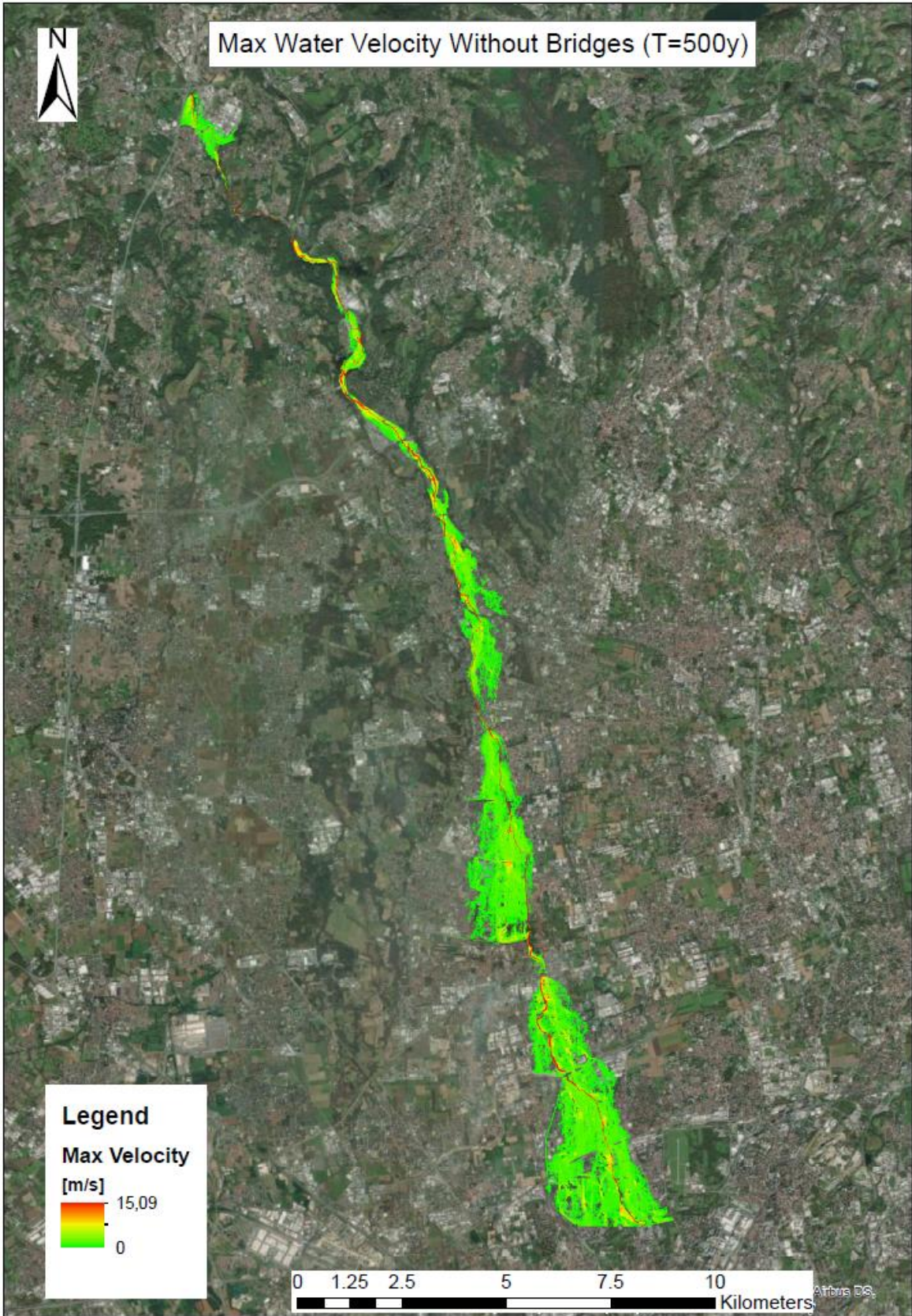


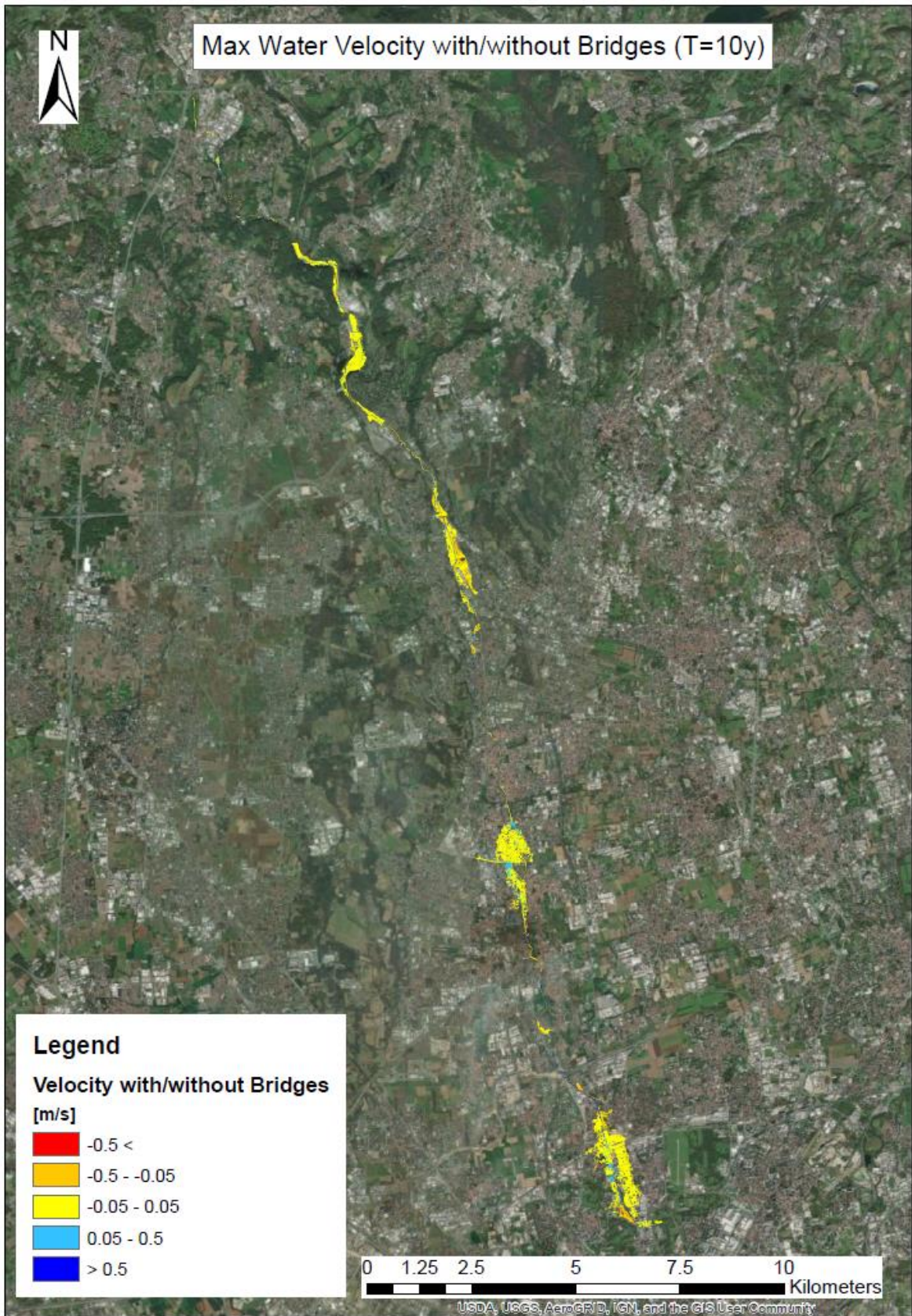


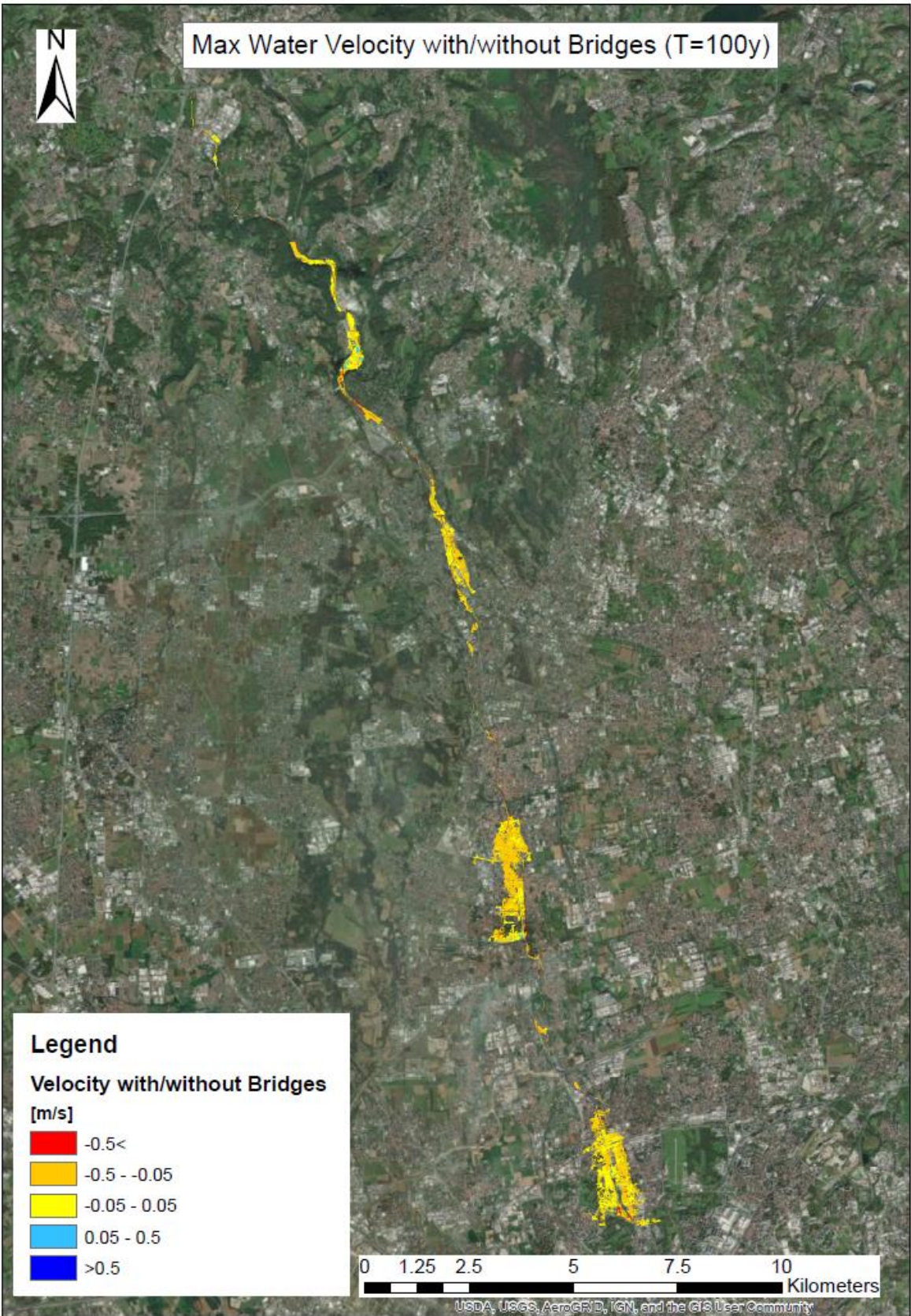


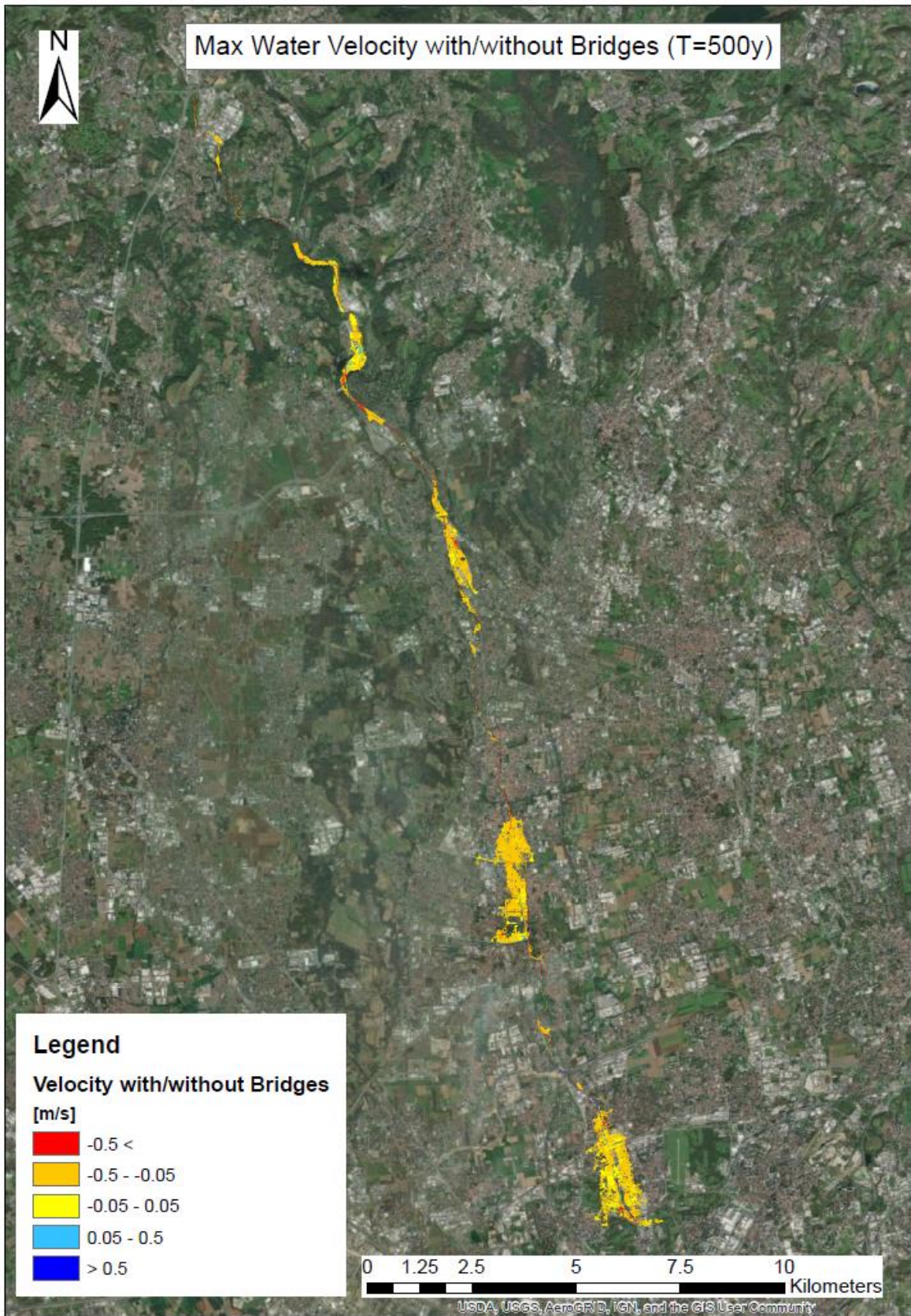












4.2 Bozzente

4.2.1 Longitudinal peak flow rate distribution and its discretization

Figure 4.8 represents the longitudinal peak flow rate distribution for the Bozzente: the values provided by the previous PGRA study have been taken as a reference to define the steps of constant values for each sub-reach.

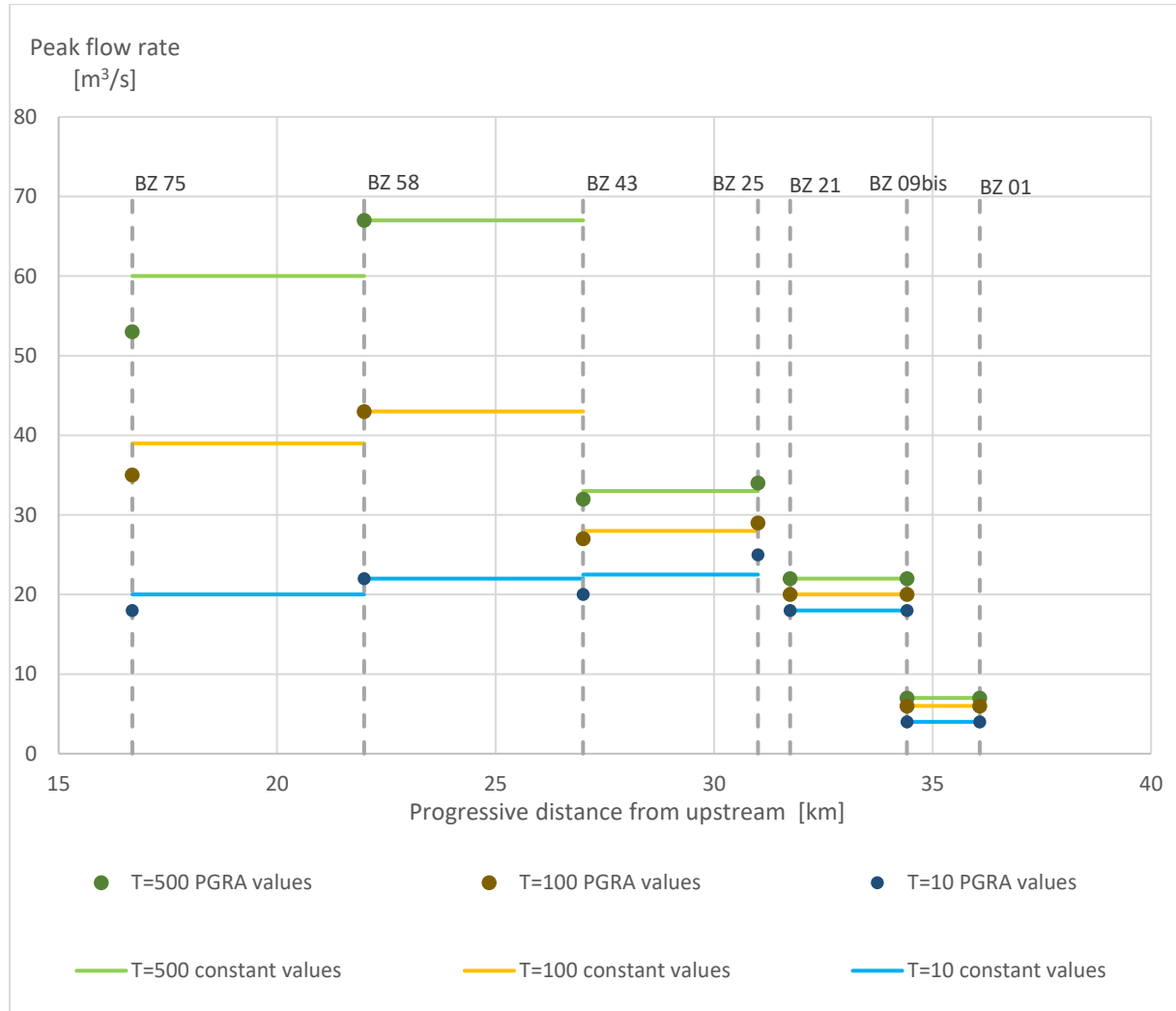


Figure 4.8: Peak flow rate distribution for the Bozzente

As one can notice, in the case of sections where the peak Q increases (i.e. BZ 75 - BZ 58 and BZ 43 - BZ 25), the average value has been set, because, differently from what already seen for the Seveso (Cfr. Section 4.1.1), those steps in discharge are not due to the presence of punctual inflows. So that, to take in account the distributed water discharge along those sections, without overestimating their contribution, the average between the values at the respective boundaries has been considered worthwhile. On the other hand, between BZ 58 and BZ 43, a conservative choice has led to set the maximum value as peak discharge. A further

consideration concerns the trend of the discharge values which decrease in the downstream reach of the Bozzente: this is due to the presence of a flood retention basin between sections BZ 25 and BZ 21 and a relief channel in correspondence of section BZ 09bis.

Figure 4.9 shows the subdivision of the Bozzente consequence of the peak flow distribution.

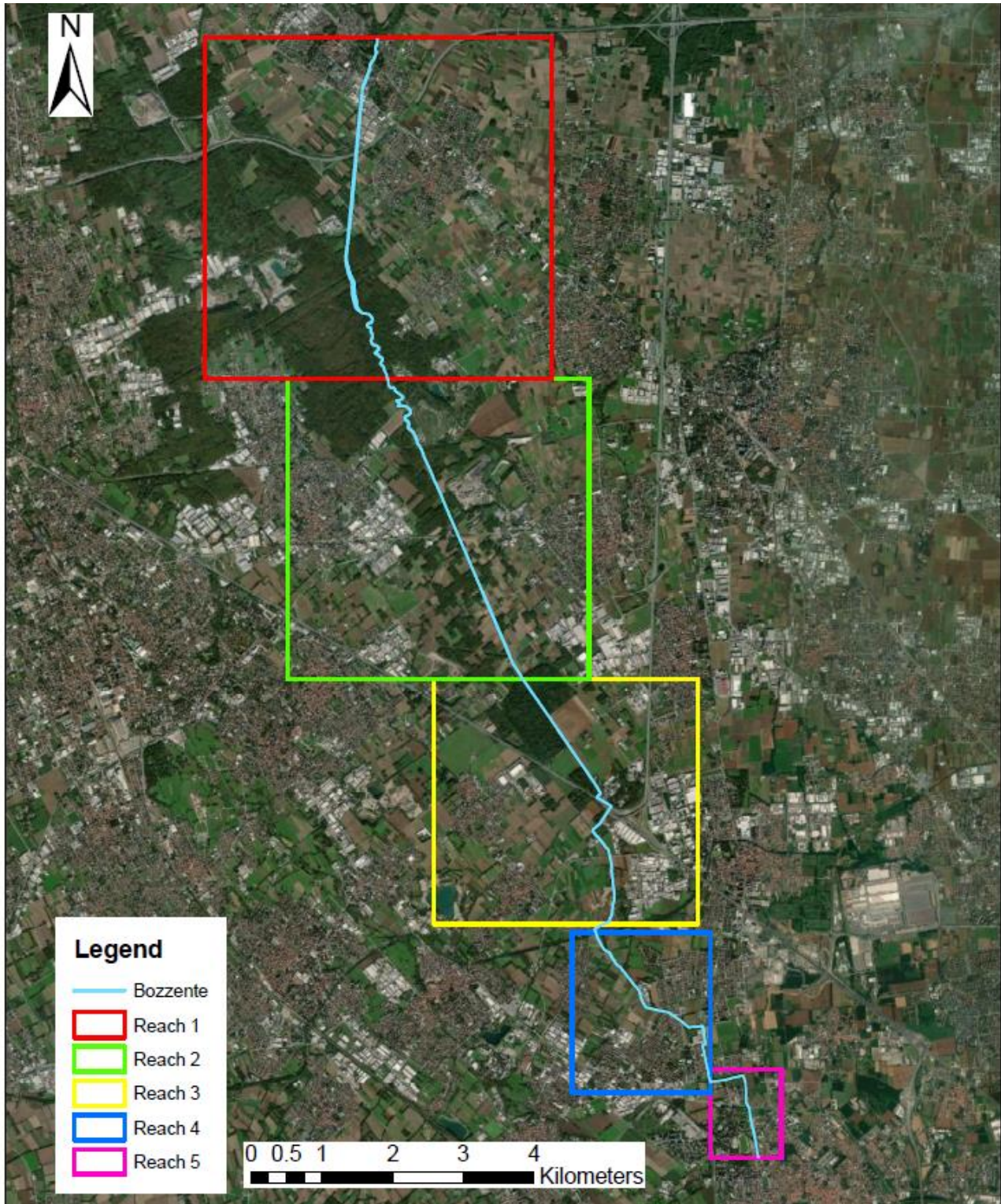
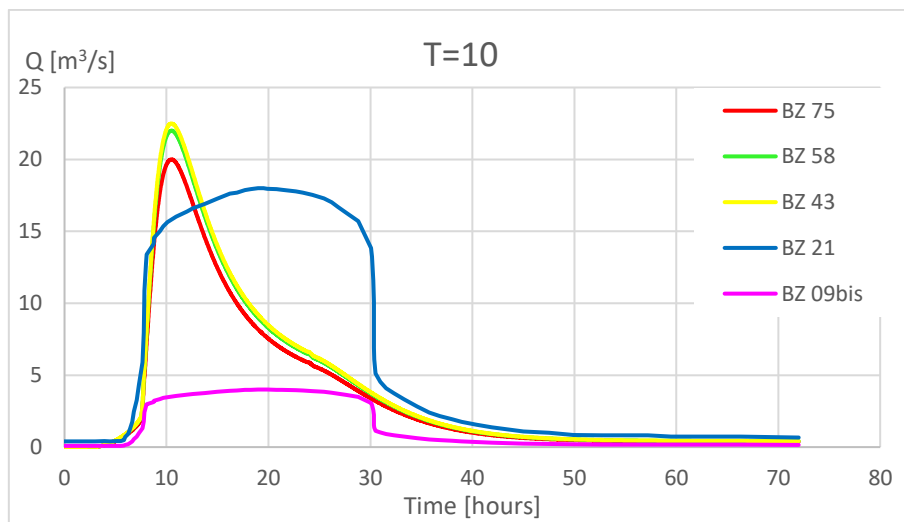


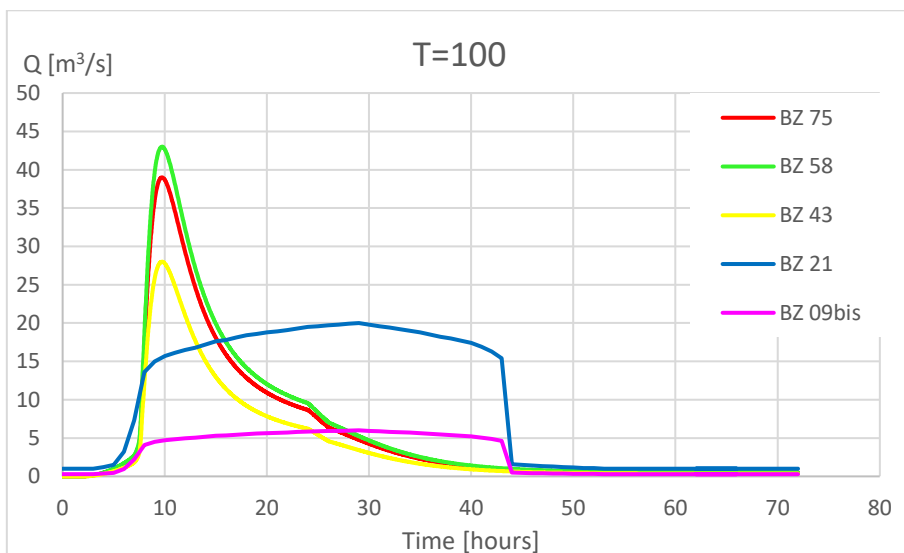
Figure 4.9: Subdivision of the Bozzente

4.2.2 Boundary conditions

Figures 4.10 a-c show the hydrographs applied as boundary conditions in correspondence of the upstream section of each sub-reach, for the three return periods. Even though the Bozzente is shorter than the Seveso, the hydrographs for the former describe an event which lasts 72 hours. This is a consequence of the presence of the flood retention basin upstream section BZ 21, which makes the distribution of the flow rate delayed over time, reducing the peak value of the discharge. Thus, the need of extending the run time of the simulation to let the flood wave completely extinguish its effect downstream the retention work.



a



b

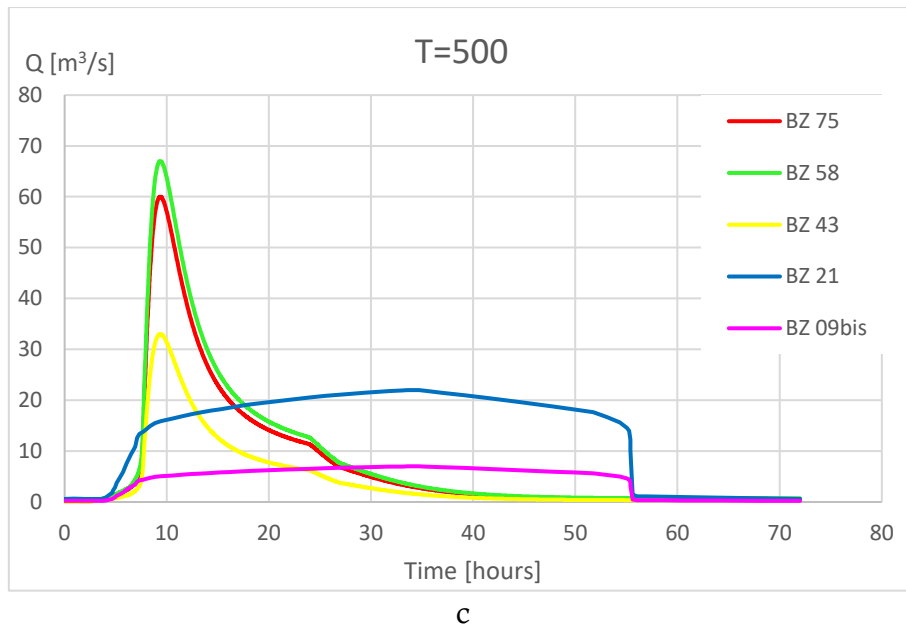
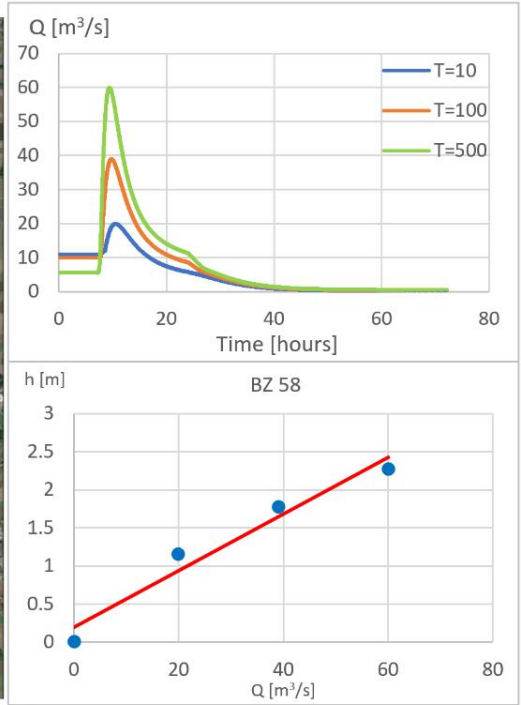
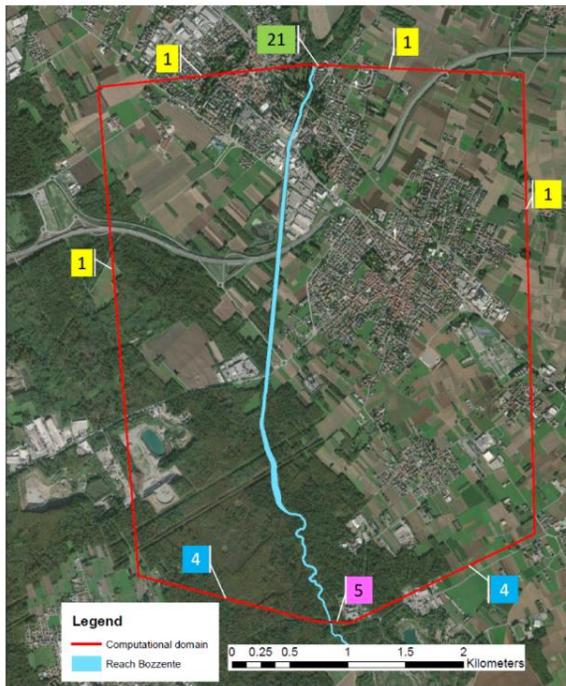


Figure 4.10 a-c: Hydrographs set as upstream BCs for the Bozzente for $T=10, 100, 500$ years respectively

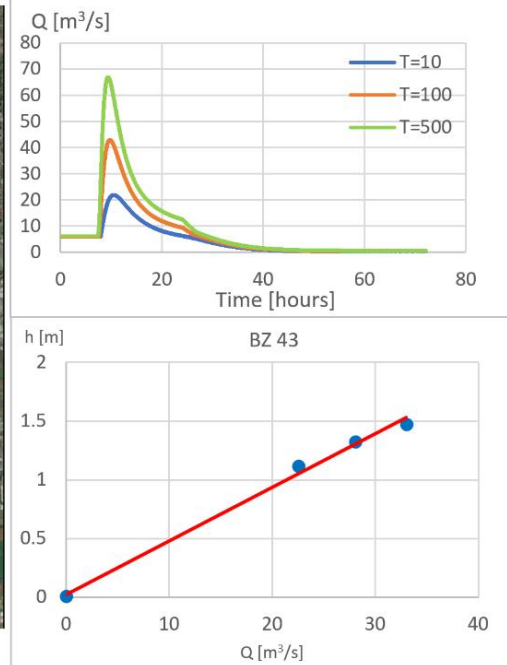
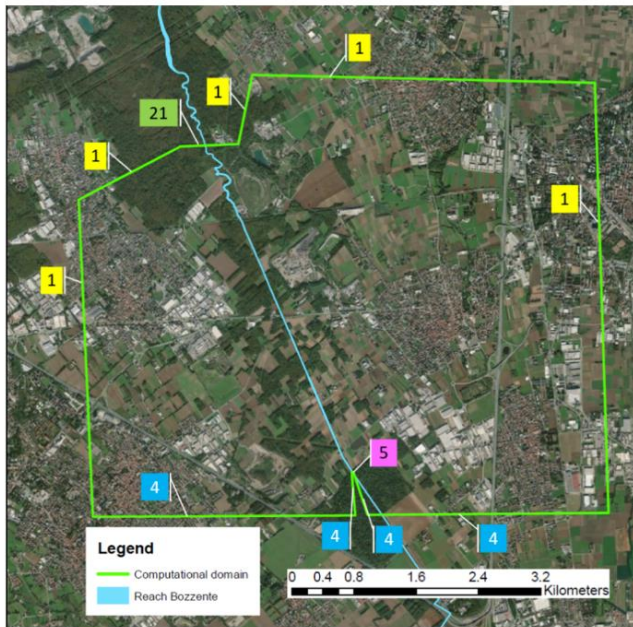
It has to be pointed out the fact that, probably due to the reduced dimensions of the river, the interaction between the boundaries of the computational domain and the polygon describing the initial condition has led, in many cases, to numerical instabilities, which could not be solved, if not by increasing the value of initial flow rate set as input for the simulations. Thus, in the following, the hydrographs represented beside the maps of the reaches, are those actually used in the simulations.

Another difference with respect to the study of the Seveso consists in the definition of the rating curves as boundary conditions. Indeed, here the law which best interpolates the known values from the PGRA 2015 is linear (with the exception of reach 5, where the downstream BC was already available at the section BZ 01).

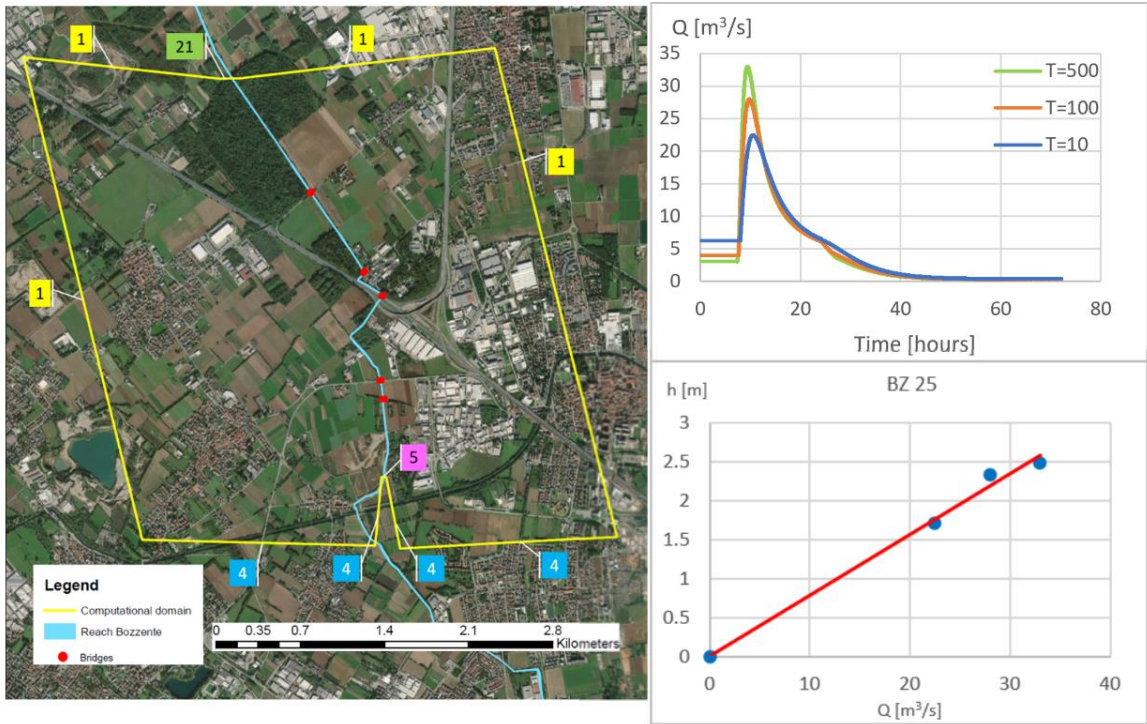
Reach	Length [km]	Upstream section	Downstream section	Transversal structures	Q (T=10) [m ³ /s]	Q (T=100) [m ³ /s]	Q (T=500) [m ³ /s]
1	5.31	BZ 75	BZ 58	0	20	39	60



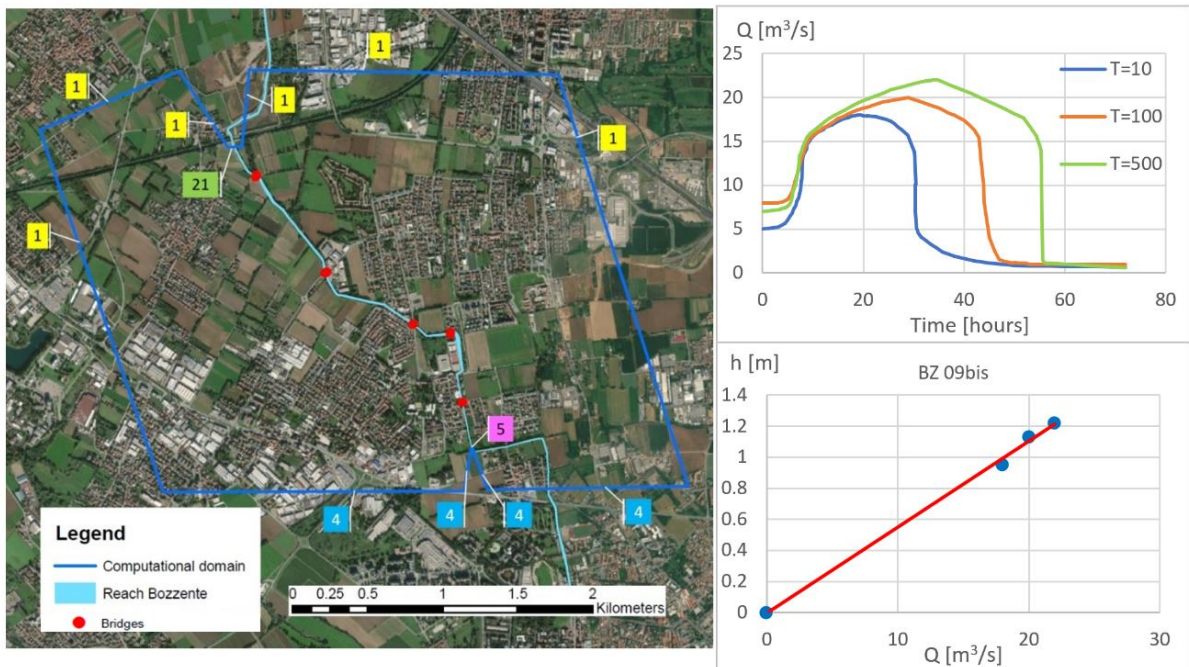
Reach	Length [km]	Upstream section	Downstream section	Transversal structures	Q (T=10) [m ³ /s]	Q (T=100) [m ³ /s]	Q (T=500) [m ³ /s]
2	5	BZ 58	BZ 43	0	22	43	67



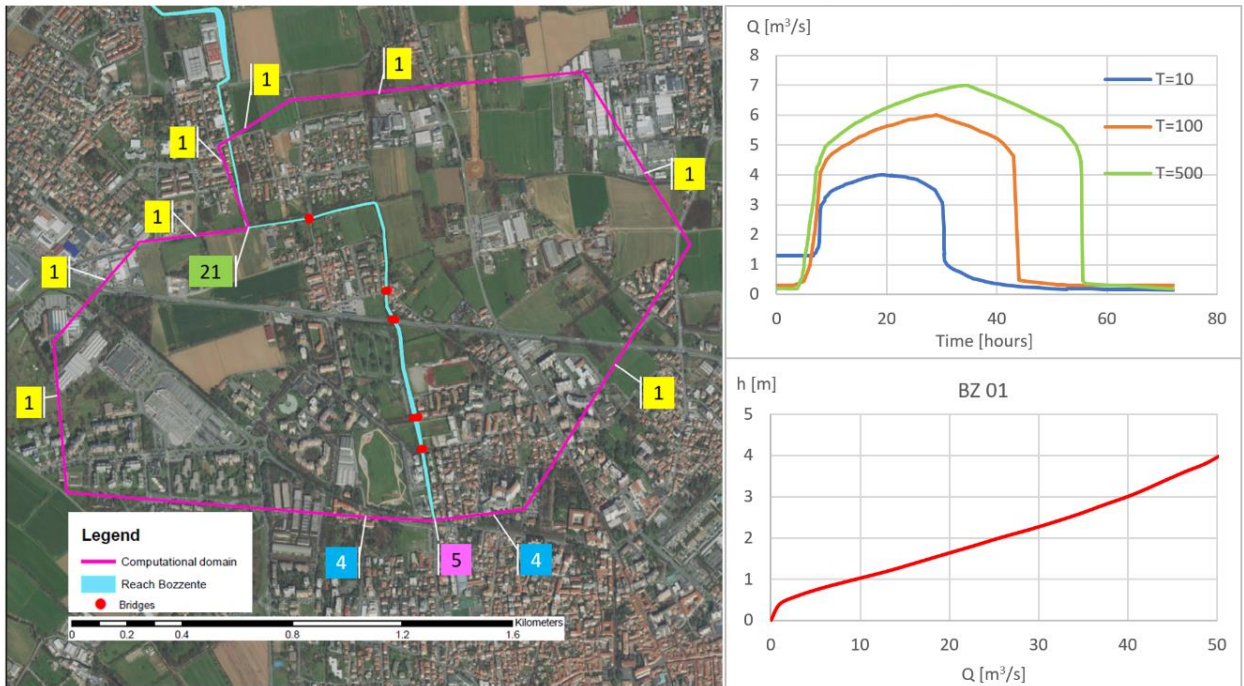
Reach	Length [km]	Upstream section	Downstream section	Transversal structures	Q (T=10) [m ³ /s]	Q (T=100) [m ³ /s]	Q (T=500) [m ³ /s]
3	4	BZ 43	BZ 25	5	22.5	28	33



Reach	Length [km]	Upstream section	Downstream section	Transversal structures	Q (T=10) [m ³ /s]	Q (T=100) [m ³ /s]	Q (T=500) [m ³ /s]
4	4	BZ 25	BZ 09bis	5	18	20	22



Reach	Length [km]	Upstream section	Downstream section	Transversal structures	Q (T=10) [m ³ /s]	Q (T=100) [m ³ /s]	Q (T=500) [m ³ /s]
5	1.67	BZ 09bis	BZ 01	5	4	6	7



4.2.3 Control sections for the flow rate distribution

Also in the case of Bozzente, a comparison between two different reaches for the same return period ($T=100$ y) is here illustrated. Reach 1 (Figure 4.11) and reach 3 (Figure 4.12) are shown with the respective flood maps and control sections. The hydrographs extracted from the control sections Bozzente are plotted in Figures 4.13 and 4.14.

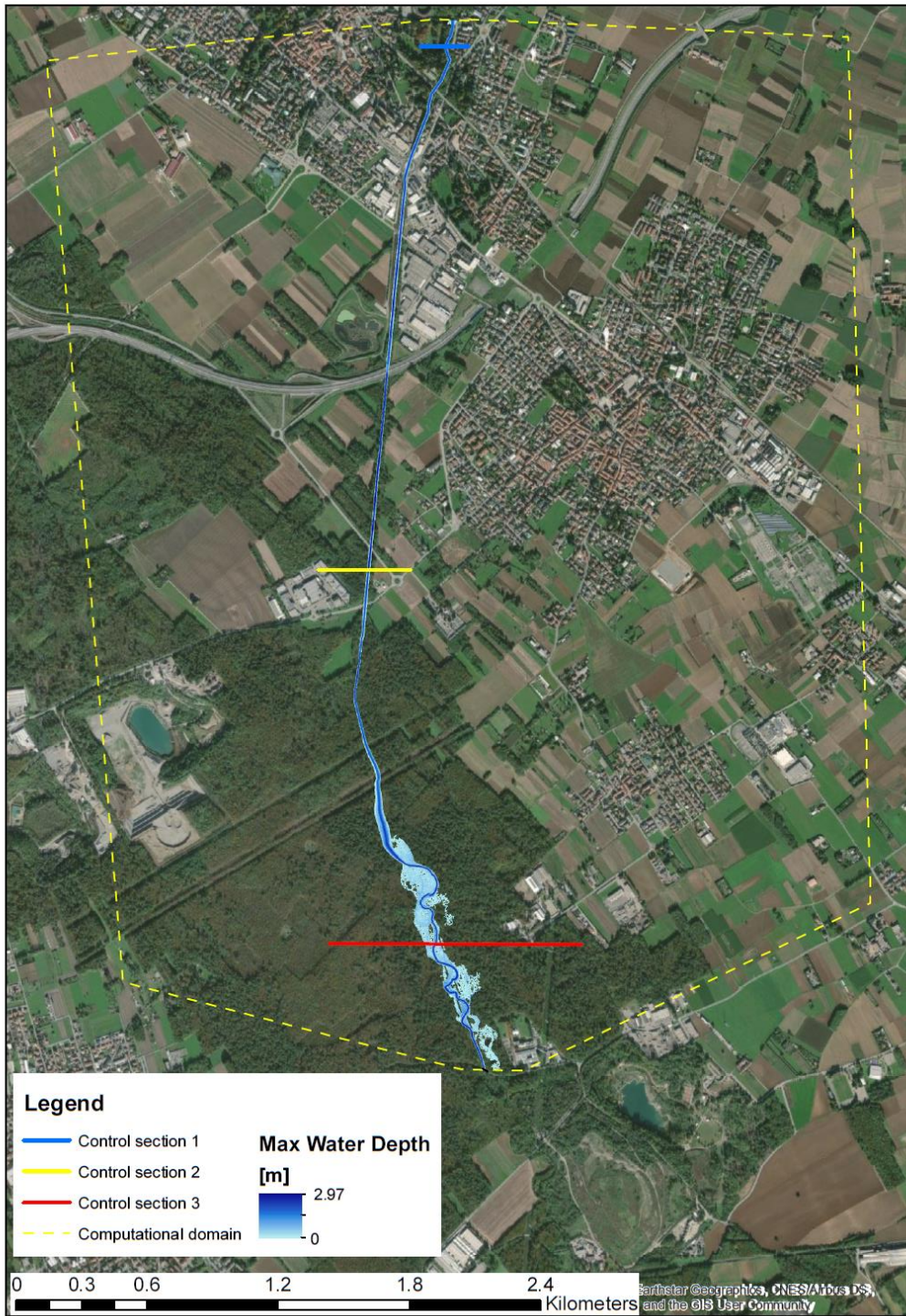


Figure 4.11: Control sections for the reach 1

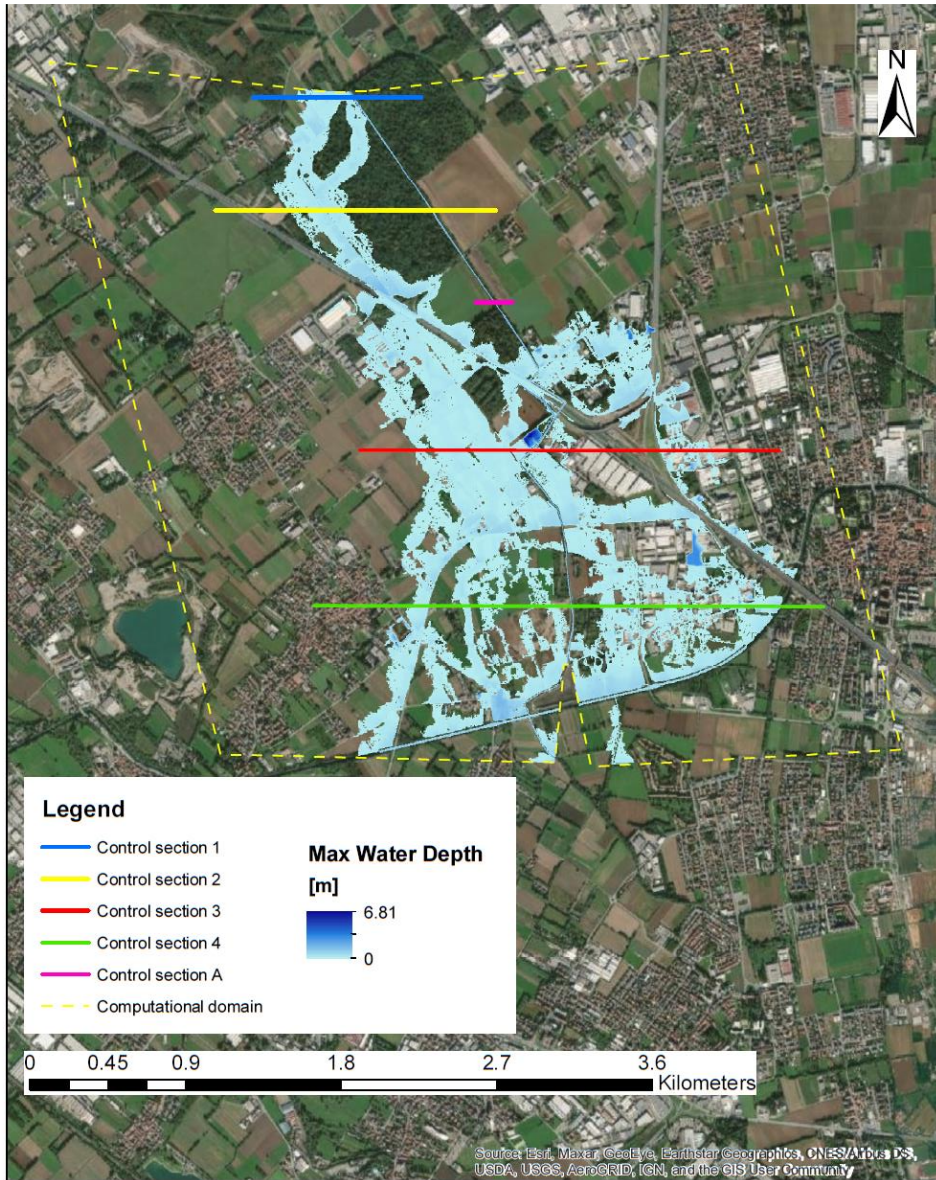


Figure 4.12: Control sections for the reach 3

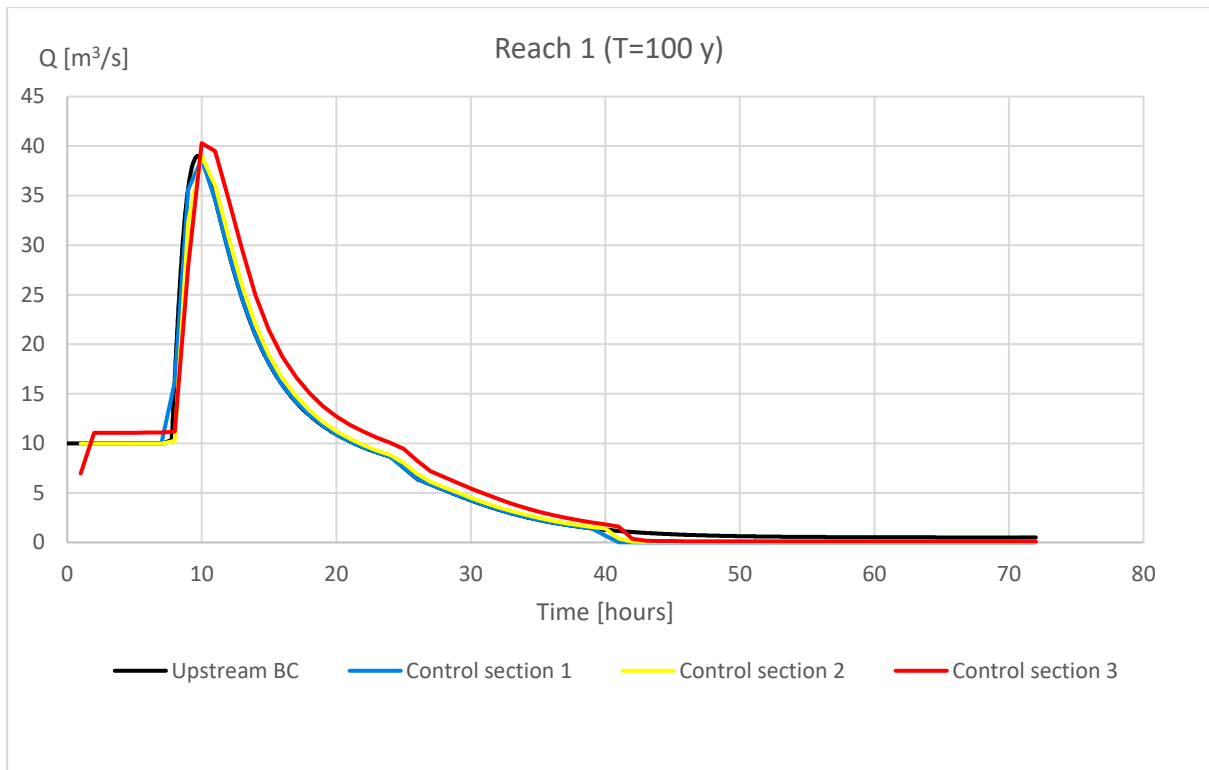


Figure 4.13: Hydrographs extracted from the control sections for the reach 1

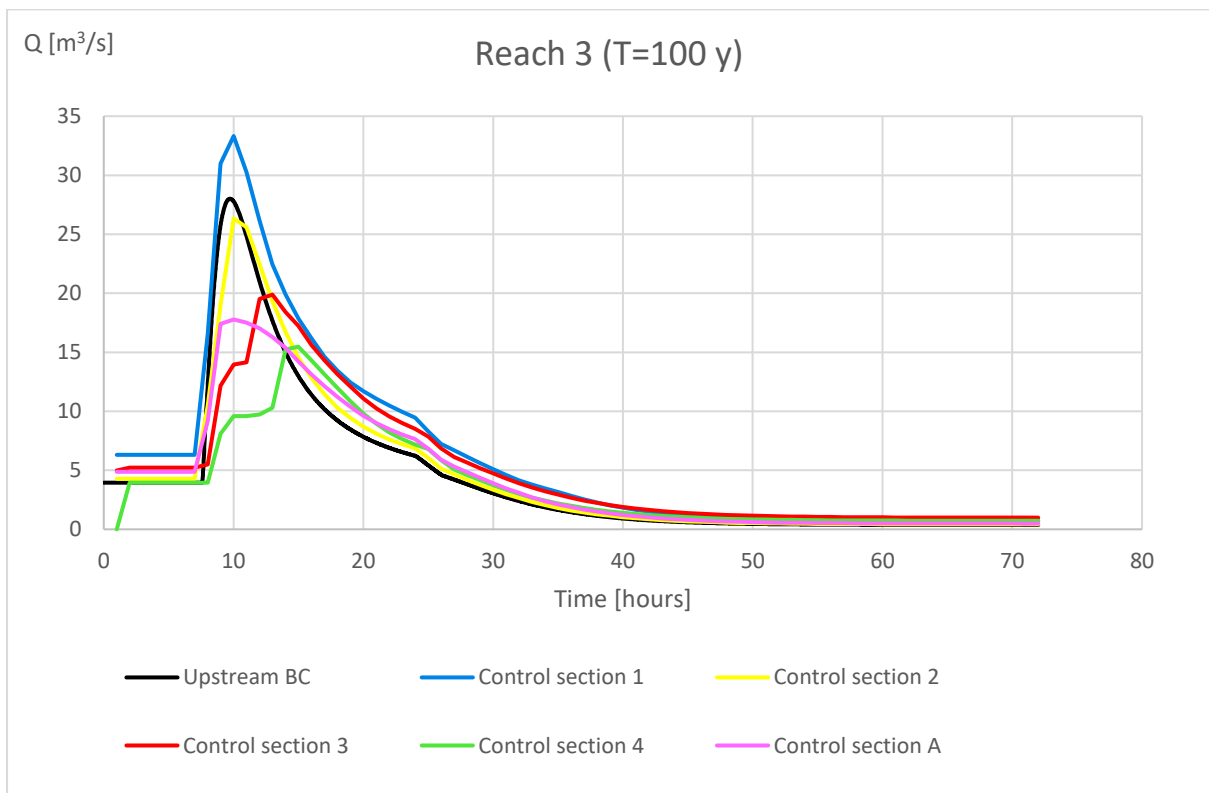
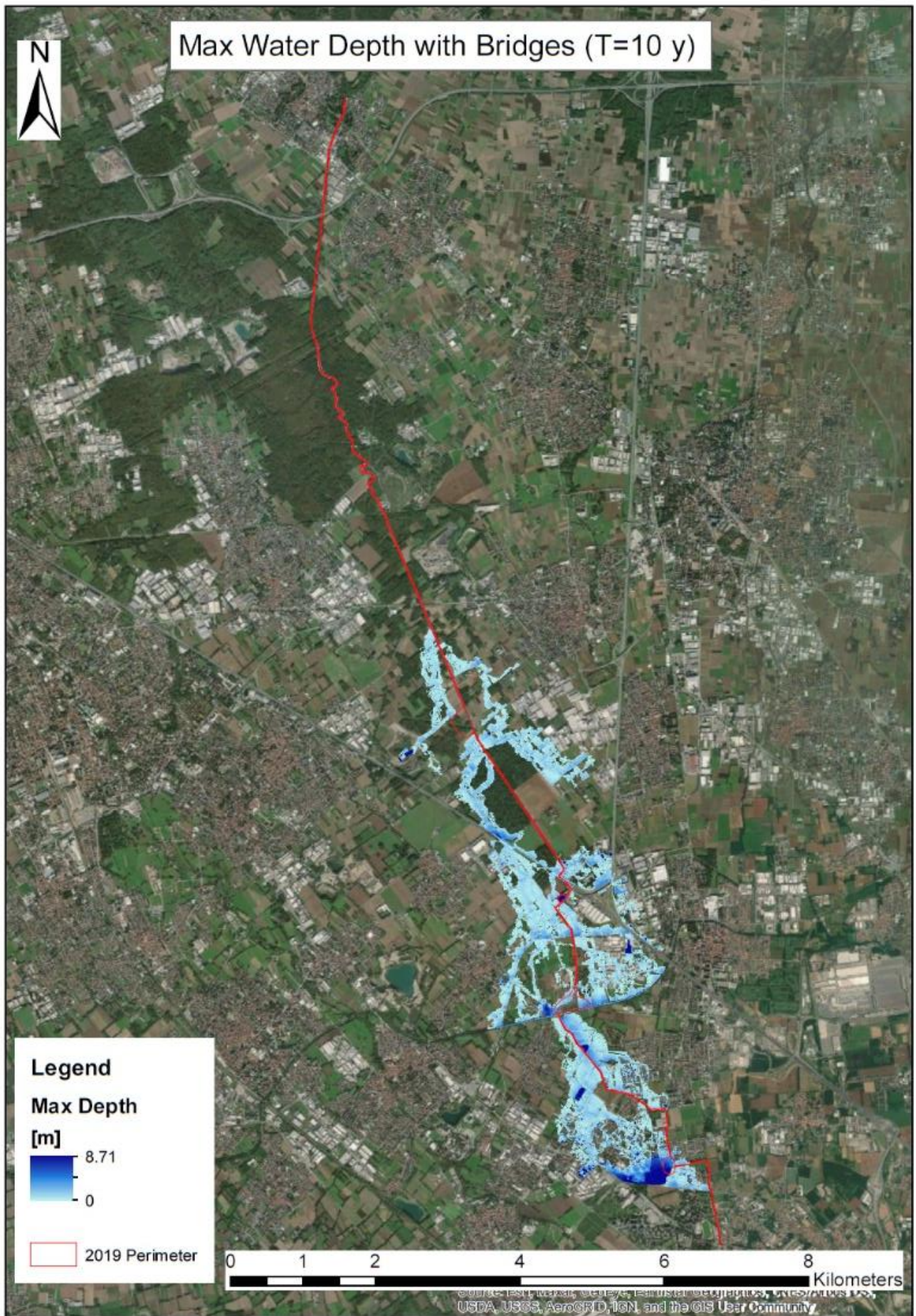


Figure 4.14: Hydrographs extracted from the control sections for the reach 3

4.2.4 Maps of the results

Max Water Depth	
Spatial distribution with bridges compared with the perimeter of the flood maps from 2019	Pp. 84-86
Spatial distribution without bridges	Pp. 87-89
Differences between max water depth distribution with and without bridges	Pp. 90-92
Max Velocity	
Spatial distribution with bridges compared with the perimeter of the flood maps from 2019	Pp. 93-95
Spatial distribution without bridges	Pp. 96-98
Differences between max velocity distribution with and without bridges	Pp. 99-101



Max Water Depth with Bridges (T=100 y)

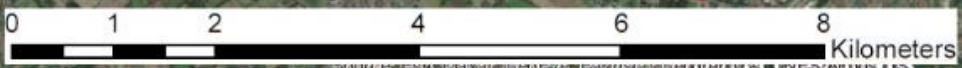


Legend

Max Depth
[m]

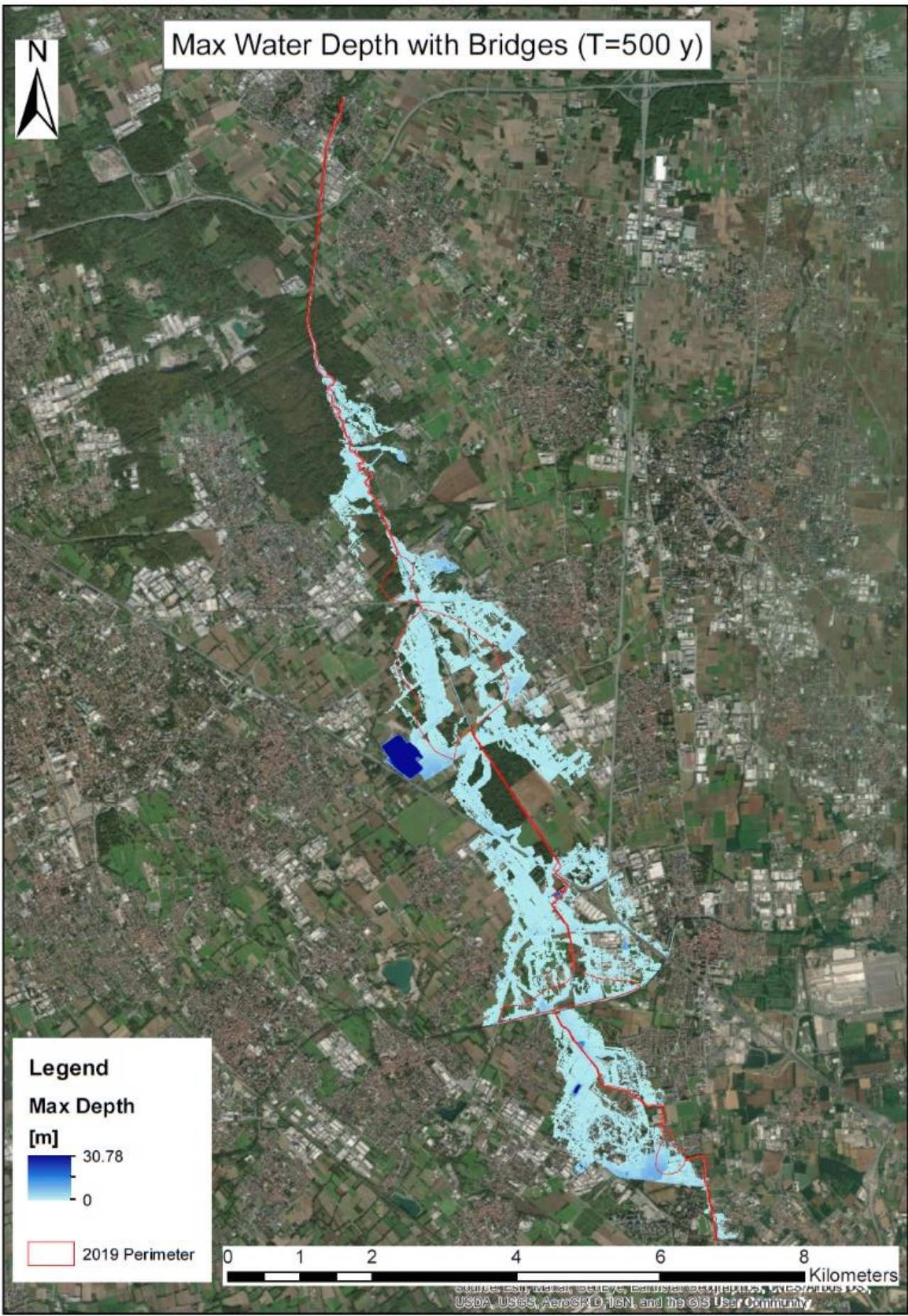
 30.78
0

 2019 Perimeter



© 2019 Esri, DeLorme, Garmin, IBM Corp., Intel, Intergraph, GEBCO, USGS, AeroGRID, IGN, and the GIS User Community

Max Water Depth with Bridges (T=500 y)



Legend

Max Depth
[m]

30.78
0

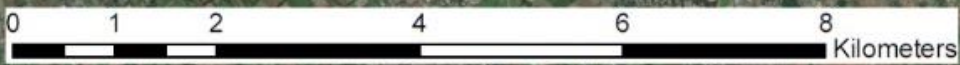
2019 Perimeter

0 1 2 4 6 8 Kilometers

Source: Esri, DigitalGlobe, GeoEye, Earthstar (Earthstar), CNES/Airbus DS, USDA, USGS, AeroGRID, IGN, and the GIS User Community

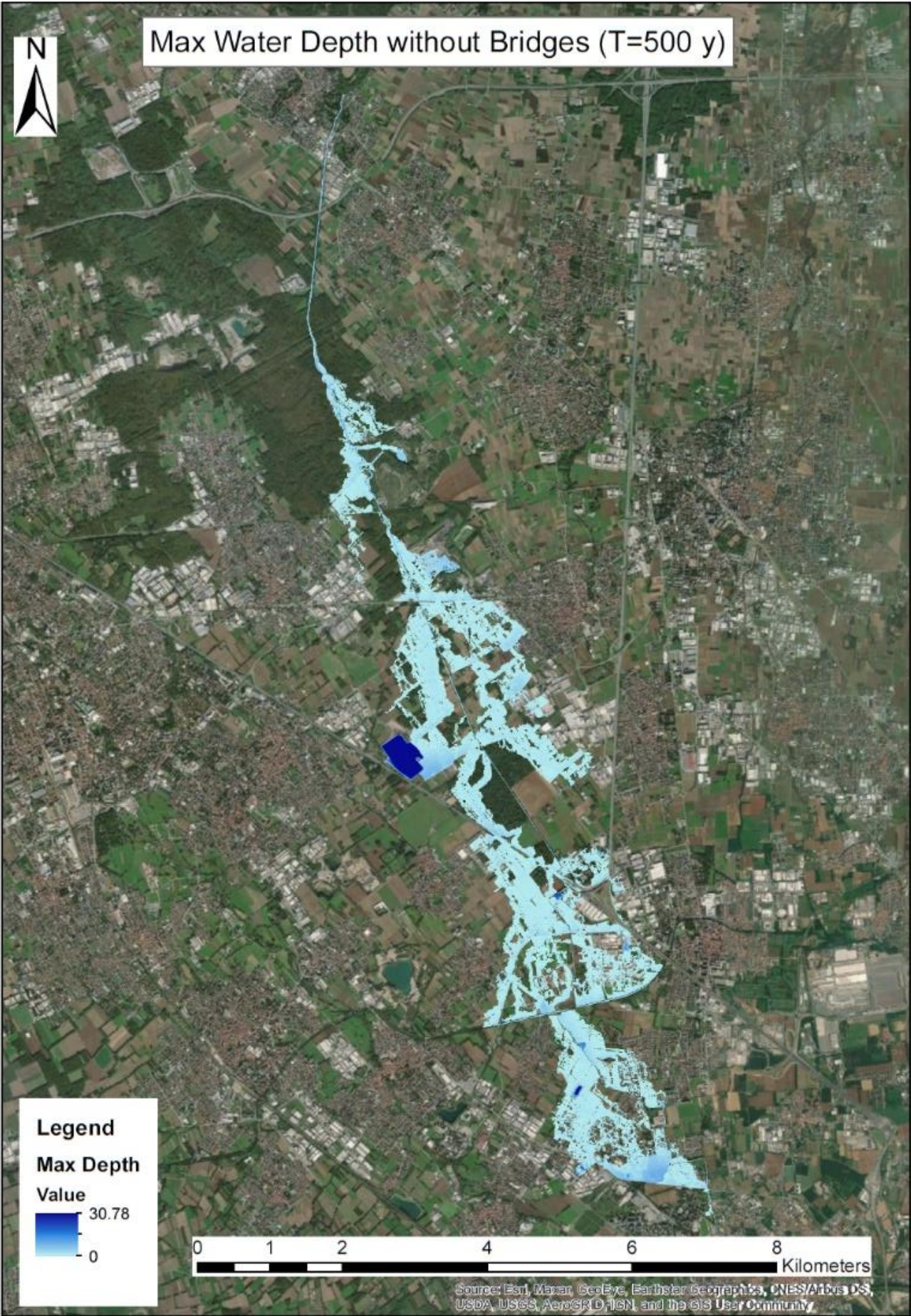


Max Water Depth without Bridges (T=100 y)

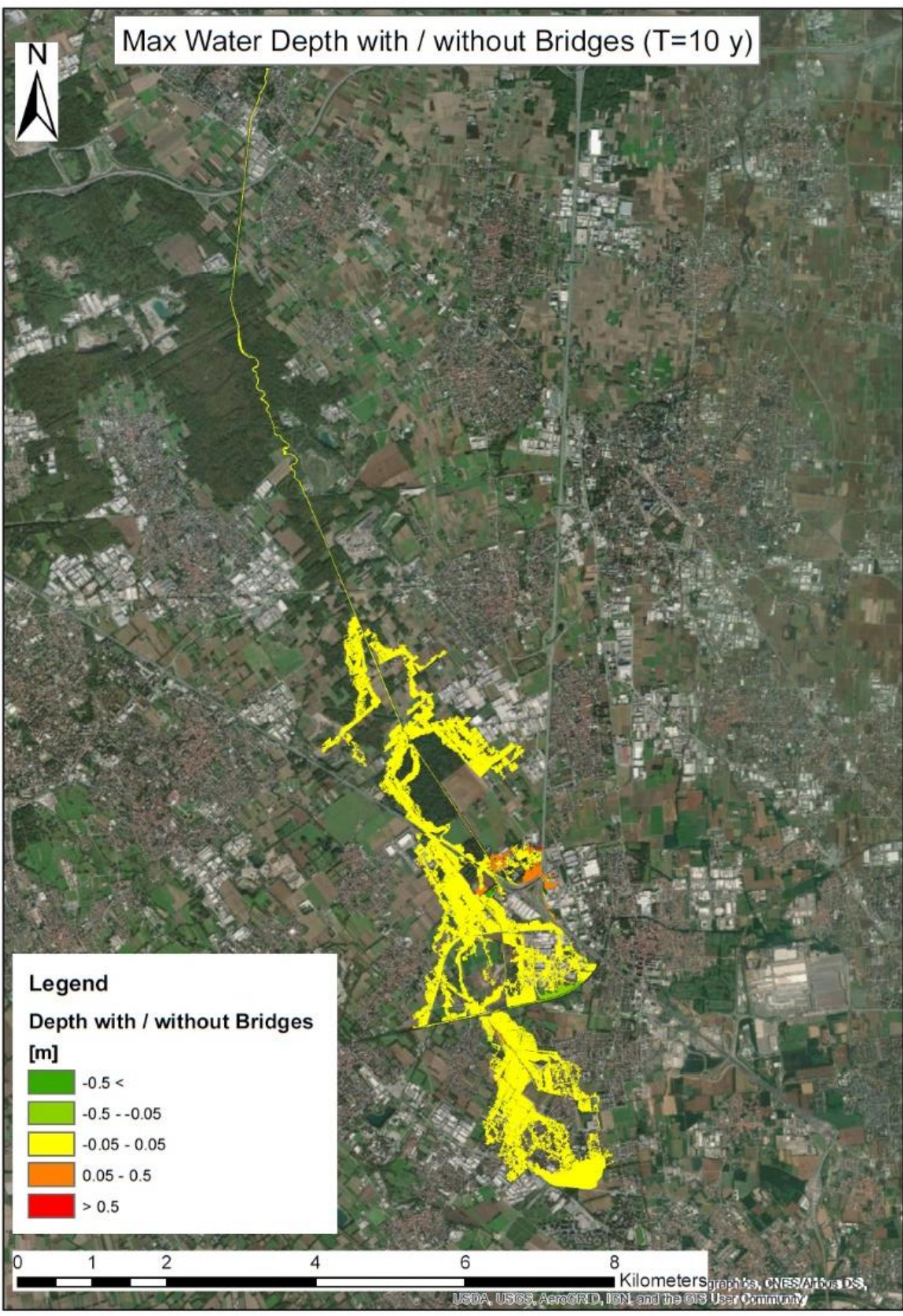


Source: Esri, Maxar, GeoEye, Earthstar Geographics, CNES/Airbus DS, USDA, USGS, AeroGRID, IGN, and the GIS User Community

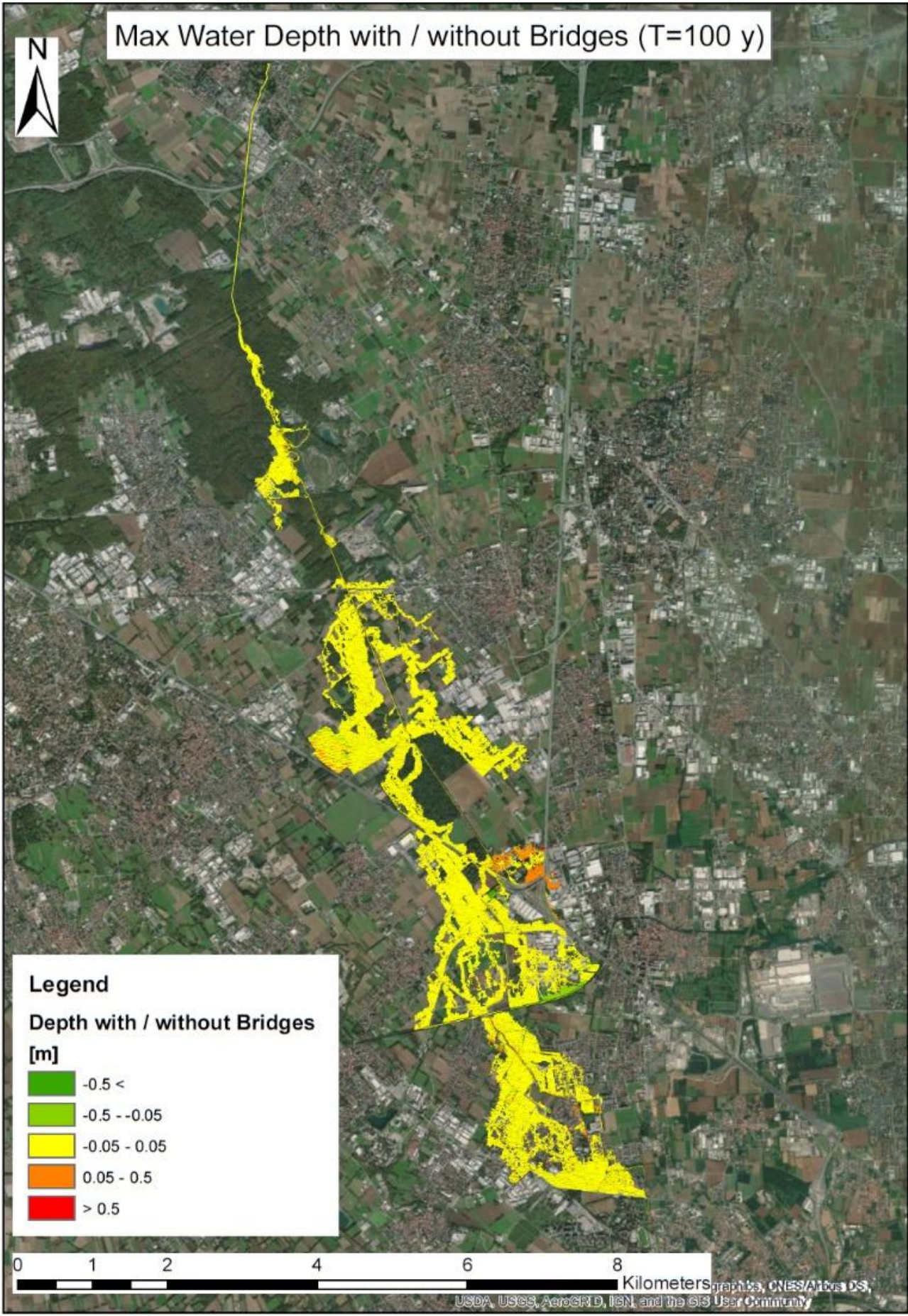
Max Water Depth without Bridges (T=500 y)



Max Water Depth with / without Bridges (T=10 y)



Max Water Depth with / without Bridges (T=100 y)

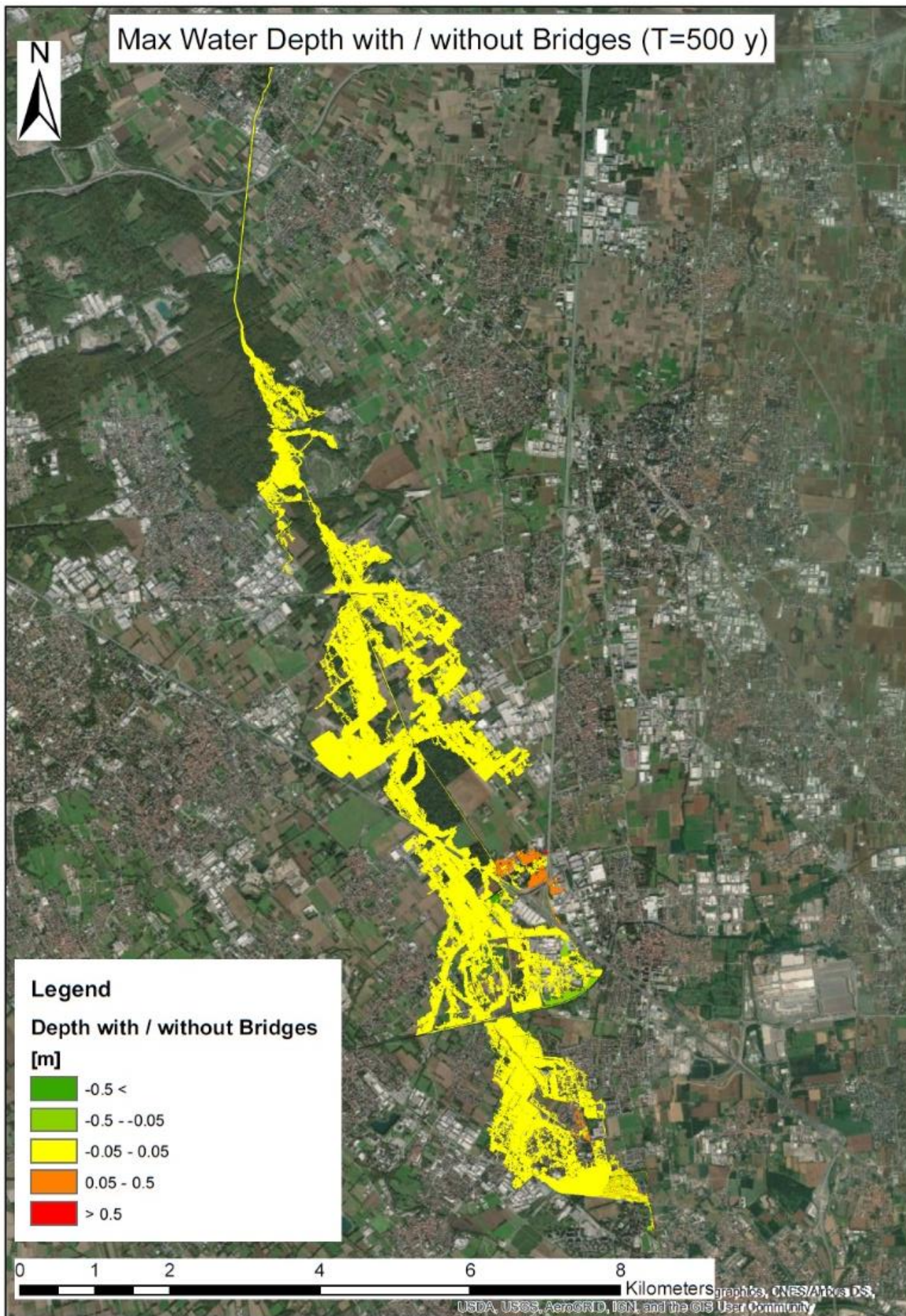


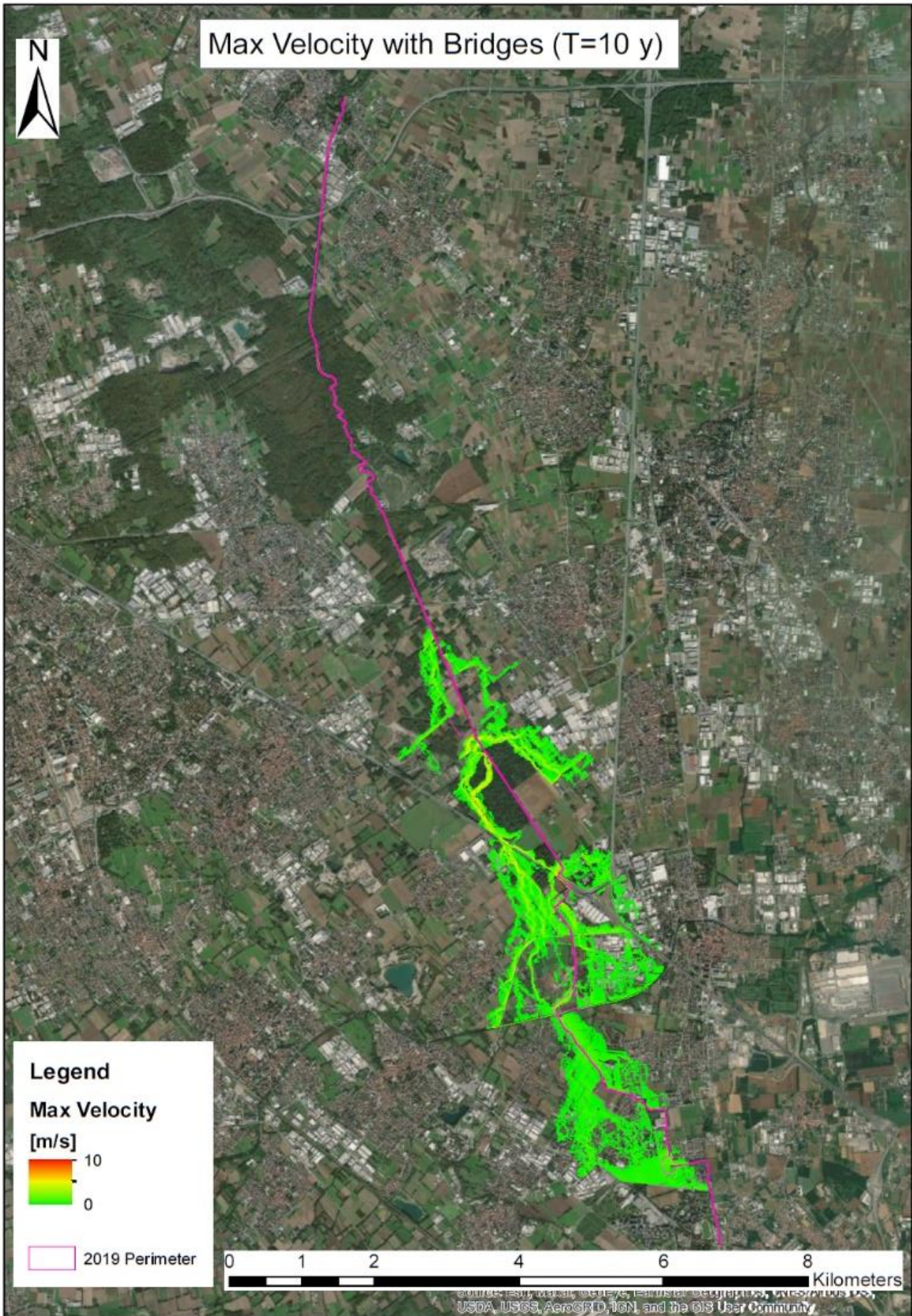
Legend
Depth with / without Bridges
[m]

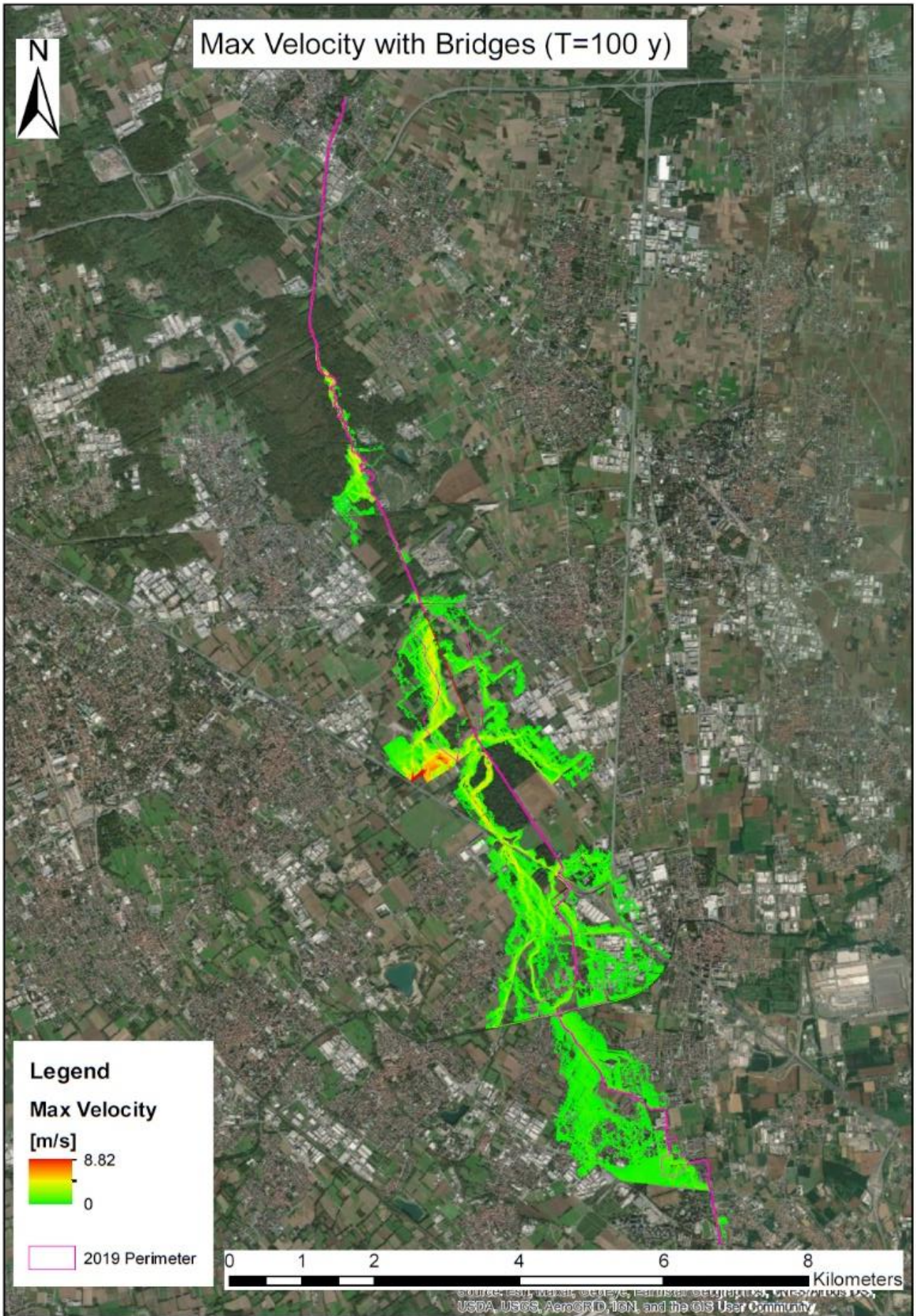
	-0.5 <
	-0.5 -- -0.05
	-0.05 - 0.05
	0.05 - 0.5
	> 0.5



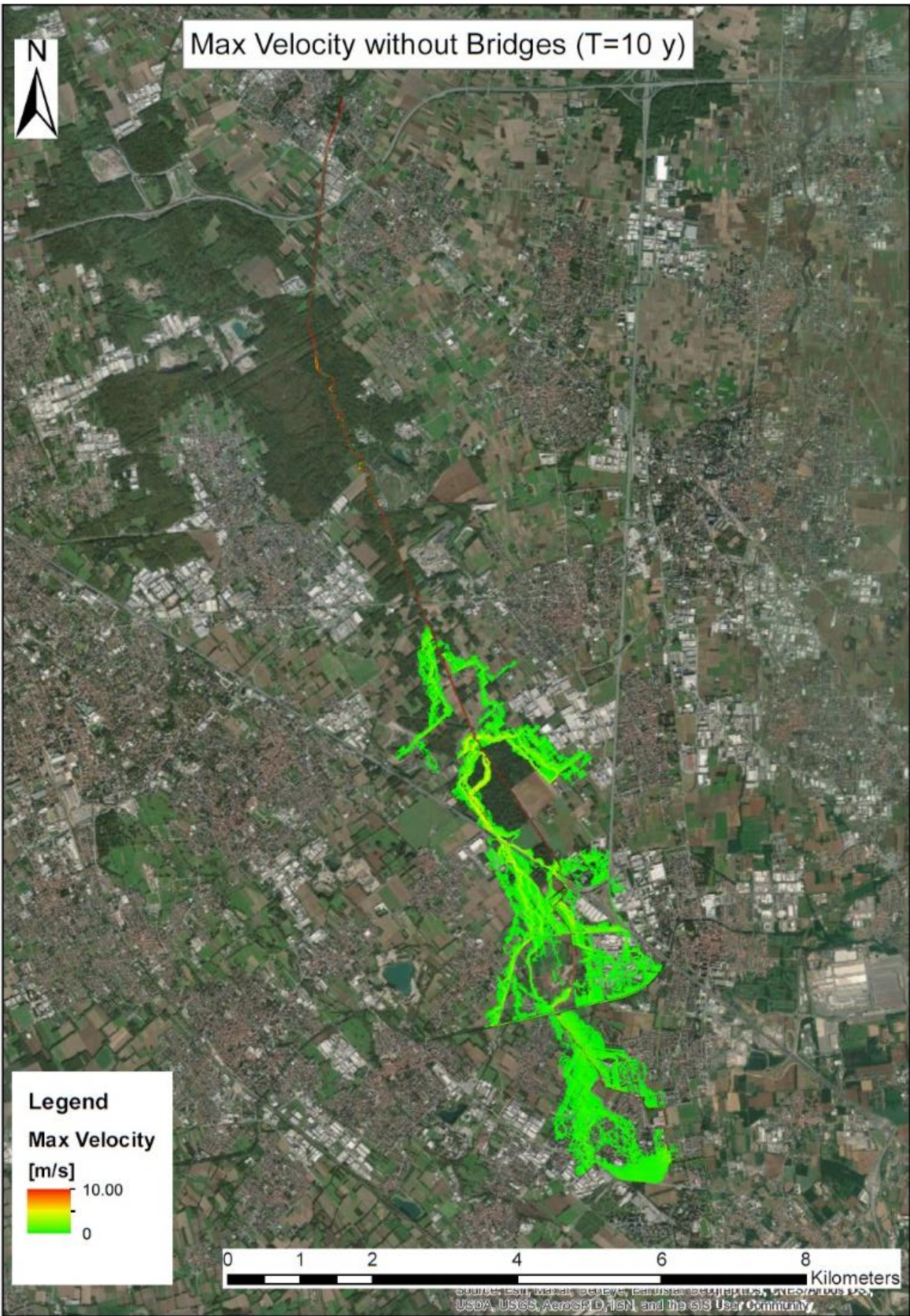
graphics, CNES/Airbus DS, USDA, USGS, AeroGRID, IGN, and the GIS User Community







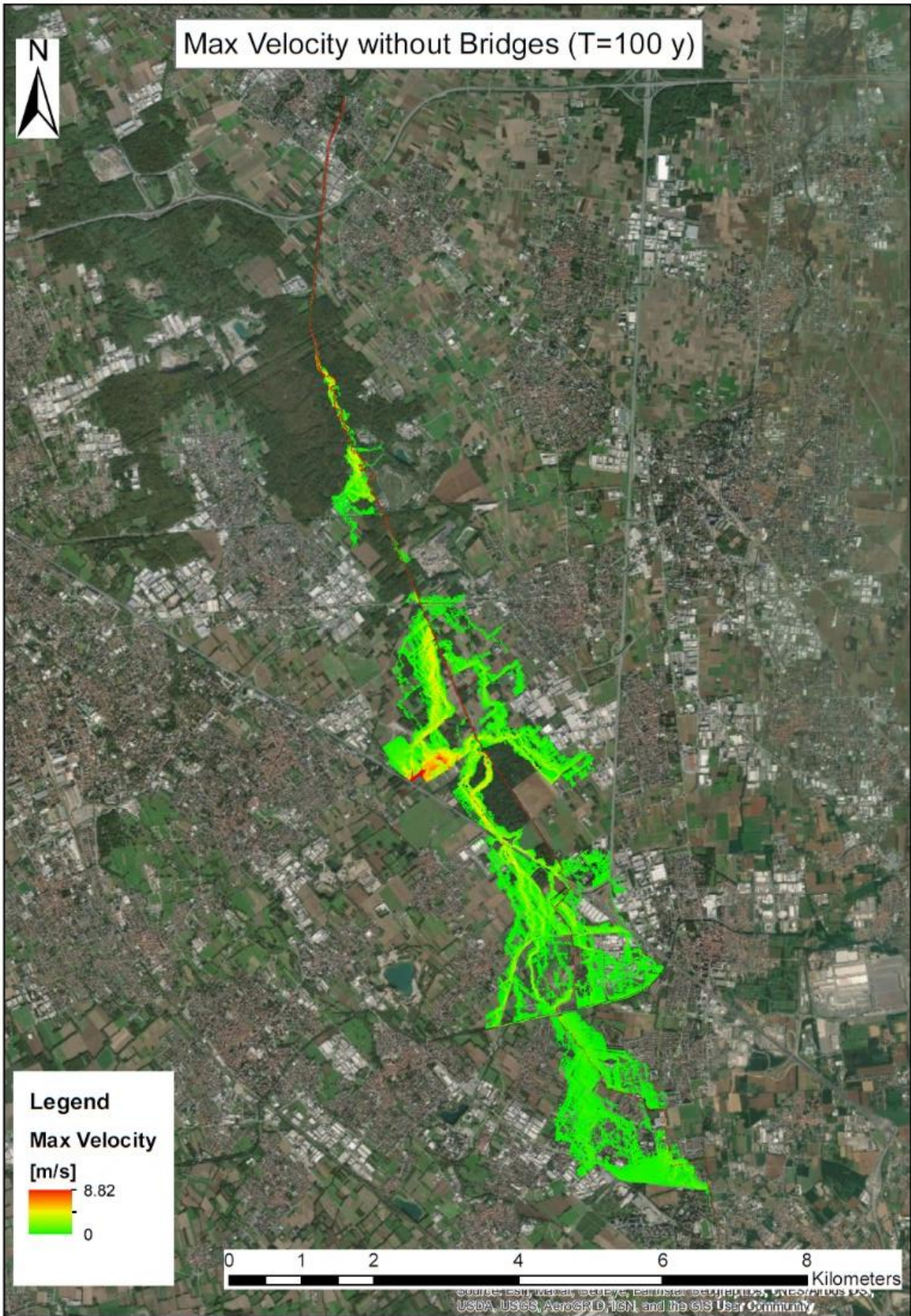
Max Velocity without Bridges (T=10 y)



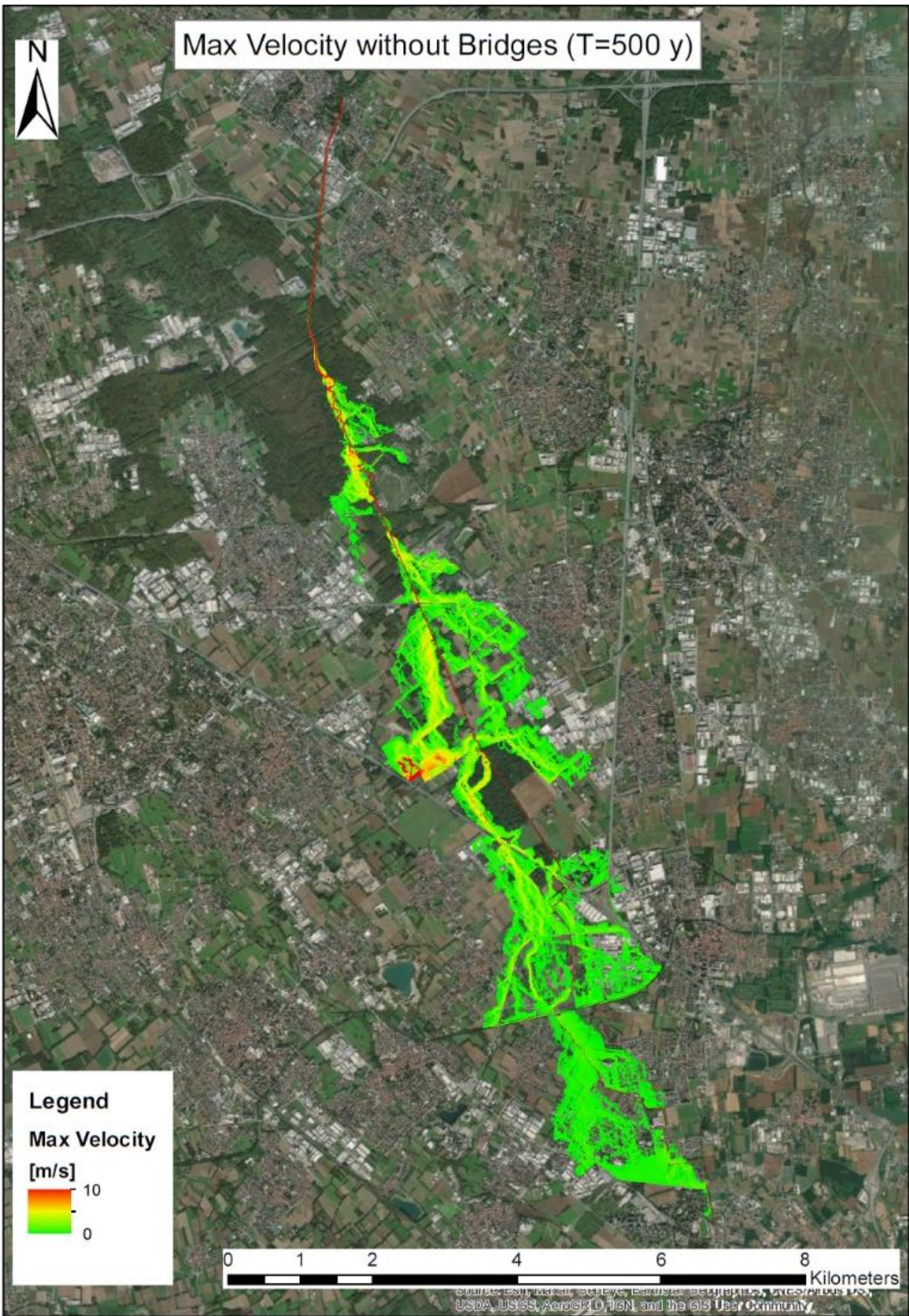
Legend
Max Velocity
[m/s]
10.00
0

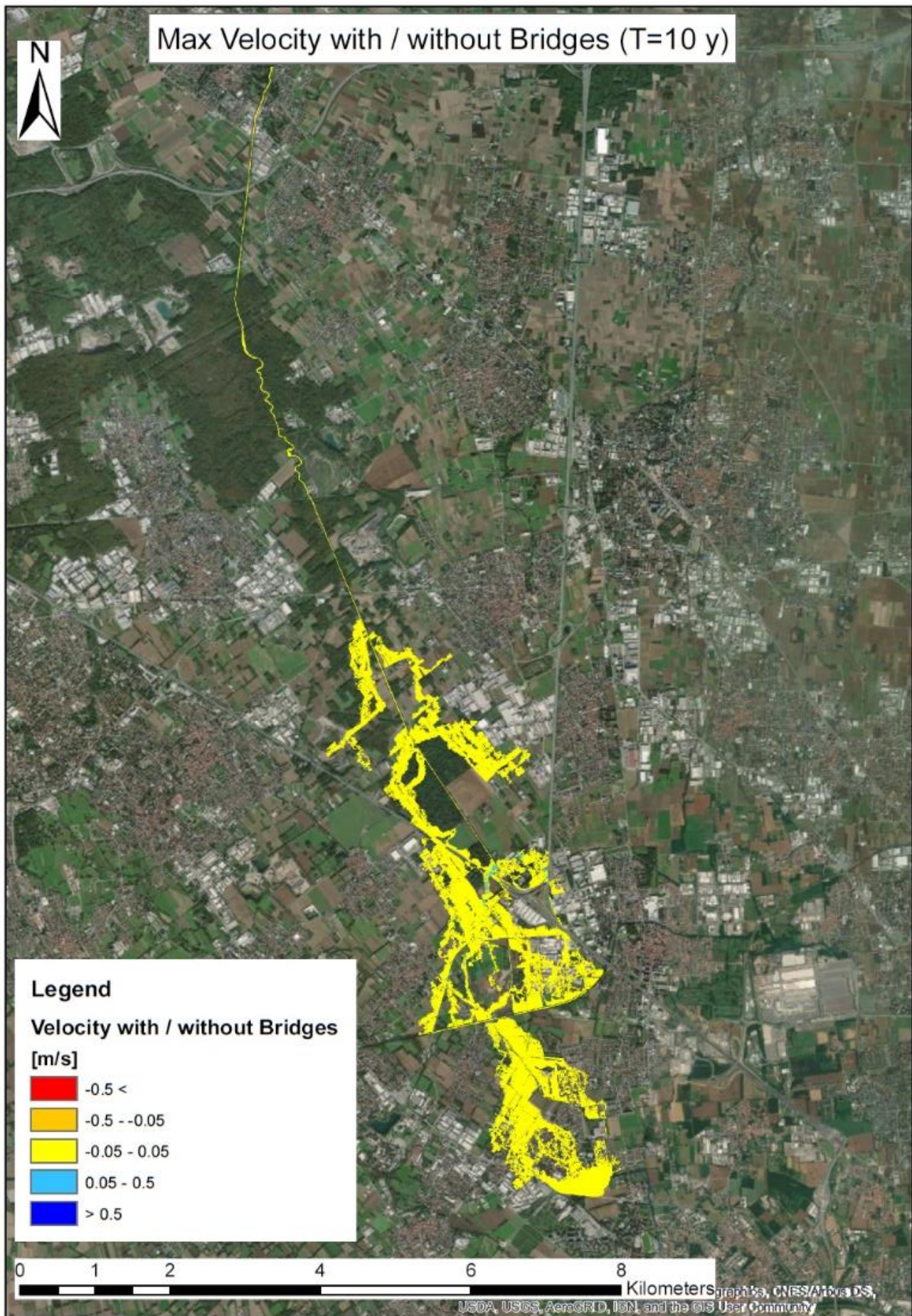
0 1 2 4 6 8 Kilometers

Source: Esri, Maxar, GeoEye, Earthstar, DigitalGlobe, GeoEye, IGN, Aerogrid, IGN, and the GIS User Community

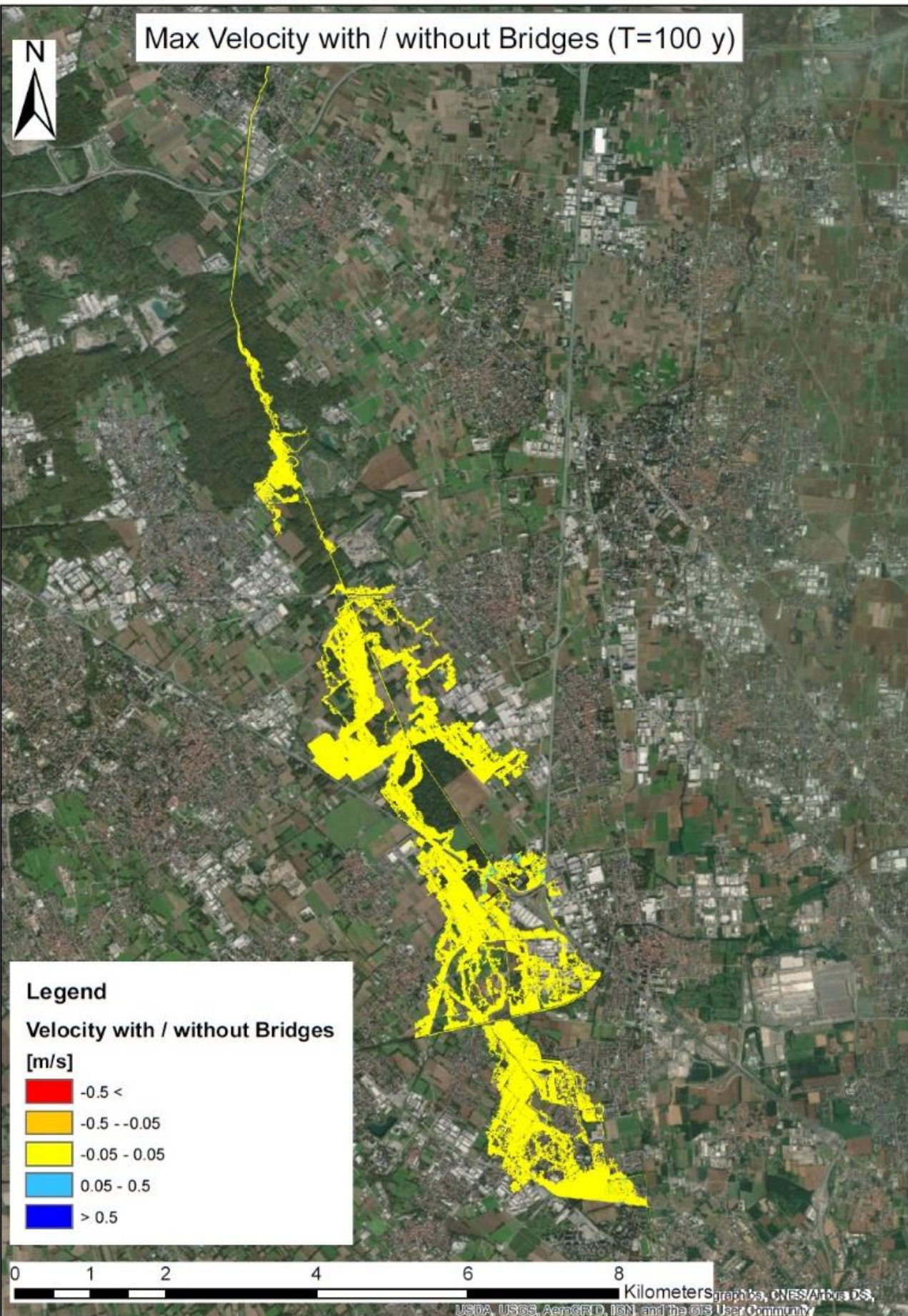


Max Velocity without Bridges (T=500 y)





Max Velocity with / without Bridges (T=100 y)



Legend

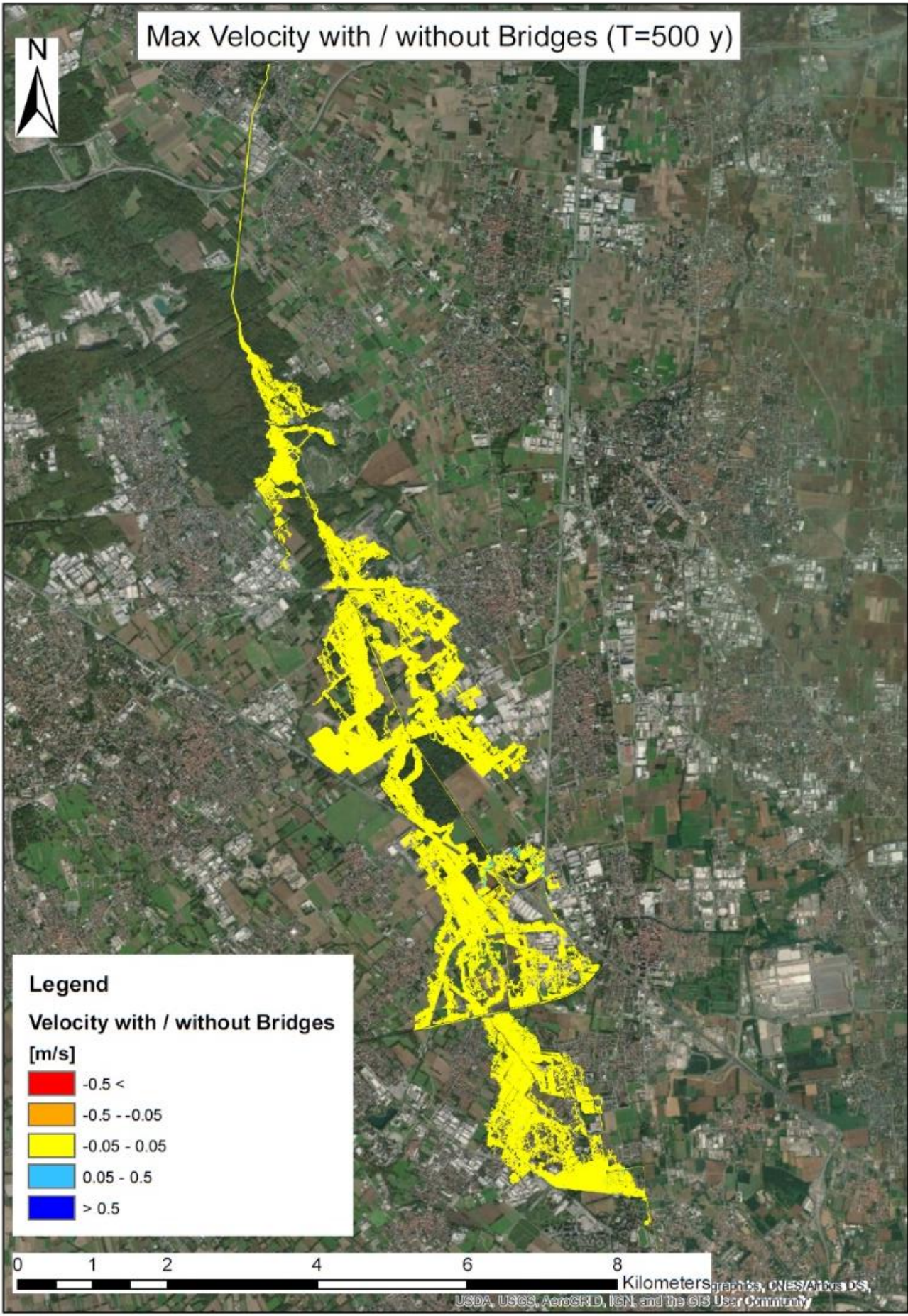
Velocity with / without Bridges

[m/s]

-  -0.5 <
-  -0.5 -- -0.05
-  -0.05 - 0.05
-  0.05 - 0.5
-  > 0.5



Max Velocity with / without Bridges (T=500 y)



4.3 General comments

As a general comment concerning the flood wave propagation for the Seveso and the Bozzente, one can say that, as expected, both the water depth and the velocity values in correspondence of the riverbed result much higher than those in the surrounding floodplains. Indeed, apart from some singularities, represented by the terrain configurations (e.g. the quarry on the hydrographic right of the Bozzente) or numerical instabilities (limited to few anomalous cases), the values are contained in physically justifiable ranges.

Furthermore, as one can notice from the flood perimeter, in the upstream reaches of the two streams, where the riverbed is closer to the natural conformation, the flooded areas are more restricted with respect to the downstream, more urbanized, regions. Indeed, moving from North to South in the area of the APFSR, the ground elevation gradient attenuates, so the flood perimeter extent is more likely to widen, even for low return periods.

As a further consideration, it is worth pointing out that the effect of the introduction of the bridges in the modelling is more evident in terms of water depth values, than in terms of flood extension. In particular, as expected, the differences in depth are higher in the proximity of the bridges than elsewhere.

Finally, as one can notice from the maps of the differences between simulations with and without bridges, in the case of Bozzente, the distribution of values is centred on the class close to zero. This does not happen in the case of the Seveso, because of the strong effect that the bridges have on the flow. The reason for this can be found in the fact that, in the model for the Bozzente, only 15 transversal structures could be inserted, while the Seveso is crossed by more than 70 bridges.

5. Critical discussion of the results and further developments

This chapter presents an overview of several issues emerged after the modelling work performed for this thesis. It is stressed that a modelling result is always a compromise between modelling objectives, data available as input, and modelling resources; therefore, high possibility for improvement of the obtained maps still exist.

5.1 Observations

5.1.1 Downstream BC

As shown in *Sections 4.1.2* and *4.2.2*, different types of boundary conditions have been applied at the downstream segments of the computational domain (numbers 1,4,5,3).

Conditions 5 and 3 are specifically applied at the outlet segment, where, respectively, a rating curve or a constant level need to be set as downstream BC. On the other hand, the segments of the computational domain which do not intersect the river need to be characterized as capable to be crossed by water or not. Thus, a different flood propagation is expected according to the presence of condition 1 (wall) or 4 (free flow or “far field”) on the segments at issue (Cfr. *Section 3.5*). Moreover, because the rating curve used as downstream BC comes from a correspondence elevation/discharge computed through a 1D model from the “Studio di fattibilità”, the section along which this correspondence has been defined could not be the same as to the downstream section of the computational domain defined in the 2D model. Thus, uncertainty can arise about the most representative condition to impose.

As an example, *Figure 5.1* shows the effect of the condition 4 “far field” on the water depth distribution, whose extension decreases due to the capability of the water to flow undisturbed through the boundaries of the computational domain.

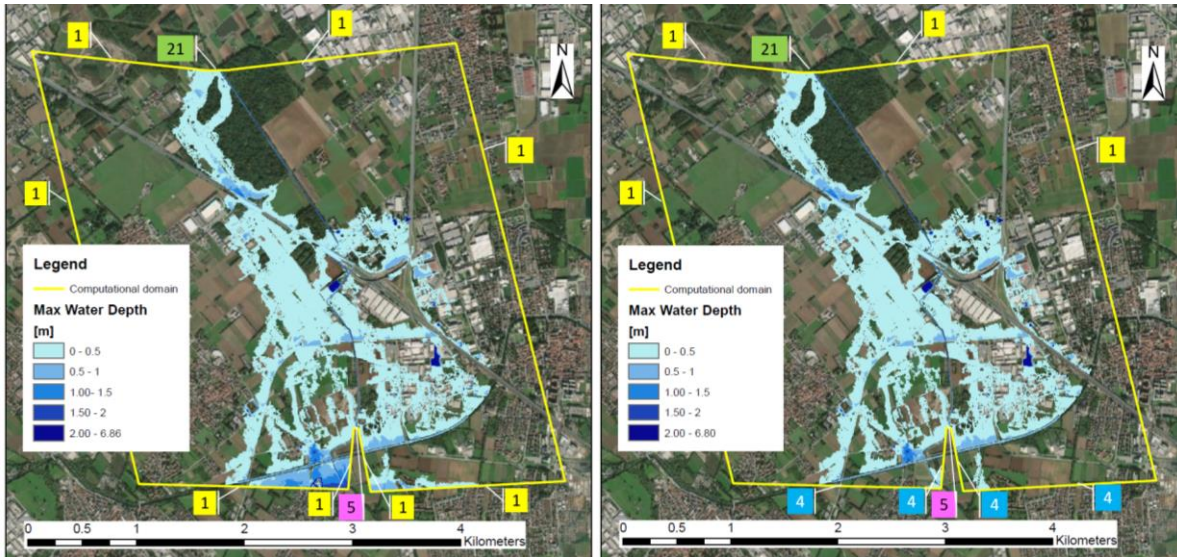


Figure 5.1: Comparison between results imposing condition 5 (left) and condition 4 (right)

A consequence of the behaviour illustrated in pictures above, could be that, by selecting the far field as boundary, an underestimation of the flooded area can occur.

5.1.2 PARFLOOD vs Perimeters 2019

As already mentioned in *Section 1.4*, the motivation behind this thesis work is represented by the need to for defining a methodology suitable for a full 2-dimensional flood modelling on a large scale. In this way, an update of the maps produced in 2019 has been achieved. A comparison between the two version of the flood maps for the Seveso and Bozzente has therefore been performed, as explained in *Section 3.7.4*.

It has to be said that, as a general observation about the similarity between the two results, the flood maps obtained with PARFLOOD are characterized by a wider extent with respect to those from 2019. In the areas of the rivers in which the thalweg is depressed enough with respect to the surrounding ground level, or where the embankments are tall enough not to be overtopped, or finally where the valley is narrow and V shaped, the boundaries of the 2019 maps follow quite accordingly those of the maps made with PARFLOOD. Elsewhere, large differences exist between the perimeters returned by the two approaches.

5.2 Limitations of the model

5.2.1 Boundary conditions for consecutive reaches

As a direct consequence of the partition of the watercourse in sub-reaches, the flow hydrograph obtained at the downstream end of a reach is not necessarily equal to that used as upstream BC for the following one. Indeed, from *Figure 5.2*, an example can be seen referring to the joint between downstream section of reach 2 and upstream BC of reach 3.

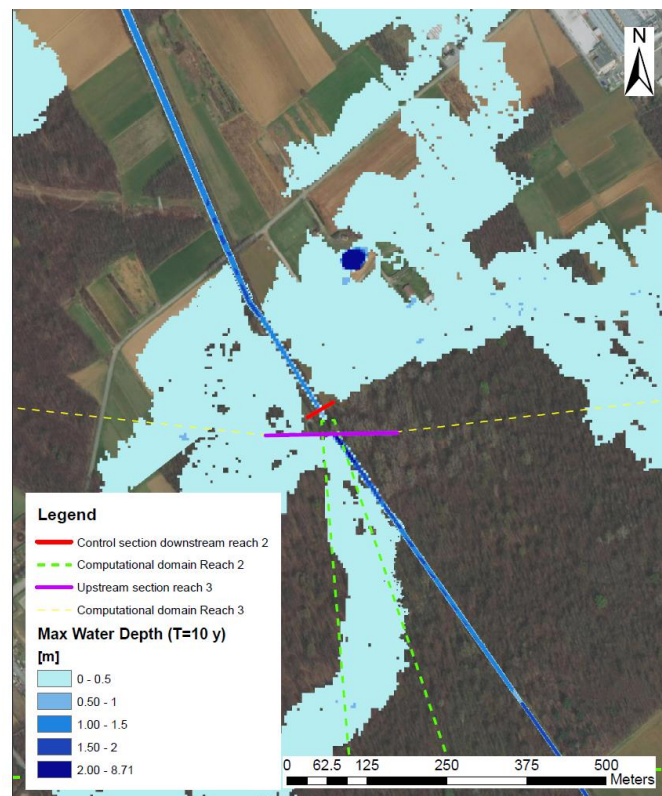


Figure 5.2: Representation of control section of reach 2 and upstream section of reach 3, Bozzente river

The flow rate distribution at the control section downstream reach 2 and the hydrograph used as upstream BC in reach 3 are plotted together in *Figure 5.3*. In the chart, the hydrograph set as upstream BC for reach 2 is represented as well. The two BCs are almost identical to each other, while the hydrograph obtained at the end of reach 2 is much lower due to a significant flooding occurred in reach 2 according to the numerical model.

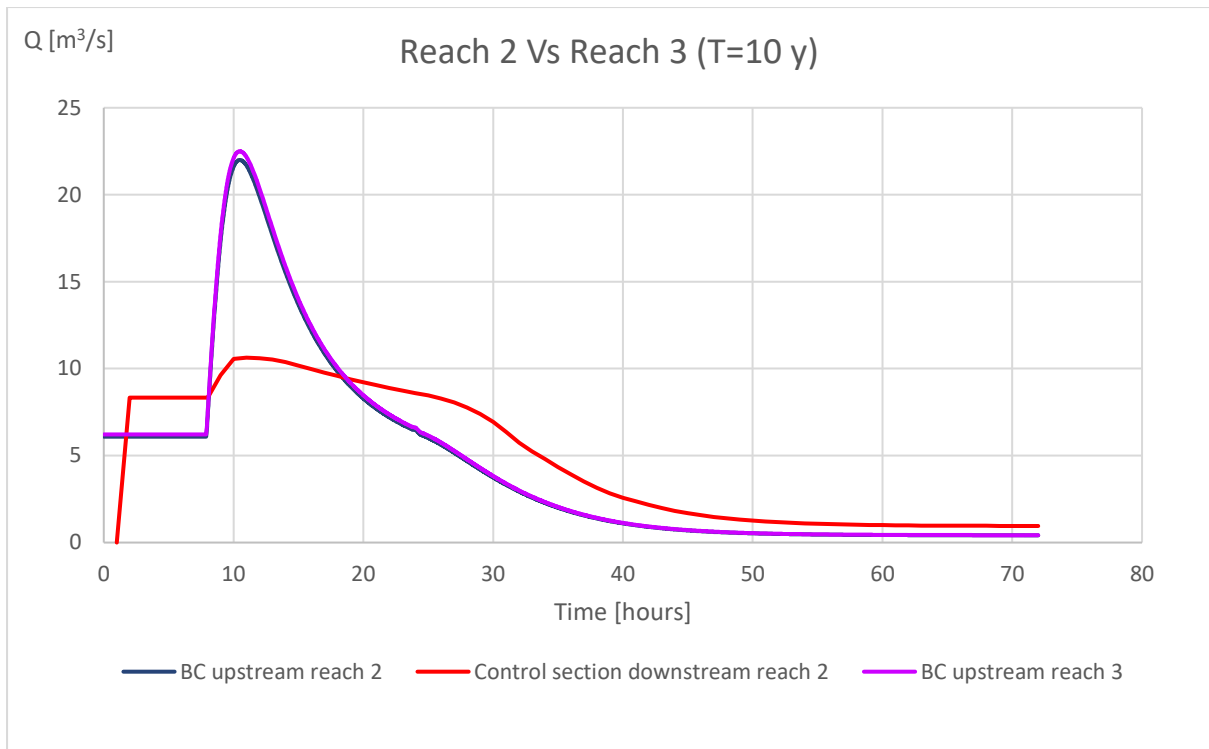


Figure 5.3: Flow rate distributions at downstream control section reach 2 and input hydrograph reach 3

5.2.2 Punctual inflows

In the current model deployed for Seveso and Bozzente, the presence of water inflows in the main watercourses has been approached introducing some simplifications regarding:

- Punctual inflows due to the urban drainage system: their contribution has been taken into account by updating, for every sub reach, the upstream boundary condition. In this way, where necessary, the flow rate in the hydrograph, upstream a specific reach, results increased according to the presence of punctual inflows along the reach immediately upstream. This is the case, for example, of the Bozzente, where the peak values of the flow rate related to consecutive reaches (the downstream value higher than the upstream one), have been averaged not to completely disregard the inflow coming from the urban drainage system.
- Junctions between the main watercourses and the relative tributaries, such is the case of the Seveso: the stream receives water from the Rio Acquanegra, Serenza and Certesa, whose contribution is taken into account with the increase in peak discharge in correspondence of the section immediately after the confluences (Cfr. Figure 4.1). Also in this case, this results in updating the BC upstream the following sub reach.

In the case of the urban drainage inflows, the only possible solution to take them into account would be piercing the computational domain as shown in *Figure 5.4*. In this way, the segment adjacent to the watercourse could be considered as inflow section where the boundary condition describing the inflow should be applied. Unfortunately, this obviously would create an interference with the flood propagation, with the boundary of the computational domain that cuts the floodplain.

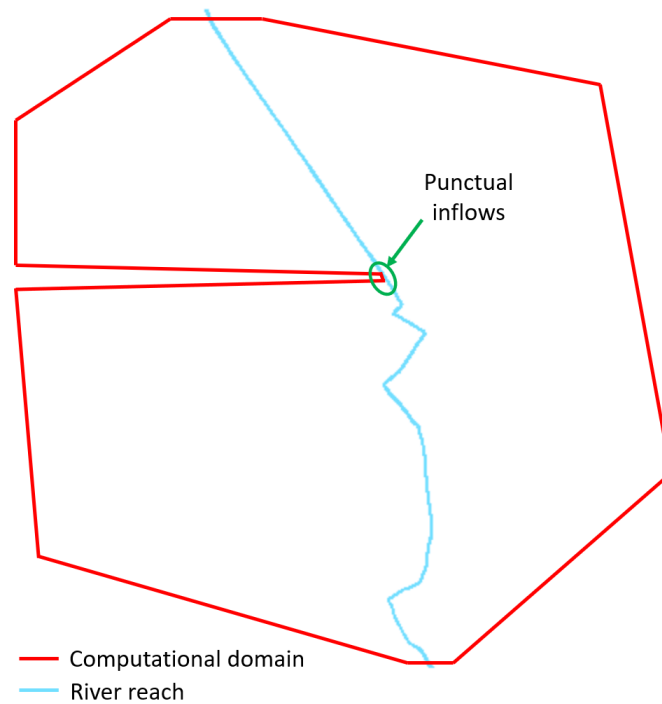


Figure 5.4: Sketch of computational domain needed to insert punctual inflows

On the other hand, to model the confluence of the tributaries in the mainstream, the computational domain should be outlined in such a way to have to entrance sections in correspondence of the main watercourse and the affluent (*Figure 5.5*), both characterized by the correspondent upstream boundary condition (i.e. hydrograph). The difficulty in this approach consists of the lack of data necessary to characterize the affluent, both in terms of geometry and hydrographs. Indeed, as a part of the computational domain, the 2-dimensional modelling needs to run in correspondence of the tributary as well.

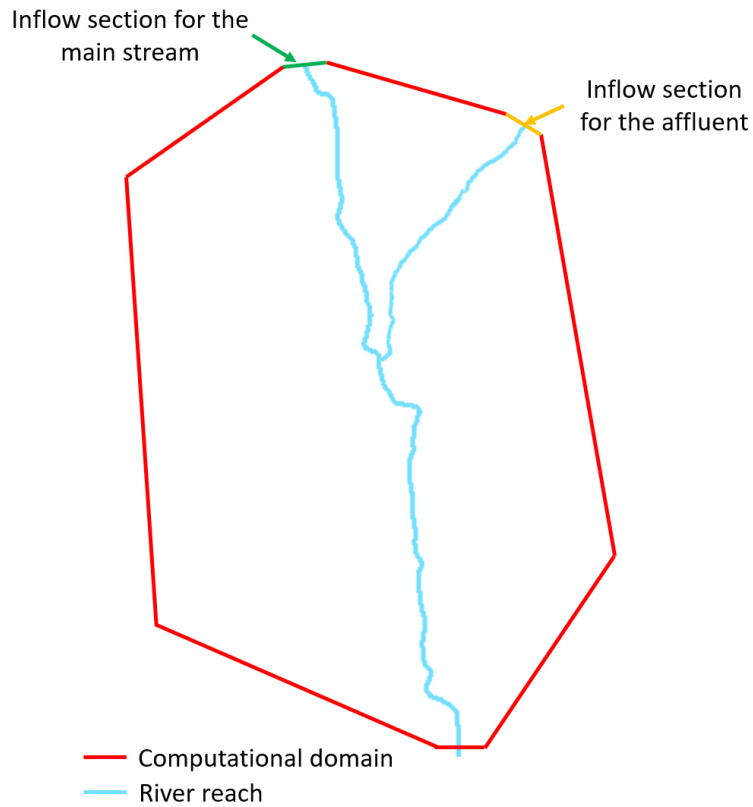


Figure 5.5: Sketch of computational domain needed to insert affluent, if affluent sections are available

Furthermore, provided that some information about the upstream boundary condition at the confluence from the side of the affluent is available, it is not always possible to insert the correspondent entrance section in the boundary of the computational domain. Indeed, as one can see from *Figure 5.6*, this would create a shrinkage of the domain in the upstream area of the reach, with possible consequences on the flood propagation in case of interaction between the same boundaries and the water.

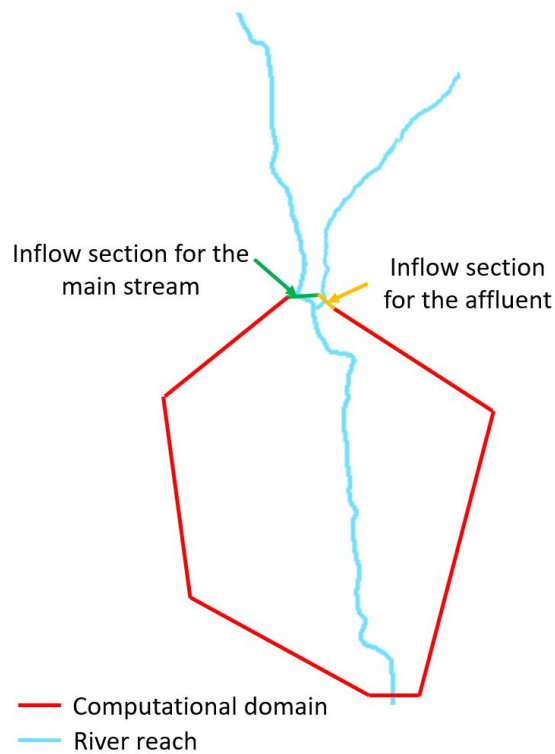


Figure 5.6: Sketch of shrinkage of the domain in the upstream area of the reach

5.2.3 Junction of maps for consecutive reaches

Another consequence of the partition of the watercourse in sub-reaches is represented by the junctions of the flood maps resulted from two consecutive reaches. Indeed, because the respective computational domains often intersect, there is the possibility of having the same area interested by presence of water coming from the two different simulations. To clarify this concept, *Figure 5.7* shows an example in correspondence of the junction between reaches 4 and 5.

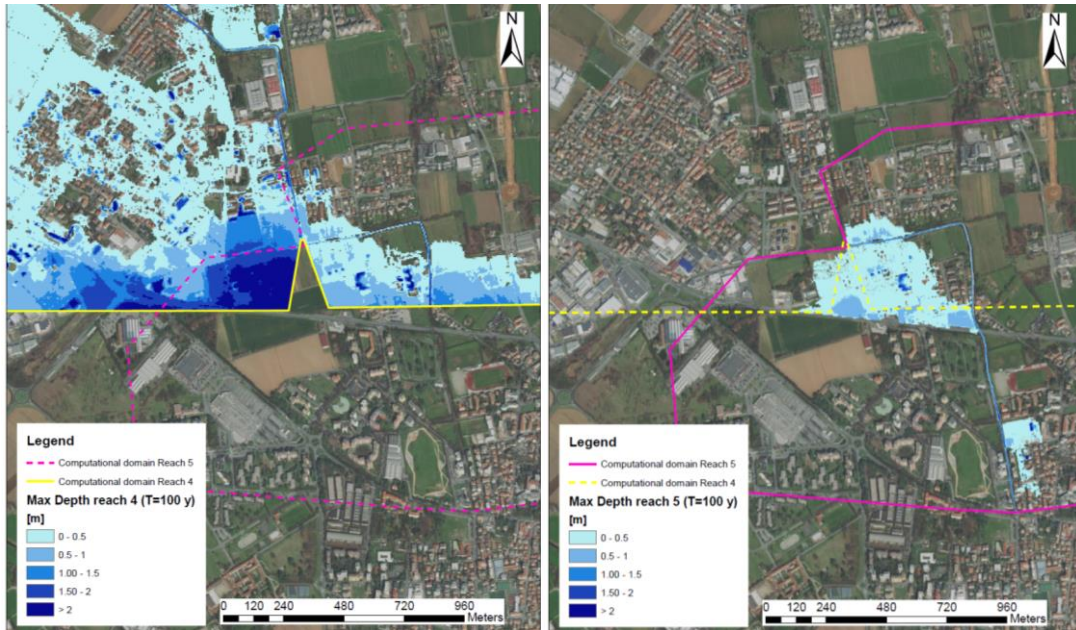


Figure 5.7: Example of junction between partition 4 (left) and partition 5 (right) of Bozzente river

As one can see, the two computational domains enclose some common regions, thus the “conflict” between the two flooded perimeters. In this case, as in the others, the flooded area in correspondence of the downstream segments of the upstream reaches has been clipped to follow the boundaries of physical entities such as roads or buildings, due to the uncertainty which affects the actual distribution beyond the limits of the computational domain. Then, to solve the superposition between flooded areas, a mosaic operation has been performed on a GIS environment, setting as a conservative value the maximum between the ones from the two reaches. The result is shown in *Figure 5.8*, from which it is possible to notice that the water distribution at the junction is discontinuous, because the presence of a step in values of depth is not avoidable.

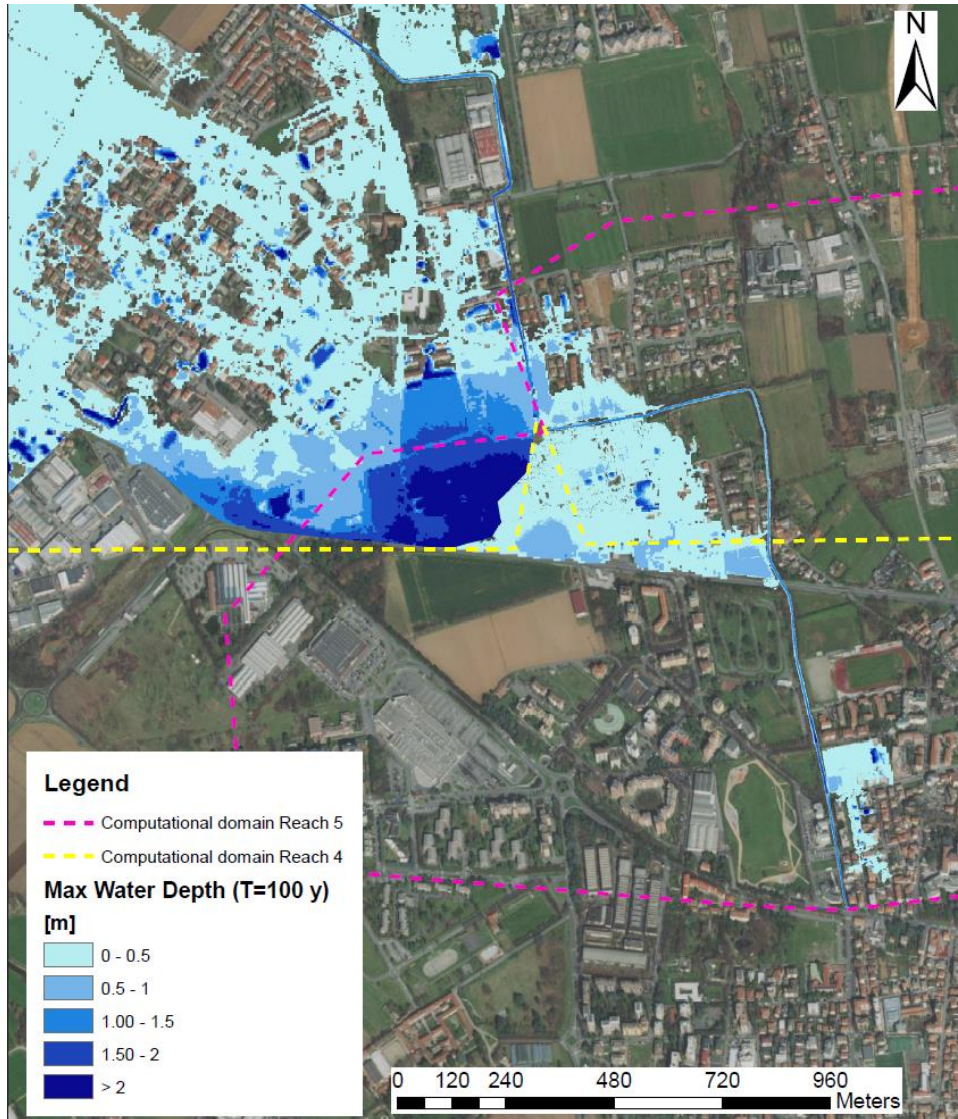


Figure 5.8: Result of junction between partitions 4 and 5 of Bozzente river

5.2.4 Bathymetry: construction and sections geometry

As explained in *Section 3.1*, the terrain model used as input for the modelling through PARFLOOD code is the result of the combination between a 5x5 DTM from *Geoportale della Lombardia*, a 1x1 DTM from the MATTM, and a raster with resolution of 1 meter produced by a MATLAB code and following interpolation of a point cloud. In particular, the latter has been obtained starting from the available surveyed sections (Cfr. *Appendix B*). The process of raster construction starting from a series of points, which are the vertices of the surveyed sections, presents several intrinsic criticalities.

Sections removal

The MATLAB code used to create the bathymetry of the riverbed (Cfr. *Appendix B*), generated an error when projecting a section that intersects the river axis at multiple points (this can happen as the river flow is not straight). This has resulted in some sections being excluded in the bathymetry construction phase and, in turn, in differences arising between the sections that have been surveyed and those from the output provided by MATLAB code in the vicinity of the removed ones.

Spatial resolution

The sections provided to the MATLAB code to create the point cloud of the riverbed, are those which faithfully describe the actual terrain model, in the sense that they contain the elevations of riverbed, embankments and surrounding floodplains. The series of interpolations performed by the MATLAB code do not alter the geometry in correspondence of the same sections. Nevertheless, in the GIS environment, the operation to move from a point cloud (dense enough after the abovementioned interpolations) to a raster terrain model could lead to some discrepancies between the original sections and the respective one that can be extracted from the final raster. Two examples of this are displayed in *Figure 5.9* and *Figure 5.10*.

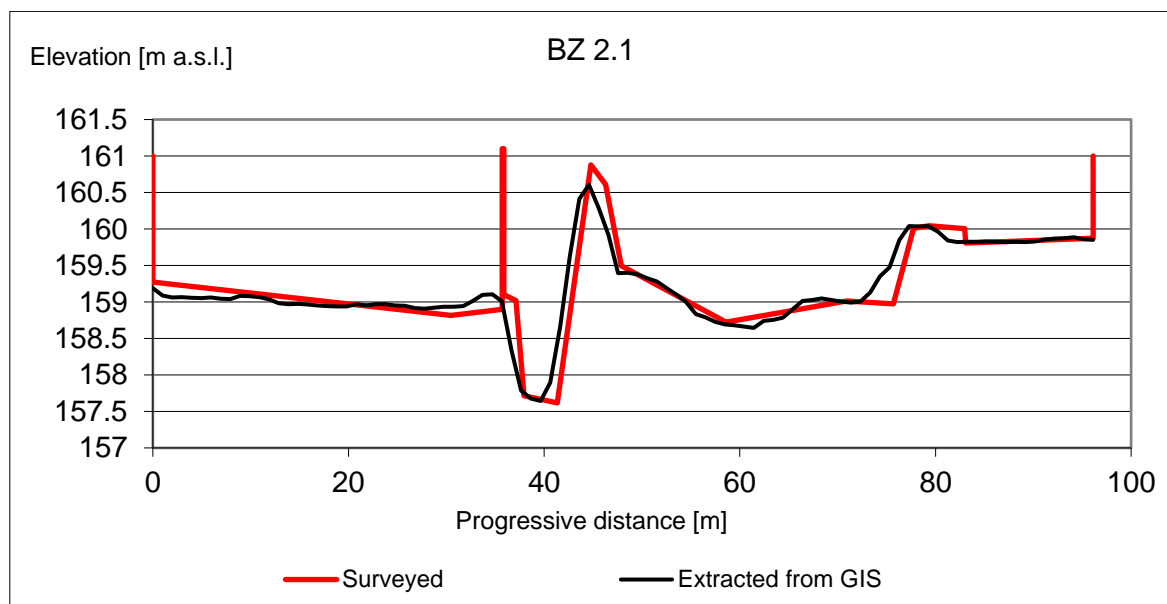


Figure 5.9: Comparison between surveyed section BZ 2.1 and its representation in GIS

Figure 5.9 represents a clear example of how the 1x1 DTM representing the input for the modelling is not always suitable to insert in the simulation structures which are expected to have a crucial role in the flood propagation. Indeed, as one can notice from the same picture, the wall, present in the left side of the riverbed section in the graph, is too thin to be successfully represented in the interpolated surface, while the one on the right side of the graph is characterized by a thickness comparable with the cell size. Although less pronounced, the same problem persists in the riverbed. In fact, the channel elevation is different between the surveyed sections and extracted sections in GIS. This is again since the maximum resolution of 1 metre used in the PARFLOOD is still quite rough considering the width of the riverbed in its narrowest part. This problem holds in the situation of 2-dimensional flood modelling based on a terrain model described by a grid. This is the case of PARFLOOD, where the only way to effectively represent containment walls and similar structures, is to define a cell size close enough to the thickness of those because the manually correction is not usable due to the large scale of the study.

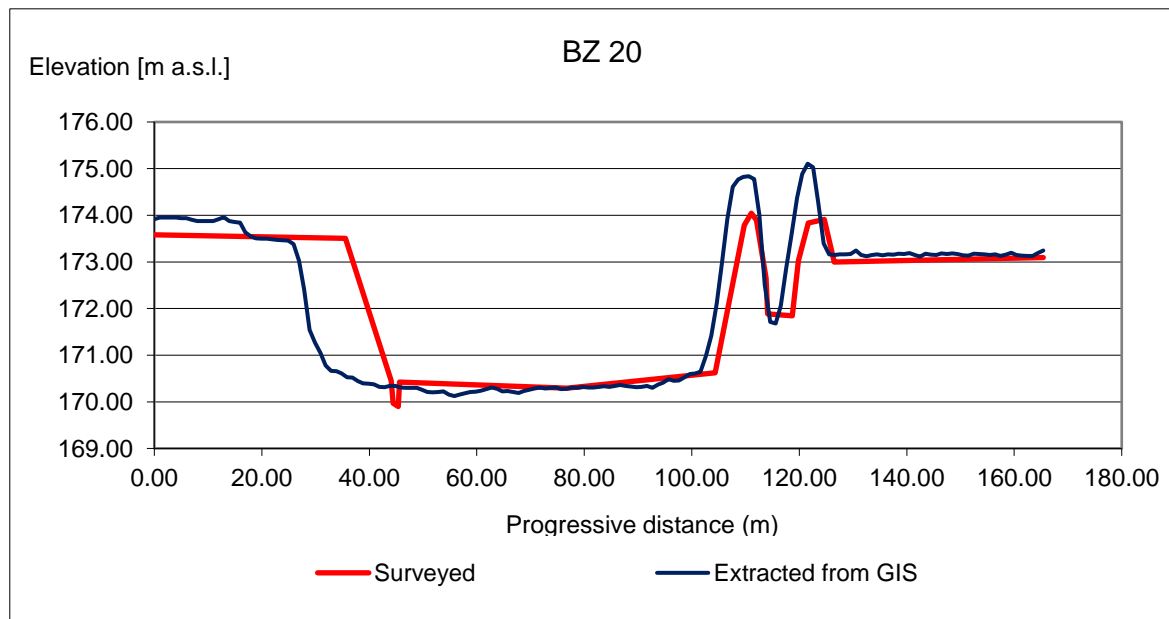


Figure 5.10: Comparison between surveyed section BZ 20 and its representation in GIS

Figure 5.10, on the other hand, presents an additional criticality: even though the embankments beside the cross section of the river (around a progressive distance of 110-120 meters) are reproduced in the final raster, they are deformed, as also the rest of the section and the left side of the depression in the ground placed at around 40 m of progressive distance.

5.2.5 Bridge input

As explained in *Section 2.2*, PARFLOOD generates some problems because of lateral water flow near the bridges. In fact, because of the backwater immediately upstream of a bridge, it could happen that the height of water downstream of the bridge is considered higher than upstream by the code. This leads to a flow from downstream to upstream that, if persistent, generates the interruption of the simulation. Hence it has been necessary to delete some bridges, as shown in *Figure 5.11*:

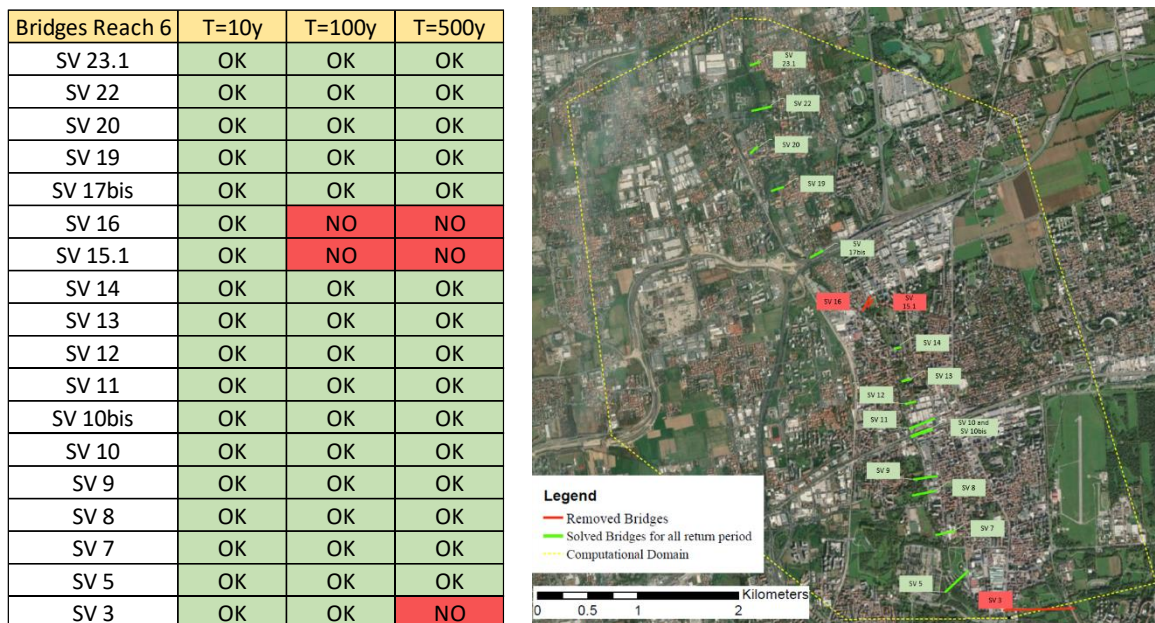


Figure 5.11: Representation of removed bridges in red, and the inserted one in green - reach 6 of Seveso stream

Furthermore, in the one-dimensional bridge equations used by PARFLOOD, the bridge extension in the direction longitudinal to the flow is not considered. This is obviously only a problem in the circumstance when the bridge is overtopped.

5.2.6 Culvert representation

Using the PARFLOOD code it is impossible to model a culvert, as the code does not include an appropriate module. One possibility to cope with this is to model a culvert using the module for bridges. For this reason, in this work the culverts present along the Bozzente (the modelled reach for the stream Seveso does not contain culverts) have been described in the model just

by their entrance section, as shown in *Figure 5.12*. It is worth to point out that this reasoning can hold just if the information about the geometry of the entry section of the culvert (i.e. surveyed section) is available for the culvert at issue. Unfortunately, in some cases, the fact that the culvert has been realized after the survey occurred in 2003 with the “Studio di fattibilità” does not make possible to include the presence of the structure, even by means of the first section.



Figure 5.12: Representation of culvert section in Bozzente River

Considering a culvert in the same way as the bridges are introduced in the model, obviously introduces a heavy simplification. First, the fact that PARFLOOD does not consider a length for a bridge becomes much more relevant in case a culvert is long. Second, even more evidently, the water is more prone to flow back into the main channel after a possible outflow at the entry section of the culvert, due to the consideration of a free surface for the stream, as well as outflows in the culvert reach are not limited by the presence of a lid.

5.3 Future developments

As explained above, the contours of the update flooding areas are larger than expected. In particular, the scenario H is hardly representative of reality. This problem could be linked to

all the limitations explained above. Therefore, the proposed future developments are aimed at increasing the model reliability. Two different ways are proposed:

- 1) Using 2D modelling, with PARFLOOD software. In particular, to correct the bathymetry, it is proposed to modify the MATLAB shown in *Appendix B*, to fictitiously enlarge the banks so that the edges are captured when interpolating the point cloud in GIS. This should solve the embankments problem described above but would insert fictitious structures into the model. Furthermore, still it would not improve the representation of the bed. In fact, the problem of the riverbed elevations described in *Section 5.2.4* would persist. The second intervention proposed, again using a two-dimensional model, is to define a resolution grid that is characterized by square cells smaller than 1 m². For example, by using a grid with a square mesh size of 20 cm per side, the walls could be well represented. Also the riverbed elevations would be better represented. Obviously in this case it should be ensured that the inevitable increase in computational cost does prevent a solution from being obtained.
- 2) Using a 1D – 2D coupled model. It is proposed to use a one-dimensional model to represent the main channel and a 2D model for the floodplains. This choice would solve the problem of representing the bathymetry for narrow rivers. In fact, the verges would be captured, and the sections could all be inserted within the model. In addition to this, there could be the further advantage of being able to insert punctual inflows and culverts more easily and therefore it may not be necessary to subdivide the model (Cfr. *Section 3.3*).

Regardless of the followed approach, further developments could certainly include a successive cycle of modelling by using updated hydrological and geometric input data. This would allow, on the one hand, to improve as much as possible the reliability of the collected data, and, on the other hand, to better describe the present conformation of the terrain, also including the interfering structures or mitigation measures introduced after 2003 (e.g. bridges, water detention basins).

In addition, to increase the level of detail, an attempt in completing the dataset from OSM containing the footprint at a scale of the single building could be targeted: in this way, the buildings can be excluded from the computational space by creating voids (Cfr. *Section 2.3*). Obviously, a comparison between the results obtained by the voids method and the one

followed in the present work (roughness method) would be useful to understand the influence of the urban fabric representation in a large-scale modelling.

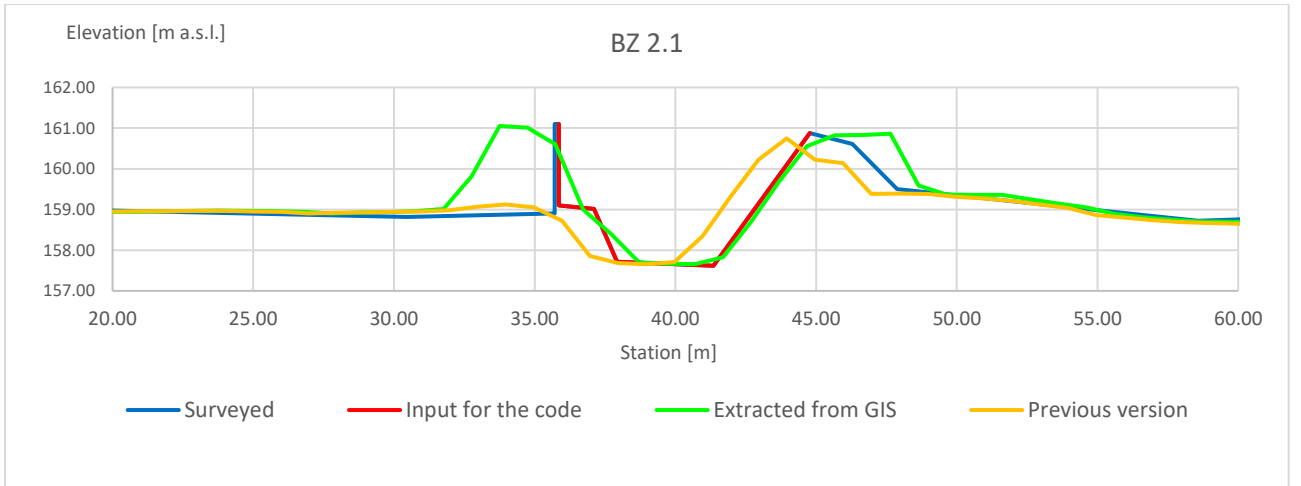
To increase the level of confidence of the results obtained from the simulations with PARFLOOD, a validation of the model would be needed, by comparing the results of the model with the flood propagation occurred during past events. In the frame of the present work, a validation has not been performed due to the fact that the level of confidence toward the obtained results is not sufficiently high; nevertheless an attempt in reducing the level of uncertainty has been performed dividing the whole streams in shorter sub reaches, in correspondence of the sections at which information from the 1D model were available. Indeed, the input data, in terms of hydrographs and peak flow rate values, which have been deployed, are the result of previous, already validated, analysis, such as the “Studio di fattibilità” from 2003.

5.4 Attempt to implement some improvements

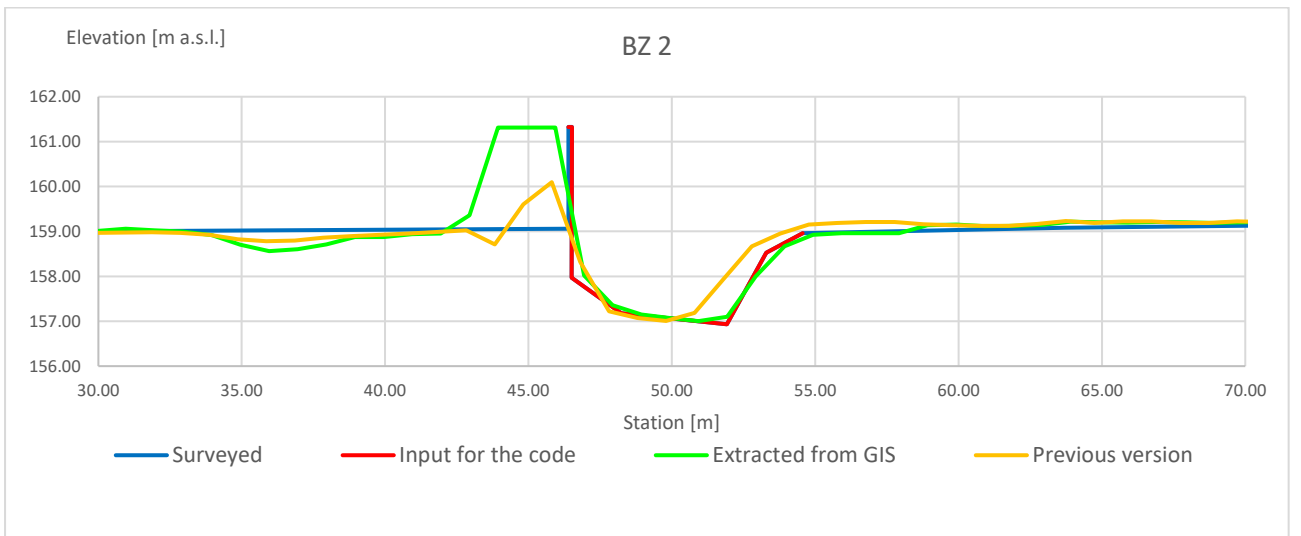
In the following, some applications of what proposed in *Section 5.3* are targeted. Due to the obvious impossibility of repeating the modelling for the entire domain of study, two sub reaches have been chosen for a pilot application: reach 4 for the Seveso and reach 5 for the Bozzente.

5.4.1 Reconstruction of the bathymetry

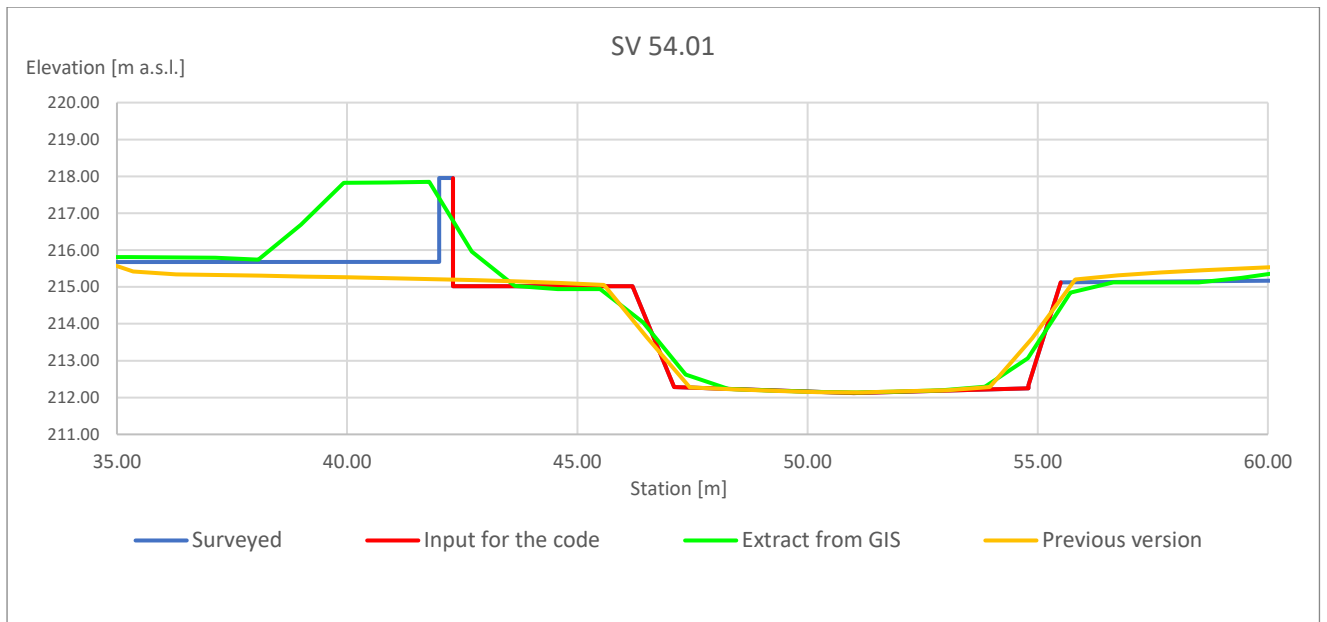
First, the MATLAB code used to create the geometry of the riverbed has been modified in order to fictitiously enlarge the embankments or any structure delimiting the riverbed (with the top elevation maintained for 3 m on each side), so that the edges are captured when interpolating the point cloud in GIS. As shown in *Figure 5.13 a-d*, this operation has considerably improved the representation of the edges of the embankments in the bathymetry, so that, at least in correspondence of the surveyed sections, the level of reliability of the geometry has drastically increased in terms of lateral wall elevation (accepting, on the other hand, the possibility that a thin wall becomes more similar to an earthen embankment).



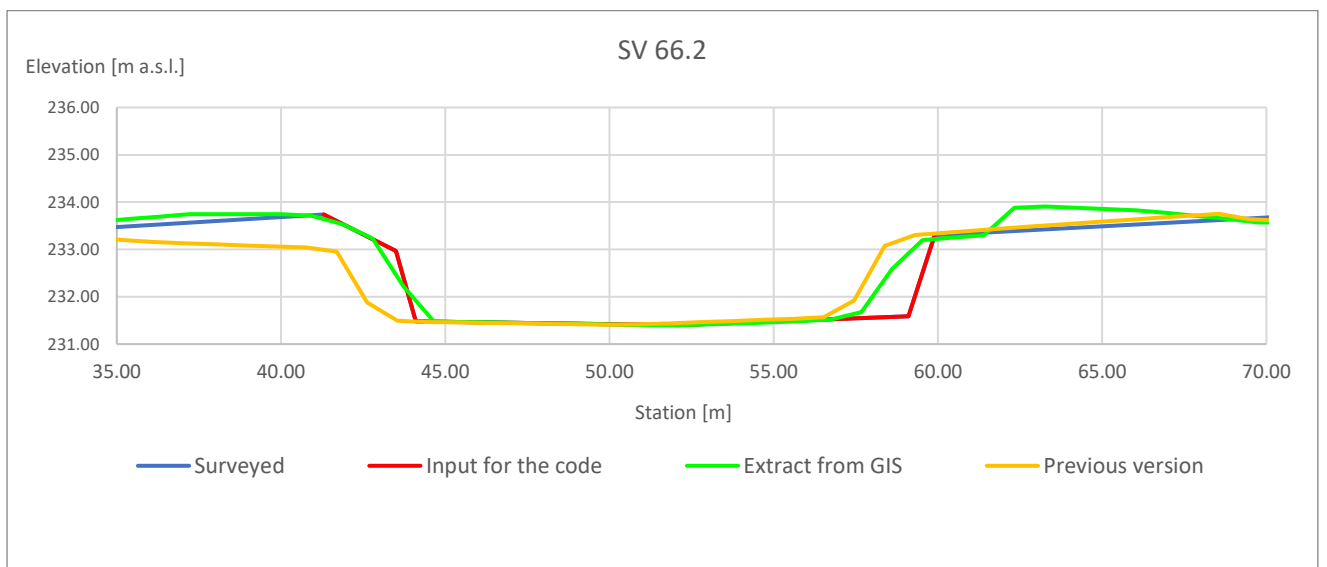
a



b



c



d

Figure 5.13: Sections representation in the bathymetry of the Bozzente (a-b) and of the Seveso (c-d)

In the pictures above, the blue line represents the surveyed section used as input for the model: more specifically, only the portion coloured in red has been inserted in the MATLAB code as representing the riverbed. The yellow line, referred to as “Previous version”, represents the section extracted from the DTM used for the simulations which led to the results shown in Chapter 4, so before the intervention of the edges of the banks. Finally, the green line is the

section from the new DTM built with an arbitrary thickening of the embankments and the retaining structures.

In the *Figures 5.13 a-c* it can be seen how the retaining walls, present in all those cases in the hydraulic left (left part of the plot), were completely disregarded by the previous version of the bathymetry, while their presence is taken in account by the new geometry (green lines), as mentioned above, by means of fictitiously large embankments. On the other hand, *Figure 5.13 d* represents an example in which one of the banks (here on the left) was unsuccessfully described, because its elevation was about 1 meter lower with respect to the surveyed section: also in this case, the new version of the code has successfully improved the situation.

5.4.2 2D model with PARFLOOD with the new bathymetry

New PARFLOOD simulations have been run with the new DTMs as input, referring to the event with a high probability of occurrence ($T=10$ years). The maps, respectively for the Bozzente and for the Seveso are displayed in *Figures 5.14* and *5.15*.

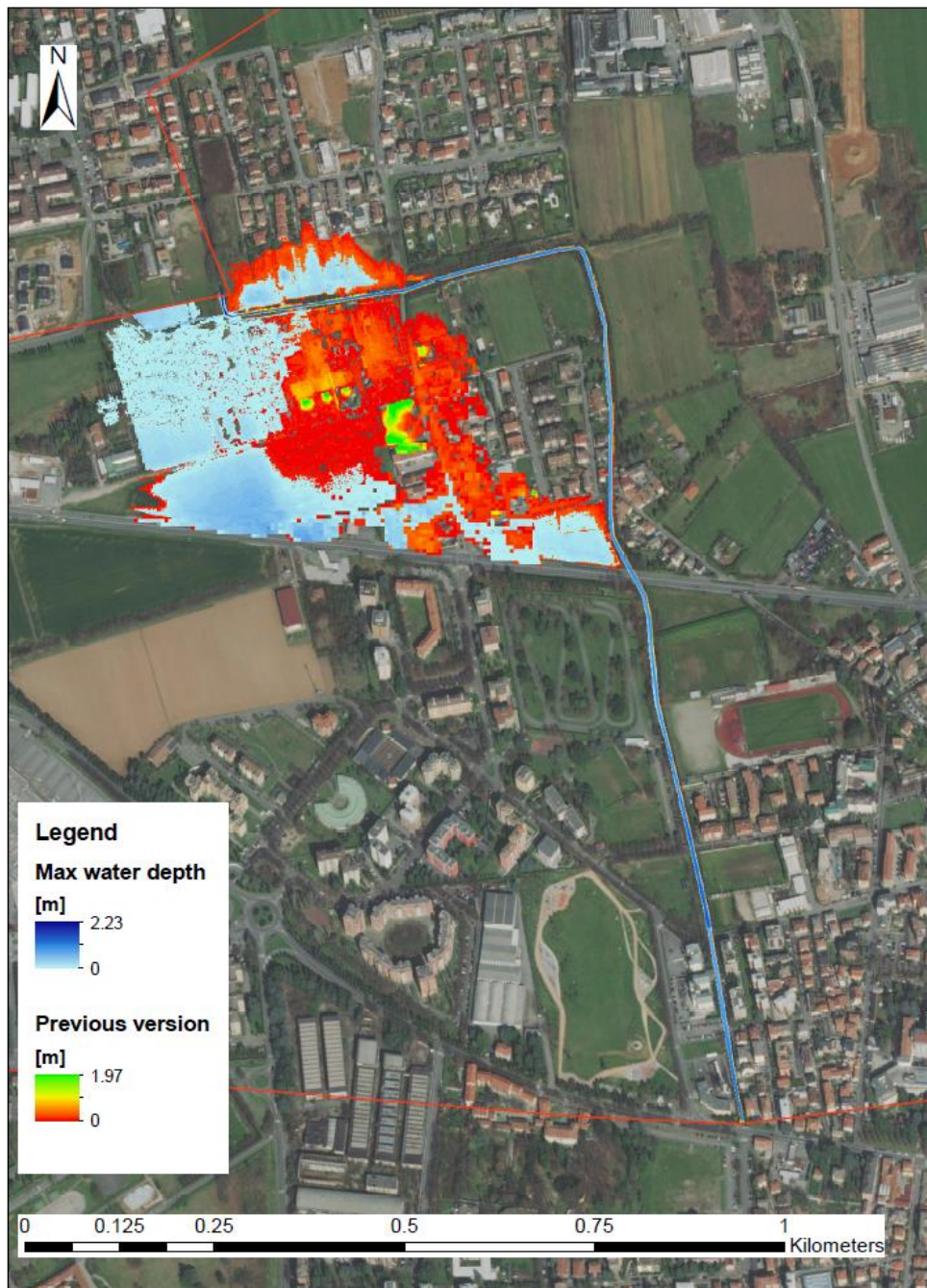


Figure 5.14: Flood maps for the Bozzente - Reach 5 ($T=10$ y)

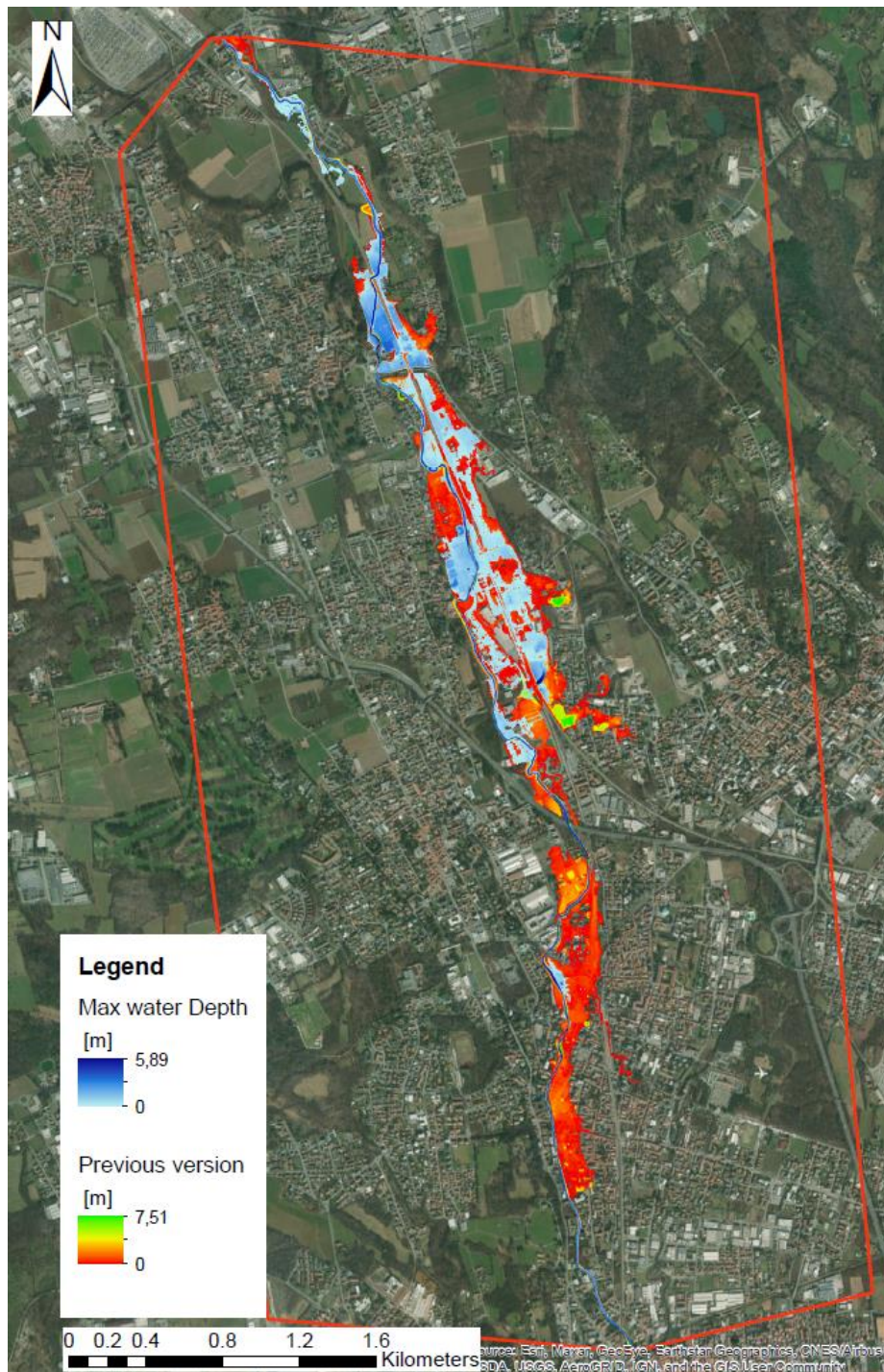


Figure 5.15: Flood maps for the Seveso - Reach 4 ($T=10$ y)

The maps above represent a comparison in terms of flood extent between the simulations performed with the corrected bathymetry (blue palette) and the previous ones (red-green palette) whose results were displayed in *Chapter 4*. As one can notice from the maps, the flooded areas have been reduced by the intervention on the verges of the banks; nevertheless,

wide inundation areas are still predicted and they seem still too large to consider these maps as representative of the reality.

By focusing on the riverbed geometry immediately downstream the overflowing portion of the streams, some anomalies have been spotted for both the Seveso and the Bozzente. In particular, it has been possible to observe that sometimes the DTM presents some incongruous shrinkages of the riverbed between two consecutive surveyed sections, despite the quite accurate representation of these last. Here is the case of the Bozzente, illustrated below as an example, which shows how an overflow occurs downstream section BZ 9 bis (*Figure 5.16*).



Figure 5.16: Overflow of the Bozzente between section BZ 9 bis and BZ 8

This could be due to the narrowing of the channel that takes place in correspondence of the bend (highlighted in the red oval in *Figure 5.16*) and which can be spotted by the help of the DTM visualization in *Figure 5.17*: here, indeed, it is shown how the elevation of the riverbed has been artificially modified to widen the opening of the channel. So, the presence of the green colour in the riverbed increases after the correction because the elevation has been forced to a value of 162.86 m.

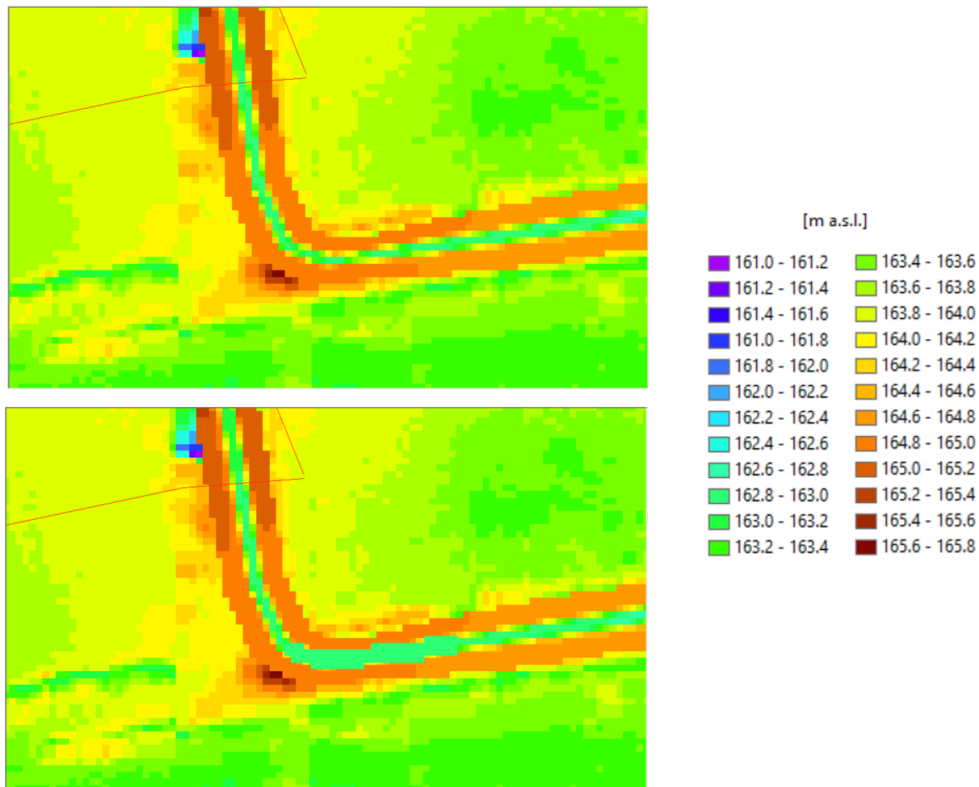


Figure 5.17: Local correction of the riverbed elevation

After the correction of the riverbed, the simulation on PARFLOOD has been repeated to check the effectiveness of the intervention: *Figure 5.18* shows the map of the maximum water depth distribution. From the picture one can notice how the widening of the channel section has led to a decrease in the water surface elevation, so that now the stream does not overtop the banks. Nevertheless, *Figure 5.19* shows how the level is still high in correspondence of the curve.

5.4.3 1D modelling for comparison

To investigate whether the riverbed is sufficient or not to contain the peak of the flood wave (as the perimeters from 2019 indicate in the case of both the sub reaches at issue), a 1D model has been built in HEC-RAS for both the streams. More in detail, a steady flow with the peak discharge of the respective hydrographs representing the upstream BC of the two the reaches has been modelled. It is worth pointing out that, for the sake of simplicity, the transverse structures have not been considered in the model at issue. The resulting profiles are plotted in *Figures 5.20 and 5.21*.

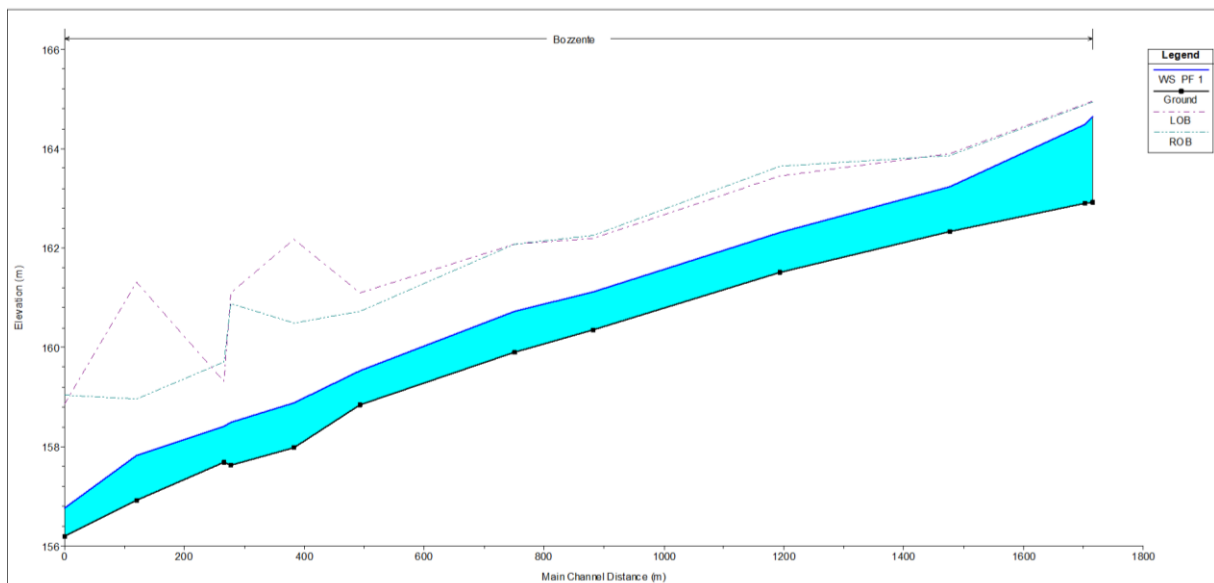


Figure 5.20: HEC-RAS profile for the Bozzente – Reach 5

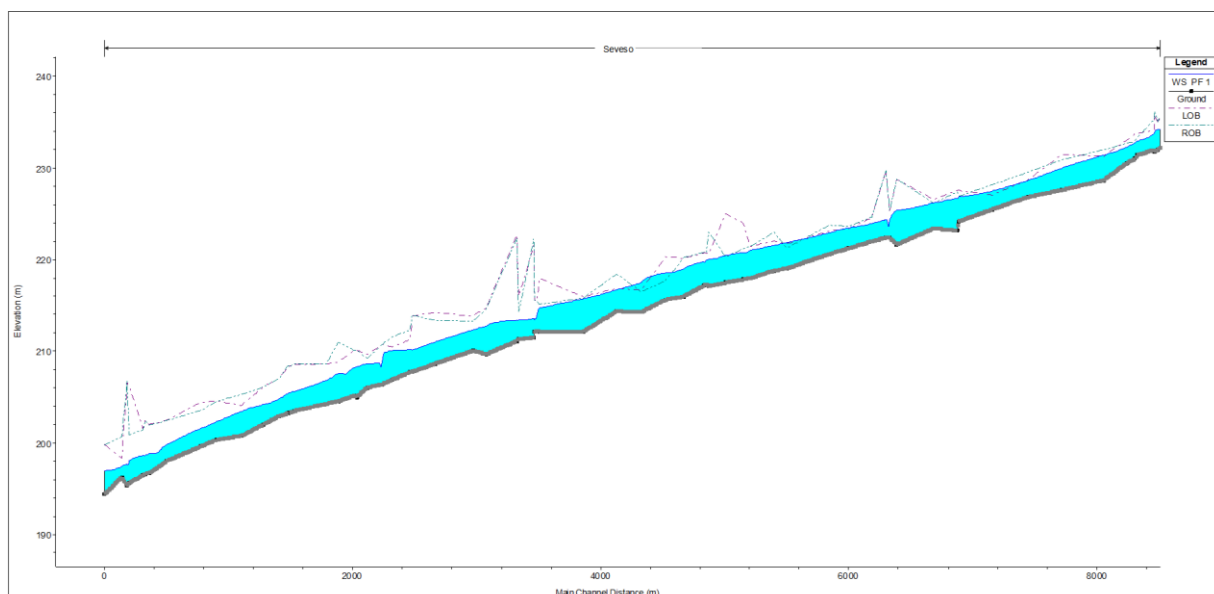


Figure 5.21: HEC-RAS profile for the Seveso – Reach 4

In *Figure 5.22* and *5.23*, the profiles from the PGRA 2015 and the 1D modelling from HEC-RAS have been superposed. For the Bozzente (*Figure 5.22*), the plot also shows the profile of the maximum water elevation obtained, in correspondence of the riverbed, in the 2D simulation with PARFLOOD (the model is the one referred to in *Section 5.4.2*).

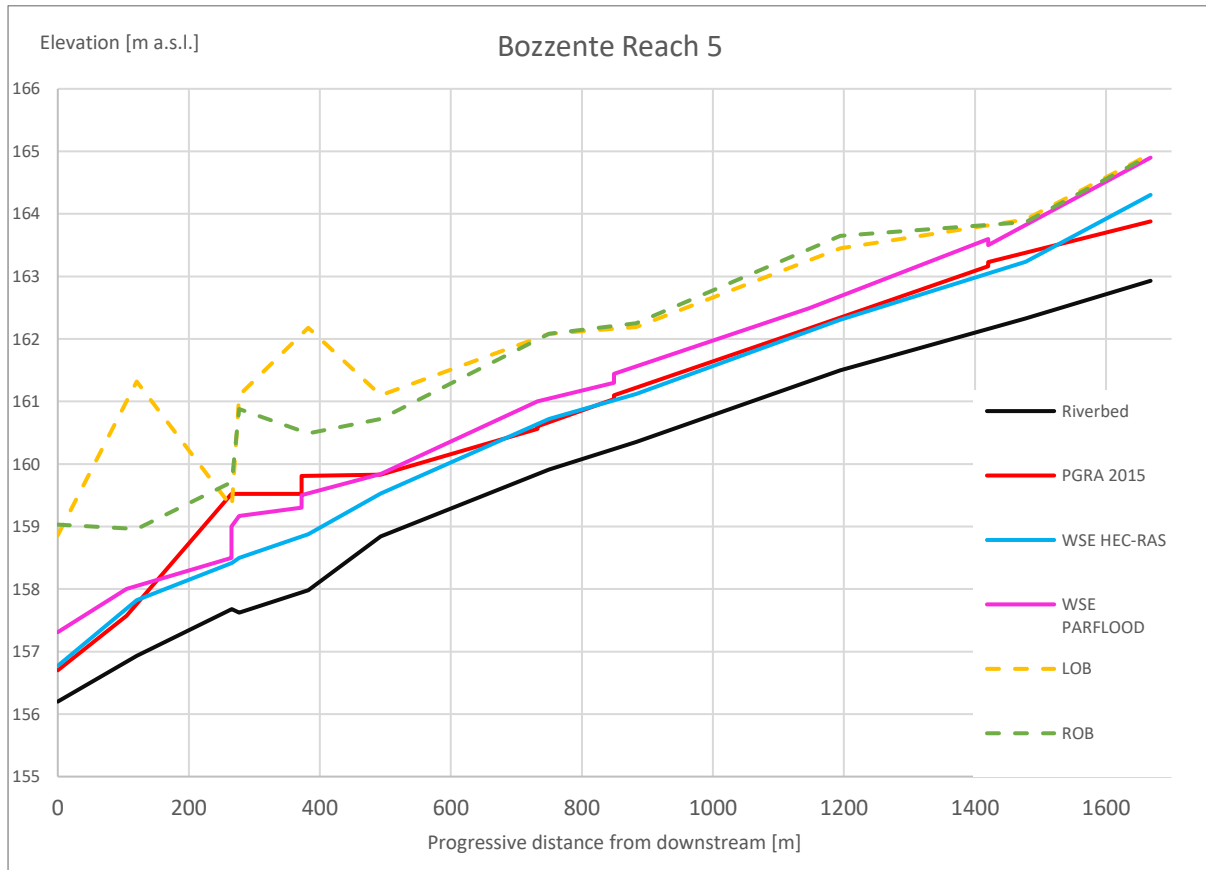


Figure 5.22: Superposition of the profiles for the Bozzente

From the comparison of the profiles, it is inferred that:

1. The profiles coming from PGRA and HEC-RAS are characterized by a good grade of similarity (apart from the backwater around the progressive 250 m which is not captured by HEC-RAS because of the absence of bridges)
2. The profile from PARFLOOD is characterized by a trend which becomes progressively higher, with respect to those mentioned in point 1, moving from downstream to upstream. This leads to a water level which, in correspondence of the upstream section, is close to the overtopping of the banks, as already shown in *Figure 5.19*.

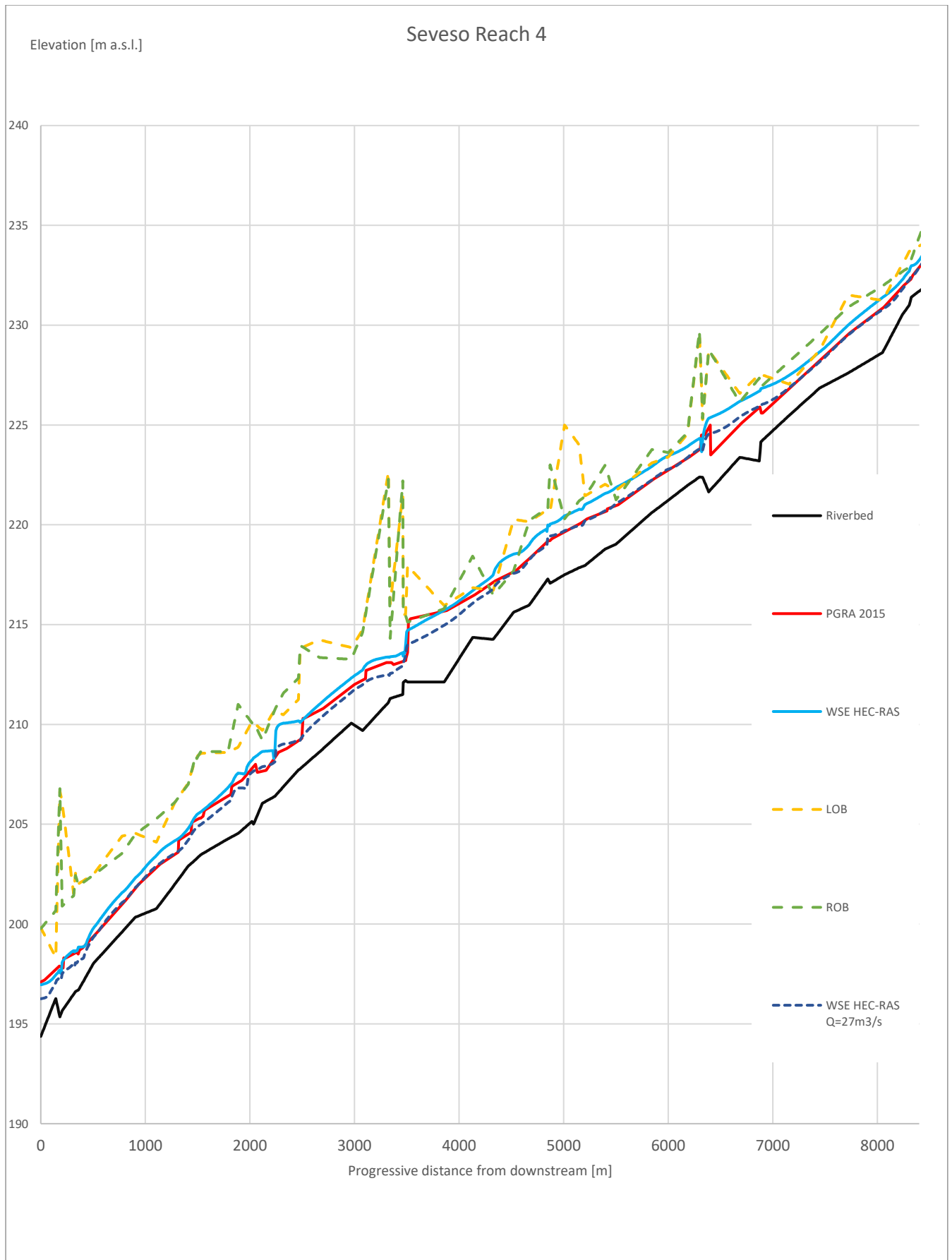


Figure 5.23: Superposition of the profiles for the Seveso

In the case of the Seveso, the situation differs from that of the Bozzente. In particular:

1. The profile obtained by the 1D model in HEC-RAS is higher than the one outlined by the data from the PGRA; the former still returns outflow in sections where the latter is quite below the edge of the banks (e.g. at a distance of around 7000 m in the hydrographic right)
2. In order to address this difference in levels, a sensitivity analysis has been carried out to set a value of discharge that can take the profile from HEC-RAS closer to the one from the PGRA; the peak flow rate of 43.9 m³/s used in the first model in HEC-RAS (and in the models in PARFLOOD for this reach) has been replaced with 27 m³/s (that was the discharge of incipient outflow in the 2D models with unsteady flow), with a considerable reduction in water level which makes the two profiles almost coincide (apart from the differences due to the absence of bridges in HEC-RAS, such as in the case of the distances around 6500 m and 3500 m).

5.4.4 Observations

In summary, the attempt above has followed the first strategy mentioned in *Section 5.3* (improving the current modelling approach) and has considered a distributed problem and solution (widening the banks everywhere), local corrections to the river bed in places where unrealistic inundation were predicted, and adding a step to the modelling procedure (also running a 1D model for comparison). The attempt has been limited to the models for the scenario H and to two pilot reaches. Based on the obtained outcome, the following observations are made:

- Although the MATLAB code performs better with respect to the representation of the verges and the sections extracted from the new DTM are quite satisfactory in the comparison with the surveyed ones, some anomalies arise along the riverbed; their effect could vary from a local to a larger scale, considering that a possible overflow could determine an important flood in such a flat territory surrounding the streams. The solution of these issues would require the manual intervention which surely represents a challenge in the context of the large scale which characterized the models targeted by the present work. An enrichment of the database used as input for the bed geometry (i.e. surveyed sections) could be a more favourable starting point for the riverbed representation.

- In the case of the reach 5 of the Bozzente, it has been noticed how the correction of some geometrical irregularities could be not enough to reach a high grade of trustworthiness toward the model. In particular, the profile of the maximum water depth extracted from the PARFLOOD model (*Figure 5.22*) could suggest that a further analysis of the upstream BC influence on the water level could provide more information to interpret the discrepancy between the 2D and the 1D models.
- On the other hand, the analysis of the reach 4 of the Seveso has led to the need of further investigations regarding the flow rate expected to represent the event under study. Both the 2D model from PARFLOOD and the 1D from HEC-RAS describe a water level distribution which is able to overtop the banks, in disagreement with the profile from the PGRA which remain below the level of the embankments.

6. Conclusions

Riverine flood impact may be reduced by appropriate measures, whose design needs to be supported by appropriate assessment of the spatial distribution of hazard and risk. During the last decades, in order to face the flood risk, the European Union has implemented the Directive 2007/60/EC, that is the reference for flood risk assessment and management in Europe. The directive requires all Member States to assess flood hazard and risk and to adopt measures for reducing the adverse impacts of flood events.

The present thesis work is motivated by the need for defining a methodology for extensive two-dimensional hydrodynamic flood modelling in the “APSF_R Milano Nord” (APSF_R = Area at Potential Significant Flood Risk). Indeed, with the PGRA 2021 the AdBPo intends to redefine the boundaries of the flood-prone areas in this APSFR, shifting from the maps produced with the simplified methods in 2019 to an extensive two-dimensional modelling of all the main waterways included in the network that crosses the Metropolitan City of Milan and other provinces in Lombardia. This represents a major update to the previous PGRA 2015 (PGRA = flood risk management plan) and the additional maps produced in 2019. In particular, the present thesis work is focused on two of the nine main waterways in the APSFR, the Bozzente and the Seveso. These two streams have been chosen because their different characteristics pose multiple challenges to a numerical solver and its operation. Indeed, the Seveso is almost twice longer than the Bozzente and it is crossed by around 70 bridges. On the other hand, the Bozzente is narrower than the Seveso, thus the same resolution of the spatial grid for the model is less representative for describing the geometry of the former; moreover, in the case of the Bozzente, only 15 bridges could be inserted in the simulations. Like many of the other streams in the area, they have a consolidated conformation with progressively decreasing flow capacity from upstream to downstream. This is due to the density of the surrounding urban fabric, which increases moving closer to the metropolitan area of Milan.

The background of the present thesis work is represented by the previous studies and models for the APSFR, carried out first in 2003 in the frame of the “Studio di fattibilità della sistemazione idraulica”, whose results have been the starting point for the following update occurred in 2019. In the case of this last study, the assessment of the flood hazard is based on zero-dimensional models, that reconstruct the spatial distribution of the water surface elevation by interpolation, starting either from the results of a one-dimensional model (where possible) or from the perimeter of the flooded area where no other results were available.

In the present work, the two-dimensional modelling has been performed with the PARFLOOD code, for the purpose of having a comprehensive and numerically affordable model, as required by the scale of the project. The code is run using a specific hardware that drastically reduces the computational times compared to those for other academic software for two-dimensional modelling.

Several operations have been required to build the digital terrain model (DTM) to be used in the simulations for the APSFR. Three elevation data were used jointly: the DTM, already available, with 1x1 m resolution, provided by the “MATTM, Ministero dell'ambiente e della tutela del territorio e del mare (ed. 2008)”; the “DTM 5x5 – Modello digitale del terreno (ed. 2015)”, which is a free dataset with 5 m resolution available in the Geoportale della Lombardia; finally, a cloud of elevation points produced interpolating cross section data, in order to correct the misrepresentation of the river bed in the DTMs. The river cross sections employed to describe the geometry of the riverbed were surveyed in the context of the “Studio di Fattibilità (2003)”. The variability of land use and cover has been used to parameterize the surface roughness: three levels of roughness in terms of Manning coefficient have been used to differentiate the river bed ($n = 0.035 \text{ s/m}^{1/3}$), urbanized areas ($n = 0.4 \text{ s/m}^{1/3}$) and the remaining areas ($n = 0.08 \text{ s/m}^{1/3}$). This choice is justified by the need to have a first hazard assessment for the whole rivers, nevertheless, a refinement of the roughness description is required in the following models.

To address the issue of extending the flood modelling to the scale of the APSFR, the involved rivers have been partitioned according to the data for the spatial distribution of the peak flow rate for given return period. In general, the peak discharge values have been taken from the PGRA 2015, unless later redetermination was available. The maps produced for the single modelling reaches have been connected to obtain the hazard maps for the whole streams, related to three different return periods ($T=10, 100$ and 500 years). The obtained flood perimeters have been compared with the previous ones, defined in the earlier stage of the project in 2019. As expected, it has been not possible to find a direct correspondence between them, as they are the product of different modelling approaches. In particular, the flooded areas modelled with PARFLOOD are much wider than those previously described in the former version of the maps. This is mostly evident in the case of the scenario corresponding to high probability of occurrence ($T=10$ years).

The full two-dimensional flood modelling on a large scale presents several intrinsic criticalities, such as the need to find a proper compromise between computational cost and resolution of the grid. In the present work, the spatial grid with a resolution of 1 meter is supposed to suit

the case of such long reaches. Nevertheless, even the maximum resolution of 1 meter used in the PARFLOOD is not consistent with the width of the riverbed in its narrowest part. Moreover, the impossibility of considering the presence of punctual inflows or affluents along the reach has led to the subdivision of the whole streams in sub-reaches, with the arising of possible inconsistencies between boundary conditions for consecutive reaches. Another consequence of the partition of the watercourse in sub-reaches is represented by the difficulties in linking the flood maps resulted from two consecutive reaches. In addition, specifically for the case of the PARFLOOD, because bridges and culverts are modelled as mono dimensional, it results impossible to represent their entire longitudinal length.

Further developments with respect to the present work could be represented by improving the current model with a better definition of the terrain geometry, by increasing the resolution in order to include the presence of structures, such as the thin embankments which cannot be described by a cell with the side of 1 m. In the case this implicates a prohibitive computational cost, an alternative could be exaggerating artificially the width of the walls bounding the river sections, to preserve their top elevation, crucial for the containment of the flood wave in the final DTMs.

An attempt to apply the procedure to correct the bathymetry, in order to fictitiously enlarge the embankments or any structure delimiting the riverbed (with the top elevation maintained for 3 m on each side), has been limited to the models for the scenario H and to two pilot reaches. This has led to a reduction in terms of flooded area, but still some improvements are deemed necessary, on the side of anomalies in the geometry of the riverbed that heavily influence the results. Moreover, on the basis of a comparison with the 1D models, further investigations are suggested regarding the boundary conditions and the value of flow rate applied in the simulations at issue.

Additional developments can be made by considering an alternative modelling strategy, coupling a one-dimensional and a two-dimensional models, the former for the main channel and the latter for the floodplains. This choice could solve some problems, such as the representation of the bathymetry including the verges of the embankments and the insertion of punctual inflows. The strong limitation of the coupled model is certainly the definition of the interactions between riverbed and floodplain.

However, it would be useful to perform another modelling cycle collecting, when available, more updated data, both in terms of geometric and hydrological information. This could solve the problem that the urban development over the years is not described in the model the input

sections deployed to shape the terrain geometry. Therefore, further surveys would be necessary to include in the geometry of the model the new structures built in correspondence of the riverbed, so that their influence of the flood propagation is not neglected. Moreover, an update in the hydrological inputs is crucial to be as close as possible with the current situation.

Bibliography

European Environmental Agency (EEA), 2010:

<https://www.eea.europa.eu/highlights/natural-hazards-and-technological-accidents>

European Commission, The EU Floods Directive:

https://ec.europa.eu/environment/water/flood_risk/

Regione Lombardia, Scheda informativa - Piano di Gestione Rischio Alluvioni nel bacino del fiume Po (PGRA):

<https://www.regione.lombardia.it/wps/portal/istituzionale/HP/DettaglioRedazionale/servizi-e-informazioni/Enti-e-Operatori/territorio/pianificazione-di-bacino/piano-gestione-rischio-alluvioni/piano-gestione-rischio-alluvioni>

MATTM, Geoportale Nazionale - La Direttiva 2007/60/CE:

<http://www.pcn.minambiente.it/mattm/direttiva-alluvioni/>

Autorità di Bacino Distrettuale del Fiume Po, Prevenzione Frane e Alluvioni:

<https://adbpo.gov.it/categoria-suolo-e-rischio/>

Autorità di Bacino Distrettuale del Fiume Po, Territorio:

<https://adbpo.gov.it/territorio-di-competenza/>

Piano di gestione del rischio di alluvioni (PGRA), Mappe della pericolosità e del rischio di alluvione:

<https://pianoalluvioni.adbpo.it/mappe-della-pericolosita-e-del-rischio-di-alluvione/>

[Alcrudo, 2004] Alcrudo, F. (2004). “*Mathematical modelling techniques for flood propagation in urban areas. Project report: IMPACT Project*”.

[Benquè et al., 1982] Benquè, J.P., Hauguel, A., Viollet, P.L., and Preissmann, A. (1982). “*Engineering applications of computational hydraulics*”. Pitman.

[Bradley, 1978] Bradley, J.N. (1978). “*Hydraulics of Bridge Waterways*”. US Department of Transportation Federal Highway Administration.

[Cunge, 2003] Cunge, J. A. (2003). “*Of data and models. Journal of Hydroinformatics*”, 5(2):75–98.

[Dazzi et al., 2018] Dazzi, S., Vacondio, R., Dal Palu`, A., and Mignosa, P. (2018). “*A local time stepping algorithm for GPU-accelerated 2D shallow water models*”. *Advances in Water Resources*, 111:274–288.

[Dazzi et al., 2019] Dazzi, S., Vacondio, R., and Mignosa, P. (2019). “*Integration of a levee breach erosion model in a GPU-accelerated 2D shallow water equations code*”. *Water Resources Research*, 55(1):682–702.

[Dazzi et al., 2020] Dazzi, S., Vacondio, R., and Mignosa, P. (2020). “*Internal boundary conditions for a GPU-accelerated 2D shallow water model: Implementation and applications*”. *Advances in Water Resources*

- [Landau and Lifshitz, 1959] Landau, L. D., and Lifshitz, E. M. (1959). *“Fluid mechanics”*. Course of theoretical physics, Oxford: Pergamon Press, 1959.
- [Liang and Borthwick, 2009] Liang, Q., and Borthwick, A. G. (2009). *“Adaptive quadtree simulation of shallow flows with wet–dry fronts over complex topography”*. Computers & Fluids, 38(2):221–234.
- [Rogers et al., 2003] Rogers, B.D., Borthwick, A.G., and Taylor, P.H. (2003). *“Mathematical balancing of flux gradient and source terms prior to using Roe’s approximate Riemann solver”*. Journal of Computational Physics, 192(2):422–451.
- [Spurk, 1997] Spurk, J. H. (1997). *“Stream filament theory. In Fluid Mechanics”*, pages 302–398.
- [Toro, 2001] Toro, E. F. (2001). *“Shock-capturing methods for free-surface shallow flows”*, volume 868. Wiley New York.
- [Vacondio et al., 2016] Vacondio, R., Aureli, F., Ferrari, A., Mignosa, P., and Dal Palu`, A. (2016). *“Simulation of the January 2014 flood on the Secchia river using a fast and high-resolution 2D parallel shallow-water numerical scheme”*. Natural Hazards, 80(1):103–125.
- [Vacondio et al., 2014] Vacondio, R., Dal Palu, A., and Mignosa, P. (2014). *“GPU-enhanced finite volume shallow water solver for fast flood simulations”*. Environmental modelling & software, 57:60–75.
- [Vázquez-Cendón, 1999] Vázquez, M.E., and Cendón (1999). *“Improved Treatment of Source Terms in Upwind Schemes for the Shallow Water Equations in Channels with Irregular Geometry”*.

Appendix A

PARFLOOD code user guide

Code requirements

To be able to solve the SWE, PARFLOOD code needs information with reference to the studied terrain elevation or bathymetry, roughness coefficients as Manning's values, spatial computational domain and boundary conditions for the simulation, time domain and initial conditions.

The required files for the method to properly run should be uploaded into the UNIPR servers as Text Grids. To be able to set each file into the required format it is necessary to use the Surfer software. Surfer 13 belongs to the Golden Software LLC company and has been used in this thesis to export files into Surfer 6 Text Grid. Texts grids were then edited with Notepad++ software and converted into the needed extension as follows:

1. [Simulation/name].BTM: bathymetry file
2. [Simulation/name].MAN: roughness file
3. [Simulation/name].INH : file for initial conditions
4. [Simulation/name].BLN: file for spatial domain of the computation
5. [Simulation/name].BCC: file for boundary conditions.
6. [Simulation/name].PTS: file for multi-resolution
7. [Simulation/name].IBC: file for geometry of structures
8. [Simulation/name].ILN: file for the position of structures

Bathymetry file

The input file .BTM contains information about the terrain elevation of the area of study. The raster is exported into Text Grid as described previously. The importance of this file, aside from holding the terrain information, lies in the fact that it also works as a reference for other files (i.e the .MAN and .INH files must have the same dimensions in terms of columns and rows as the .BTM file).

Roughness file

The file for the roughness representation is also a Text Grid that must have the same dimensions of the bathymetry file. This file is constructed with Surfer 13, using the .BTM file as base and the tool Grid-Math to modify it. This tool helps to locate areas of the terrain to

assign a specific Manning's coefficient value. One can assign different roughness coefficients to selected areas defined by polygons as shown in *Figure A.1*.

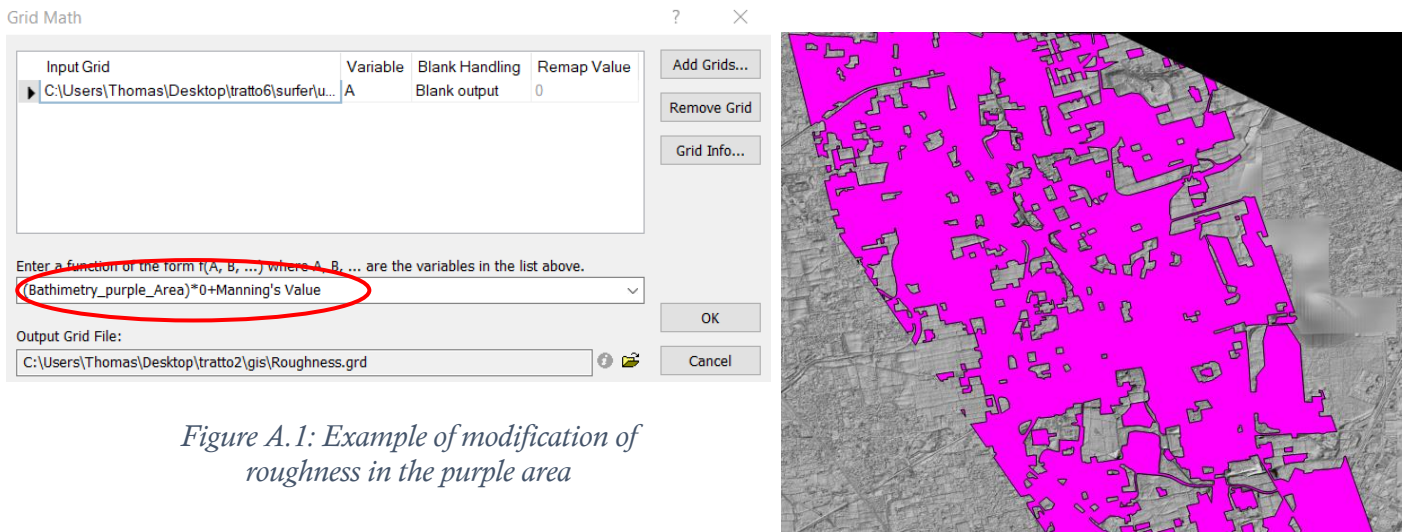


Figure A.1: Example of modification of roughness in the purple area

Afterwards, the Mosaic tool is used to merge all together the different grids with new values. The interface of the Mosaic tool can be seen in *Figure A.2*. It is important to notice that it is necessary to properly set both resample method (in orange) and the overlap method (light blue). Finally, the same procedure to save in .MAN extension as before is followed.

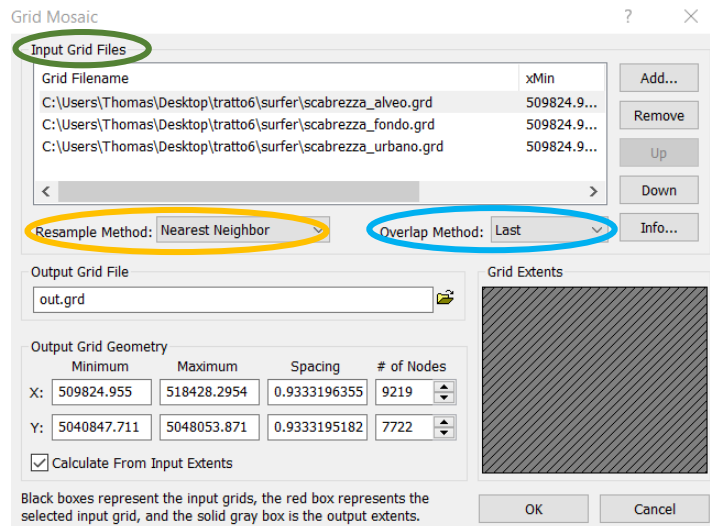


Figure A.2: Window of Mosaic tool

File for initial conditions

The initial condition file contains information about the water surface elevation in the area of study at the initial time. It is important to say that, also for dry bed, small wet areas are inserted to avoid numerical instability. These areas are defined by polygons that must intersect the

computational domain in correspondence of the inflow sections as shown in *Figure A.3*. To assign the initial water level is necessary to use Grid Math tool. Obviously in this case the initial water level is summed to the bathymetry. It is important to note that the dimensions must be the same as the .BTM file. The same procedure to save in .INH extension as before is followed.

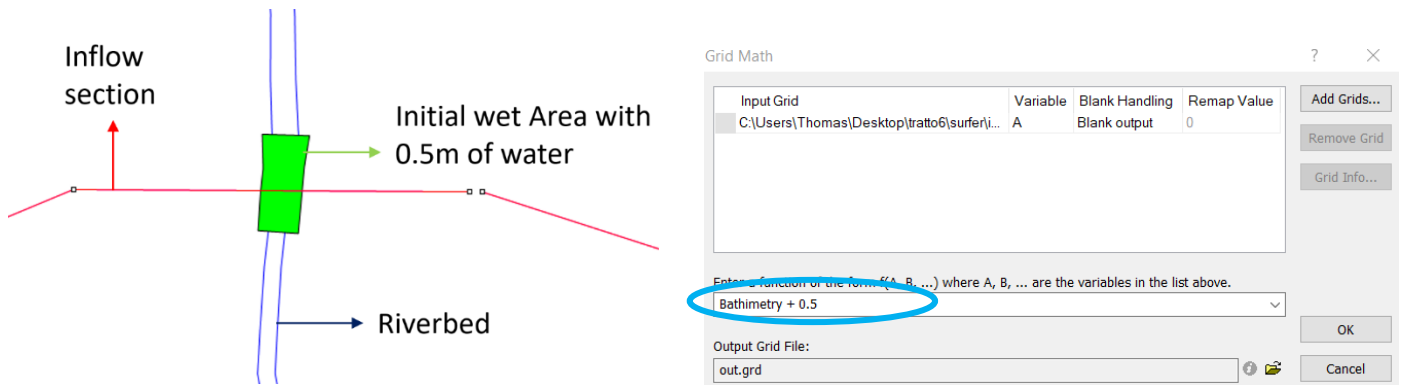


Figure A.3: Sketch of position of wet area respect the inflow section – window of Grid Math tool with an example with an example of water height assignment.

Files for spatial domain and boundary conditions

The spatial domain for the computation and the boundary conditions for the PARFLOOD code are input as two complementary files: .BLN and .BCC files. The .BLN file defines the computational domain. This is a text file created with the Digitize tool of Surfer 13. In this way, a polygon is traced to delimit the area over which the conditions will be applied. The polygon is formed by clicking over the .BTM file in a counter clockwise direction, saving the coordinates of the resulting vertices. The .bln saved file originally has three columns separated by commas, containing respectively the x-coordinate of the clicked point, y-coordinate of the clicked point and the elevation of the clicked point. With Notepad++ this file should be modified, erasing the commas and replacing them with spaces. Instead, in the third column one has to insert the specification of the boundary conditions for each segment. The different allowed types of boundary condition are:

- 21: For a discharge influx over time, i.e an input hydrograph.
- 2: For constant input discharge over time.
- 1: For a wall type boundary, meaning water cannot flow through.
- 4: For indicating a far field, meaning that water can flow away as if in an undisturbed plain terrain imposing the normal depth.
- 3: For the imposition of a water surface elevation at downstream section.

- 5: For assigning a known rating curve, meaning that on the selected downstream section the relationship between discharge in function of the water level is known.

An example of a proper .BLN file is shown in *Figure A.4*. This file is constructed by 9 points, as reported at line 1 of the file. There are boundary conditions of far field type in the fourth and sixth segments adjacent to the closing segment. At the upstream section is assigned a condition of hydrograph, with the number 21 at line 2, instead at the downstream one a rating curve condition is set, with the number 5 at line 6 of the file. Every condition in the file is set in the segment between the point where it is assigned until the subsequent point in the file. So, for the example in *Figure A.4*, the hydrograph condition is applied only in the first segment delimited by the points in lines 2 and 3.

The .BCC file is a text file that specifies each of the boundary conditions set in the .BLN file. For the condition of value 1 or 4 there is no need of any additional information, but, for the others, the user needs to input the related information. This file is structured with a header indicating how many boundary conditions there are, followed by each specification. The structure of this type of file can be seen as an example of the complementary file of the one shown in *Figure A.4* in *Figure A.5*.

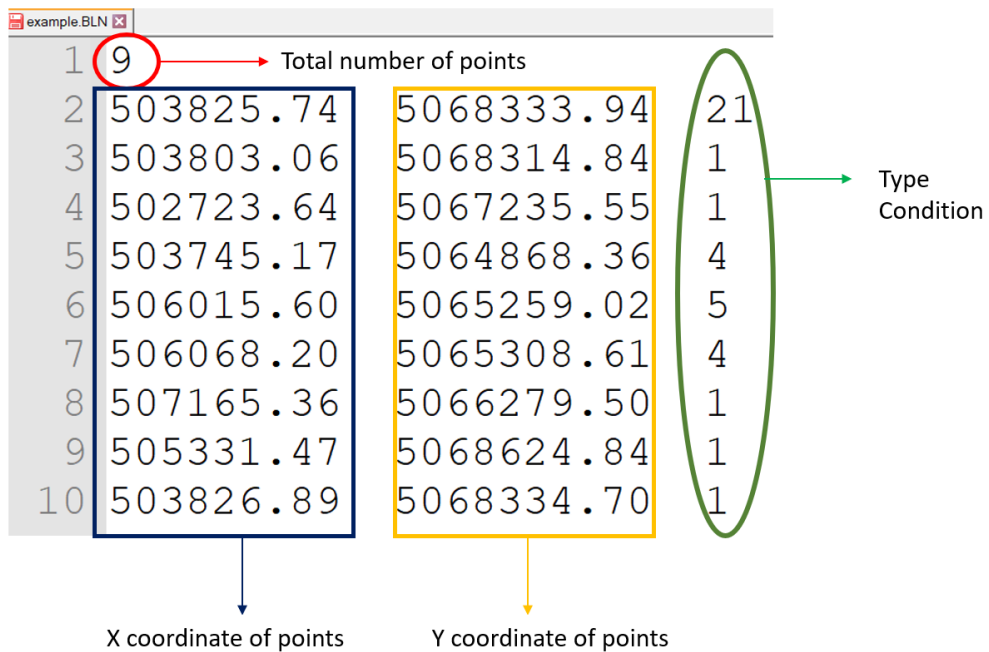


Figure A.4: Example of .BLN input file

		N° of total conditions		
	1	2		
N° of segment at which the first condition is applied	2	1	10	N° of rows that describe the first condition
	3	0	0	0
	4	300	0	5
	5	600	0	10
	6	900	0	20
	7	1200	0	30
	8	1500	0	35
	9	1800	0	30
	10	2100	0	25
	11	2400	0	15
	12	2700	0	10
N° of segment at which the second condition is applied	5	9		N° of rows that describe the second condition
	14	256.25	0	0
	15	256.53	0.5	0
	16	256.64	1.0	0
	17	256.72	1.5	0
	18	256.79	2.5	0
	19	257.85	2.5	0
	20	257.91	3.5	0
	21	258.96	4.5	0
	22	260.01	6.0	0

Figure A.5: Example of .BCC related to the above .BLN file input file

With reference to the *Figure A.5*, the header indicates that there are 2 incoming boundary condition specifications. The next line indicates, with a number 1, that the first boundary condition is valid from the first point declared in the .BLN file and consists of 10 lines of information. After the condition specifications, the values representing the hydrograph are reported, with the time information in the first column (in seconds) and the discharge corresponding values in the third column (in m^3/s). After the hydrograph is described, the values expressing the second boundary condition follow. In fact, at line 13 of the .BCC file there is 5, in concordance to the fact that the rating curve is applied at fifth segment of the computational domain, as shown in *Figure A.4*. Hence at line 13 there is also the number of data which describe the rating curve (9 in the example). Then the water surface elevation values are written in the first column, expressed in m a.s.l., while the related Q are reported in the third column (in m^3/s). For obvious reasons, depending on the type of boundary condition, the .BCC will be differently compiled. *Figure A.6* exhibits the structure of the text file for each of the possible boundary conditions that need to be specified.

Number of Boundary Conditions (hydrograph, water level and rating curve)			
Number of the line of the location of the point in which the boundary condition is called	Number indicating how many lines of information are incoming as hydrograph		
Time [s]	Water elevation [m a.s.l]	Discharge [m ³ /s]	0
Number of the line of the location of the point in which the boundary condition is called	Number indicating how many lines of information are incoming as water level values		
Time [s]	Water elevation [m a.s.l]	Discharge [m ³ /s]	0
Number of the line of the location of the point in which the boundary condition is called	Number indicating how many lines of information are incoming as rating curve		
Water elevation [m a.s.l]	Discharge in x-direction [m ³ /s]	Discharge in y-direction [m ³ /s]	///

Figure A.6: Summary table to construct .BCC file for all type of condition

Files for multi-resolution

In order to reduce the computational cost of the simulation, it is possible to use a multiresolution grid: this implicates that the cell sizes are not uniform everywhere, but are smaller where more detail is required and larger in areas of less interest. The .PTS file is used to indicate the coordinates of the points, to which cells with the desired resolution will correspond. The file has four columns: the first two represent the x and y coordinates of the points, the third shows the required resolution (1 to 4) and the fourth shows a zero.

Files for structures geometry and their positioning

The software allows two types of structures to be entered: bridges and other structures for which the scale of run-off is known. The .ILN file, containing the position of the sections on which the internal boundary conditions for bridges/structures have to be applied, is a text file structured as follows:

- Number of structures;
- Number of points on the 1st structure (typically 2);
- Value of x, y coordinates and internal boundary condition;
- Number of points in the 2nd structure (typically 2);
- Value of x, y coordinates and internal boundary condition;
- And so on.

The third value following the coordinates is the indicator for the inner boundary condition and it is always 7 in this file (even for condition type 8). It should be noted that the structure should preferably be described by only 2 points (section plotted from hydraulic left to right) and that the good functioning of the model is not guaranteed for "strange" polylines. With the help of Notepad++ software, the .ILN file will be structured as shown in *Figure A.7* (S is the number of structures, N is the number of points):

```

S
N1
XSX,1 YSX,1 CC1
XDX,1 YDX,1 CC1
N2
XSX,2 YSX,2 CC2
XDX,2 YDX,2 CC2
...

```

Figure A.7: Structure of .ILN file

The .IBC file contains additional information on the internal boundary conditions mentioned in the .ILN file. The IBC file is a text file, structured as shown schematically in *Figure A.8*.

Number of conditions		
Number of the structure on which to impose the condition (in the order of the .ILN file)	Number of values describing the geometry of the bridge	Type of internal condition (7=bridge , 8=internal rating curve)
Progressive [m] from left to right of the bridge section	Elevation of intrados [m.a.s.l.]	Elevation of talweg [m.a.s.l.]
...
Elevation of extrados [m.a.s.l.]	Overhang width of extrados [m]	
Number of the structure on which to impose the condition (in the order of the .ILN file)	Number of values describing the internal rating curve	Type of internal condition (7=bridge , 8=internal rating curve)
Water surface Elevation [m.a.s.l.]	Q [m ³ /s]	0
...

Figure A.8: Structure of .IBC file (yellow for bridges and green for rating curve structures)

An example of .ILN file and .IBC file is reported in Figure A.9.

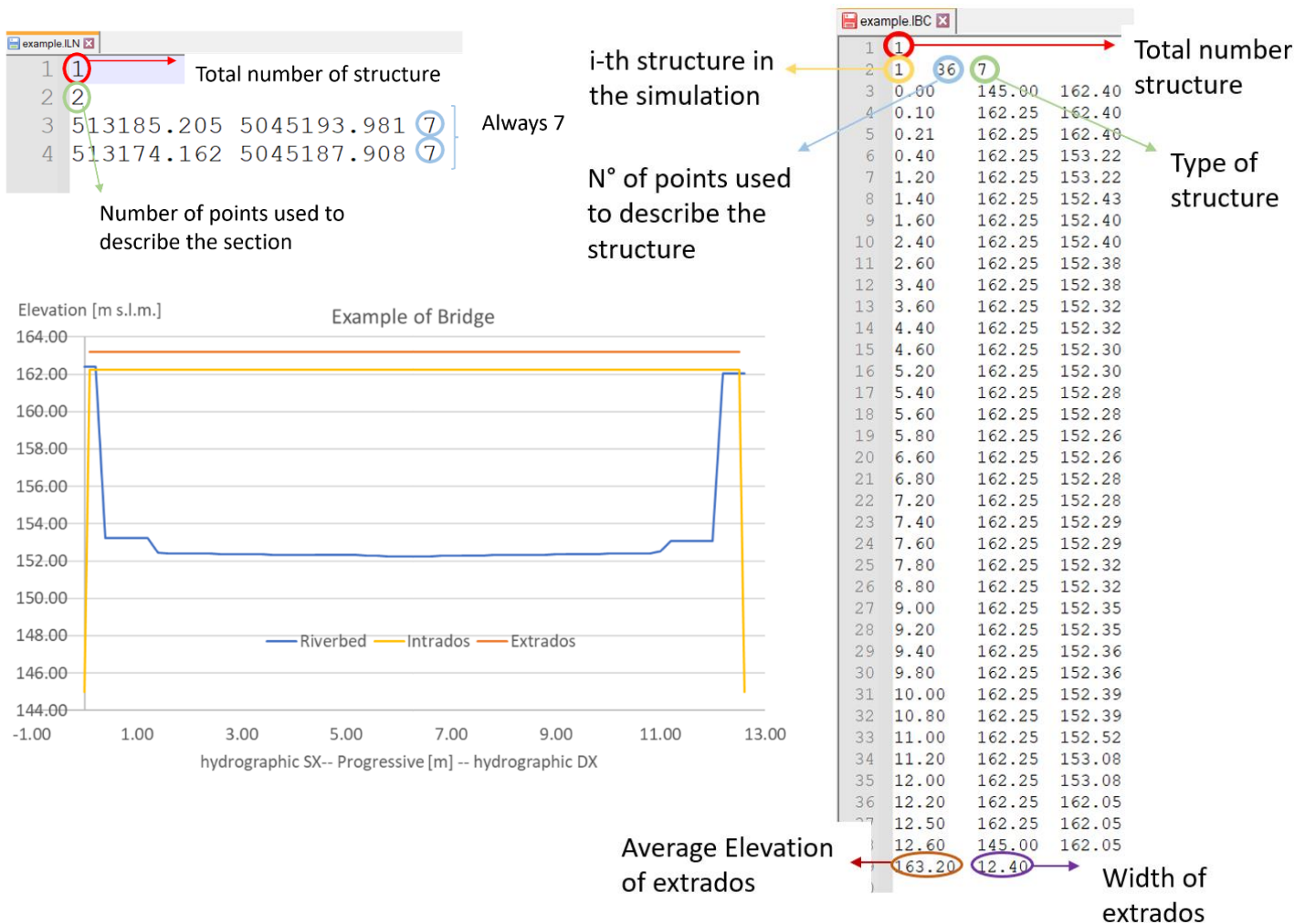


Figure A.9: Example of .ILN and .IBC files for describing the bridges shown

Code outputs

The PARFLOOD calculation provides, as available outputs, the following files:

- .WSE file, that is the water surface elevation data for each instant
- .DEP file, that is the water depth data for each instant
- .VVX and .VVY files, that are the velocity maps in the x-direction and the y-direction for each instant.

So, using the DECODE_SIMULATION file it is possible to extract the following outputs:

- Maps of depth, w.s.e., and velocity at any instant of time, for all or a part of the calculation domain.
- Maps with maximum values of depth, w.s.e. and velocity, for all or a part of the calculation domain.
- Values of depth, w.s.e. and velocity on some cells whose coordinates are required.
- Flow rate through a control section.

Appendix B

MATLAB code to build a digital terrain model for the main river channel

Description

This appendix illustrates the working principles of the MATLAB code built to correct the DTM in correspondence of the water courses.

The reconstruction of the riverbed is necessary because the original DTMs show the elevations of the water surface or of the bridges, hiding in this way the elevation of the riverbed. Since the DTMs are an input for two-dimensional hydraulic simulations, this operation is crucial.

The data necessary to correct the DTM are:

- Cross-section elevation profile
- Cross-section coordinates of at least two benchmarks
- River axis along the selected reach, Geo-referenced.

Inputs

The first step to use the code is the creations of inputs that are:

- I. a text file with the coordinates of the river axis. This text file contains two columns with the x and y coordinates for each point, as shown in *Figure B.1*.



Figure B.1: Example of input I and related map. The table has titles for clarity but the actual input files only contain numbers.

It is important to specify that the points must be ordered from upstream to downstream or vice versa. Furthermore, the code does not allow two consecutive points that have the same x or y coordinate; should such a situation arise, the code will modify the coordinates x and y of one of the two points by 5cm.

- I. One text file for each section named with a number (sections need to be sorted from upstream to downstream or vice versa, while there is no rule to be followed for the section names that do not need to be in any order). It is possible to observe that each text file is composed by 2 columns, as shown in *Figure B.2*, that contains station and elevation of riverbed surveyed points. Not all the section points are inserted in the text file, but only those that describe the riverbed, as shown in *Figure B.3*.

Station [m]	Elevation [m.a.l.s.]
77.78	142.22
82.80	138.60
86.11	138.41
88.94	138.65
93.36	142.47

Figure B.2: Example of section file named "1.txt". The table has titles for clarity but the actual input files only contain numbers.

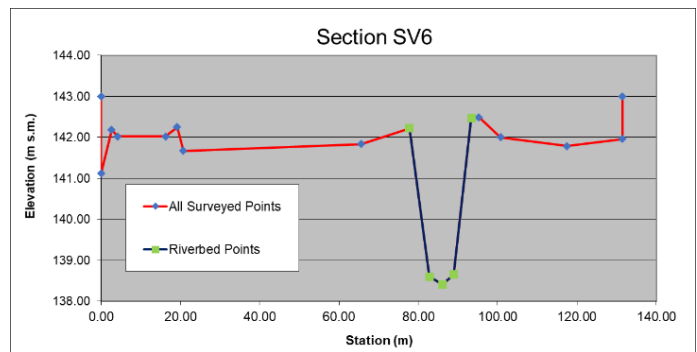


Figure B.3: Example of chosen points among those available

- II. A text file containing the coordinates of the two benchmarks for each section. The file is constructed as shown in *Figure B.4*.

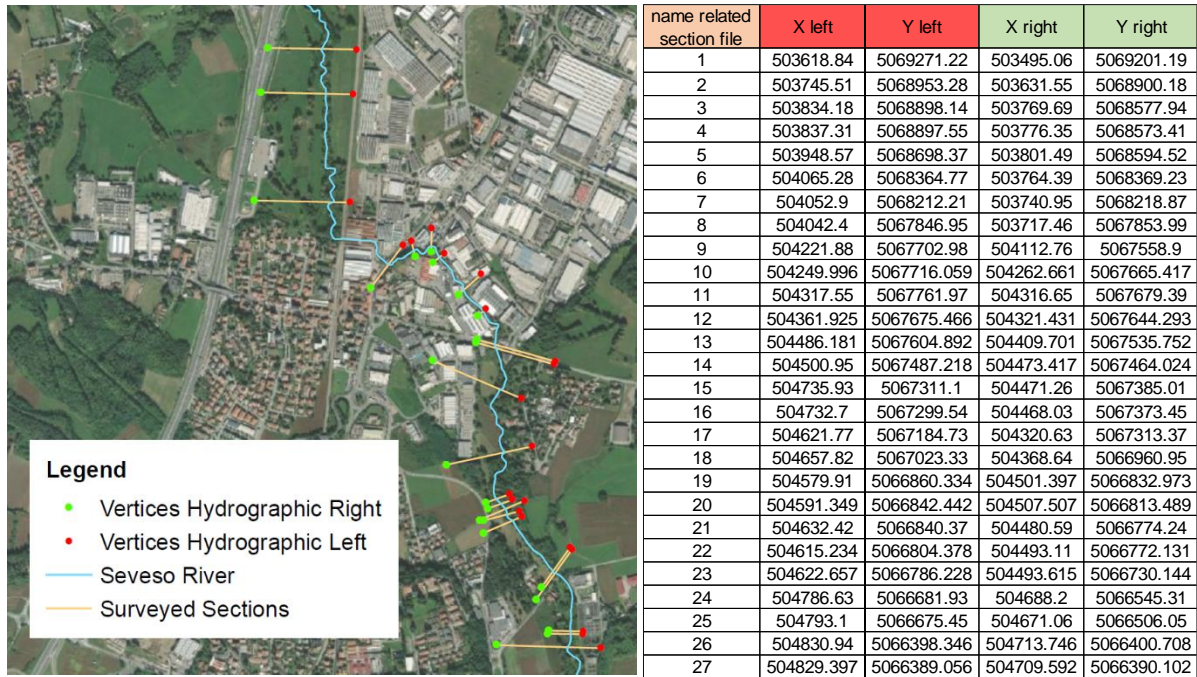


Figure B.4: Example of input II (Right table) and the related representation of vertices in the map (Left figure). The table has titles for clarity, but the actual input files only contain numbers.

Hence, there are 5 columns: in the first one there is the name of the corresponding section text file presented above. Instead, in the second and third columns there are the x-y coordinates of the benchmarks on hydrographic left, so, in the last two columns there are the coordinates referred to those on the hydrographic right.

How the code works

The code performs mainly 3 macro-operations:

- 1) In the first one the aim is to find the intersections between the sections and the segments of the river axis, defined by two successive points in the input file described above (I input). To do this, the first step carried out by the code is to transform the stations of the points of each section into x-y coordinates starting from the benchmarks. Then, for each section, the program solves n linear systems 2X2 (with n number of segments that compose the river axis) to find the intersections between the line passing through the section and the river stream. If there is more than one intersection, the code computes the distance between all possible intersections and both vertices and it chooses the intersection that has the smallest average of the distances from the vertices. An example is shown in *Figure B.5*.

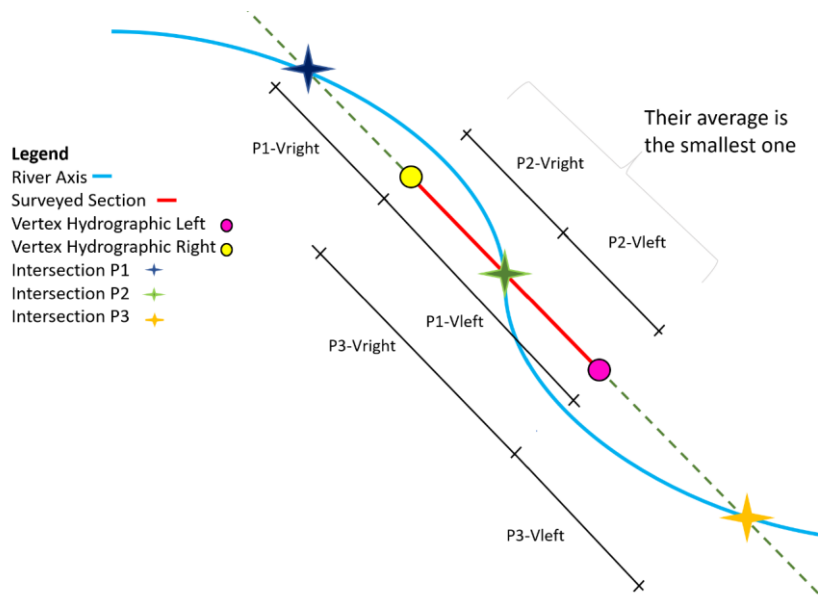


Figure B.5: Sketch of chosen closest intersection

- 2) The second part is useful for projecting the measured sections. It is convenient to have sections which are perpendicular to the river. An example is shown in *Figure B.6*. It is important to specify that the code allows the user to choose whether to project sections or not (in the initial lines with the user settings).

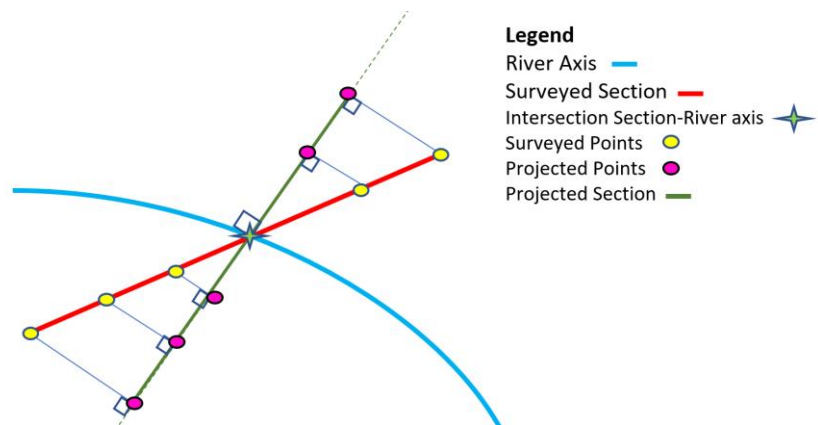


Figure B.6: Sketch of projected section

- 3) The last part of the code is where the sections are interpolated to create the bathymetry of the riverbed. There are three different interpolations:
- i) The first linear interpolation occurs within each individual section. In particular, the stations and elevations are linearly interpolated to have the same number of points on all the sections considered. The number of points is set by

the user. An example is shown in *Figure B.7* using the number of points for section equal to 10.

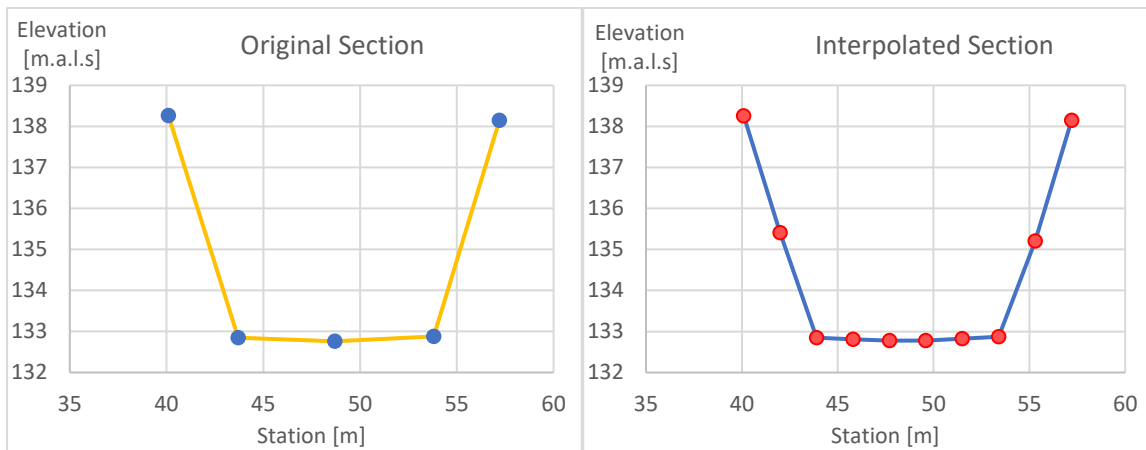


Figure B.7: Example of result after the first interpolation

- ii) The second interpolation is a linear interpolation between two successive surveyed sections, governed by a sufficiently large step imposed by the user. It is important to specify that also the centering with respect to the river axis is interpolated, this is fundamental in sections where the river axis is displaced with respect to the real riverbed. The sections obtained from this level of interpolation are georeferenced by imposing them perpendicular to the river axis. An example is reported in *Figure B.8*.

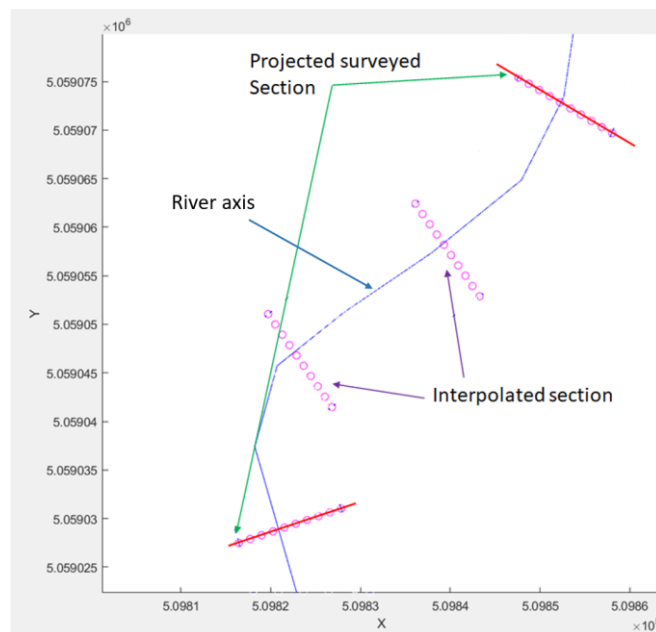


Figure B.8: Example of result after the second interpolation

iii) The last level of interpolation, which is nested with the second one, takes place between the sections obtained from the previous step. Considering the example shown in *Figure B.9*, we see the two sections in purple as the result of the previous interpolation, and the cyan ones as the result of this last interpolation. The cyan sections have stations and elevations calculated with linear interpolation between those of the purple sections. The positioning criterion is no longer the imposition of perpendicularity with respect to the axis but starting from the two angles formed with the horizontal by the purple sections (angles in orange and green in *Figure B.9*), the blue sections rotate following a linear interpolation of the section angle with the x axis in the map. The progressive variation of the angle was preferred to imposing perpendicularity to the axis in order to avoid wrong intersections between the interpolated sections, with a consequent bad representation of the banks. This last level of interpolation is governed by a step that must necessarily be smaller than that of the previous step. The user can impose this in the initial lines of the code. The contour line shown in *Figure B.9* is built by the code connecting the vertices of all sections.

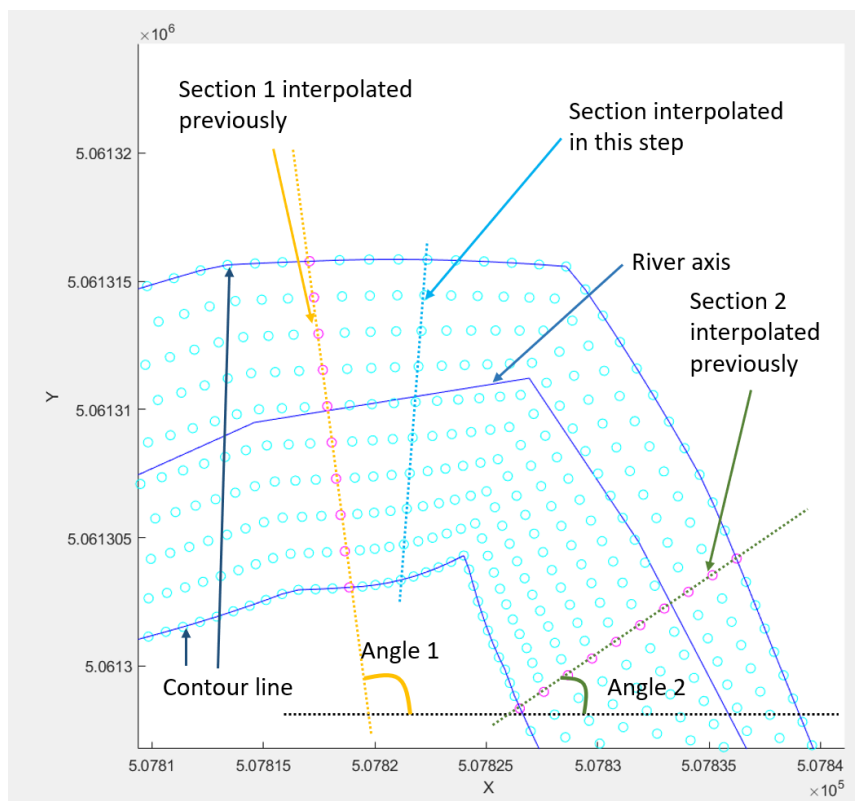


Figure B.9: Example of result after the last interpolation

Outputs

The outputs of this method are:

- 1) A text file containing the bathymetry of the riverbed to be overlaid on the original DTMs using GIS software, as explained in *Section 3.1*.
- 2) A text file containing the coordinates of the vertices of the contour line which describes the riverbed.

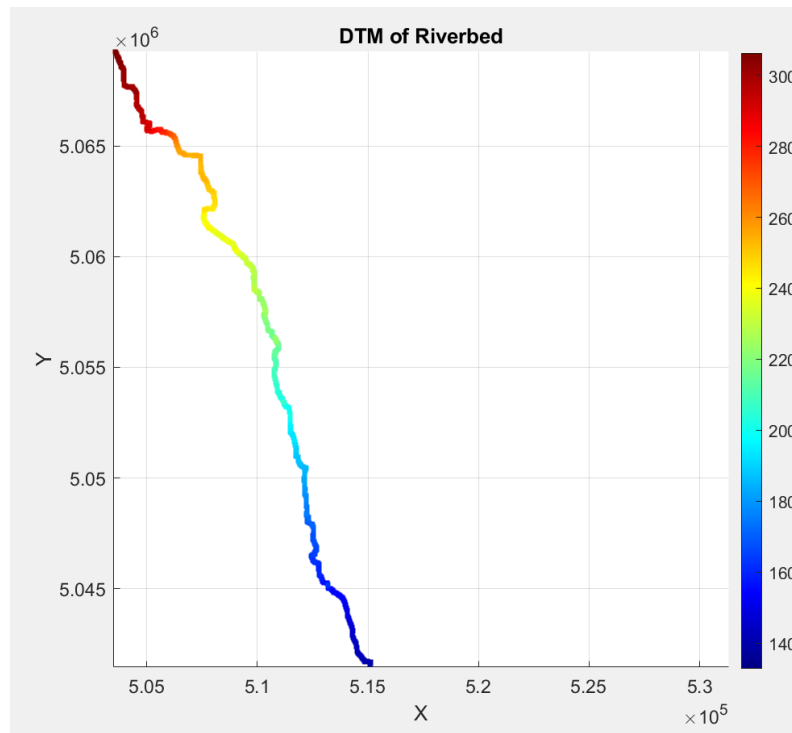


Figure B.10: Example of output DTM plotted in MATLAB

CODE

```
%% Crea una batimetria di letto partendo da:  
%% - vertici_sezioni che indica il nome delle sezioni e le coordinate dei capisaldi (sezioni viste  
da monte)  
%% - punti_asse che contiene le coordinate x,y della polilinea d'asse (da monte a valle)  
%% - file di testo nome_sezione.txt che contengono station-elevation (solo alveo)  
  
close all  
clear  
clc  
  
% PARAMETRI UTENTE  
proietta=0; % 0 per non proiettare le sezioni rilevate, 1 per proiettarle1
```

```

n_punti_sez=50; % numero punti per interpolazione station-elevation delle sezioni rilevate
delta_s=9.76; % distanza tra le sezioni interpolate, primo giro
delta_s_2=1; % distanza tra le sezioni interpolate, giro annidato
nome_file_vertici='dati_vertici_Seveso.txt';
nome_file_asse='dati_asse_Seveso.txt';

% (1) -----
% Apertura dati e visualizzazione iniziale
dati_vertici=textread(nome_file_vertici);

x_vert=cat(1,dati_vertici(:,2),dati_vertici(:,4)); y_vert=cat(1,dati_vertici(:,3),dati_vertici(:,5));
y1_plot=min(y_vert); y2_plot=max(y_vert); x1_plot=min(x_vert);
x2_plot=x1_plot+(y2_plot-y1_plot); % adesso li scopre lui

dati_asse=textread(nome_file_asse);

% eliminazione dei segmenti orizzontali e verticali
xarim=dati_asse(:,1); yarim=dati_asse(:,2);
xarim1=xarim(1:length(xarim)-1); xarim2=xarim(2:length(xarim));
yarim1=yarim(1:length(yarim)-1); yarim2=yarim(2:length(yarim));
diffx=xarim1-xarim2; diffy=yarim1-yarim2;
zerix=find(diffx==0); zeriyy=find(diffy==0);
xarim(zerix)=xarim(zerix)+0.05; yarim(zeriyy)=yarim(zeriyy)+0.05;
dati_asse=cat(2,xarim,yarim);

xarim=dati_asse(:,1); yarim=dati_asse(:,2);
xarim1=xarim(1:length(xarim)-1); xarim2=xarim(2:length(xarim));
yarim1=yarim(1:length(yarim)-1); yarim2=yarim(2:length(yarim));
diffx=xarim1-xarim2; diffy=yarim1-yarim2;
zerix=find(diffx==0); zeriyy=find(diffy==0);
xarim(zerix)=xarim(zerix)+0.05; yarim(zeriyy)=yarim(zeriyy)+0.05;
dati_asse=cat(2,xarim,yarim);

xarim=dati_asse(:,1); yarim=dati_asse(:,2);
xarim1=xarim(1:length(xarim)-1); xarim2=xarim(2:length(xarim));
yarim1=yarim(1:length(yarim)-1); yarim2=yarim(2:length(yarim));
diffx=xarim1-xarim2; diffy=yarim1-yarim2;
zerix=find(diffx==0); zeriyy=find(diffy==0);
xarim(zerix)=xarim(zerix)+0.05; yarim(zeriyy)=yarim(zeriyy)+0.05;
dati_asse=cat(2,xarim,yarim);

figure(1)
hold on
plot(dati_asse(:,1),dati_asse(:,2),'-b'),axis([x1_plot x2_plot y1_plot y2_plot]), axis square;
plot(dati_vertici(:,2),dati_vertici(:,3),'^k',dati_vertici(:,4),dati_vertici(:,5),'sk'),axis([x1_plot
x2_plot y1_plot y2_plot]), axis square;

```

```

for indice_sezione=1:size(dati_vertici,1)
    dati_sezione=textread(strcat(num2str(dati_vertici(indice_sezione,1)),'.txt'));
    numeropunti=size(dati_sezione,1);
    x1=dati_vertici(indice_sezione,2);          y1=dati_vertici(indice_sezione,3);
x2=dati_vertici(indice_sezione,4); y2=dati_vertici(indice_sezione,5);
    L_sezione=sqrt((x2-x1)^2+(y2-y1)^2);
    x_sezione=[]; y_sezione=[];
    for i_punto=1:numeropunti
        st_punto=dati_sezione(i_punto,1);
        x_sezione(i_punto)=x1+(x2-x1)*st_punto/L_sezione;
        y_sezione(i_punto)=y1+(y2-y1)*st_punto/L_sezione;
    end
    plot(x_sezione,y_sezione,'k');
end

% (2) -----
% Ora devo trovare le intersezioni con l'asse, le progressive, i beta e gli angoli
% se lo decido, proietto le sezioni rilevate per renderle perpendicolari all'asse
% (2a) -----
% Progressive lungo l'asse
x_asse=dati_asse(:,1); y_asse=dati_asse(:,2);
numero_segmenti_asta=length(x_asse)-1;
prog_asse(1)=0;
indice_progressive=2;
while indice_progressive<=numero_segmenti_asta+1
    prog_asse(indice_progressive)=prog_asse(indice_progressive-1)+...
        sqrt((x_asse(indice_progressive)-x_asse(indice_progressive-1))^2+...
            (y_asse(indice_progressive)-y_asse(indice_progressive-1))^2);
    indice_progressive=indice_progressive+1;
end
% (2b) -----
% Intersezioni, progressive, beta e angoli delle sezioni (con eventuale proiezione)
intersezioni=[]; % inizializzazione di una matrice vuota; avrà cinque colonne (nome_sezione,
indice_segmento_asta, x_intersezione, y_intersezione, progressiva intersezione)
% ciclo sulle sezioni
numero_sezioni=size(dati_vertici,1); % sono quelle rilevate
dati_vertici_p=dati_vertici; % conterrà le proprietà delle sezioni eventualmente proiettate
tabella_gamma_ril=[]; % conterrà i valori dei gamma
for indice_sezione=1:numero_sezioni
    % qualche proprietà della sezione
    nome_sezione=dati_vertici(indice_sezione);
    dati_sezione=textread(strcat(num2str(nome_sezione),'.txt'));
    numeropunti=size(dati_sezione,1);
    x1=dati_vertici(indice_sezione,2);          y1=dati_vertici(indice_sezione,3);
x2=dati_vertici(indice_sezione,4); y2=dati_vertici(indice_sezione,5);
    L_sezione=sqrt((x2-x1)^2+(y2-y1)^2);
    x_sezione=[]; y_sezione=[];
    for i_punto=1:numeropunti
        st_punto=dati_sezione(i_punto,1);
        x_sezione(i_punto)=x1+(x2-x1)*st_punto/L_sezione;
        y_sezione(i_punto)=y1+(y2-y1)*st_punto/L_sezione;
    end
end

```

```

m_sezione=(y_sezione(length(x_sezione))-y_sezione(1))/(x_sezione(length(x_sezione))-
x_sezione(1));
q_sezione=y_sezione(1)-m_sezione*x_sezione(1);
% ricerca intersezione (ciclo su tutti i segmenti dell'asse e verifico)
intersezioni_candidati=[]; % avrà cinque colonne: x, y, check che intersechi davvero il
segmento, progressiva, distanza)
for indice_segmento=1:numero_segmenti_asta
    % punti del segmento, equazione della retta relativa, progressive
    x1_a=x_asse(indice_segmento); y1_a=y_asse(indice_segmento);
    x2_a=x_asse(indice_segmento+1); y2_a=y_asse(indice_segmento+1);
    m_segmento=(y2_a-y1_a)/(x2_a-x1_a); q_segmento=y1_a-m_segmento*x1_a;
    p1=prog_asse(indice_segmento); p2=prog_asse(indice_segmento+1);
    % punto di intersezione e controllo; aggiunta alla matrice
    x_intersezione_cand=(q_sezione-q_segmento)/(m_segmento-m_sezione);
    y_intersezione_cand=m_segmento*x_intersezione_cand+q_segmento;
    if x_intersezione_cand>=min(x1_a,x2_a) && x_intersezione_cand<=max(x1_a,x2_a)
    && y_intersezione_cand>=min(y1_a,y2_a) && y_intersezione_cand<=max(y1_a,y2_a)
        controllo=1; % intersezione buona
    else
        controllo=0; % intersezione non buona
    end
    progressiva_cand=p1+sqrt((x_intersezione_cand-x1_a)^2+(y_intersezione_cand-
y1_a)^2);
    distanza_cand=0.5*(sqrt((x_intersezione_cand-x1)^2+(y_intersezione_cand-
y1)^2)+sqrt((x_intersezione_cand-x2)^2+(y_intersezione_cand-y2)^2));
    intersezioni_candidati=cat(1,intersezioni_candidati,[x_intersezione_cand
y_intersezione_cand controllo progressiva_cand distanza_cand]); % righe=numero segmenti,
spero un solo 1 nella colonna 3
end
% scelta del punto di intersezione
x_candidati=intersezioni_candidati(:,1);
y_candidati=intersezioni_candidati(:,2);
controllo_candidati=intersezioni_candidati(:,3);
prog_candidati=intersezioni_candidati(:,4);
dist_candidati=intersezioni_candidati(:,5);
if length(find(controllo_candidati==1))==1
    posizione=find(controllo_candidati==1);
    x_intersezione=x_candidati(posizione);
    y_intersezione=y_candidati(posizione);
    prog_intersezione=prog_candidati(posizione);
    intersezioni=cat(1,intersezioni,[nome_sezione posizione x_intersezione y_intersezione
prog_intersezione]);
else
% stringa=strcat('troppi alla sezione:',num2str(nome_sezione));
% disp(stringa);
x_candidati_check=x_candidati(find(controllo_candidati==1));
y_candidati_check=y_candidati(find(controllo_candidati==1));
prog_candidati_check=prog_candidati(find(controllo_candidati==1));
dist_candidati_check=dist_candidati(find(controllo_candidati==1));
posizione_mindist=find(dist_candidati_check==min(dist_candidati_check));
posizione=posizione_mindist;
x_intersezione=x_candidati_check(posizione_mindist);

```

```

y_intersezione=y_candidati_check(posizione_mindist);
prog_intersezione=prog_candidati_check(posizione_mindist);
intersezioni=cat(1,intersezioni,[nome_sezione posizione x_intersezione y_intersezione
prog_intersezione]);
end
% proietto la sezione se decido di farlo; creo la matrice dei nuovi vertici e il nuovo file di
testo delle sezioni
if proietta==1 % devo proiettare
% segmento dell'asse e retta corrispondente
x1a=x_asse(posizione); y1a=y_asse(posizione);
x2a=x_asse(posizione+1); y2a=y_asse(posizione+1);
ma=(y2a-y1a)/(x2a-x1a); qa=y2a-ma*x2a;
% retta perpendicolare all'asse
mp=-1/ma; qp=y_intersezione-mp*x_intersezione;
% proiezione dei punti della sezione
x_sezione_p=((y_sezione-ma*x_sezione)-qp)/(mp-ma);
y_sezione_p=mp*x_sezione_p+qp;
% proiezione dei vertici
x1_p=((y1-ma*x1)-qp)/(mp-ma); x2_p=((y2-ma*x2)-qp)/(mp-ma);
y1_p=mp*x1_p+qp; y2_p=mp*x2_p+qp;
% station-elevation della sezione proiettata
station_p=[];
for gg=1:length(x_sezione_p)
station_p(gg)=sqrt((x_sezione_p(gg)-x1_p)^2+(y_sezione_p(gg)-y1_p)^2);
end
dati_sezione_p=cat(2,station_p,dati_sezione(:,2));
dati_vertici_p(indice_sezione,2)=x1_p;
dati_vertici_p(indice_sezione,3)=y1_p;
dati_vertici_p(indice_sezione,4)=x2_p;
dati_vertici_p(indice_sezione,5)=y2_p;
else
x_sezione_p=x_sezione;
y_sezione_p=y_sezione;
x1_p=x1; x2_p=x2;
y1_p=y1; y2_p=y2;
dati_sezione_p=dati_sezione;
end
nomesalva_p=strcat(num2str(nome_sezione),'_p.txt');
save(nomesalva_p,'dati_sezione_p','-ascii');
plot(x1_p,y1_p,'^m',x2_p,y2_p,'sm');
% plot([x1_p x2_p],[y1_p y2_p],'sg');
plot(x_sezione_p,y_sezione_p,'-m');
% ora posso calcolare il beta e aggiungerlo come colonna 6 alla dati_vertici_p
x_sx=x_sezione_p(1); x_dx=x_sezione_p(neropunti);
y_sx=y_sezione_p(1); y_dx=y_sezione_p(neropunti);
d_sx=sqrt((x_intersezione-x_sx)^2+(y_intersezione-y_sx)^2); d_dx=sqrt((x_intersezione-
x_dx)^2+(y_intersezione-y_dx)^2);
l_sezione=sqrt((x_dx-x_sx)^2+(y_dx-y_sx)^2);
if d_sx<=l_sezione && d_dx<=l_sezione % la sezione interseca l'asse
beta=d_sx/l_sezione; % sar  < 1
elseif d_sx>l_sezione && d_dx>d_dx % la sezione   a sinistra dell'asse
beta=d_sx/l_sezione; % sar  > 1

```

```

elseif d_dx>1_sezione && d_sx<d_dx % la sezione è a destra dell'asse
    beta=-d_sx/1_sezione; % sarà < 0
else
    disp(strcat('non riesco a calcolare beta alla ',num2str(nome_sezione)));
end
dati_vertici_p(indice_sezione,6)=beta;
% determino infine l'angolo gamma (radianti) con l'asse delle x
m_sezione=(y_dx-y_sx)/(x_dx-x_sx);
if (x_dx-x_sx)<0
    dati_vertici_p(indice_sezione,7)=atan(m_sezione)+pi;
elseif (x_dx-x_sx)>0 && (y_dx-y_sx)>0
    dati_vertici_p(indice_sezione,7)=atan(m_sezione);
elseif (x_dx-x_sx)>0 && (y_dx-y_sx)<0
    dati_vertici_p(indice_sezione,7)=atan(m_sezione)+2*pi;
end

tabella_gamma_ril=cat(1,tabella_gamma_ril,cat(2,nome_sezione,dati_vertici_p(indice_sezio
ne,7)));
end
% aggiungo le intersezioni al diagramma
plot(intersezioni(:,3),intersezioni(:,4),'xk');

% (3) -----
% Ciclo di interpolazione sezioni, referenziazione e aggiunta al risultato finale
% (3a) -----
% inizializzo le matrici del risultato
batimetria=[]; batimetria_interna=[]; linea_clip_sx=[]; linea_clip_dx=[];
% (3b) -----
% ciclo sulle sezioni rilevate
for indice_sezione=1:(numero_sezioni-1)
    % (3b1) sezione 1
    nome_1=dati_vertici_p(indice_sezione);
    dati_1=textread(strcat(num2str(nome_1),'_p.txt'));
    station_1=dati_1(:,1); station_start=station_1(1); station_end=station_1(length(station_1));
    % rimozione dei punti duplicati
    station_1_1=station_1(1:length(station_1)-1);
    station_1_2=station_1(2:length(station_1));
    diff_st=station_1_1-station_1_2;
    zeri=find(diff_st==0);
    station_1(zeri)=station_1(zeri)-0.01; % tolgo 1 cm

    station_1_1=station_1(1:length(station_1)-1);
    station_1_2=station_1(2:length(station_1));
    diff_st=station_1_1-station_1_2;
    zeri=find(diff_st==0);
    station_1(zeri)=station_1(zeri)-0.01; % tolgo 1 cm

    station_start=station_1(1); station_end=station_1(length(station_1));

% interpolazione
passo_int=(station_end-station_start)/(n_punti_sez-1);

```

```

elevation_1=dati_1(:,2);
station_1_int=station_start:passo_int:station_end; % e avrà il numero di punti che ho scelto
all'inizio
elevation_1_int=interp1(station_1,elevation_1,station_1_int);
% creo la x,y,z della sezione 1 e aggiungo alla batimetria
x11=dati_vertici_p(indice_sezione,2); y11=dati_vertici_p(indice_sezione,3);
x21=dati_vertici_p(indice_sezione,4); y21=dati_vertici_p(indice_sezione,5);
L_sezione1=sqrt((x21-x11)^2+(y21-y11)^2);
x_sezione1=[]; y_sezione1=[];
for i_punto=1:n_punti_sez
    st_punto=station_1_int(i_punto);
    x_sezione1(i_punto)=x11+(x21-x11)*st_punto/L_sezione1;
    y_sezione1(i_punto)=y11+(y21-y11)*st_punto/L_sezione1;
end
batimetria_aggiungere=cat(2,x_sezione1',y_sezione1',elevation_1_int');
batimetria=cat(1,batimetria,batimetria_aggiungere);
% (3b2) sezione 2
nome_2=dati_vertici(indice_sezione+1);
dati_2=textread(strcat(num2str(nome_2),'_p.txt'));
station_2=dati_2(:,1); station_start=station_2(1); station_end=station_2(length(station_2));
% rimozione dei punti duplicati
station_2_1=station_2(1:length(station_2)-1);
station_2_2=station_2(2:length(station_2));
diff_st=station_2_1-station_2_2;
zeri=find(diff_st==0);
station_2(zeri)=station_2(zeri)-0.01; % tolgo 1 cm

station_2_1=station_2(1:length(station_2)-1);
station_2_2=station_2(2:length(station_2));
diff_st=station_2_1-station_2_2;
zeri=find(diff_st==0);
station_2(zeri)=station_2(zeri)-0.01; % tolgo 1 cm

station_start=station_2(1); station_end=station_2(length(station_2));

% interpolazione
passo_int=(station_end-station_start)/(n_punti_sez-1);
elevation_2=dati_2(:,2);
station_2_int=station_start:passo_int:station_end; % e avrà il numero di punti che ho scelto
all'inizio
elevation_2_int=interp1(station_2,elevation_2,station_2_int);
% (3b3) qui il ciclo per interpolare le sezioni
% (3b3a) progressive, distanza, distanza interpolare, beta
prog_1=intersezioni(indice_sezione,5); prog_2=intersezioni(indice_sezione+1,5);
passo_prog=delta_s;
beta_1=dati_vertici_p(indice_sezione,6); beta_2=dati_vertici_p(indice_sezione+1,6);
gamma_1=dati_vertici_p(indice_sezione,7);
gamma_2=dati_vertici_p(indice_sezione+1,7);

```

% (3b3a1) trasformo la prima sezione rilevata in una "interpolata precedente" per semplificare l'interpolazione interna

```

beta_int_prec=beta_1; gamma_int_prec=gamma_1;
station_int_prec=station_1_int; elevation_int_prec=elevation_1_int;
prog_int_prec=prog_1;
% (3b3b) ciclo sezioni interpolate
prog_attuale=prog_1+passo_prog;
while prog_attuale<prog_2
    % (3b3b1) determino station ed elevation e beta
    station_interpolata=station_1_int+(prog_attuale-prog_1)/(prog_2-
prog_1)*(station_2_int-station_1_int);
    elevation_interpolata=elevation_1_int+(prog_attuale-prog_1)/(prog_2-
prog_1)*(elevation_2_int-elevation_1_int);
    beta_interpolata=beta_1+(prog_attuale-prog_1)/(prog_2-prog_1)*(beta_2-beta_1);
    % (3b3b2) referenzio la sezione interpolata
    % faccio le seguenti operazioni:
    % 1- trovo i punti dell'asse appena prima e appena dopo
    % 2- trovo la retta che corrisponde a quel segmento dell'asse
    % 3- trovo la retta perpendicolare, che conterrà la sezione
    % 4- genero i punti x,y della sezione
    % 1-
    indice_punto_prima=max(find(prog_asse<prog_attuale));
    indice_punto_dopo=min(find(prog_asse>prog_attuale));
    xa1=x_asse(indice_punto_prima);
    ya1=y_asse(indice_punto_prima);
    xa2=x_asse(indice_punto_dopo);
    ya2=y_asse(indice_punto_dopo);
    pa1=prog_asse(indice_punto_prima);
    pa2=prog_asse(indice_punto_dopo);
    % 2-
    ma=(ya2-ya1)/(xa2-xa1);
    % 3-
    ms=-1/ma;
    alpha=atan(abs(ms)); % considero il valore assoluto, i segni sono tenuti in conto dopo
    if (ya2-ya1)<0
        gammasez=atan(ms)+pi;
    elseif (ya2-ya1)>0 && (xa2-xa1)<0
        gammasez=atan(ms);
    elseif (ya2-ya1)>0 && (xa2-xa1)>0
        gammasez=atan(ms)+2*pi;
    end
    % 4-
    % 4.1- coordinate x,y da attribuire al punto in asse della sezione
    % (intersezione delle due rette)
    xc=(prog_attuale-pa1)/(pa2-pa1)*(xa2-xa1)+xa1;
    yc=(prog_attuale-pa1)/(pa2-pa1)*(ya2-ya1)+ya1;
    % 4.2- lunghezza e punto in asse della sezione
    x_sezione=[]; % inizializzazione
    y_sezione=[]; % inizializzazione
    numero_punti=n_punti_sez;
    lunghezza_sez=station_interpolata(numero_punti)-station_interpolata(1);

```

```

stc=station_interpolata(1)+lunghezza_sez*beta_interpolata; % station del punto di
intersezione con l'asse
% 4.3- determinazione di x,y a partire dalla station (con
% riconoscimento del quadrante in base alla direzione dell'asse)
if xa2>xa1 && ya2<ya1 % quadrante 4
    for k=1:n_punti_sez
        station_punto=station_interpolata(k);
        x_sezione(k)=xc-(station_punto-stc)*cos(alpha);
        y_sezione(k)=yc-(station_punto-stc)*sin(alpha);
    end
elseif xa2<xa1 && ya2<ya1 % quadrante 3
    for k=1:n_punti_sez
        station_punto=station_interpolata(k);
        x_sezione(k)=xc-(station_punto-stc)*cos(alpha);
        y_sezione(k)=yc+(station_punto-stc)*sin(alpha);
    end
elseif xa2<xa1 && ya2>ya1 % quadrante 2
    for k=1:n_punti_sez
        station_punto=station_interpolata(k);
        x_sezione(k)=xc+(station_punto-stc)*cos(alpha);
        y_sezione(k)=yc+(station_punto-stc)*sin(alpha);
    end
elseif xa2>xa1 && ya2>ya1 % quadrante 1
    for k=1:n_punti_sez
        station_punto=station_interpolata(k);
        x_sezione(k)=xc+(station_punto-stc)*cos(alpha);
        y_sezione(k)=yc-(station_punto-stc)*sin(alpha);
    end
else
    disp('ERRORE GIACITURA ASSE FLUVIALE');
    return
end
% (3b3b3) aggiornamento della matrice x,y,z
batimetria_aggiungere=cat(2,x_sezione',y_sezione',elevation_interpolata');
batimetria=cat(1,batimetria,batimetria_aggiungere);
% (3b4) ciclo dell'interpolazione interna
% le progressive vanno da prog_int_prec a prog_attuale;
% i gamma vanno da gamma_int_prec a gammasez;
% i beta vanno da beta_int_prec a beta_interpolata;
% le station vanno da station_int_prec a station_interpolata;
% le elevation vanno da elevation_int_prec a elevation_interpolata
%%%%%%%%%%
%%%%%%%%%%
%%%%%%%%%%
gammamodificati=0;
gammasezmod=0;
%%%%%%%%%%
%%%%%%%%%%
%%%%%%%%%%
%%%%%%%%%%

```

```

prog_attuale_interna=prog_int_prec+delta_s_2;
while prog_attuale_interna<prog_attuale
    % (3b3b1) determino station ed elevation, beta e m
    station_interpolata_interna=station_int_prec+(prog_attuale_interna-
prog_int_prec)/(prog_attuale-prog_int_prec)*(station_interpolata-station_int_prec);
    elevation_interpolata_interna=elevation_int_prec+(prog_attuale_interna-
prog_int_prec)/(prog_attuale-prog_int_prec)*(elevation_interpolata-elevation_int_prec);
    beta_interpolata_interna=beta_int_prec+(prog_attuale_interna-
prog_int_prec)/(prog_attuale-prog_int_prec)*(beta_interpolata-beta_int_prec);
    %%%%%%%%%%%
    %%%%%%%%%%%
    %%%%%%%%%%%
    %%%%%%%%%%%
    if gamma_int_prec>0 && gamma_int_prec<pi/2 && gammasez<2*pi &&
gammasez>3/2*pi
        gamma_int_prec=gamma_int_prec+2*pi;
        gammamodificati=1;
    elseif gamma_int_prec>3/2*pi && gamma_int_prec<2*pi && gammasez<pi/2 &&
gammasez>0
        gammasez=gammasez+2*pi;
        gammamodificati=1;
        gammasezmod=1;
    end

    %%%%%%%%%%%
    %%%%%%%%%%%
    %%%%%%%%%%%
    %%%%%%%%%%%
    gamma_interpolata_interna=gamma_int_prec+(prog_attuale_interna-
prog_int_prec)/(prog_attuale-prog_int_prec)*(gammasez-gamma_int_prec);
    %%%%%%%%%%%
    %%%%%%%%%%%
    %%%%%%%%%%%
    %%%%%%%%%%%
    if gamma_interpolata_interna>2*pi
        gamma_interpolata_interna=gamma_interpolata_interna-2*pi;
    end
    if gammamodificati==1
        gammamodificati=0;
    end

    %%%%%%%%%%%
    %%%%%%%%%%%
    %%%%%%%%%%%
    %%%%%%%%%%%

    % referenzio la sezione interpolata interna
    % faccio le seguenti operazioni:
    % 1- trovo i punti dell'asse appena prima e appena dopo

```

```

% 2- trovo la retta che corrisponde a quel segmento dell'asse
% 3- considero il coefficiente m appena trovato e interseco
% 4- genero i punti x,y della sezione
% 1-
indice_punto_prima=max(find(prog_asse<prog_attuale_interna));
indice_punto_dopo=min(find(prog_asse>prog_attuale_interna));
xa1=x_asse(indice_punto_prima);
ya1=y_asse(indice_punto_prima);
xa2=x_asse(indice_punto_dopo);
ya2=y_asse(indice_punto_dopo);
pa1=prog_asse(indice_punto_prima);
pa2=prog_asse(indice_punto_dopo);
% 2-
ma=(ya2-ya1)/(xa2-xa1);
% 3-
m_interpolata_interna=tan(gamma_interpolata_interna);
alpha=atan(abs(m_interpolata_interna)); % considero il valore assoluto, i segni sono
tenuti in conto dopo
% 4-
% 4.1- coordinate x,y da attribuire al punto in asse della sezione
% (intersezione delle due rette)
xc=(prog_attuale_interna-pa1)/(pa2-pa1)*(xa2-xa1)+xa1;
yc=(prog_attuale_interna-pa1)/(pa2-pa1)*(ya2-ya1)+ya1;
% 4.2- lunghezza e punto in asse della sezione
x_sezione=[]; % inizializzazione
y_sezione=[]; % inizializzazione
numero_punti=n_punti_sez;
lunghezza_sez=station_interpolata_interna(numero_punti)-
station_interpolata_interna(1);
stc=station_interpolata_interna(1)+lunghezza_sez*beta_interpolata_interna; %
station del punto di intersezione con l'asse
% 4.3- determinazione di x,y a partire dalla station (con
% riconoscimento del quadrante in base alla direzione della sezione interpolata
interna)
if gamma_interpolata_interna>pi && gamma_interpolata_interna<=3/2*pi %
quadrante 3
    for k=1:n_punti_sez
        station_punto=station_interpolata_interna(k);
        x_sezione(k)=xc-(station_punto-stc)*cos(alpha);
        y_sezione(k)=yc-(station_punto-stc)*sin(alpha);
    end
elseif gamma_interpolata_interna>pi/2 && gamma_interpolata_interna<=pi %
quadrante 2
    for k=1:n_punti_sez
        station_punto=station_interpolata_interna(k);
        x_sezione(k)=xc-(station_punto-stc)*cos(alpha);
        y_sezione(k)=yc+(station_punto-stc)*sin(alpha);
    end
elseif gamma_interpolata_interna>=0 && gamma_interpolata_interna<=pi/2 %
quadrante 1
    for k=1:n_punti_sez
        station_punto=station_interpolata_interna(k);

```

```

        x_sezione(k)=xc+(station_punto-stc)*cos(alpha);
        y_sezione(k)=yc+(station_punto-stc)*sin(alpha);
    end
elseif gamma_interpolata_interna>3/2*pi && gamma_interpolata_interna<=2*pi %
quadrante 4
    for k=1:n_punti_sez
        station_punto=station_interpolata_interna(k);
        x_sezione(k)=xc+(station_punto-stc)*cos(alpha);
        y_sezione(k)=yc-(station_punto-stc)*sin(alpha);
    end
else
    disp('ERRORE GIACITURA SEZIONE INTERPOLATA INTERNA');
    return
end
% (3b3b3) aggiornamento della matrice x,y,z
batimetria_aggiungere=cat(2,x_sezione',y_sezione',elevation_interpolata_interna');
batimetria=cat(1,batimetria,batimetria_aggiungere);
batimetria_interna=cat(1,batimetria_interna,batimetria_aggiungere);
linea_clip_sx=cat(1,linea_clip_sx,[x_sezione(1) y_sezione(1)]);
linea_clip_dx=cat(1,linea_clip_dx,[x_sezione(n_punti_sez) y_sezione(n_punti_sez)]);
% aggiornamento della progressiva interna
prog_attuale_interna=prog_attuale_interna+delta_s_2;
end
% (3b3b4) aggiornamento della progressiva e delle grandezze per l'interpolazione interna
prog_int_prec=prog_attuale;

if gammasezmod==1
    gammasez=gammasez-2*pi;
    gammasezmod=0;
end

gamma_int_prec=gammasez;
beta_int_prec=beta_interpolata;
station_int_prec=station_interpolata;
elevation_int_prec=elevation_interpolata;
prog_attuale=prog_attuale+passo_prog; % questa è la progressiva
end
% e infine devo fare l'ultimo pezzetto di interpolazione interna;
% le progressive vanno da prog_int_prec a prog_2;
% i gamma vanno da gammasez a gamma_2;
% i beta vanno da beta_int_prec a beta_2;
% le station vanno da station_int_prec a station_2_int;
% le elevation vanno da elevation_int_prec a elevation_2_int
prog_attuale_interna=prog_int_prec+delta_s_2;
while prog_attuale_interna<prog_2
    % (3b3b1) determino station ed elevation, beta e m
    station_interpolata_interna=station_int_prec+(prog_attuale_interna-
prog_int_prec)/(prog_2-prog_int_prec)*(station_2_int-station_int_prec);
    elevation_interpolata_interna=elevation_int_prec+(prog_attuale_interna-
prog_int_prec)/(prog_2-prog_int_prec)*(elevation_2_int-elevation_int_prec);

```

```

beta_interpolata_interna=beta_int_prec+(prog_attuale_interna-prog_int_prec)/(prog_2-
prog_int_prec)*(beta_2-beta_int_prec);
gamma_interpolata_interna=gamma_int_prec+(prog_attuale_interna-
prog_int_prec)/(prog_2-prog_int_prec)*(gamma_2-gamma_int_prec);
% referenzio la sezione interpolata interna
% faccio le seguenti operazioni:
% 1- trovo i punti dell'asse appena prima e appena dopo
% 2- trovo la retta che corrisponde a quel segmento dell'asse
% 3- considero il coefficiente m appena trovato e interseco
% 4- genero i punti x,y della sezione
% 1-
indice_punto_prima=max(find(prog_asse<prog_attuale_interna));
indice_punto_dopo=min(find(prog_asse>prog_attuale_interna));
xa1=x_asse(indice_punto_prima);
ya1=y_asse(indice_punto_prima);
xa2=x_asse(indice_punto_dopo);
ya2=y_asse(indice_punto_dopo);
pa1=prog_asse(indice_punto_prima);
pa2=prog_asse(indice_punto_dopo);
% 2-
ma=(ya2-ya1)/(xa2-xa1);
% 3-
m_interpolata_interna=tan(gamma_interpolata_interna);
alpha=atan(abs(m_interpolata_interna)); % considero il valore assoluto, i segni sono
tenuti in conto dopo
% 4-
% 4.1- coordinate x,y da attribuire al punto in asse della sezione
% (intersezione delle due rette)
xc=(prog_attuale_interna-pa1)/(pa2-pa1)*(xa2-xa1)+xa1;
yc=(prog_attuale_interna-pa1)/(pa2-pa1)*(ya2-ya1)+ya1;
% 4.2- lunghezza e punto in asse della sezione
x_sezione=[]; % inizializzazione
y_sezione=[]; % inizializzazione
numero_punti=n_punti_sez;
lunghezza_sez=station_interpolata_interna(numero_punti)-
station_interpolata_interna(1);
stc=station_interpolata_interna(1)+lunghezza_sez*beta_interpolata_interna; % station
del punto di intersezione con l'asse
% 4.3- determinazione di x,y a partire dalla station (con
% riconoscimento del quadrante in base alla direzione della sezione interpolata interna)
if gamma_interpolata_interna>pi && gamma_interpolata_interna<=3/2*pi %
quadrante 3
for k=1:n_punti_sez
station_punto=station_interpolata_interna(k);
x_sezione(k)=xc-(station_punto-stc)*cos(alpha);
y_sezione(k)=yc-(station_punto-stc)*sin(alpha);
end
elseif gamma_interpolata_interna>pi/2 && gamma_interpolata_interna<=pi %
quadrante 2
for k=1:n_punti_sez
station_punto=station_interpolata_interna(k);
x_sezione(k)=xc-(station_punto-stc)*cos(alpha);

```

```

        y_sezione(k)=yc+(station_punto-stc)*sin(alpha);
    end
elseif gamma_interpolata_interna>=0 && gamma_interpolata_interna<=pi/2 %
quadrante 1
    for k=1:n_punti_sez
        station_punto=station_interpolata_interna(k);
        x_sezione(k)=xc+(station_punto-stc)*cos(alpha);
        y_sezione(k)=yc+(station_punto-stc)*sin(alpha);
    end
elseif gamma_interpolata_interna>3/2*pi && gamma_interpolata_interna<=2*pi %
quadrante 4
    for k=1:n_punti_sez
        station_punto=station_interpolata_interna(k);
        x_sezione(k)=xc+(station_punto-stc)*cos(alpha);
        y_sezione(k)=yc-(station_punto-stc)*sin(alpha);
    end
else
    disp('ERRORE GIACITURA SEZIONE INTERPOLATA INTERNA');
    return
end
% (3b3b3) aggiornamento della matrice x,y,z
batimetria_aggiungere=cat(2,x_sezione',y_sezione',elevation_interpolata_interna');
batimetria=cat(1,batimetria,batimetria_aggiungere);
batimetria_interna=cat(1,batimetria_interna,batimetria_aggiungere);
linea_clip_sx=cat(1,linea_clip_sx,[x_sezione(1) y_sezione(1)]);
linea_clip_dx=cat(1,linea_clip_dx,[x_sezione(n_punti_sez) y_sezione(n_punti_sez)]);
% aggiornamento della progressiva interna
prog_attuale_interna=prog_attuale_interna+delta_s_2;
end
% (3b4) se sono all'ultima sezione creo la x,y,z della sezione 2 e aggiungo alla batimetria
if indice_sezione==(numero_sezioni-1)
    x12=dati_vertici_p(indice_sezione+1,2);    y12=dati_vertici_p(indice_sezione+1,3);
x22=dati_vertici_p(indice_sezione+1,4); y22=dati_vertici_p(indice_sezione+1,5);
L_sezione2=sqrt((x22-x12)^2+(y22-y12)^2);
x_sezione2=[]; y_sezione2=[];
for i_punto=1:n_punti_sez
    st_punto=station_2_int(i_punto);
    x_sezione2(i_punto)=x12+(x22-x12)*st_punto/L_sezione2;
    y_sezione2(i_punto)=y12+(y22-y12)*st_punto/L_sezione2;
end
batimetria_aggiungere=cat(2,x_sezione2',y_sezione2',elevation_2_int');
batimetria=cat(1,batimetria,batimetria_aggiungere);
end
end
% determinazione del contorno
linea_clip_dx=flipud(linea_clip_dx);
contorno_clip=cat(1,linea_clip_sx,linea_clip_dx);
% (3c) -----
% diagrammi
x_finale=batimetria(:,1);
y_finale=batimetria(:,2);
z_finale=batimetria(:,3);

```

```

plot(x_finale,y_finale,'om');
x_finale_interna=batimetria_interna(:,1);
y_finale_interna=batimetria_interna(:,2);
plot(x_finale_interna,y_finale_interna,'oc');
plot(contorno_clip(:,1),contorno_clip(:,2),'-b');
hold off
figure(2),scatter3(x_finale,y_finale,z_finale,25,z_finale,'s','Filled'),colormap(jet),colorbar,axis
([x1_plot x2_plot y1_plot y2_plot]),axis square;
hold on
plot(dati_asse(:,1),dati_asse(:,2),'-b');
hold off
figure,plot(tabella_gamma_ril(:,1),tabella_gamma_ril(:,2)/pi*180,'ob');
% salvataggio
save batimetria_Seveso.txt batimetria -ascii -tabs
save contorno_Seveso.txt contorno_clip -ascii -tabs

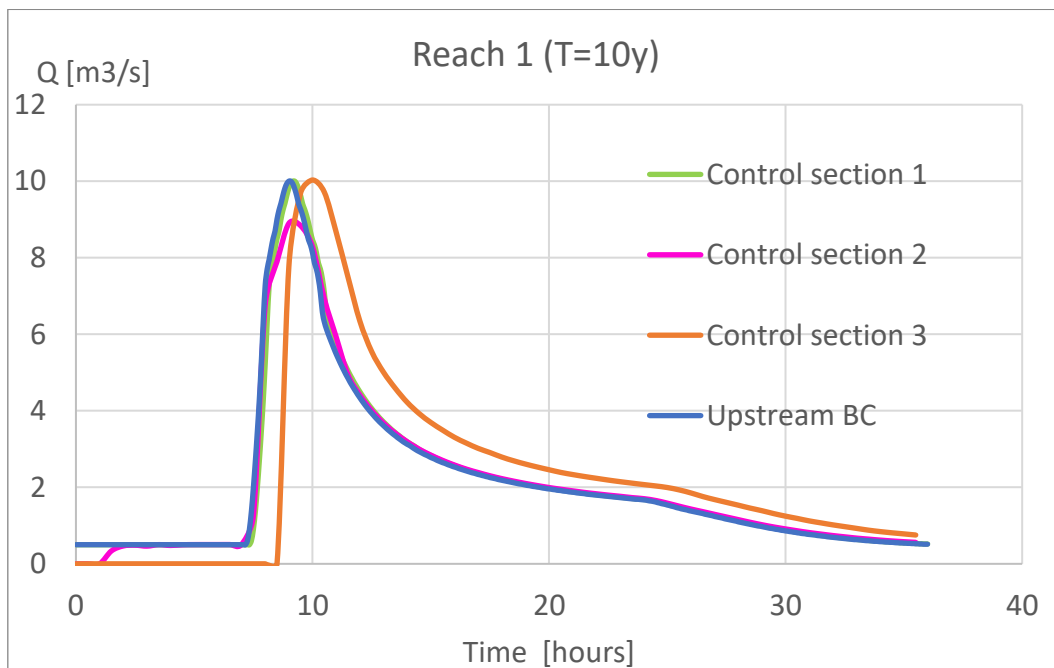
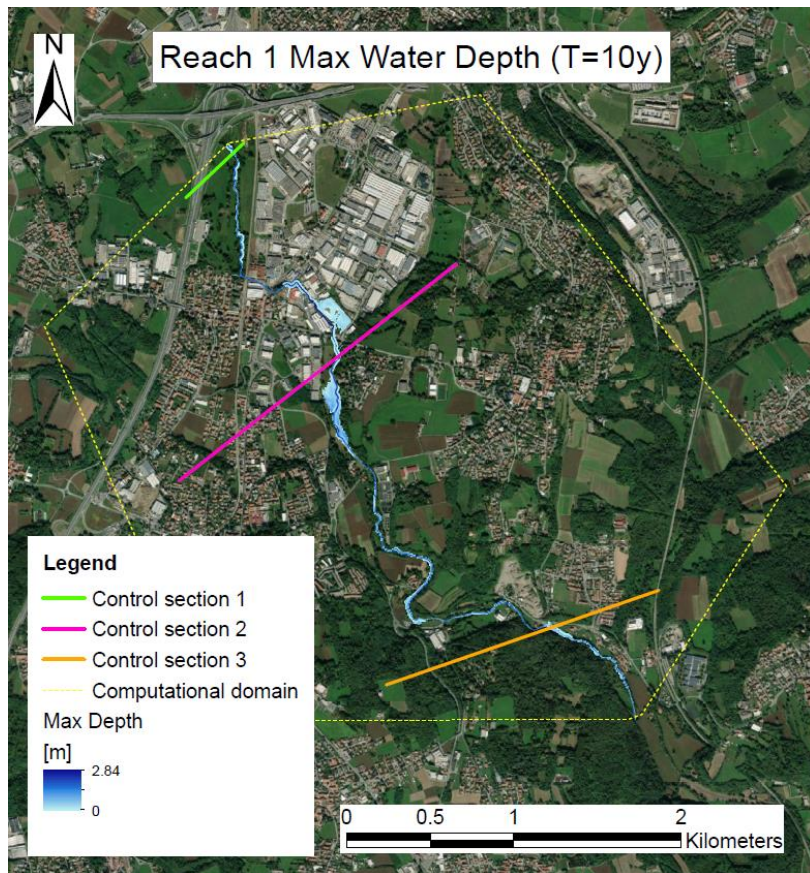
```

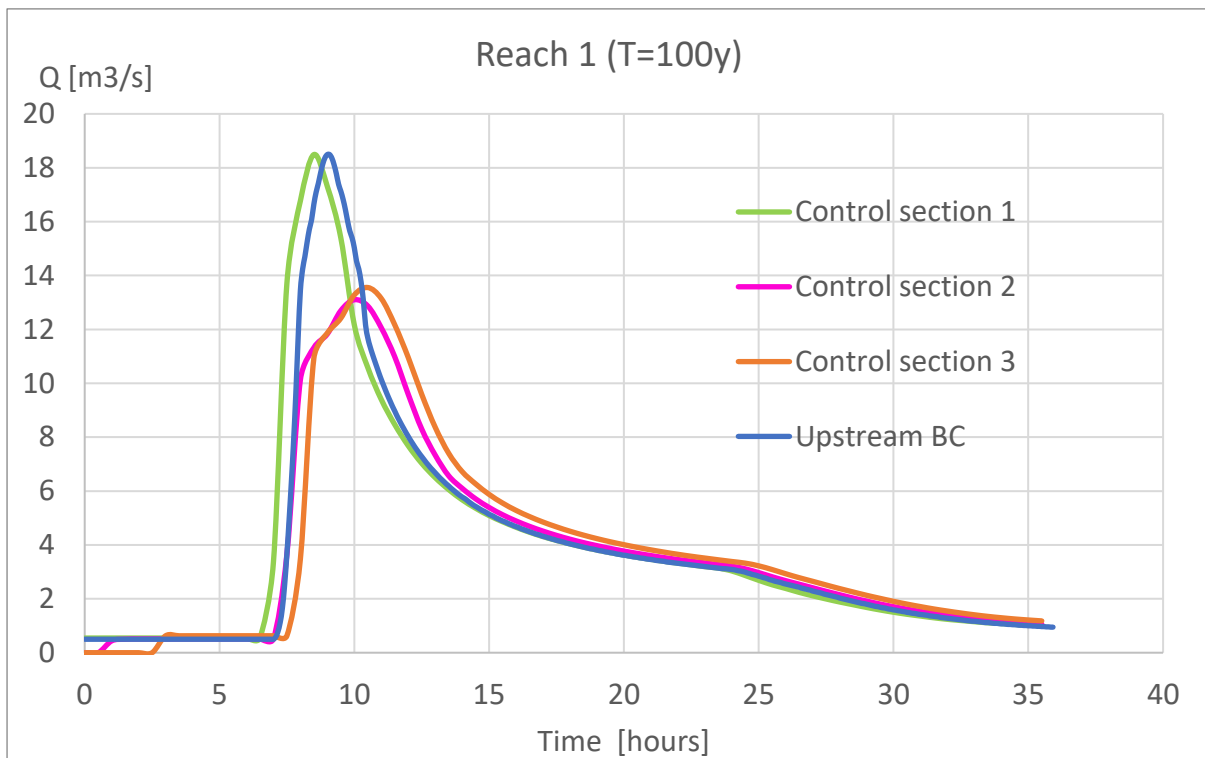
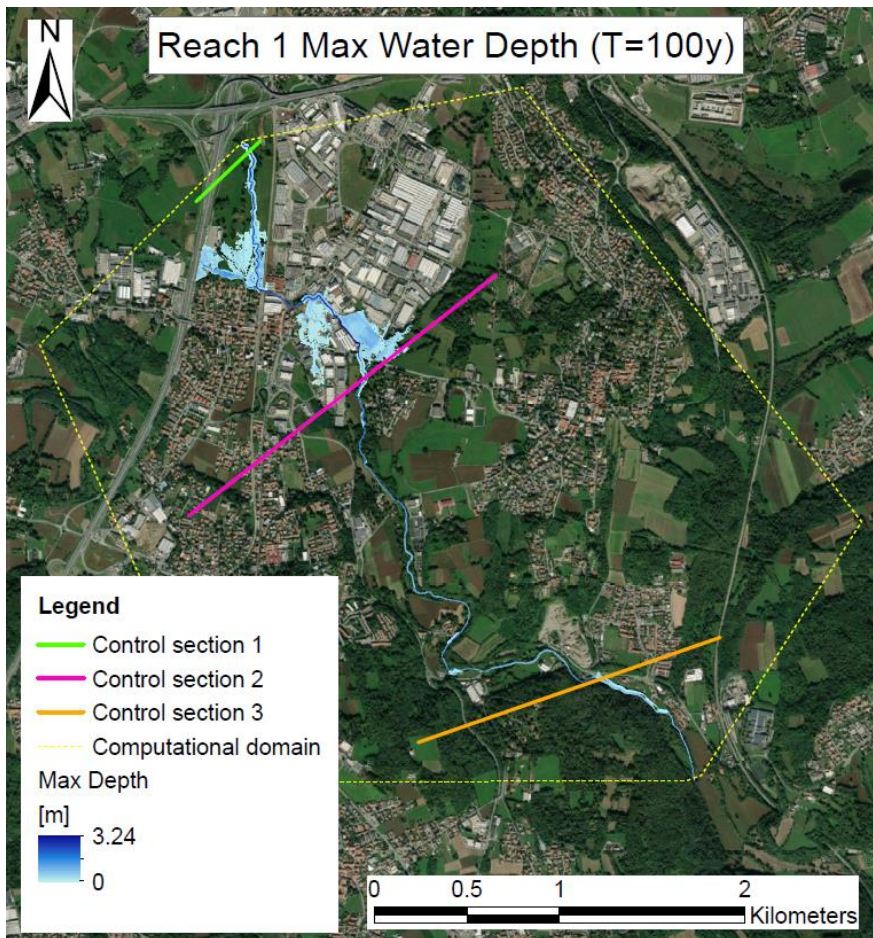
Appendix C

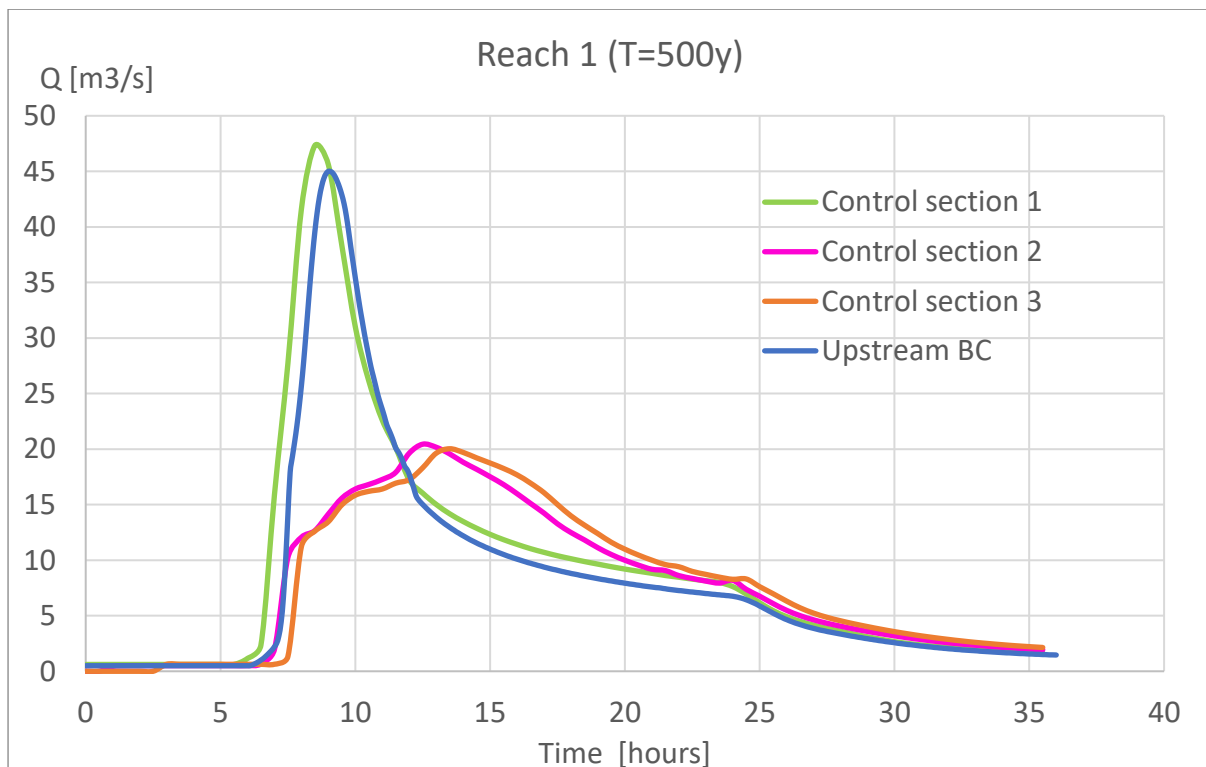
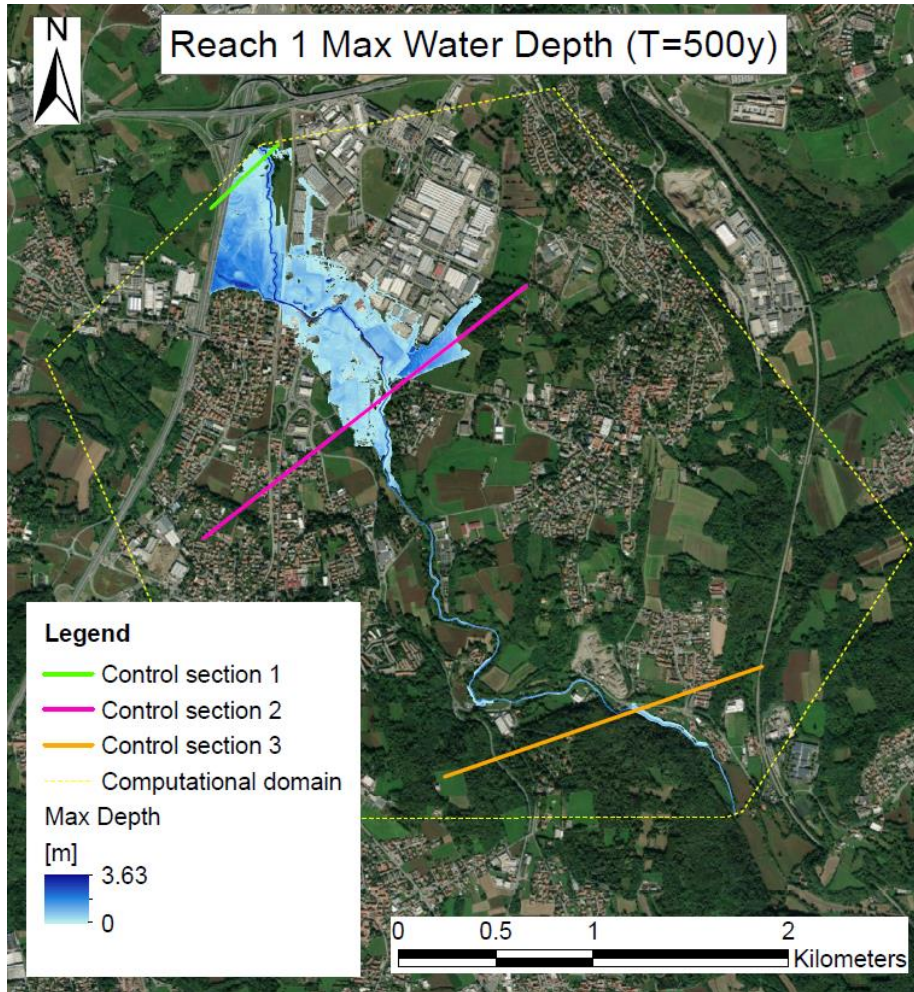
Control sections for the flow rate distribution

The present appendix illustrates all the control sections deployed to extract the flow rate trend in order to monitor the flood wave propagation along the rivers. First the maps with the respective hydrographs for the Seveso are reported, then the ones for the Bozzente.

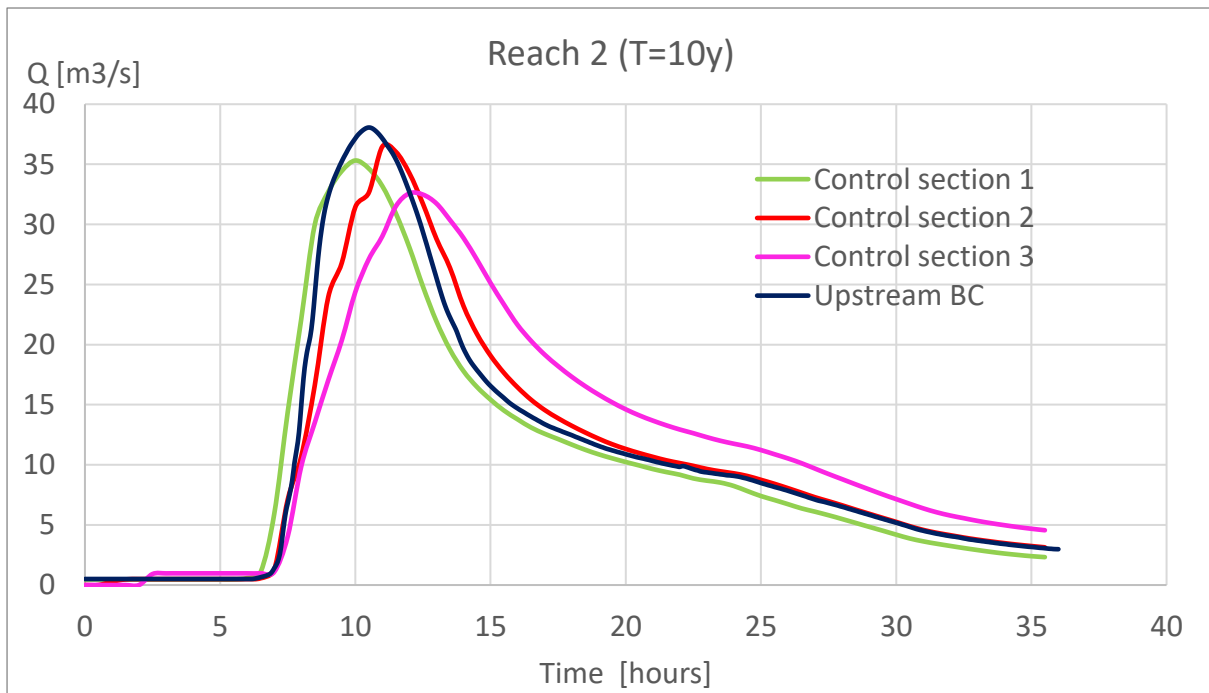
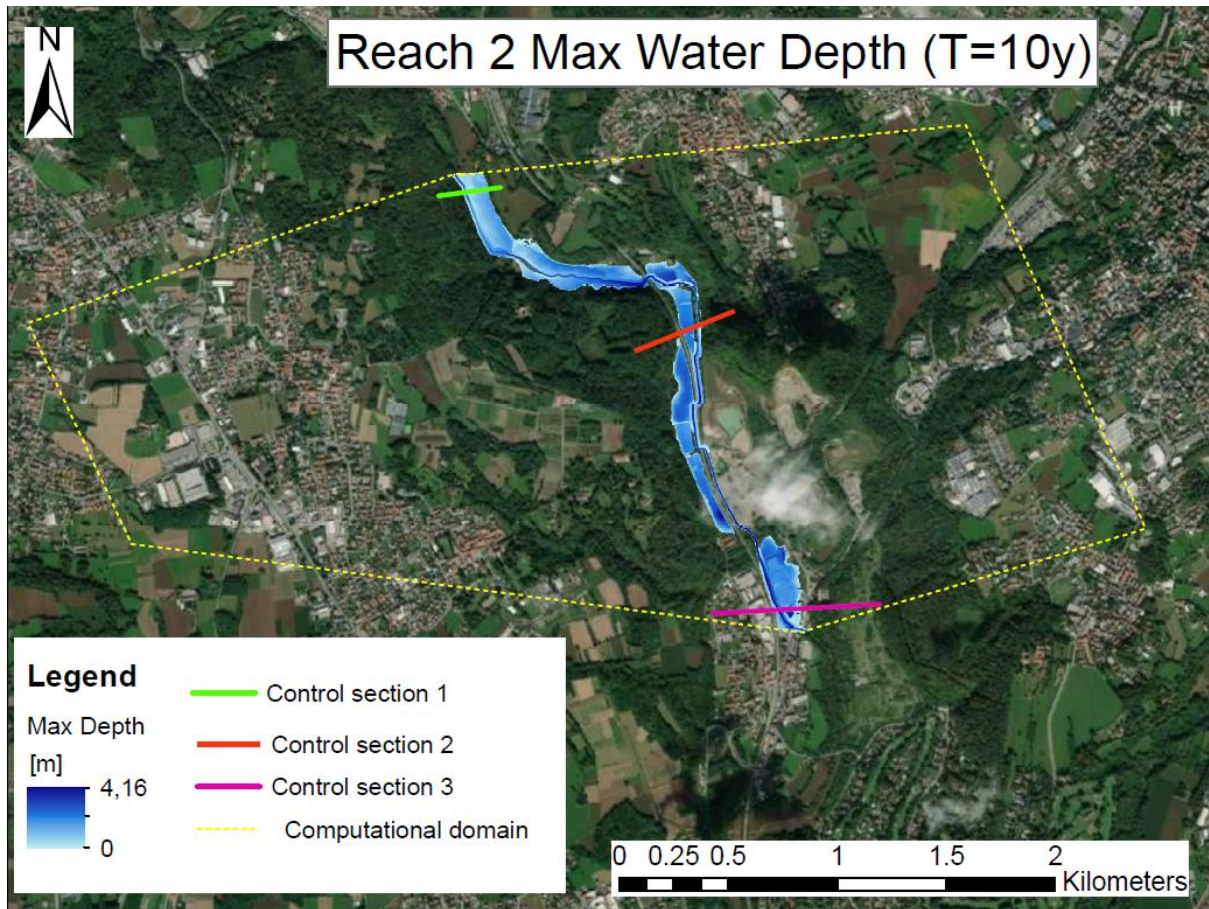
Seveso Reach 1

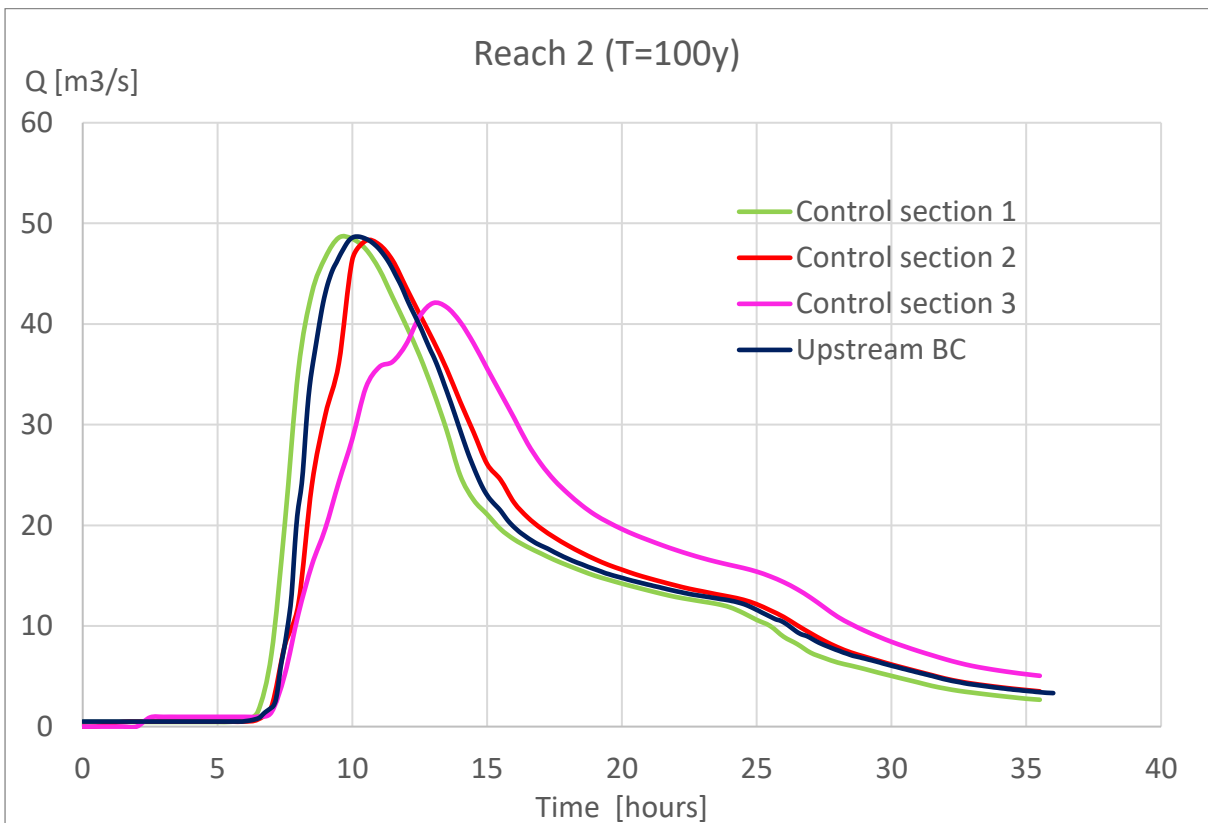
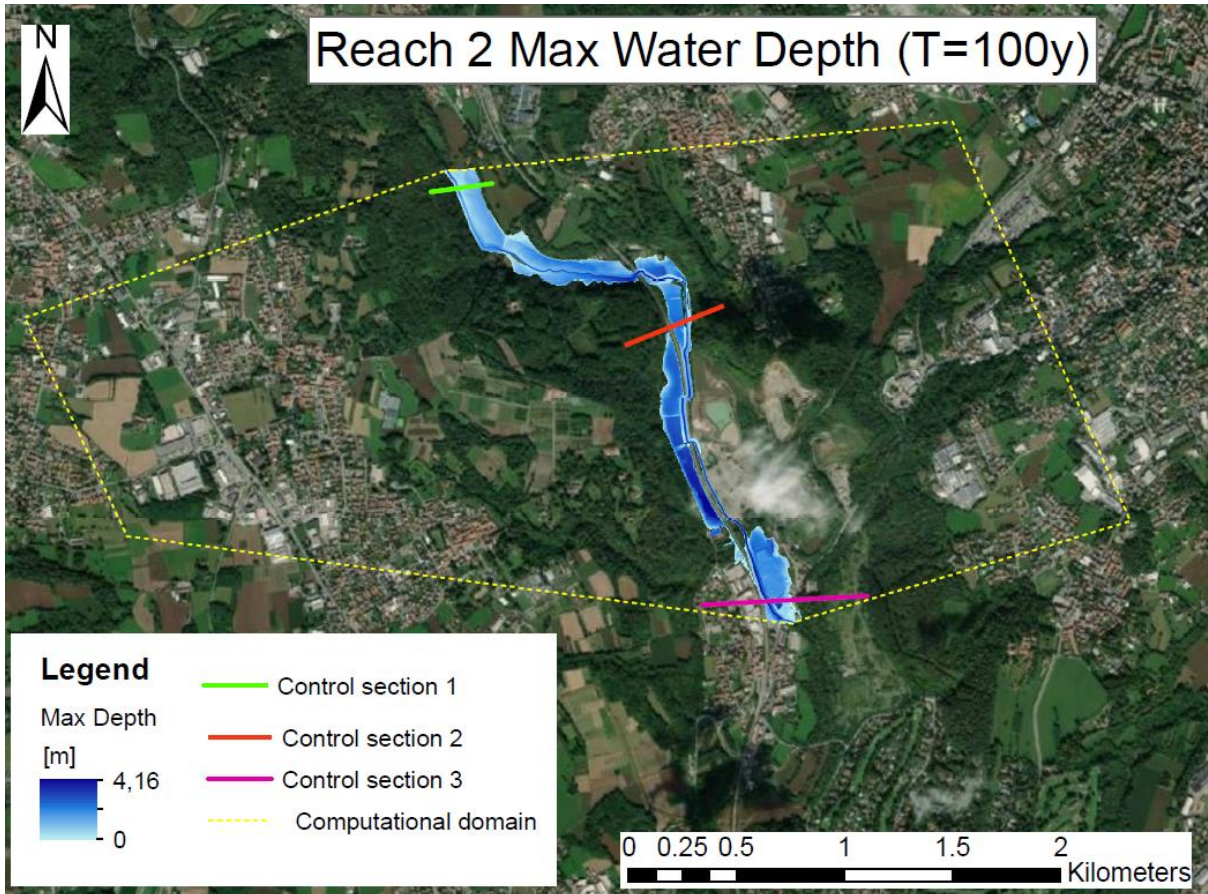


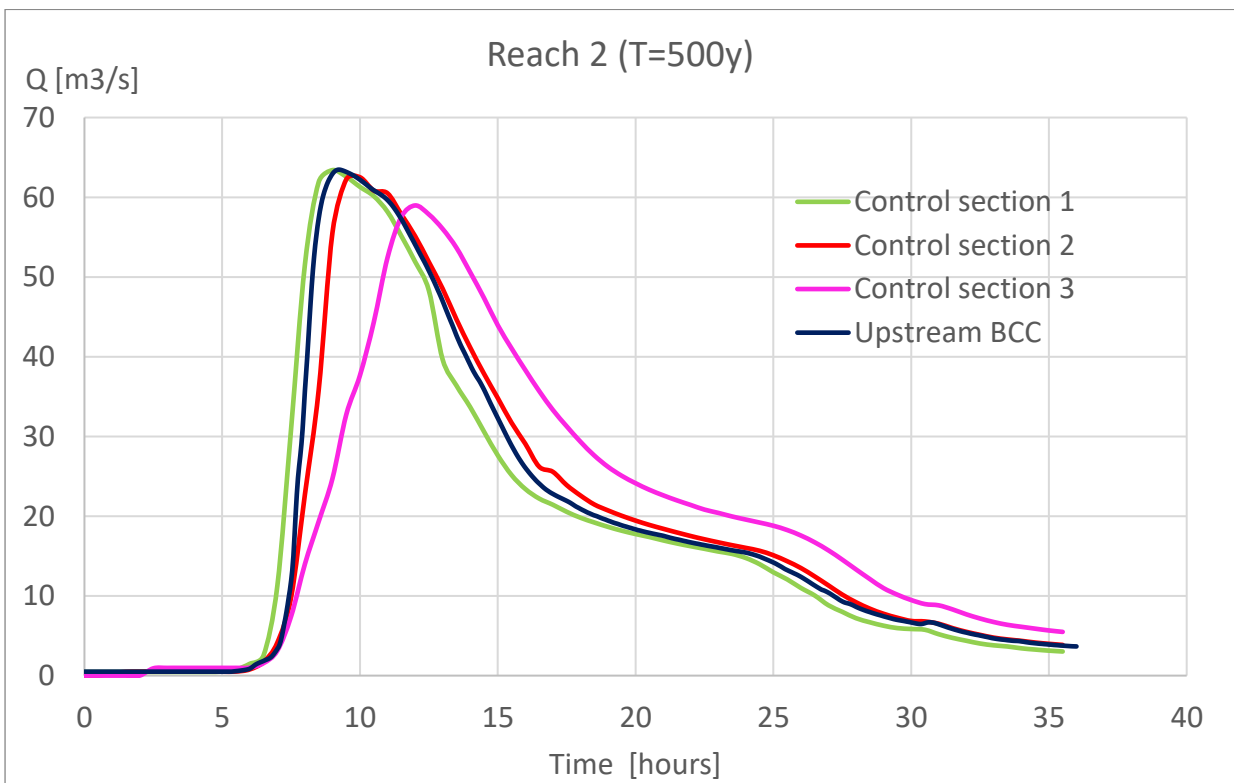
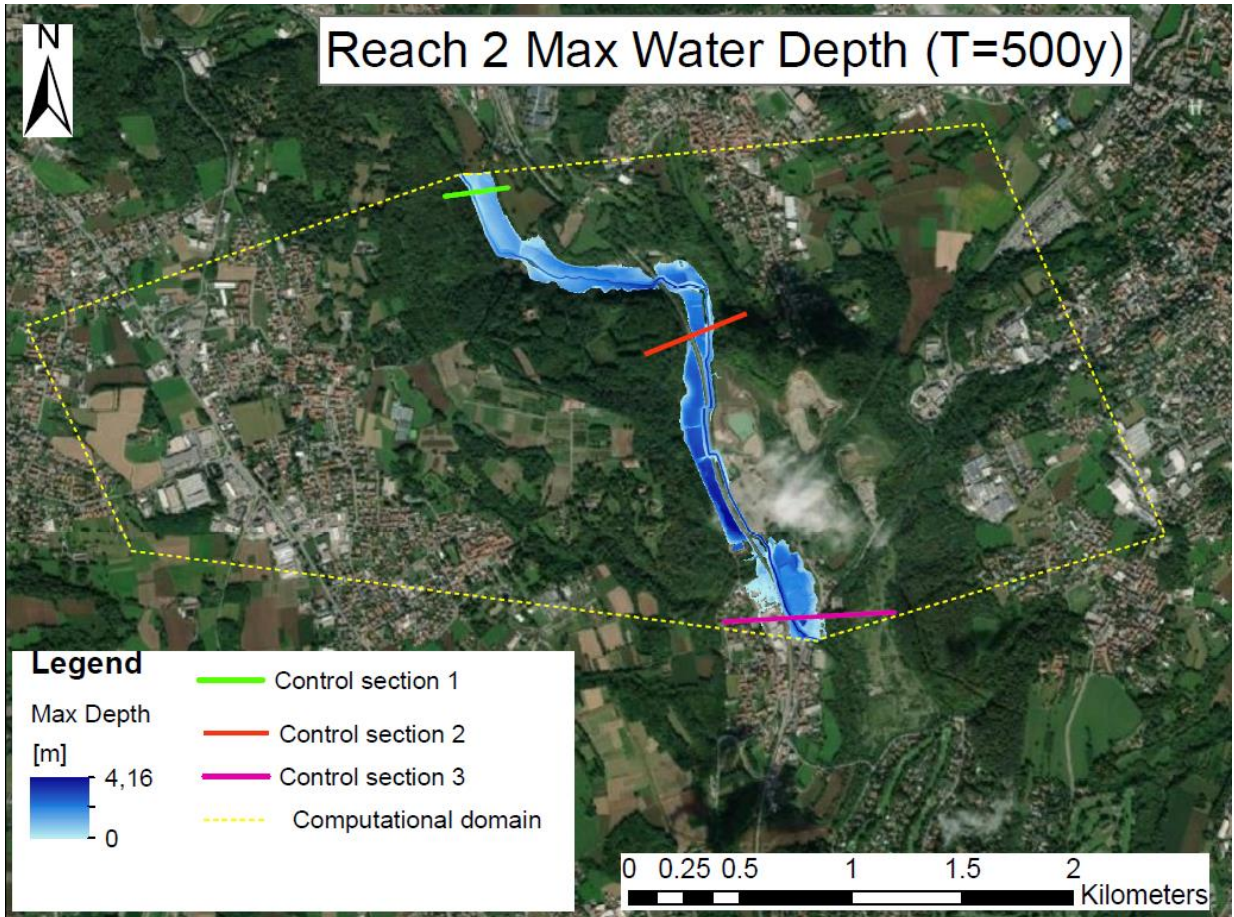




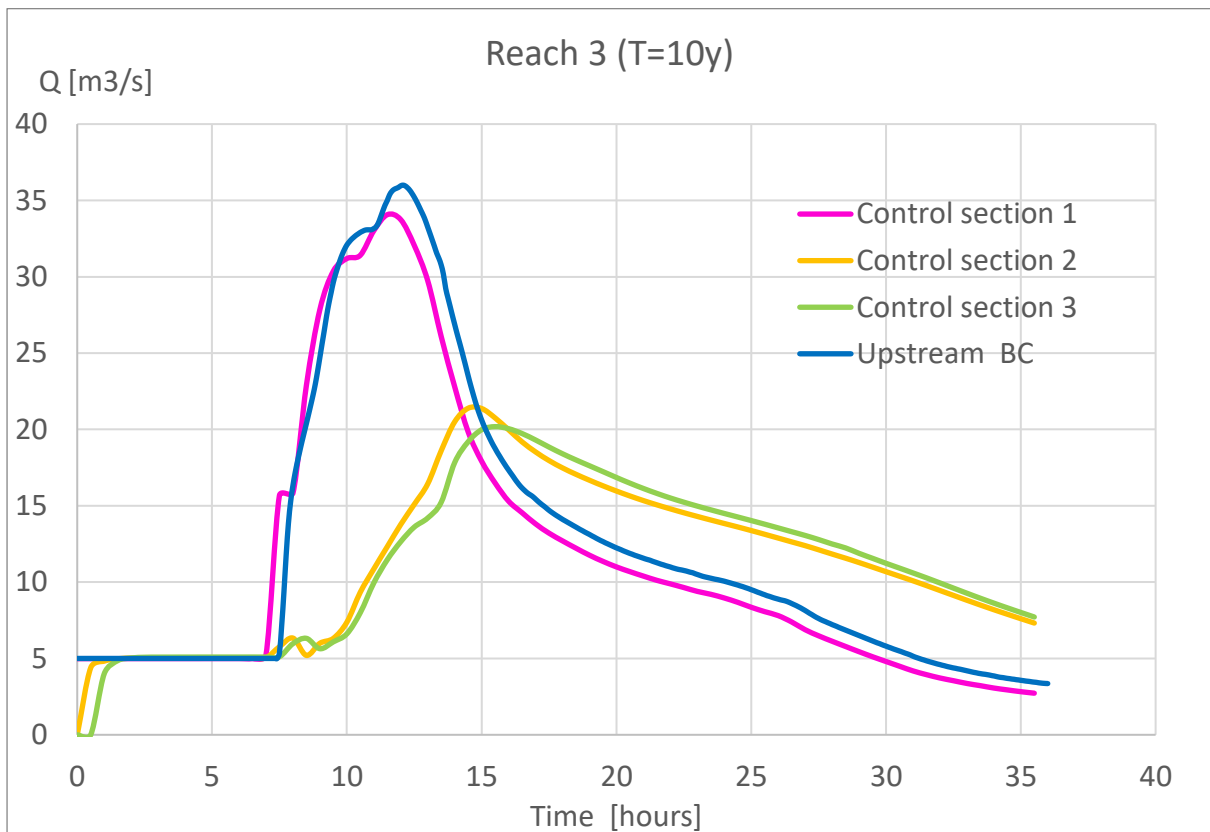
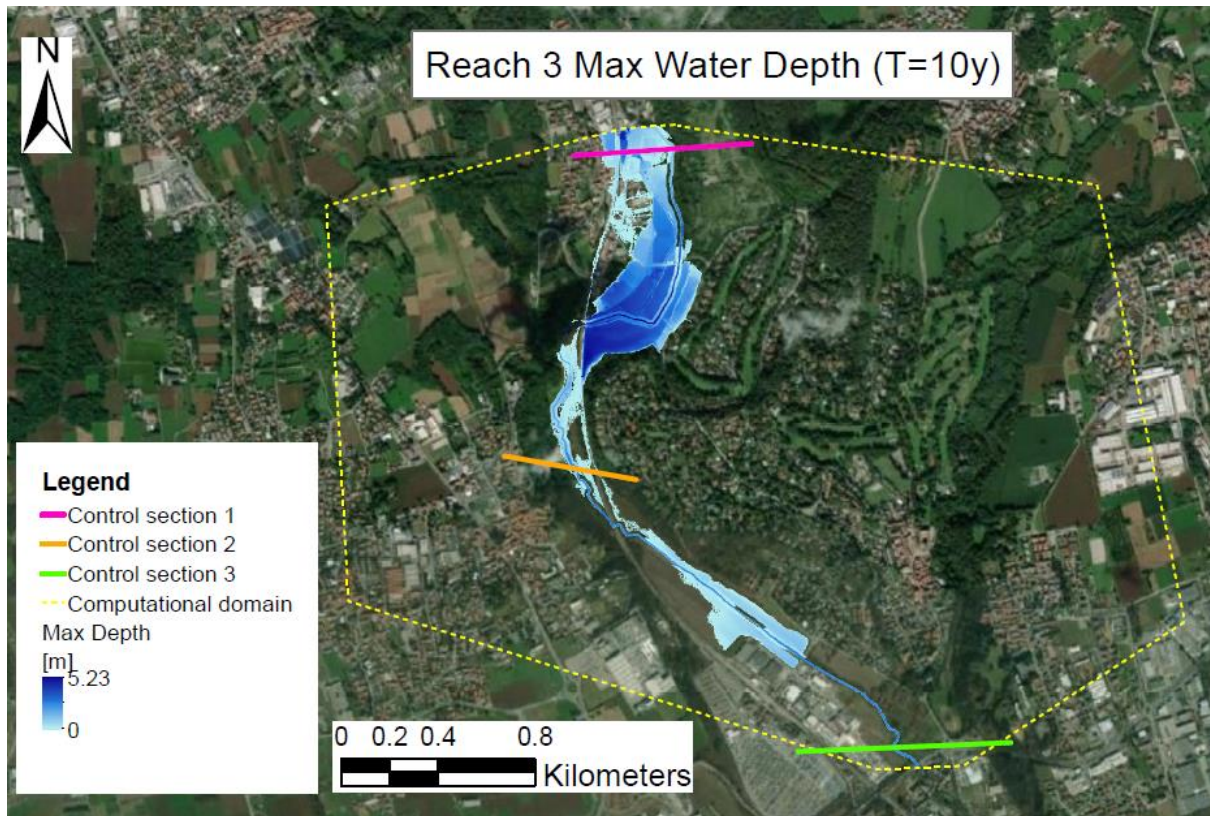
Reach 2

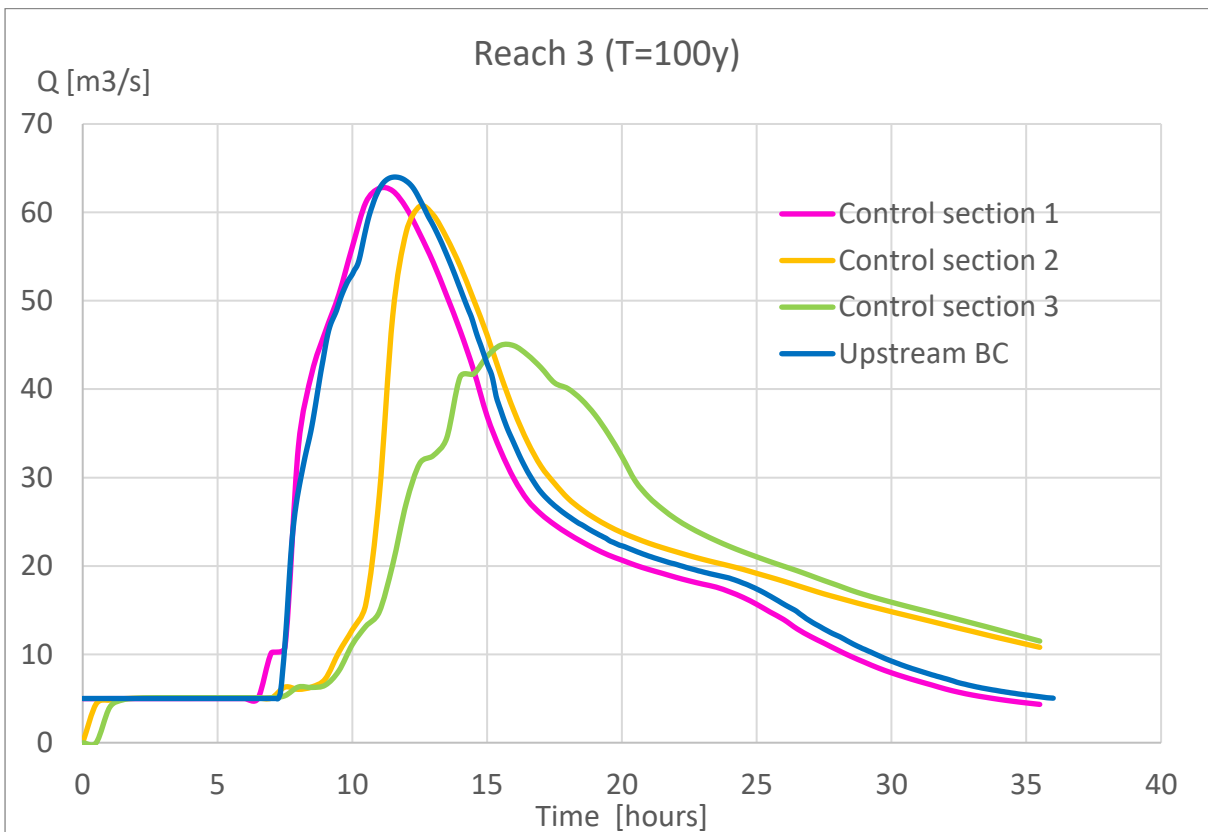
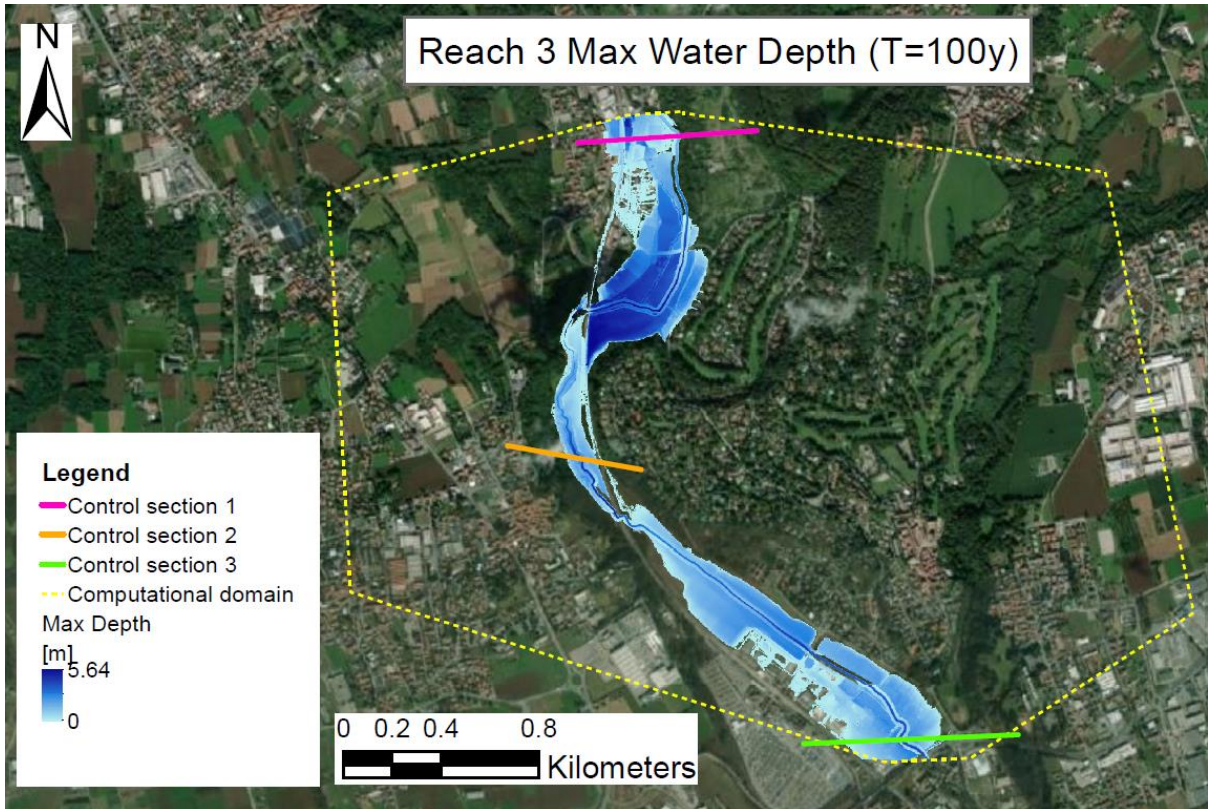


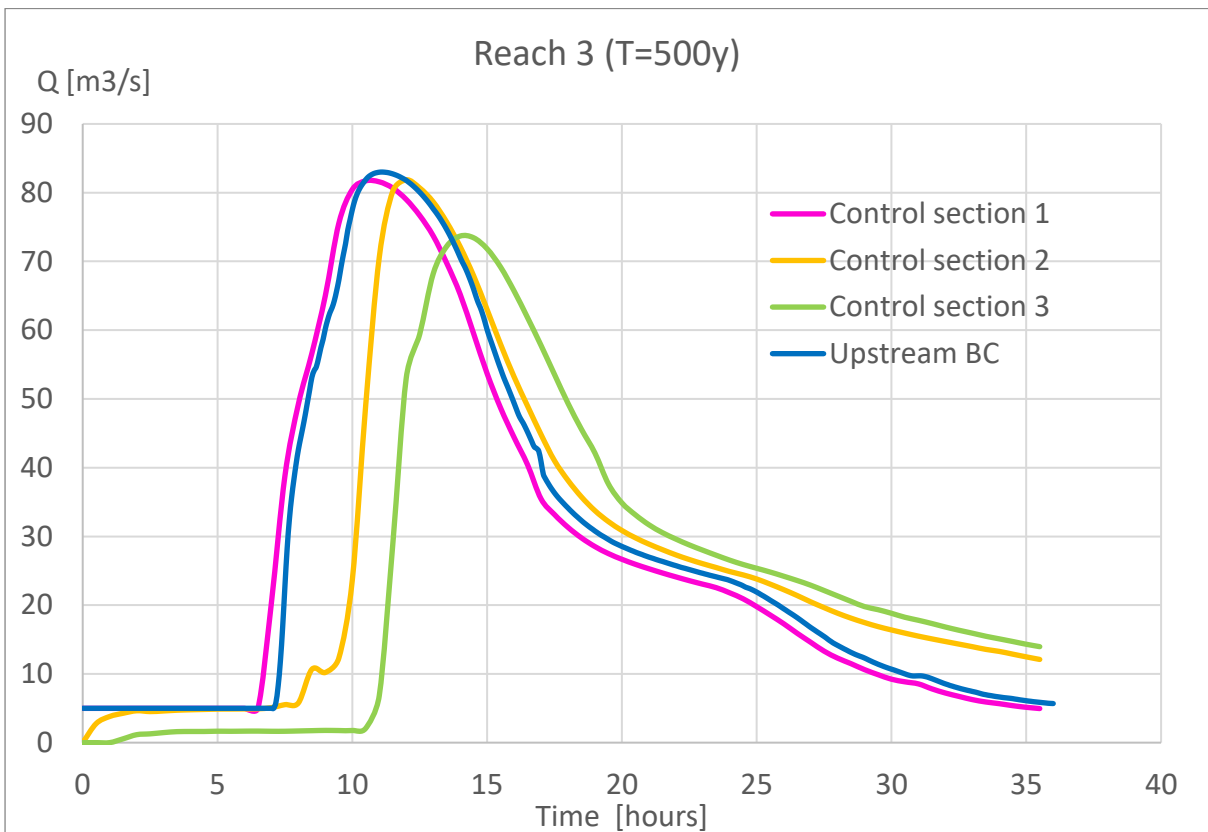
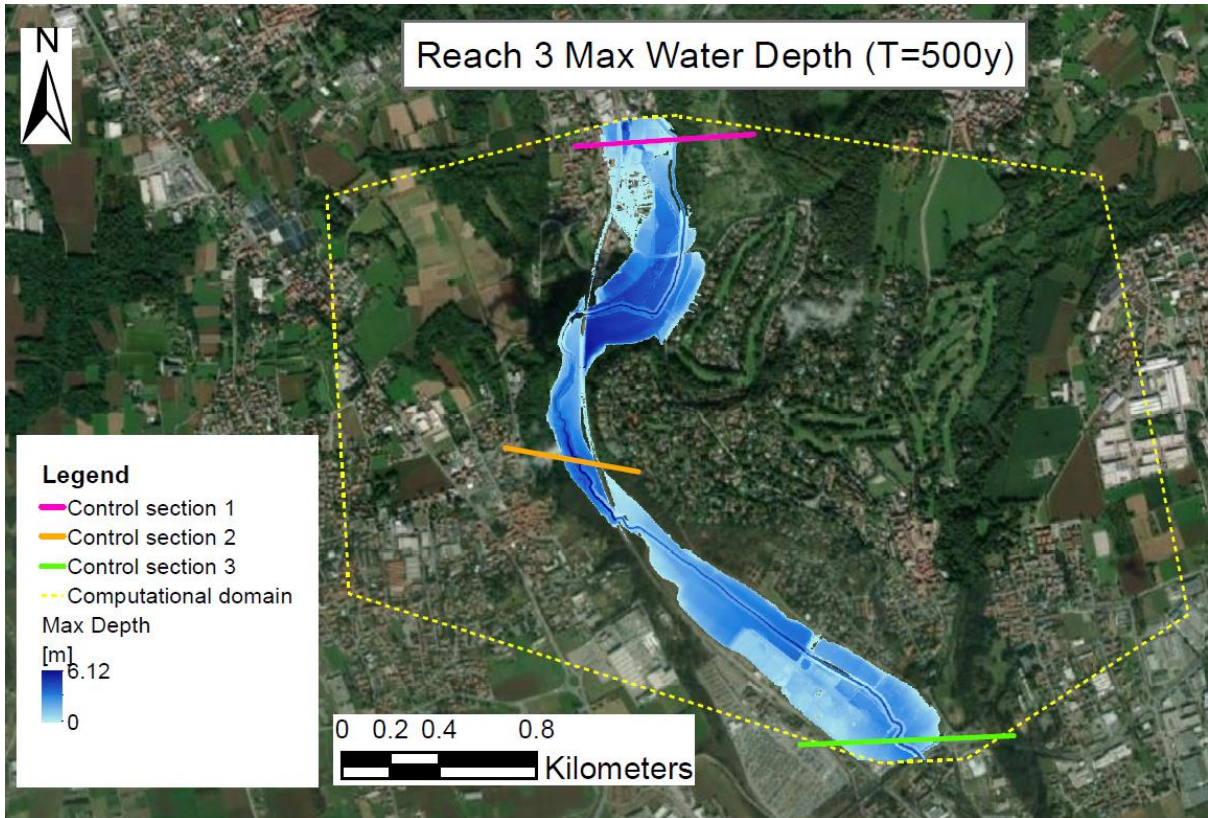




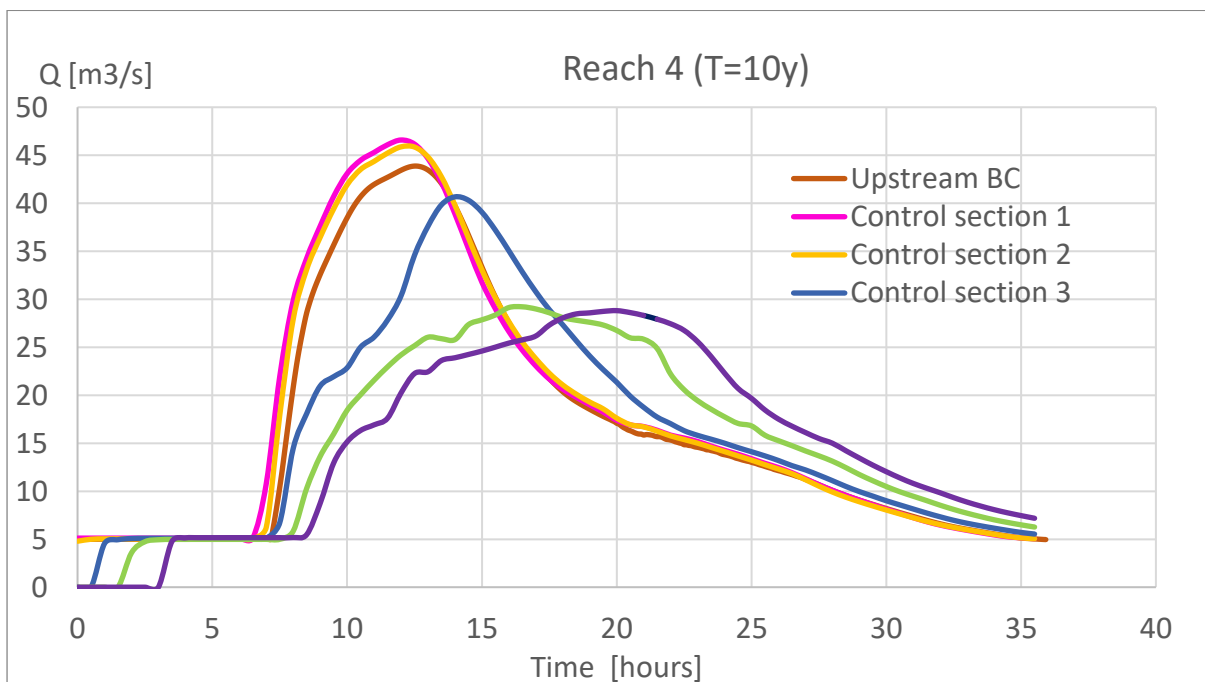
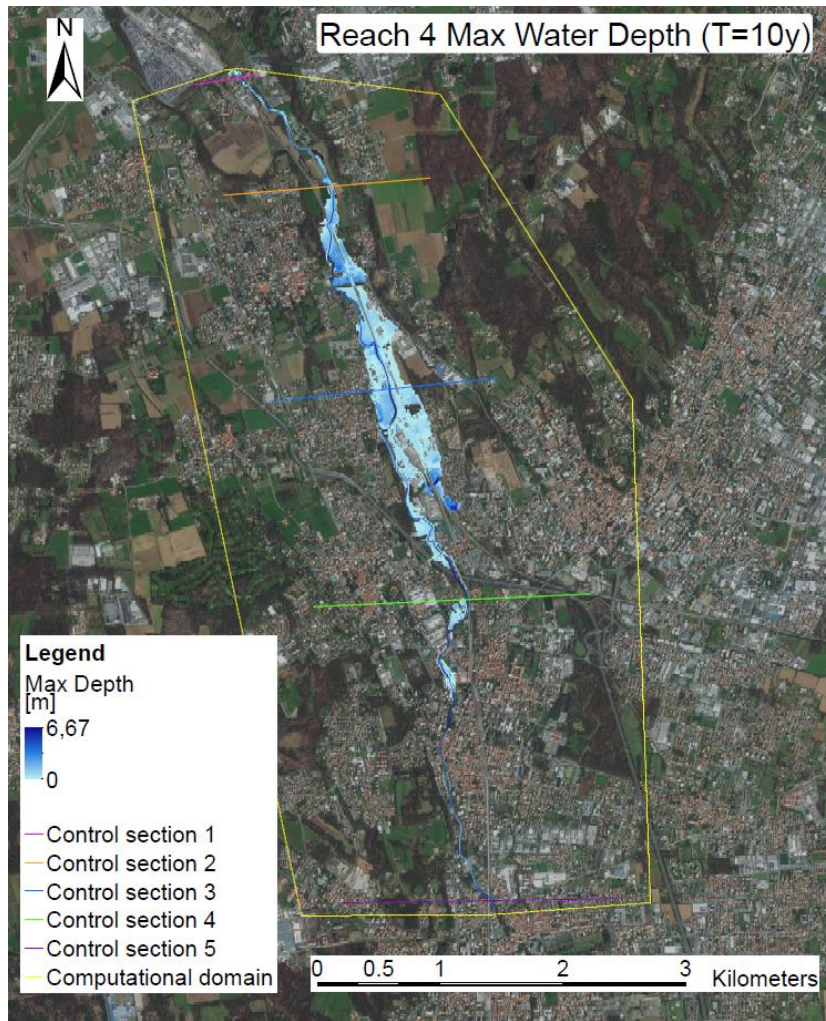
Reach 3

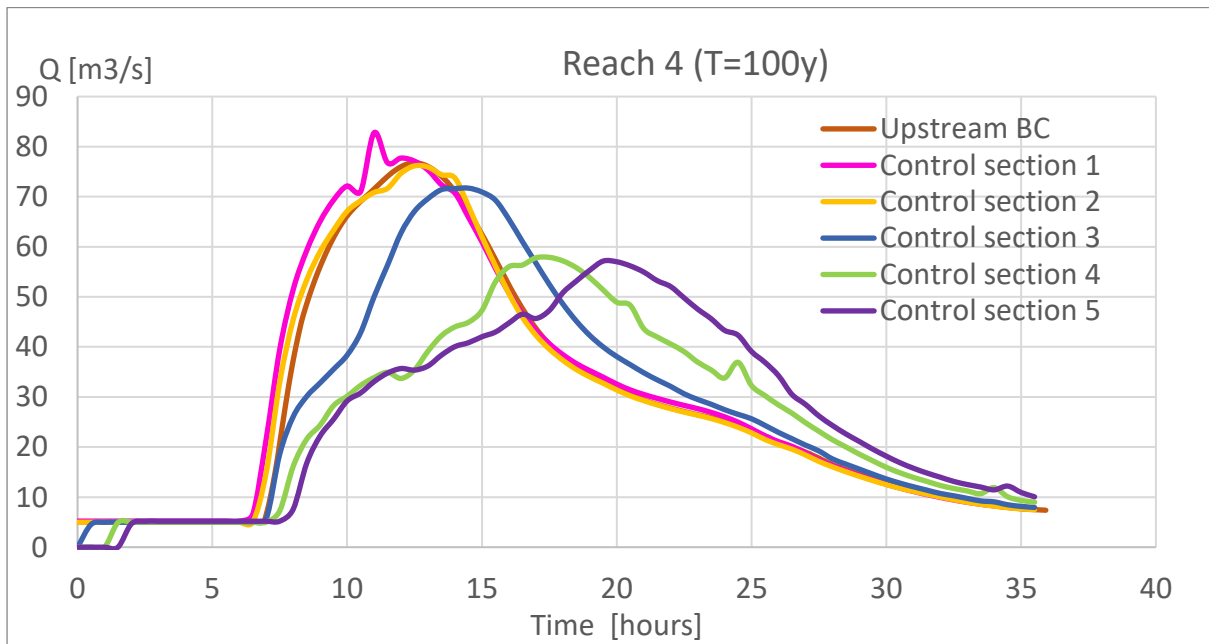
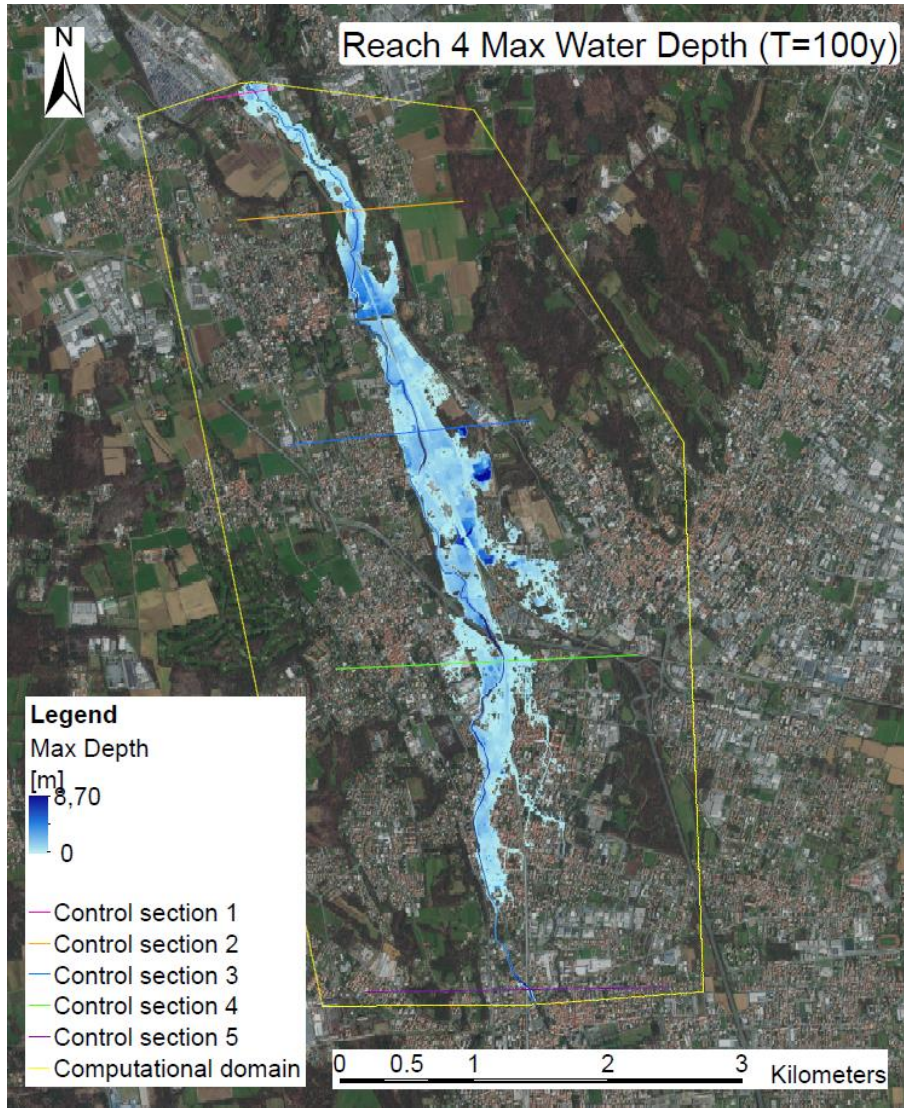


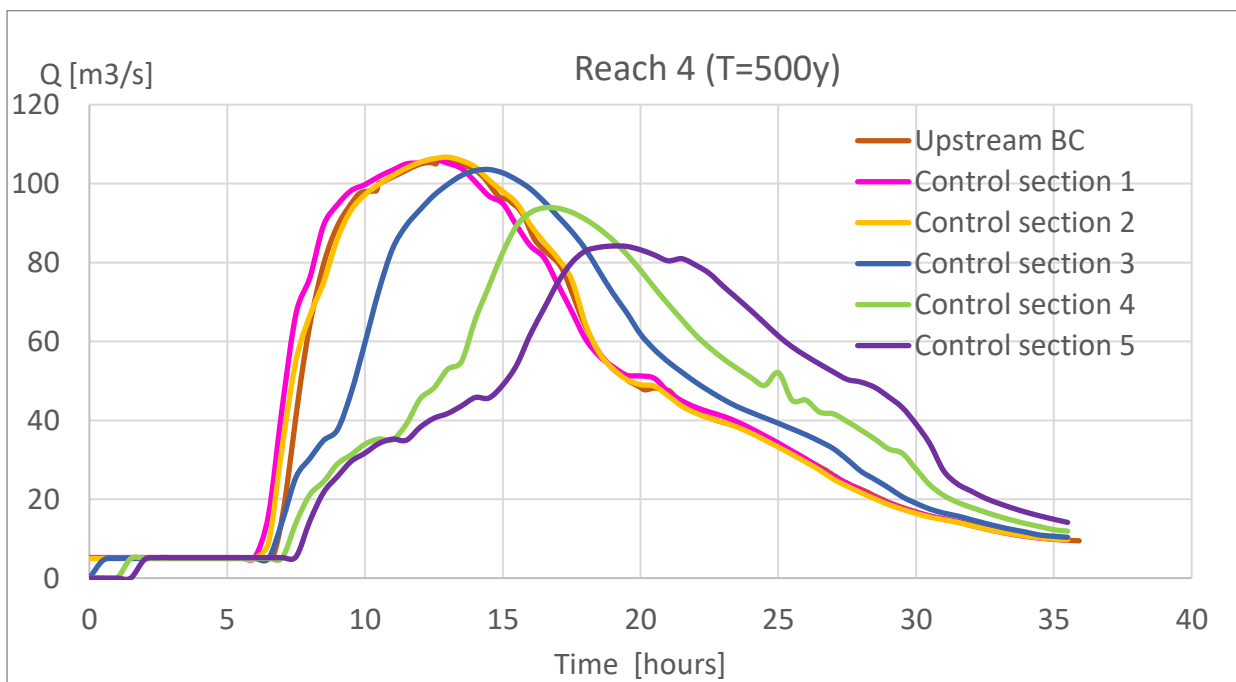
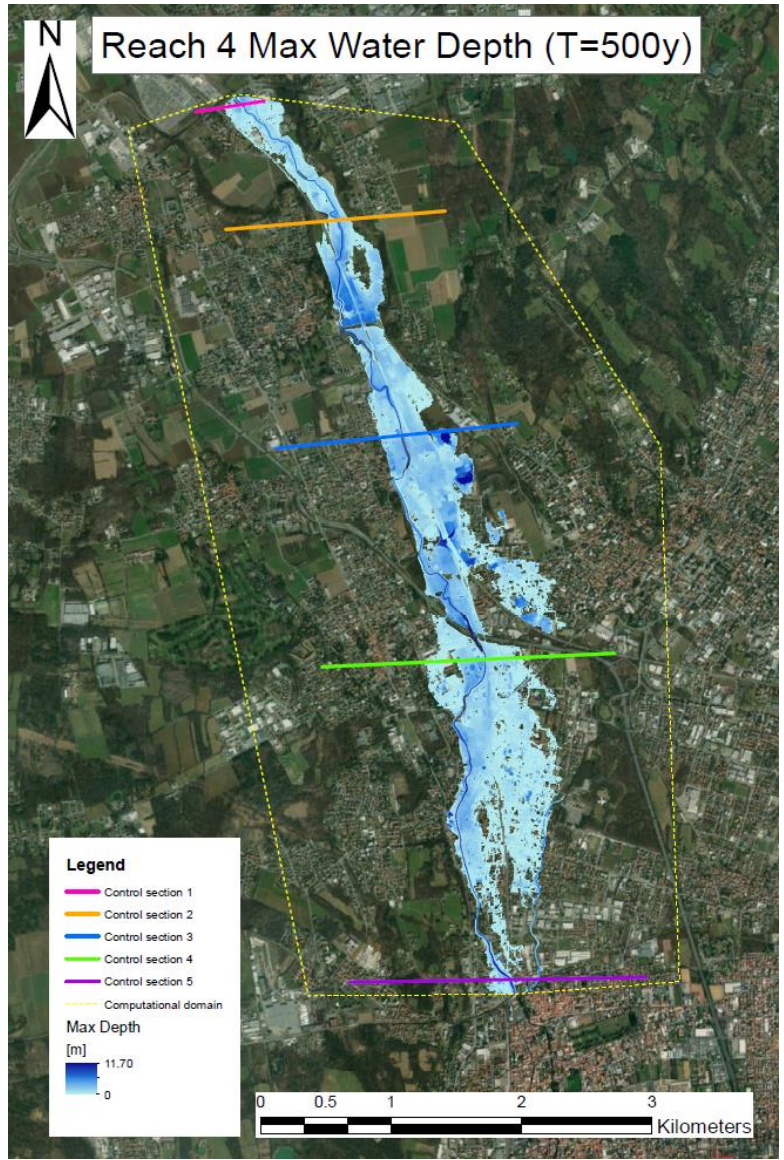




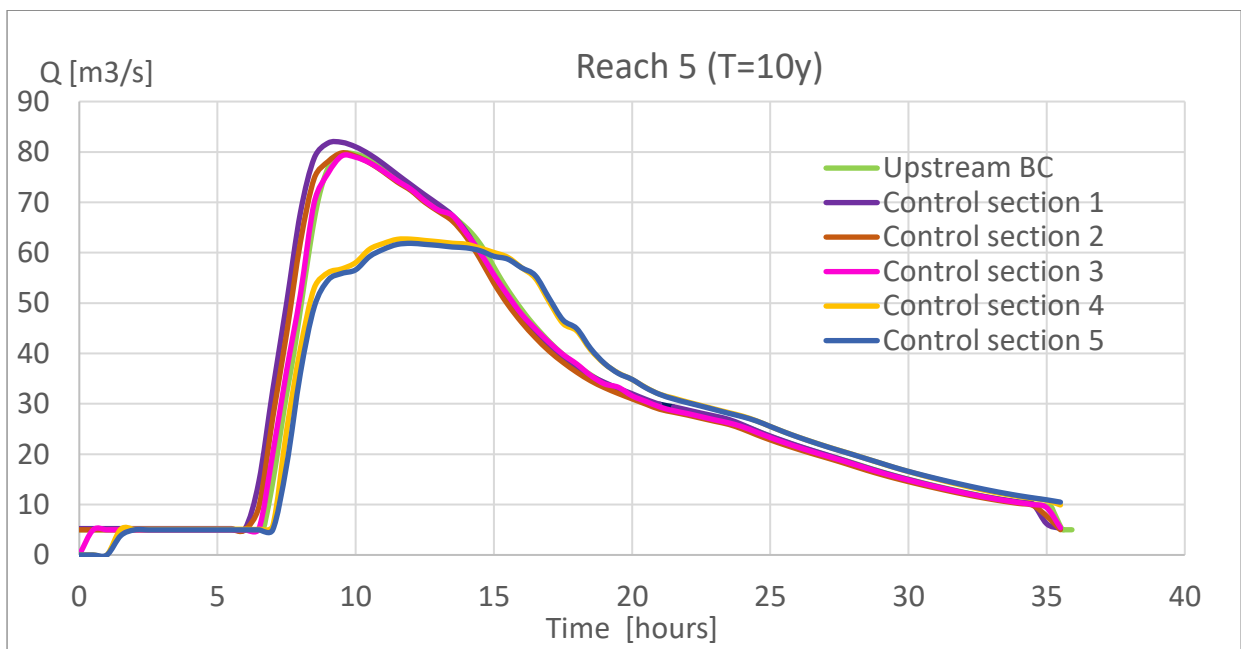
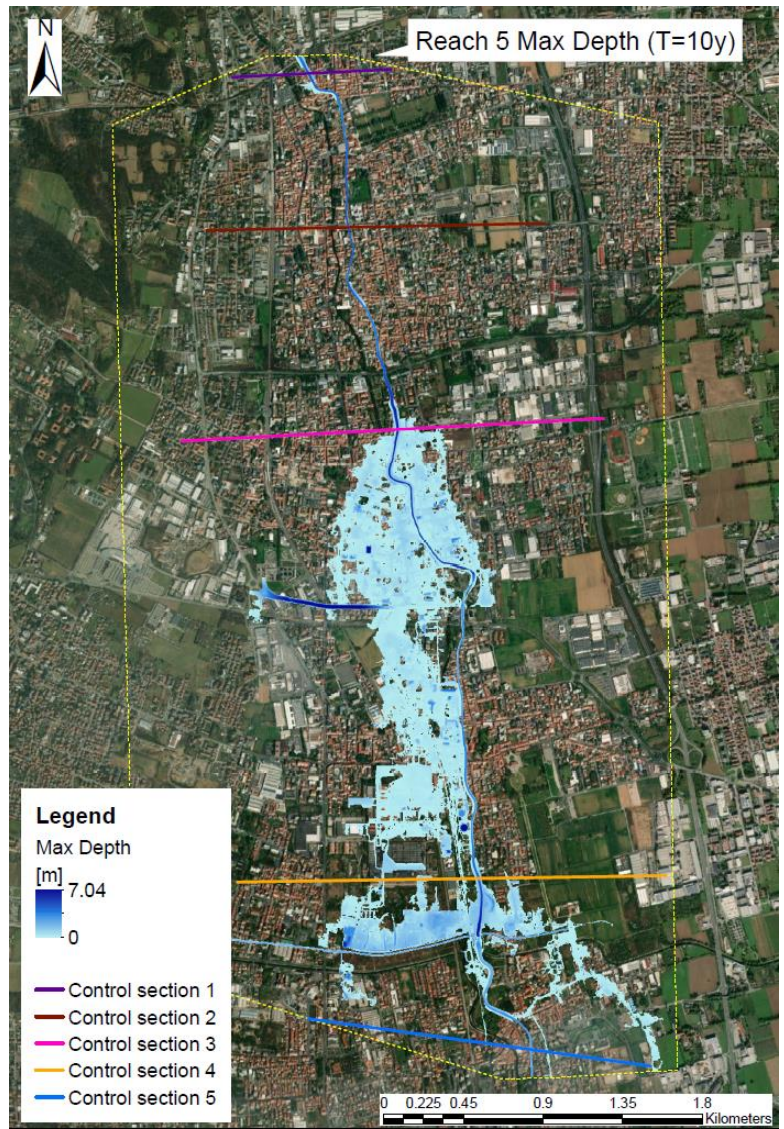
Reach 4

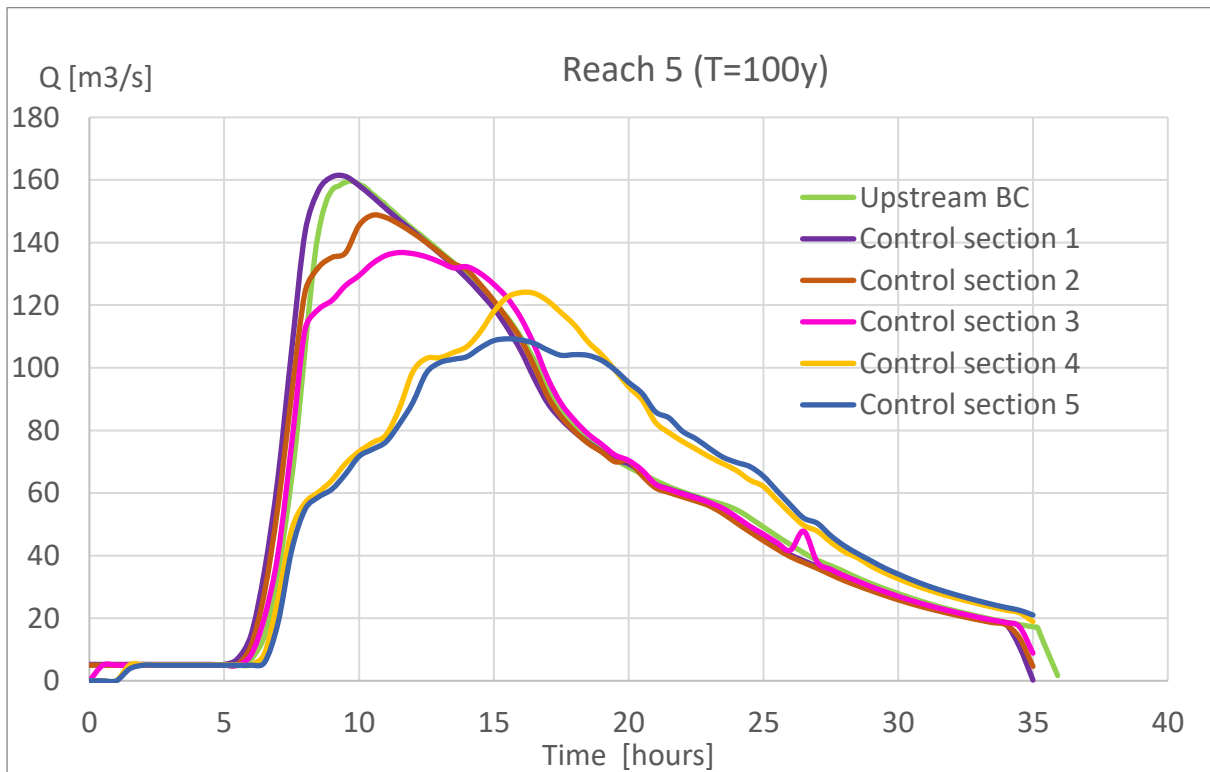
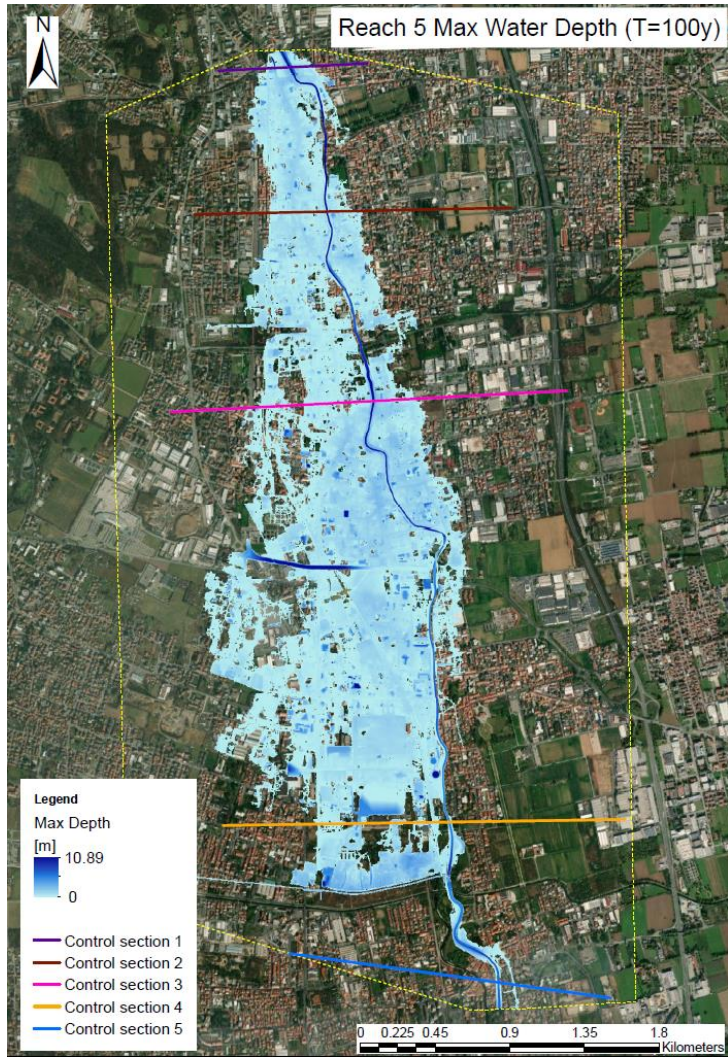


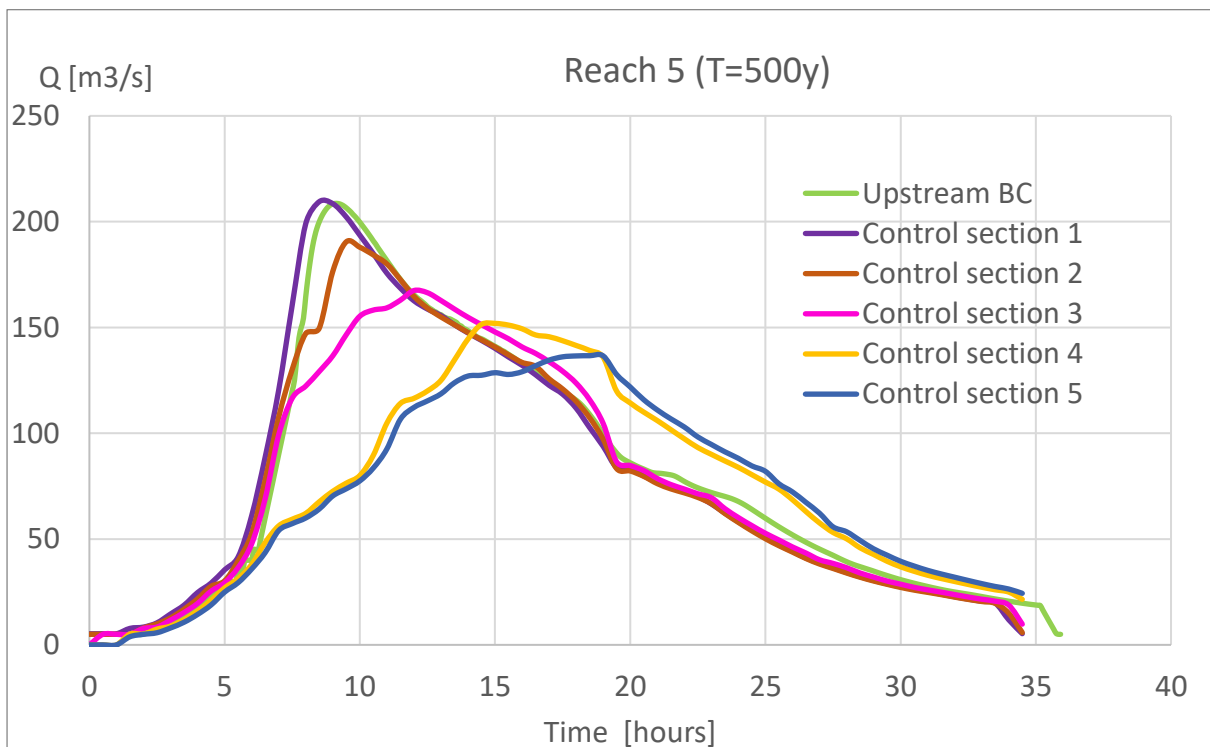
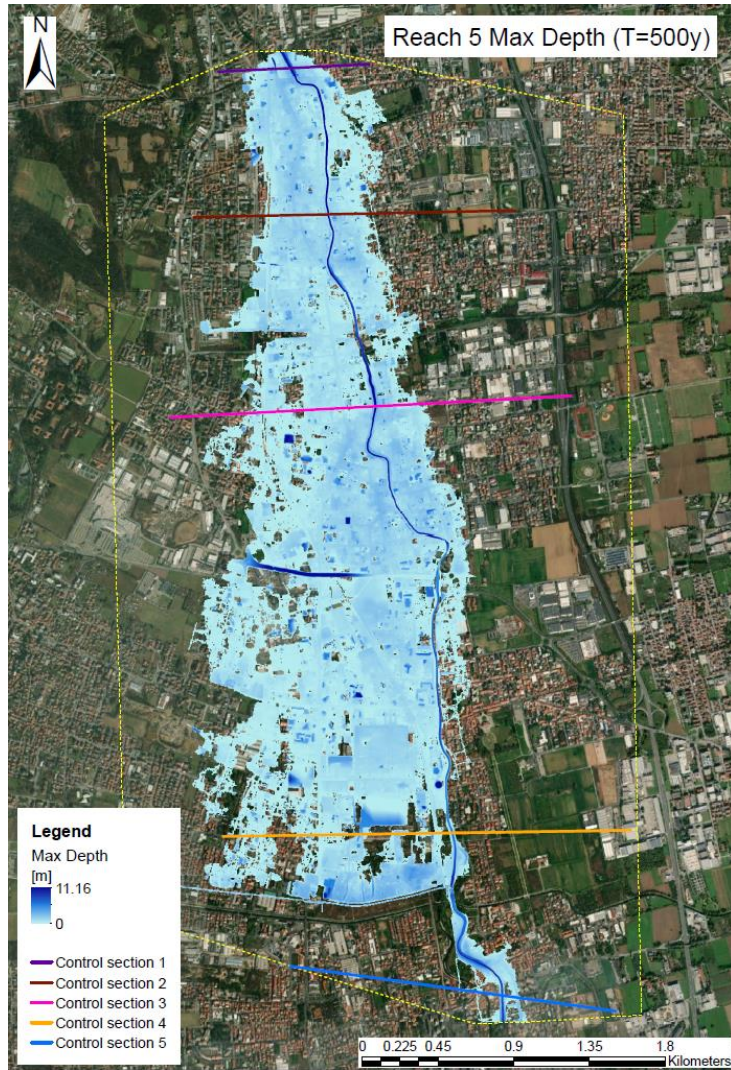




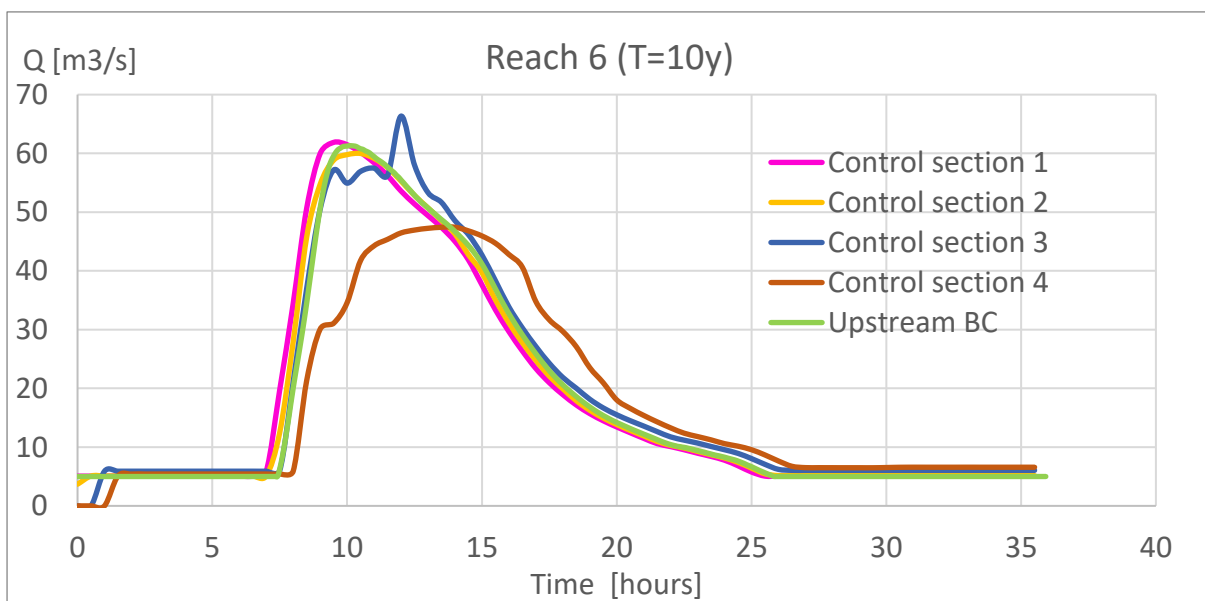
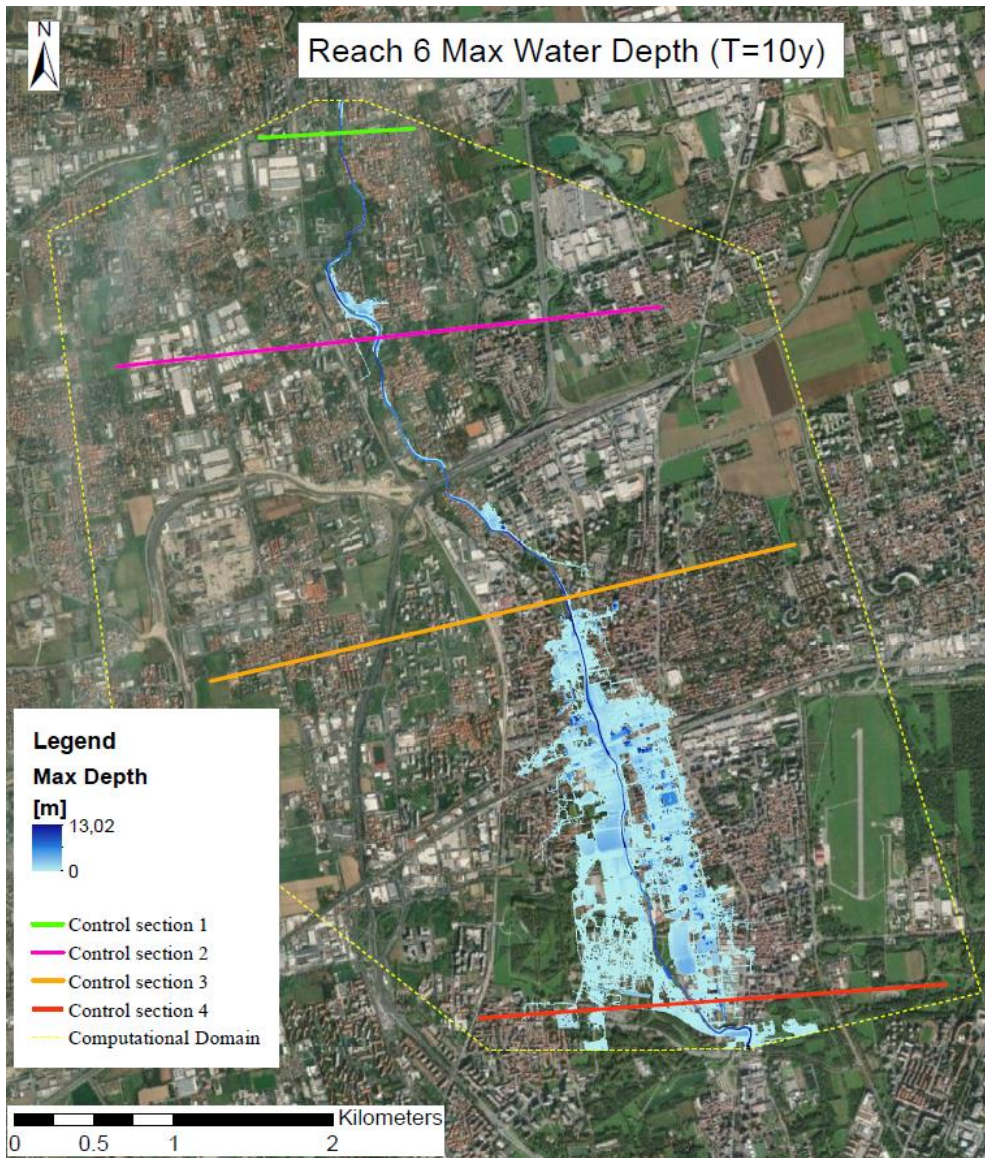
Reach 5

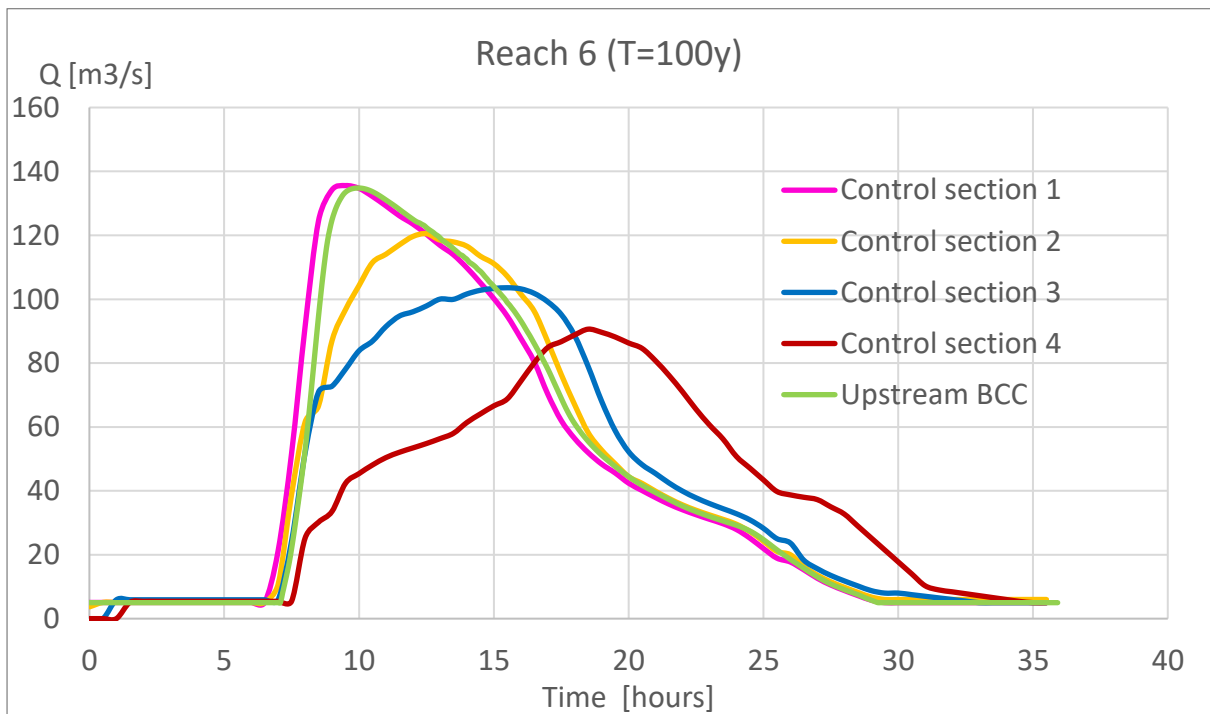
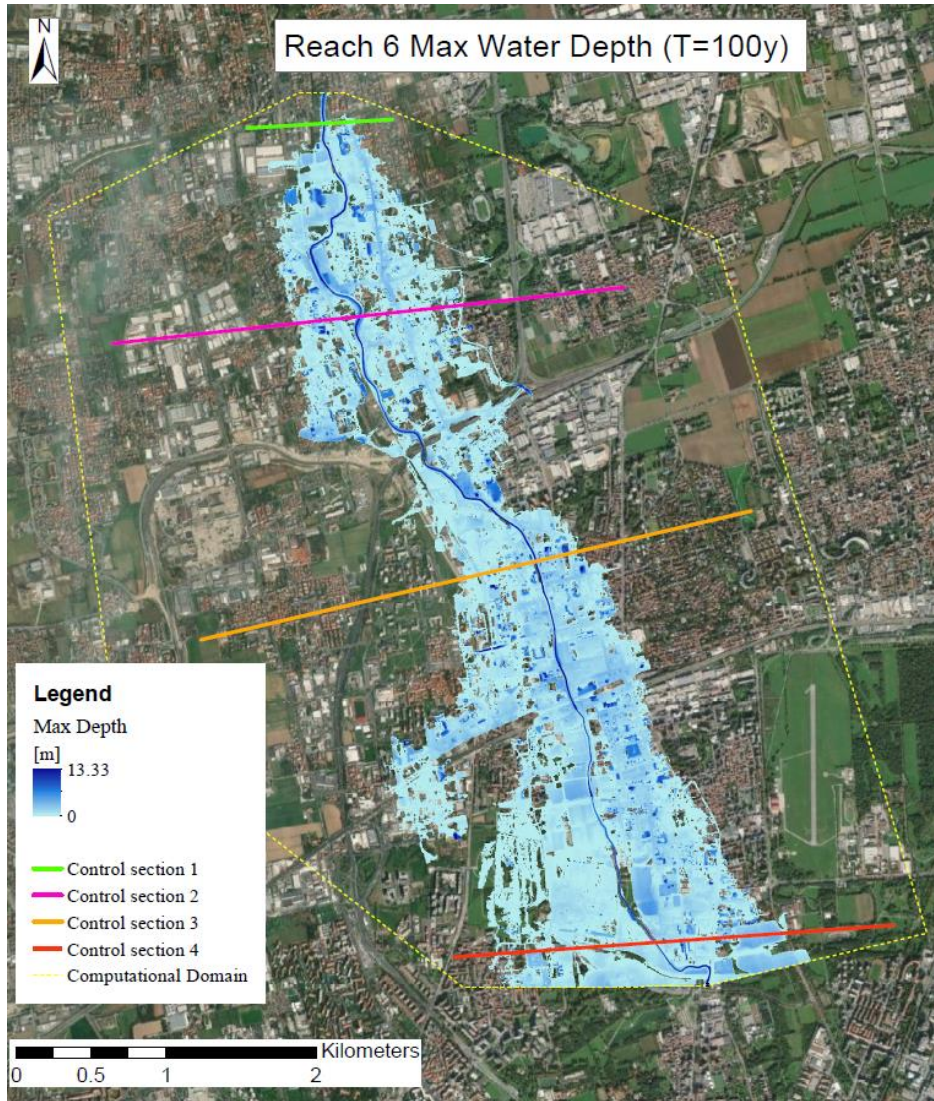


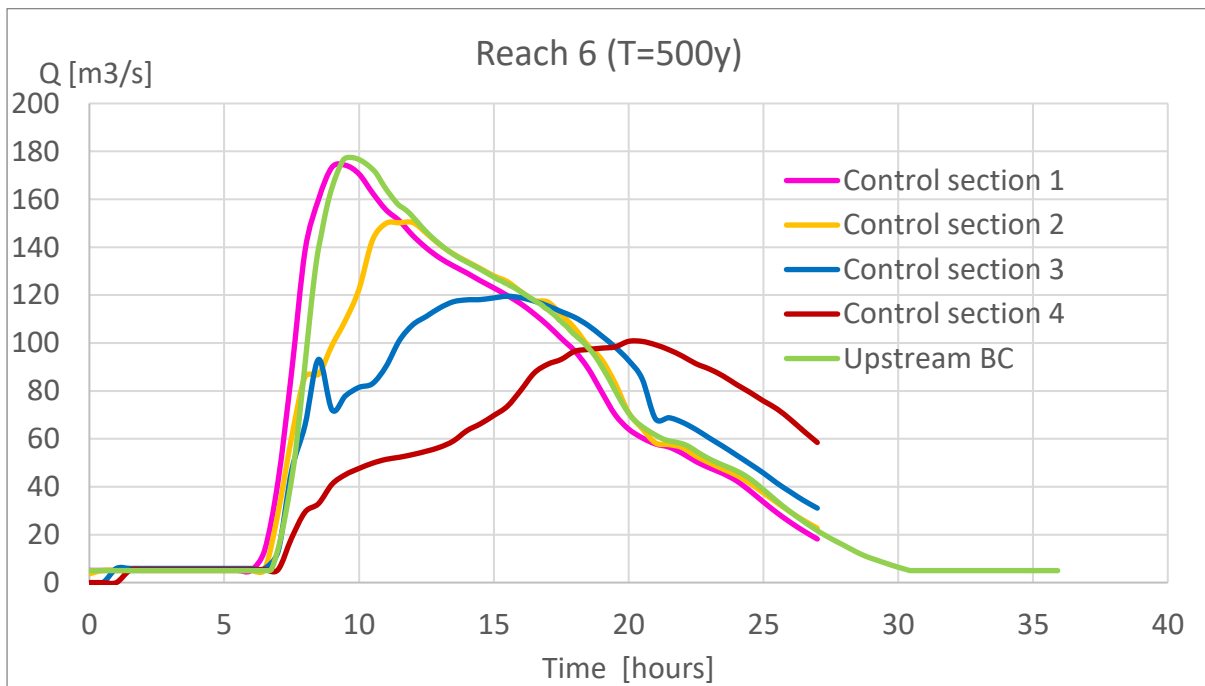
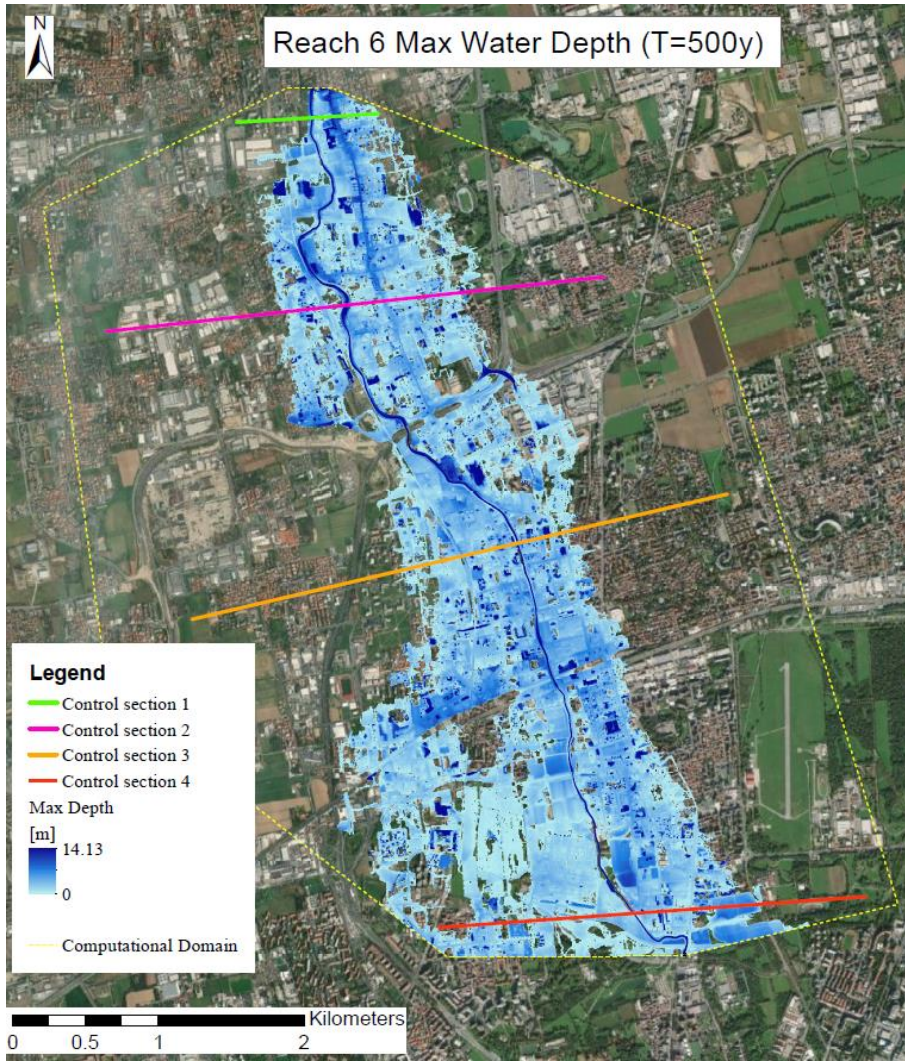




Reach 6

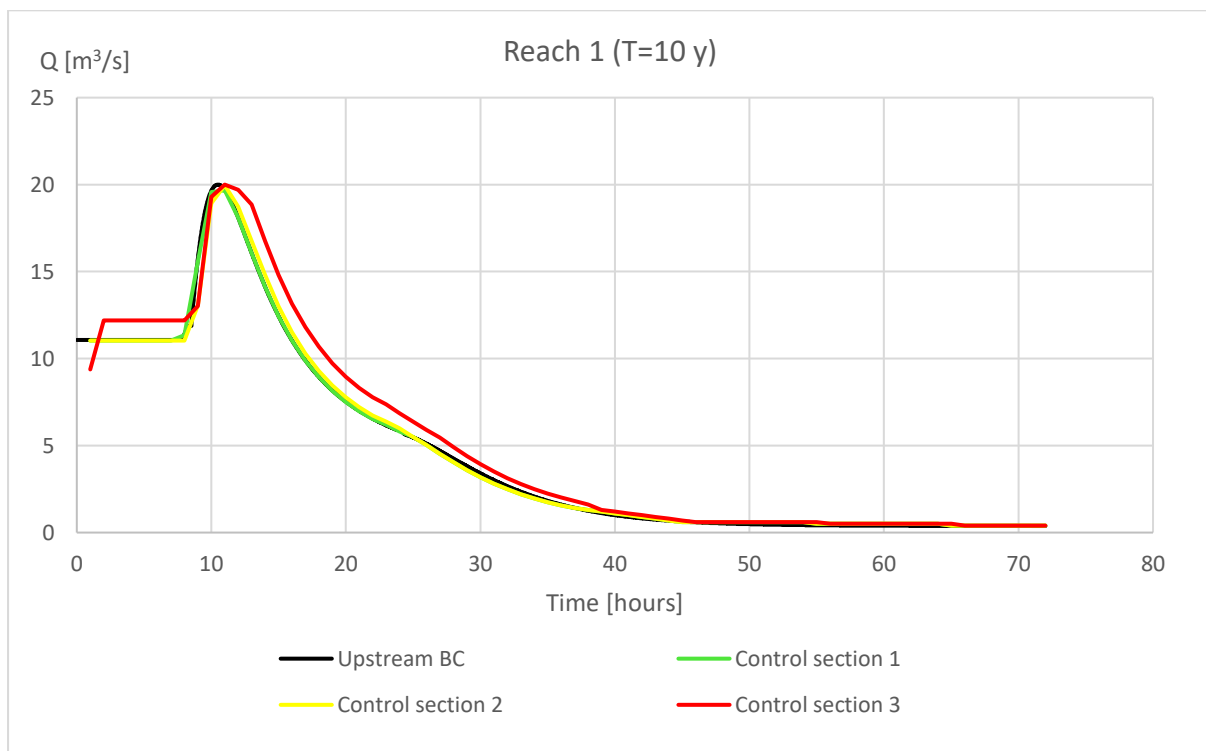
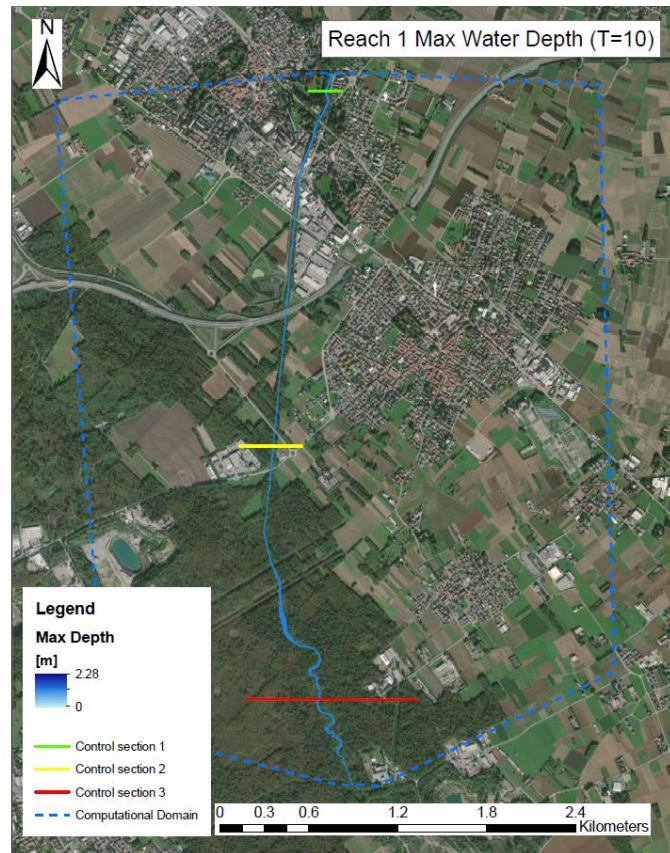


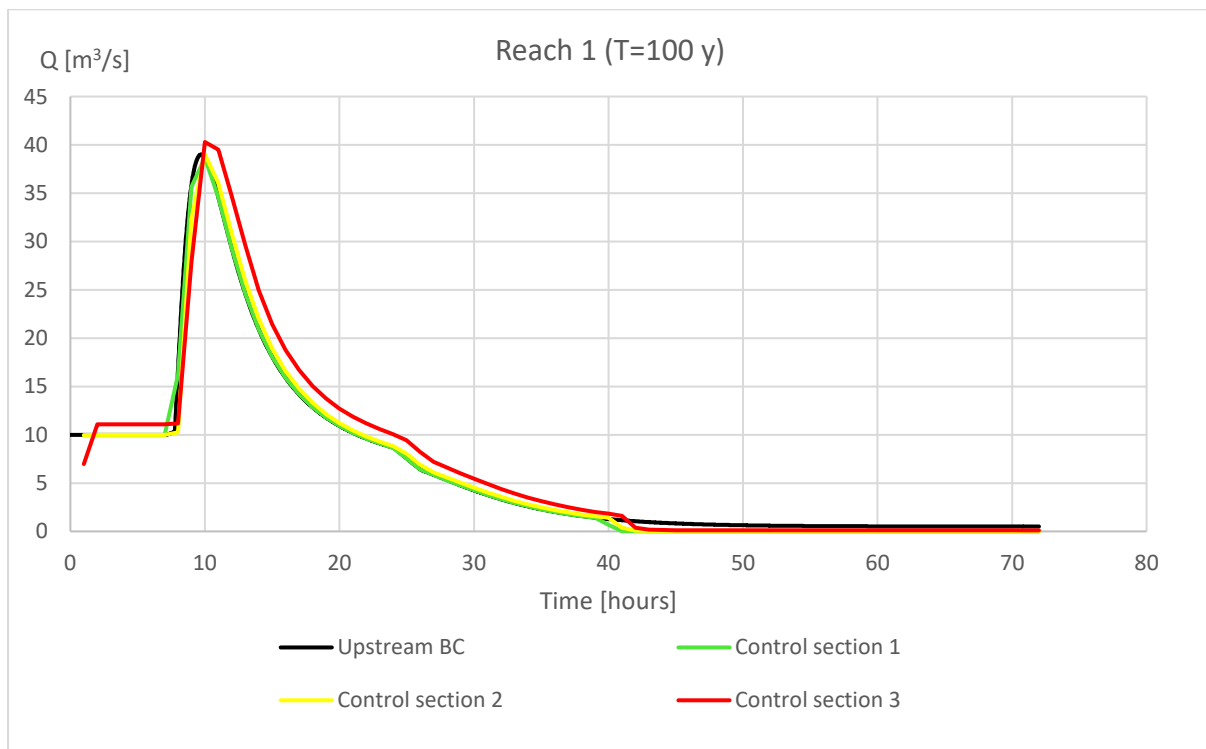
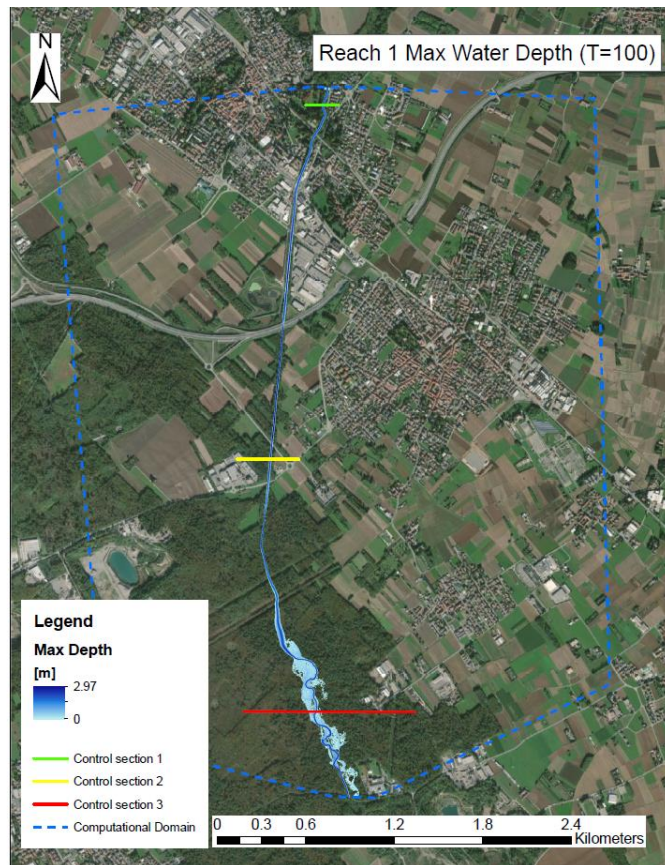


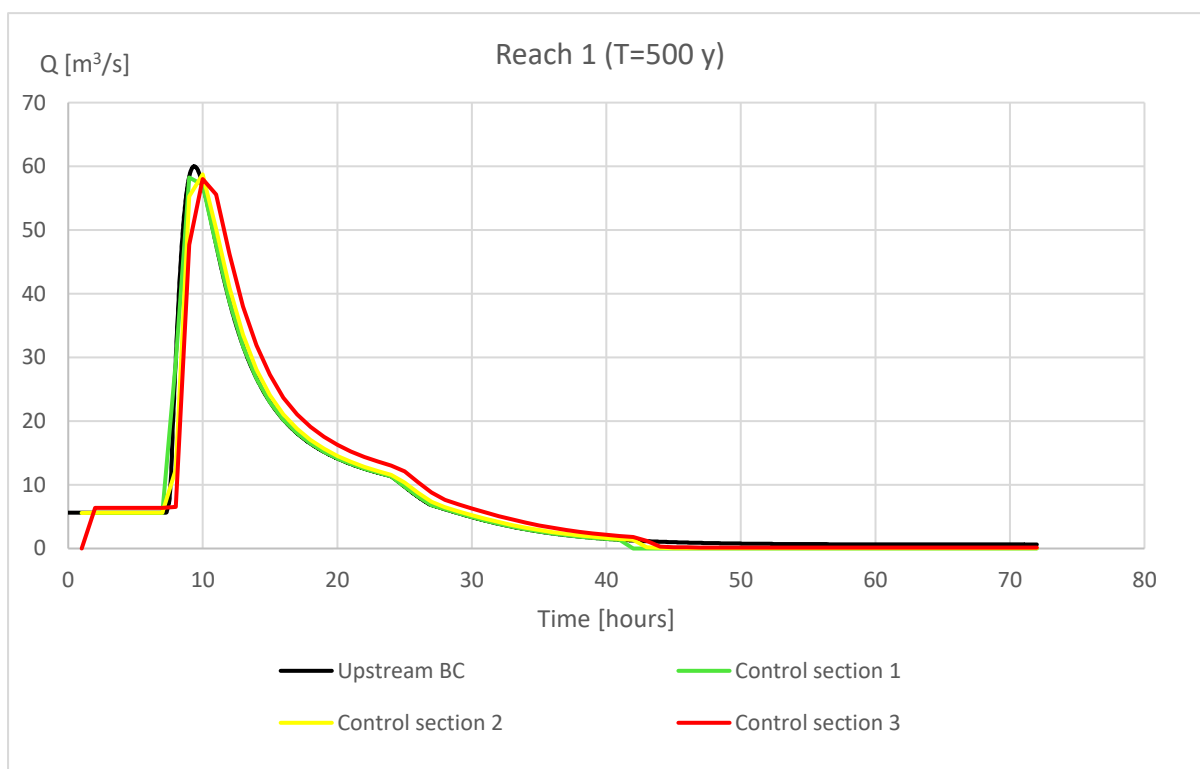
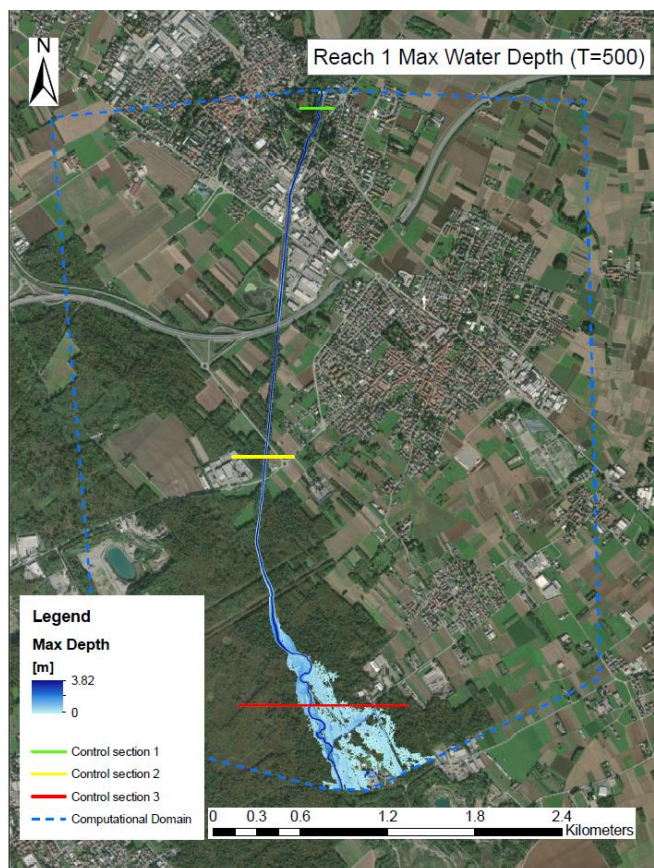


Bozzente

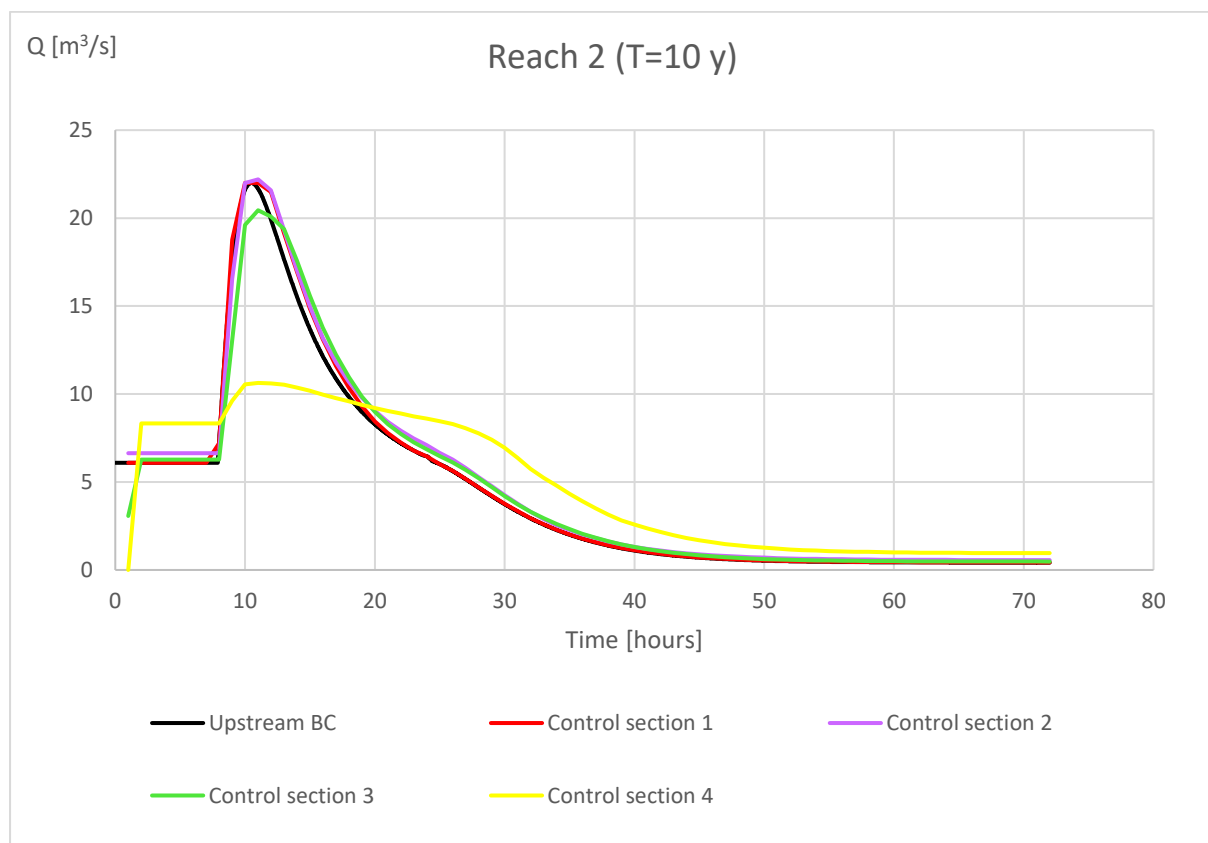
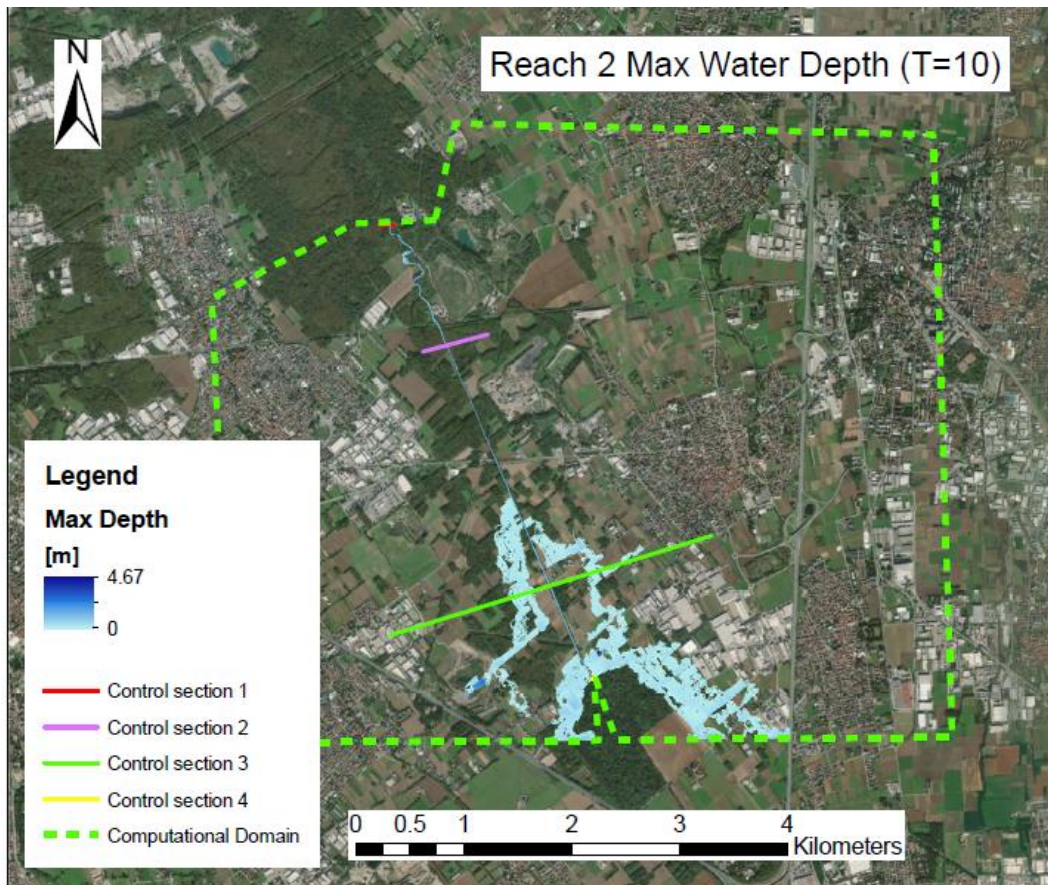
Reach 1

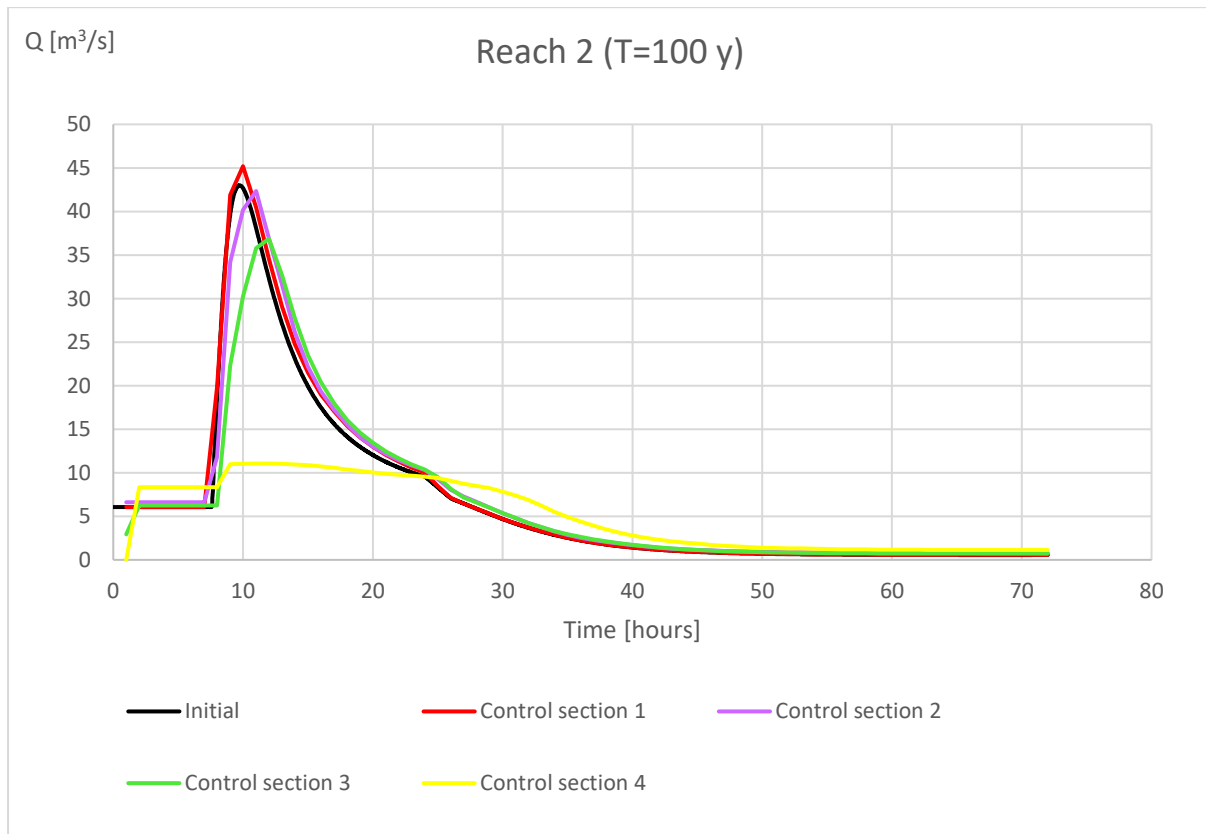
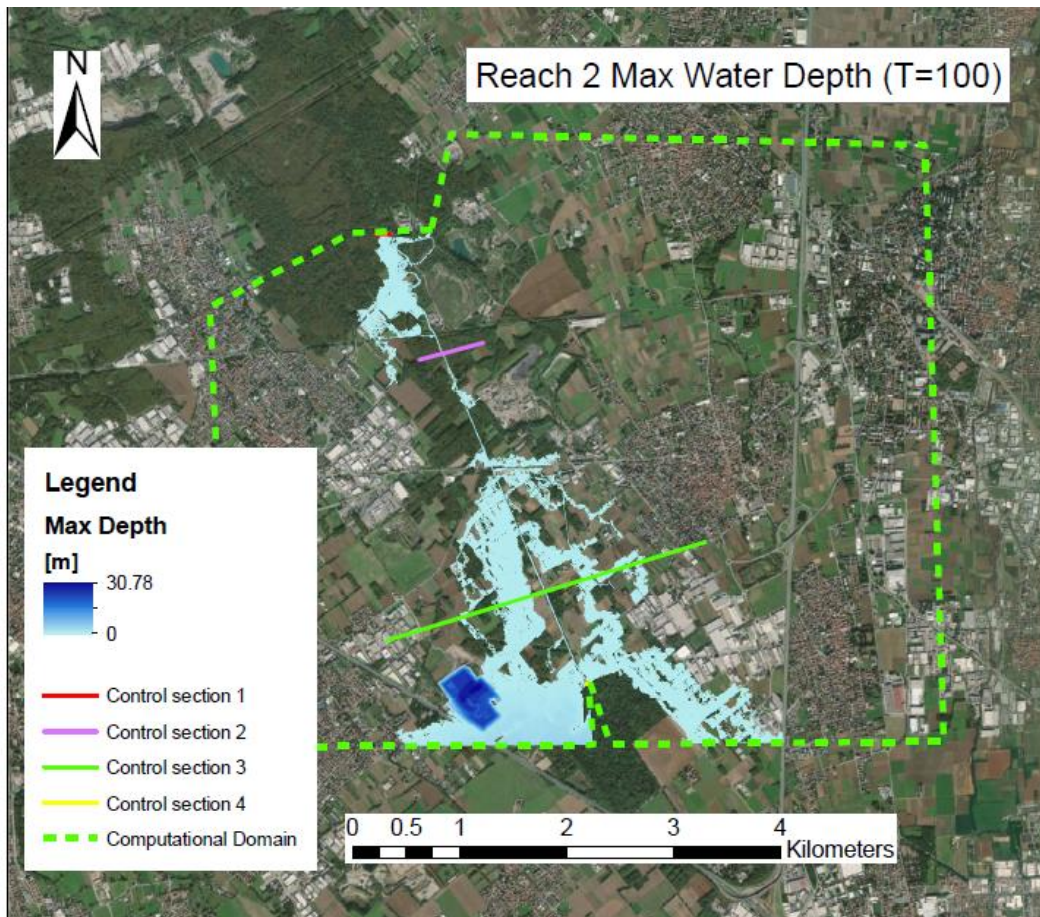


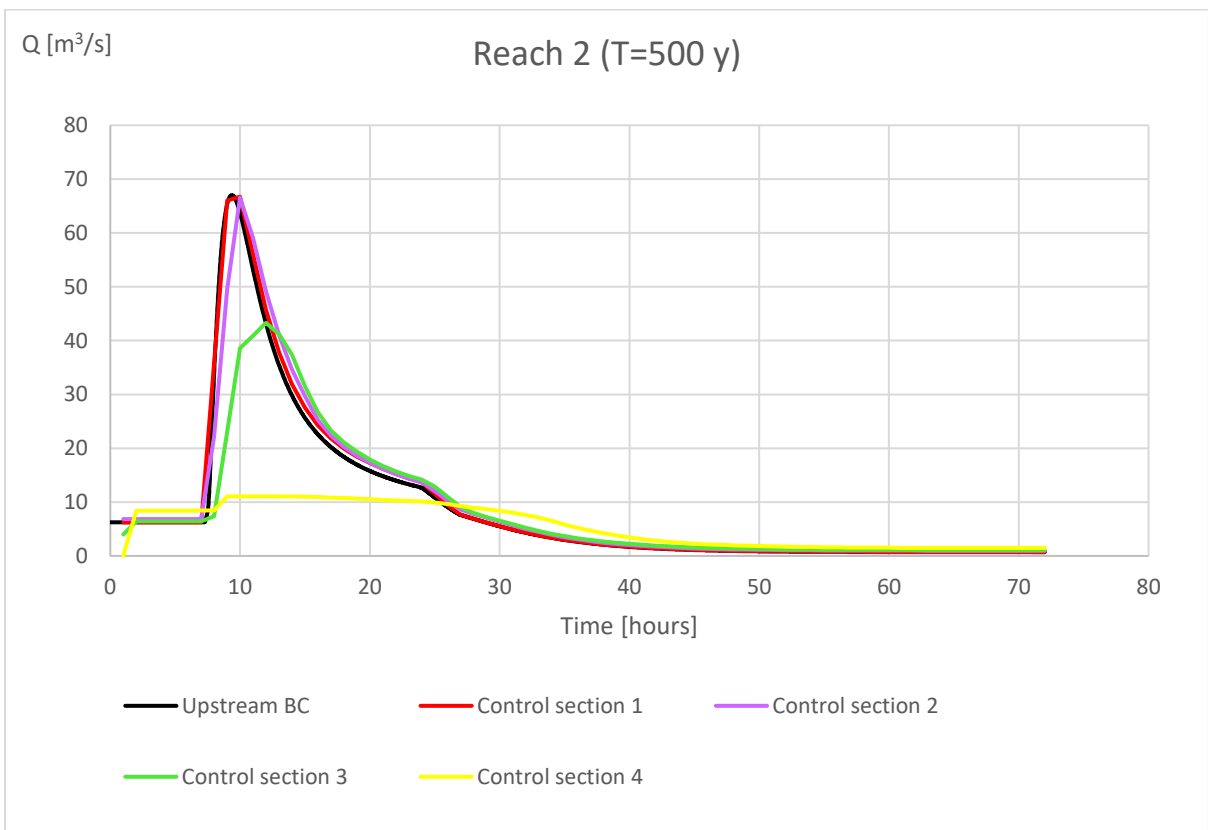
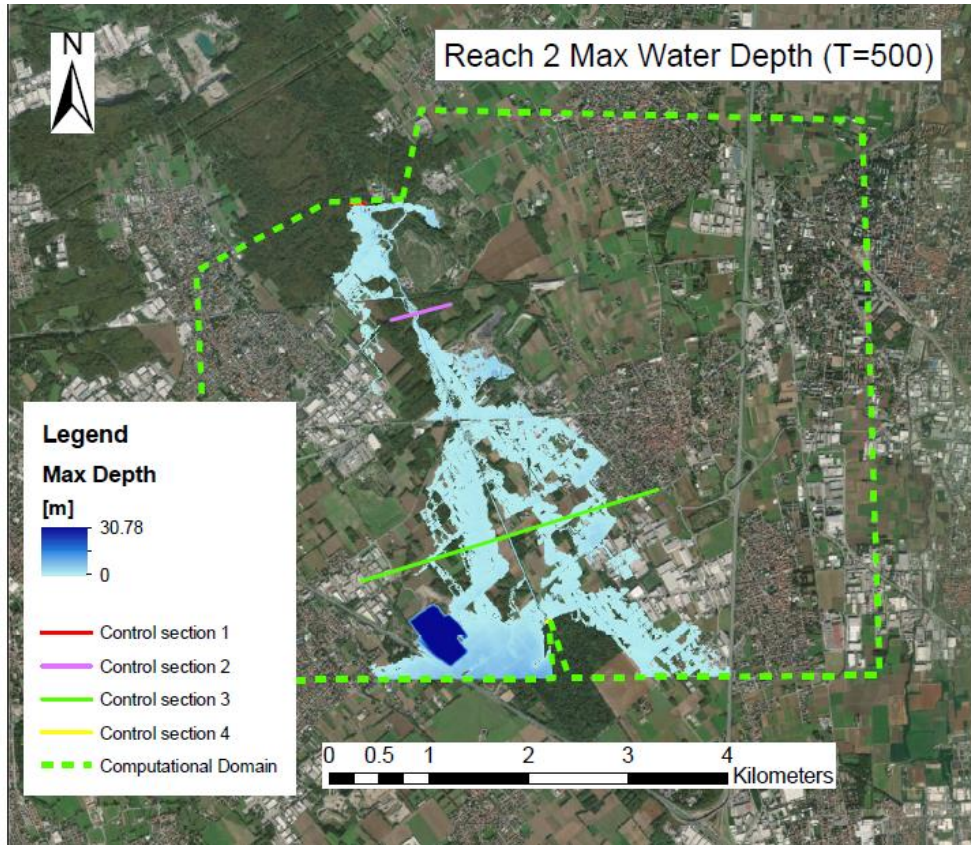




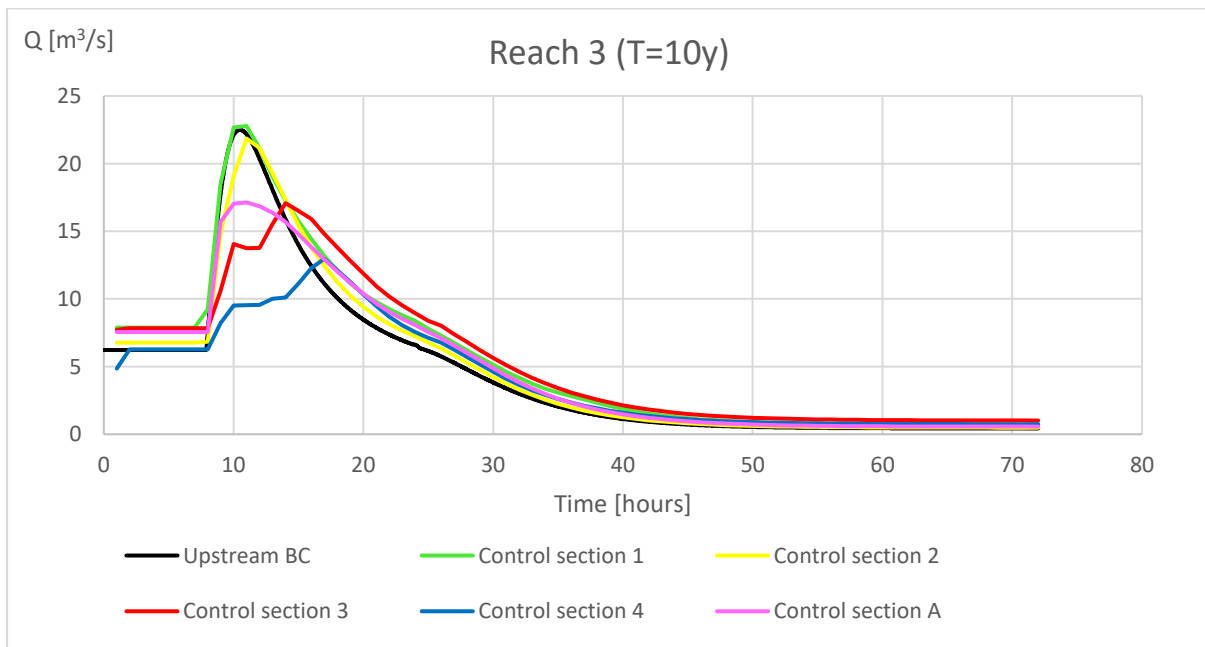
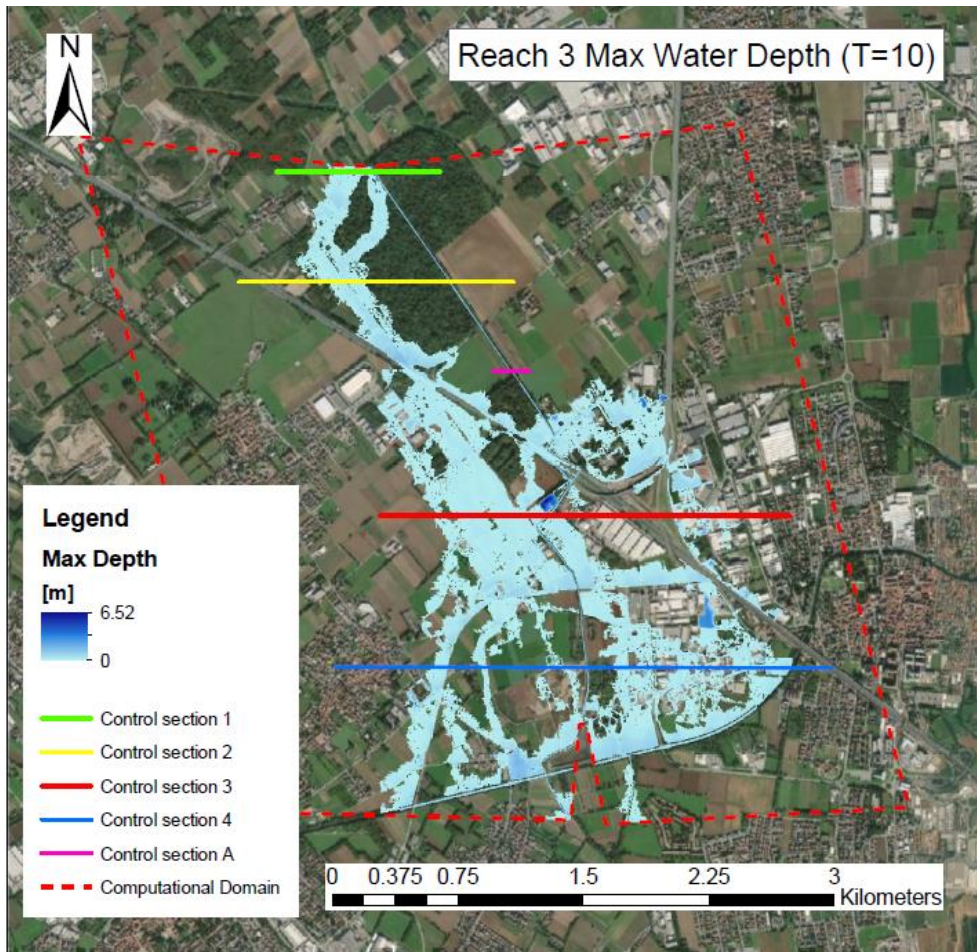
Reach 2

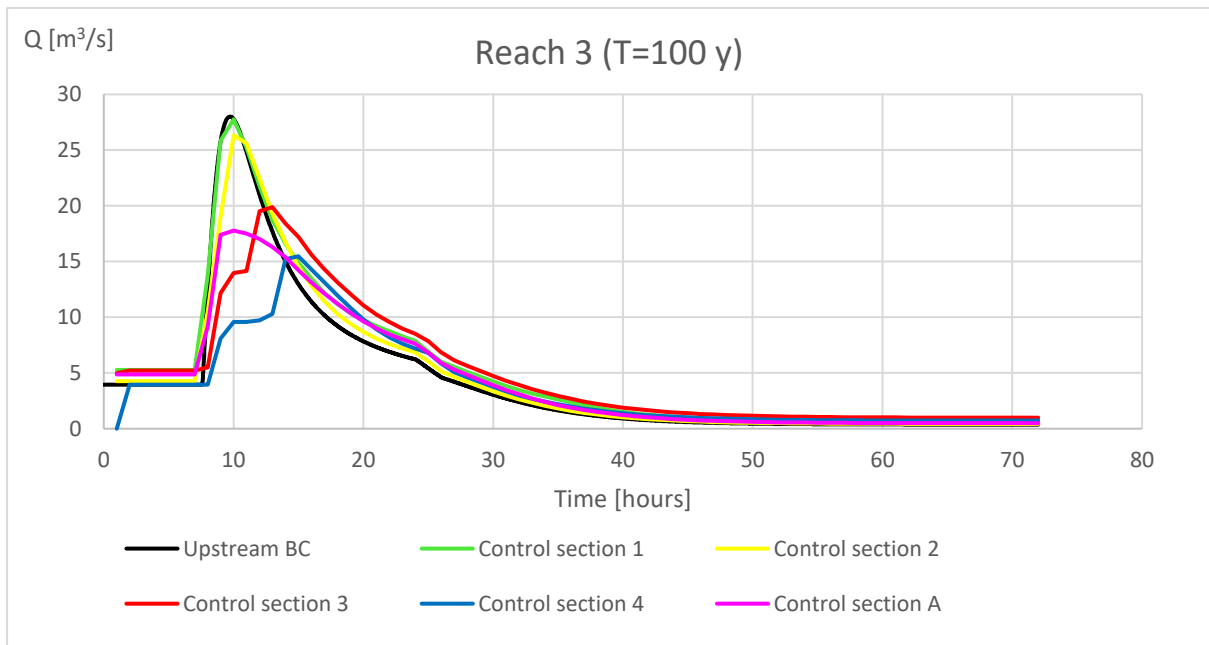
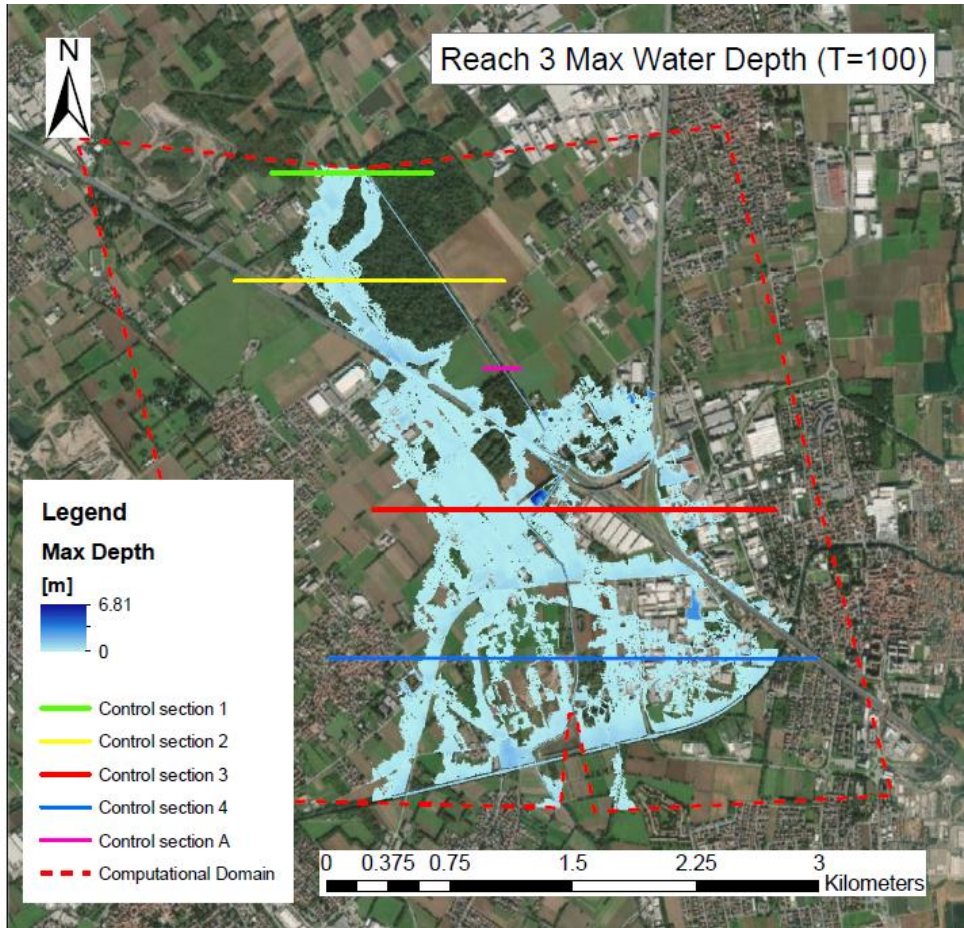


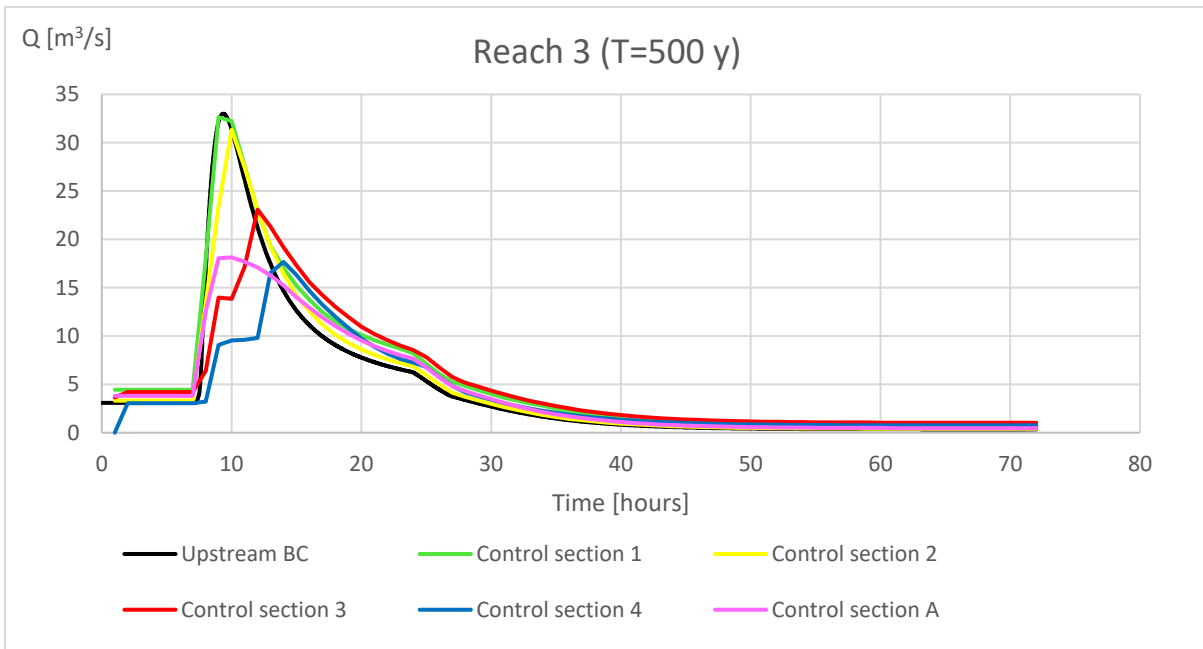
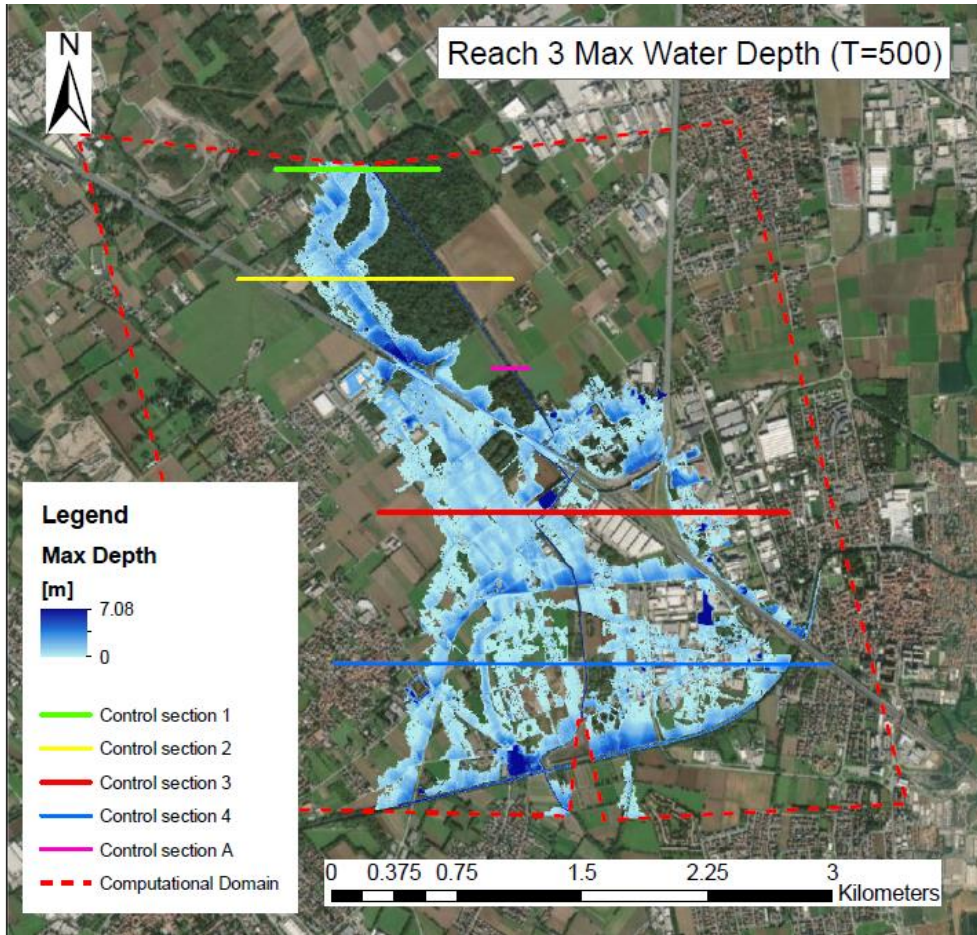




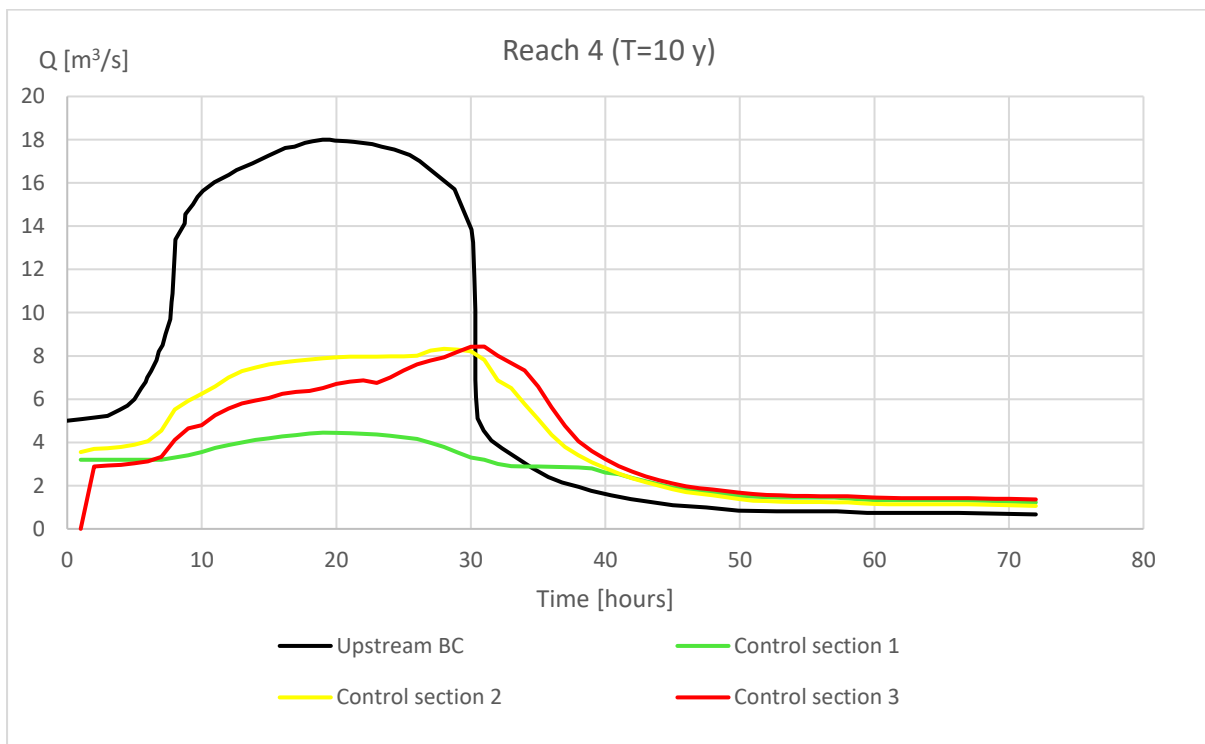
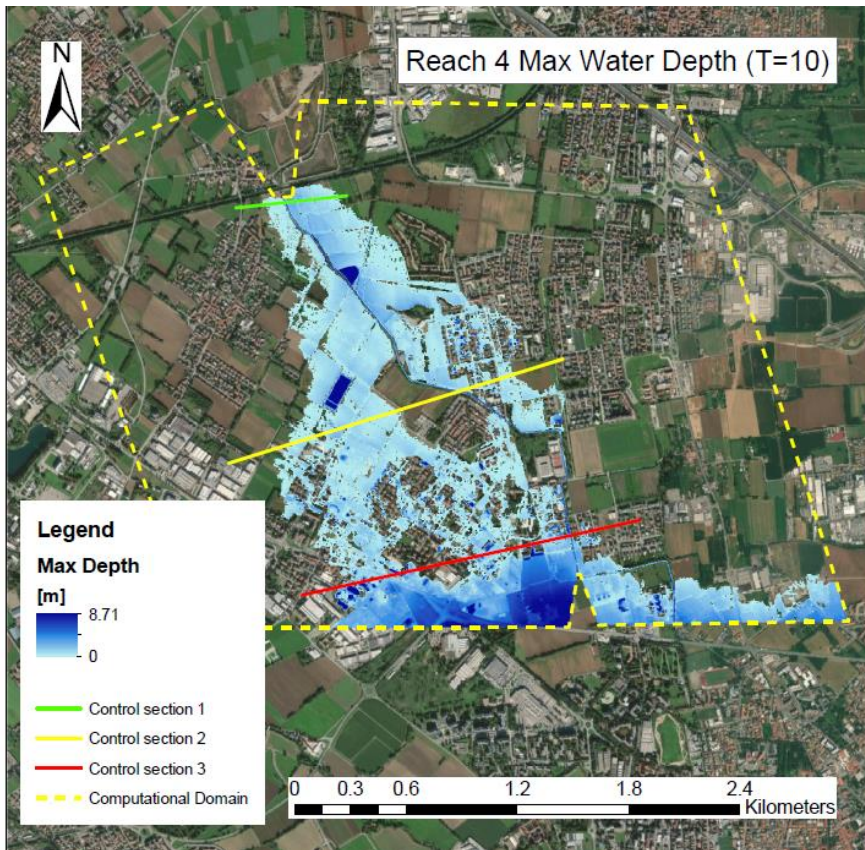
Reach 3

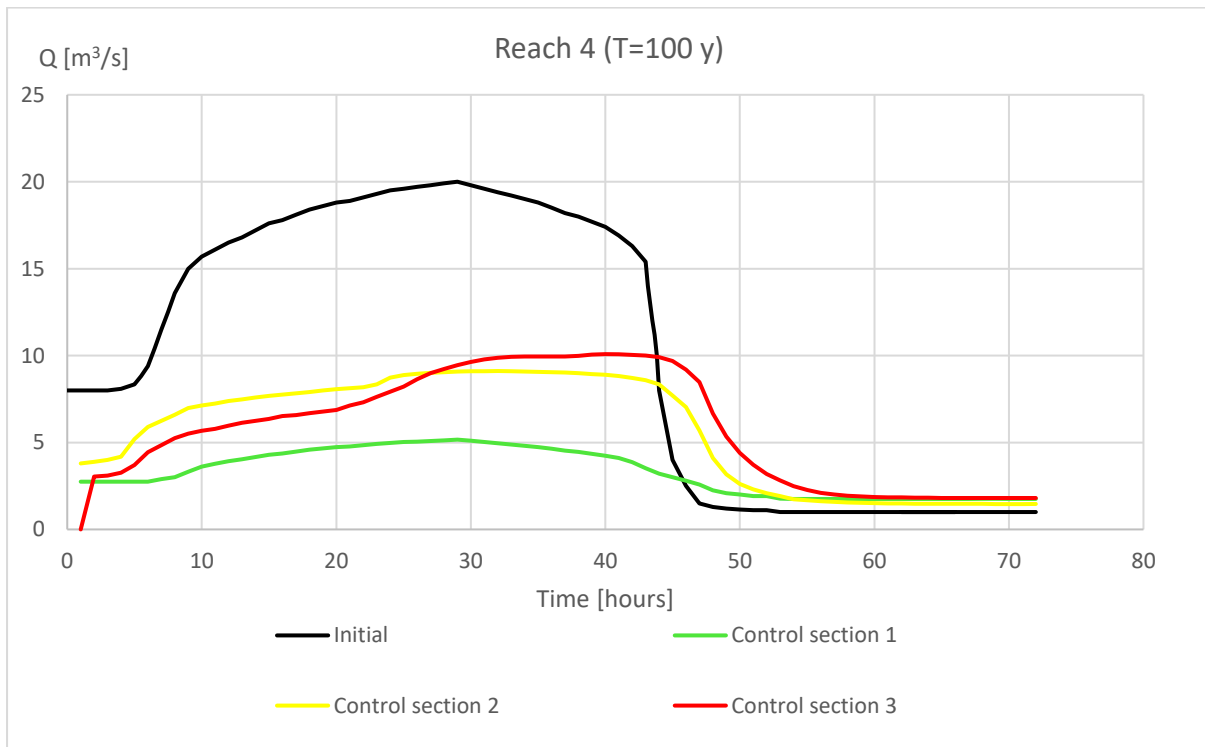
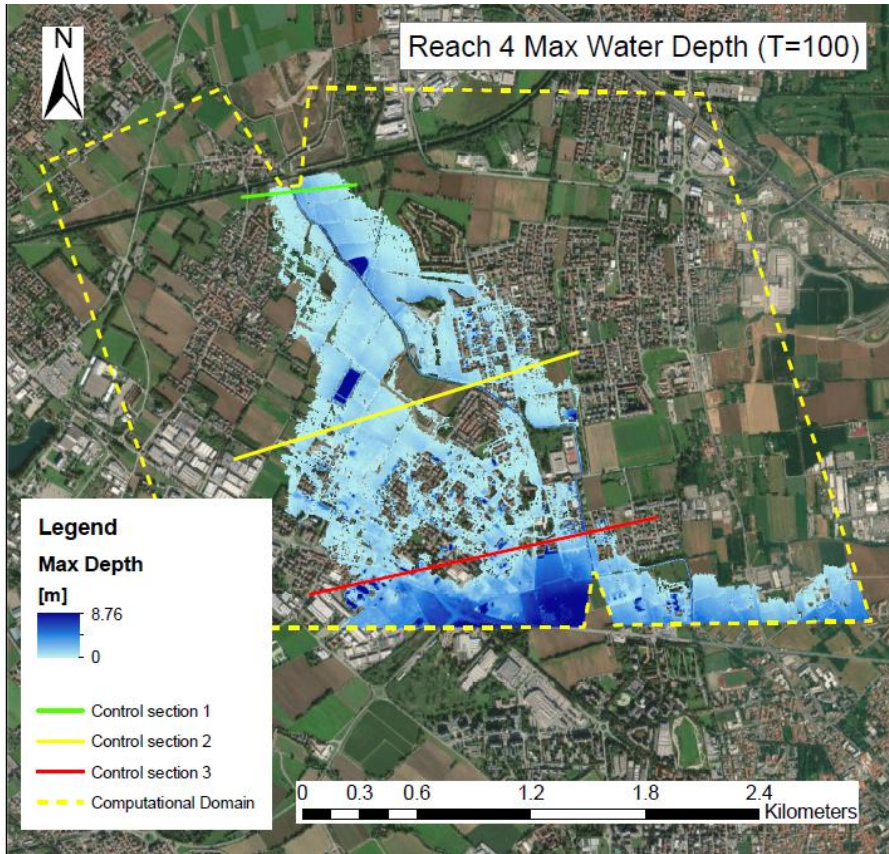


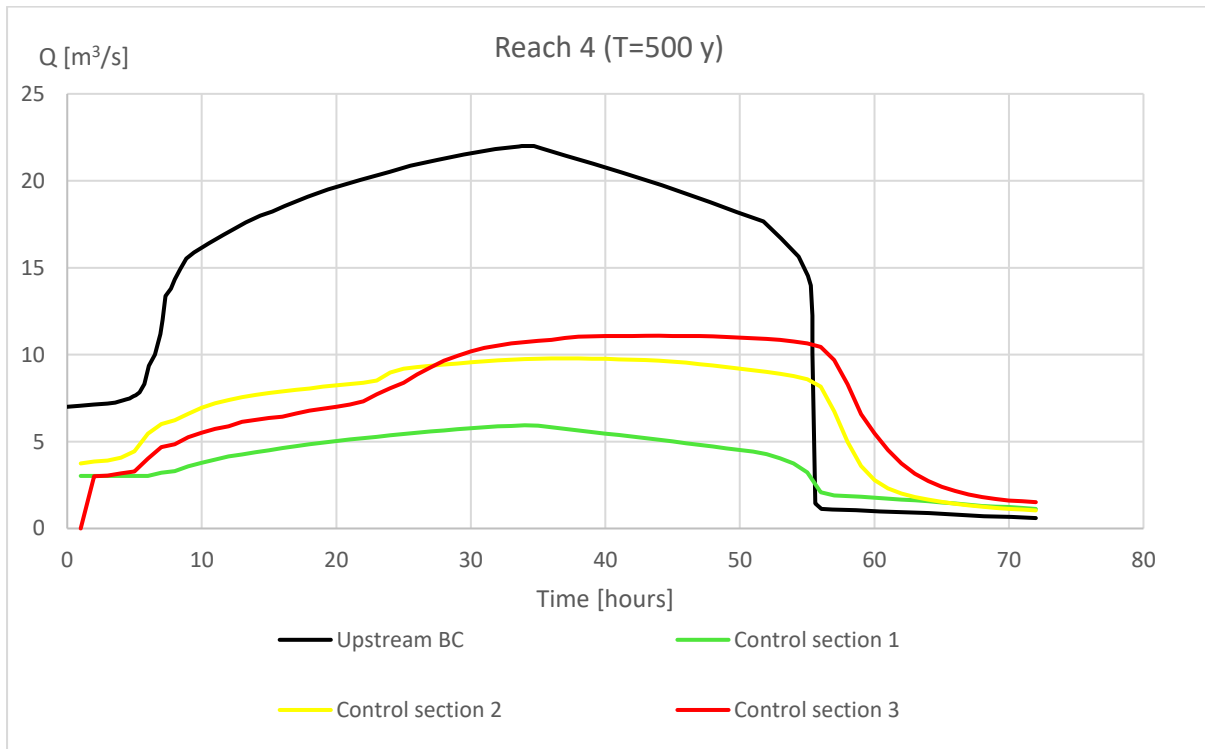
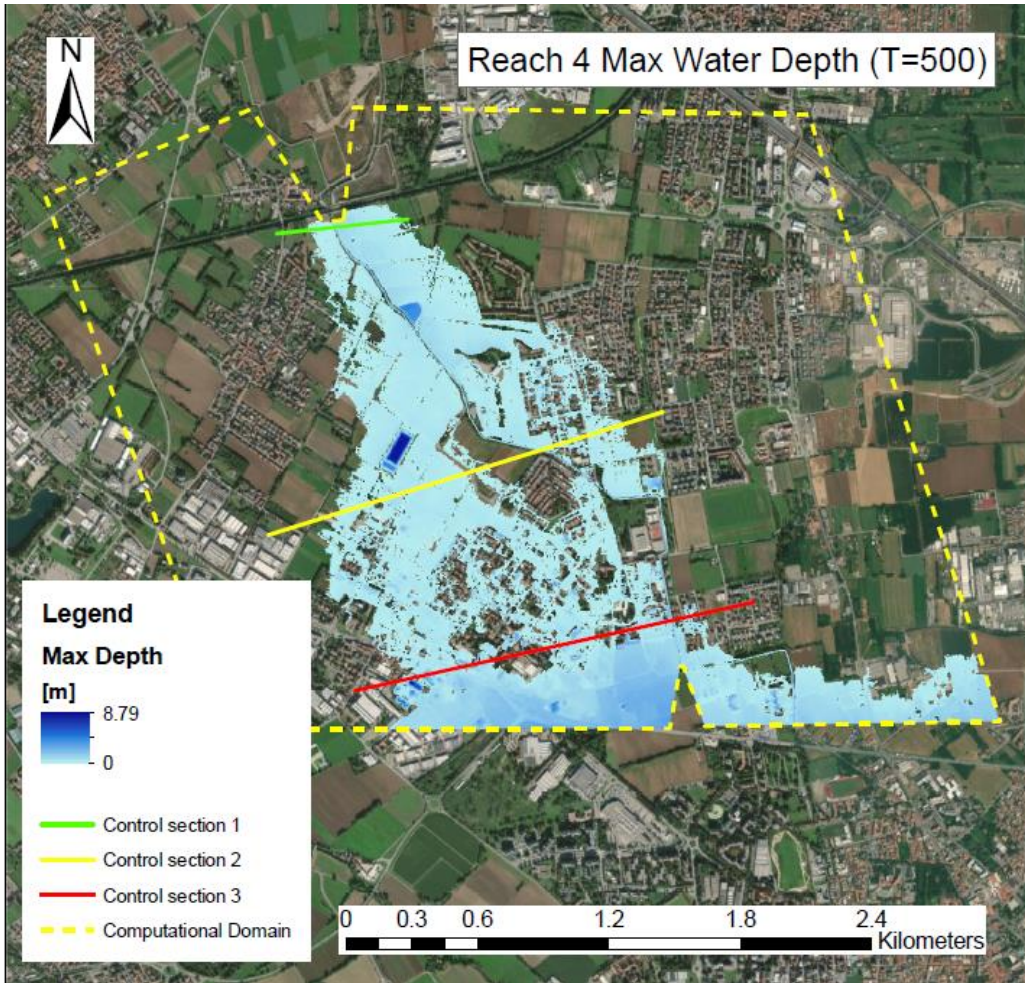




Reach 4







Reach 5

